Role of thymidine kinase 1 phosphorylation on 3'-deoxy-3'-[^{18}F]-fluorothymidine uptake by cancer cells: implication for Positron Emission Tomography

Thesis submitted for the degree of

Doctor of Philosophy

Roberta Sala

Imperial College London

Department of Surgery and Cancer

Declaration of originality

I declare that the research work discussed in this thesis has been conducted by myself, unless otherwise stated and appropriately referenced.

Abstract

Uncontrolled cell proliferation is one of the hallmarks of cancer and its inhibition is desired in cancer therapy. The thymidine analogue 3'-deoxy-3'-[^{18}F]-fluorothymidine ([^{18}F]FLT) is used to image tumour proliferation by positron emission tomography (PET). To be retained in cells, [^{18}F]FLT is phosphorylated by thymidine kinase 1 (TK1), the first enzyme in the salvage pathway for DNA synthesis, and for this reason the cellular incorporation of [^{18}F]FLT is dependent on TK1 activity. Of the mechanisms regulating TK1 activity, TK1 transcription is well recognised while post-translational enzyme modifications are less well understood.

TK1 protein phosphorylation was investigated in cancer cells, hypothesising that, throughout the cell cycle, but particularly during G2/M phase, TK1 is subjected to different types of phosphorylation, which are responsible for regulating its activity, and therefore potentially modulating [^{18}F]FLT uptake.

An acrylamide phos-tag™ gel method was validated to enable discrimination of phosphorylated TK1. Three different phosphorylated forms of TK1 were detected during progression of cells within the cell cycle, one of which was specifically produced upon G2/M arrest. There were significant changes in [^{18}F]FLT uptake subsequent to cell cycle arrest by biological means and following treatment with anti-cancer drugs and pharmacological modulators. Changes in TK1 enzyme activity were detected as variations in [^{18}F]FLT retention, with significantly reduced uptake upon serum starvation-induced G1 arrest, and marked decreased uptake during S-phase arrest and after nocodazole- or paclitaxel-induced G2/M arrest. Phosphorylation of serine-13 and serine-231 of TK1 were implicated in regulating [^{18}F]FLT uptake.

To assess whether or not [18F]FLT-PET highlighted changes in proliferation *in vivo*, HCT116 tumour-bearing mice were treated with paclitaxel. Although long term treatment resulted in tumour growth delay, in the model and at drug doses and early time points considered for imaging, no significant changes in tumour [18F]FLT retention were observed in treated animals compared to controls. This correlated with similarly unremarkable changes in Ki67 and TK1 expression in excised tumour samples.

Investigation of whether or not alternative nucleoside analogue scaffolds were incorporated into the DNA and if they were providing greater sensitivity for detecting cell proliferation, compared to [18F]FLT, was carried out. Two new radiotracers ([18F]FTT and [18F]FOT) were developed and tested for a) phosphorylation by TK1, b) accumulation into cells and c) metabolism and biodistribution. Both radiotracers proved not to be useful, being minimally phosphorylated by TK1 and therefore not retained in cells, and showing catabolism *in vivo*.

Finally, specific mitotic inhibitors were characterised *in vitro* to determine their effects on TK1 phosphorylation and proteins involved in [18F]FLT uptake, in order to verify if [18F]FLT is a suitable biomarker to highlight mitotic arrest with these modern drugs.

The key novel finding to evolve from this thesis is that measurement of tumour proliferation by [18F]FLT-PET is modulated by TK1 phosphorylation. This changes the notion that [18F]FLT uptake simply reflects changes in S-phase arrest/DNA synthesis to one that represents broad sensitivity to proliferation including G2/M arrest. New radiotracers that are specifically incorporated into DNA and whose uptake is TK1-independent could provide additional selectivity for imaging DNA synthesis.

Acknowledgements

I would like to thank Professor Eric Aboagye for the opportunity to be a PhD student in the Comprehensive Cancer Imaging Centre. I also would like to thank CRUK and all the other funding bodies for their financial support. Thanks to Graham and Laurence for the development and radiolabelling of the novel radiotracers and a big thank you to everyone in the CCIC.

A special acknowledgement goes to my family for all their support.

Grazie mamma, babbo e Claudia per tutto quello che avete fatto, fate e farete per me!!! Il vostro sostegno è uno dei pilastri della mia vita, anche lavorativa. Senza di voi non sarei mai arrivata dove mi trovo ora.

Un grazie speciale va anche al resto della famiglia. Grazie nonna Ida, zii Oriana e Renzo, Francesco, zia Cristina per credere nelle mie capacità. Grazie anche a nonno Bruno...il tuo ricordo è sempre vivo tra tutti noi!

Thanks to Giordano for being so patient and supporting even when things are not so easy to handle.

Thank you Elisa and Leo for being like a family. We shared a lot of great moments together, and I'm sure there will be more to come!

Thanks to Maria and all my friends back in Italy for making me feel welcome whenever I am there.

Thanks to the Reisegruppe (Ely, Leo, Sarah and Robin) for the amazing trips that we've organised...one more to come, woop woop!!!

Thanks to Rozy (you were my certainty during early mornings, weekends and late nights!) and all my fellow PhD colleagues: Liz, Sheena, Sebastian, Guillaume, Andreas. It's been a

real pleasure to meet all of you, and I hope that we will be able to keep in touch wherever we'll end up living!

Finally, thanks to all my London friends for the amazing times that we shared in this beautiful city.

Table of Contents

Table of Figures

Table of Tables

List of abbreviations

5-FU: 5-fluorouracil

^{11}C: Carbon-11

^{18}F: Fluorine-18

µg: microgram

µl: microliter

µM: micromolar

APH: Aphidicolin

APS: Ammonium Persulfate

ATP: Adenosine Triphosphate

BSA: Bovine Serum Albumin

CDK: Cyclin-Dependent Kinase

CIS: Cisplatin

DAPI: 4', 6-diamidino-2-phenylindole

DMEM: Dulbecco's Modified Eagle's Medium

DMSO: Dimethyl Sulfoxide

DNA: Deoxyribonucleic Acid

dNTP: Deoxyribonucleotide Triphosphate

dTDP: Deoxythymidine Diphosphate

dTMP: Deoxythymidine Monophosphate

dTTP: Deoxythymidine Triphosphate

dUMP: Deoxyuridine monophosphate

E. coli: *Escherichia coli*

EDTA: Ethylendiaminetetraaceticacid

EGFR: Epidermal Growth Factor Receptor

FACS: Fluorescence-Activated Cell Sorting

FBS: Fetal Bovine Serum

FDG: Fluorodeoxyglucose

FLT: Fluorothymidine

FMAU: 1-(2'-deoxy-2'-fluoro-β-D-arabinofuranosyl)-5-methyluracil

G1: Gap 1 phase

G2: Gap 2 phase

HRP: Horse Radish Peroxidase

ID: Injected Dose

IEF: Iso-Electric Focusing

Ig: Immunoglobulin

IP: Immunoprecipitation

i.p.: Intraperitoneal

KDa: Kilodalton

LB: Luria Broth

M: Mitosis

mg: Milligram

ml: millilitre

mM: millimolar

MRI: Magnetic Resonance Imaging

mRNA: messenger RNA

NDPK: Nucleotide Diphosphate Kinase

nM: nanomolar

NOC: Nocodazole

PAGE: Polyacrylamide Gel Electrophoresis

PAX: paclitaxel

PBS: Phosphate Buffered Saline

PBS-T: Phosphate Buffered Saline-0.1% Tween 20

PCM: Pericentriolar Material

PET: Positron Emission Tomography

PI: Propidium Iodide

pM: picomolar

RIPA: Radioimmunoprecipitation assay

RNA: Ribonucleic Acid

RNase: Ribonuclease

ROI: Region Of Interest

Rpm: rounds per minute

S: Synthetic phase

s.c.: Sub-cutaneous

SDS: Sodium Dodecyl Sulphate

Ser: Serine

shRNA: short hairpin RNA

siRNA: small interfering RNA

SOC: Super Optimal broth with Catabolite repression

TdR: Thymidine

TE: Tris EDTA buffer

TEMED: tetramethylenthylenediamine

TMPK: Thymidylate Kinase

TP: Thymidine phosphorylase

TS: Thymidylate Synthase

U: enzyme units

Chapter 1. Introduction

1.1 Cell proliferation and cancer

The eukaryotic cell cycle (or cell division cycle) is a ubiquitous, complex and vital process, which regulates growth and proliferation of cells, as well as organismal development, but it can also cause diseases such as cancer (Schafer, 1998). It coordinates a series of ordered events that are responsible for the faithful duplication of the cell and its genome. The end result is the production of two genetically identical daughter cells (Figure 1); first the DNA must be faithfully replicated to obtain two complete identical copies, then the so replicated chromosomes must be accurately subdivided into the two daughter cells, which end up having a copy of the entire genome (Alberts, 2008, Schafer, 1998).
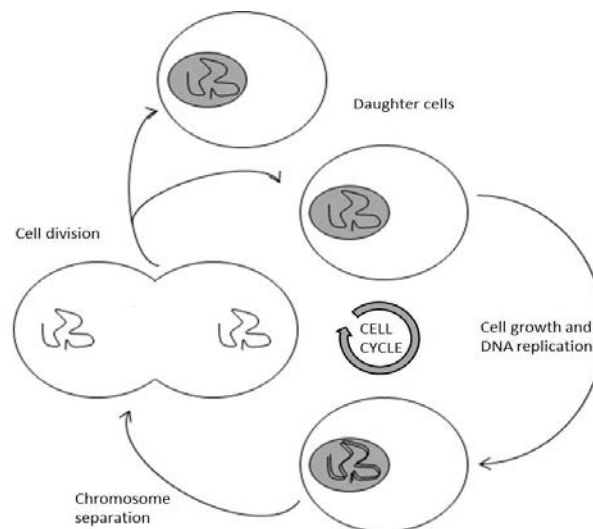
Figure 1. The main events in the mammalian cell cycle.
In order to proliferate, a cell must replicate its DNA and divide it into the two daughter cells, which will be genetically identical to the progenitor.

1.1.1 The cell cycle

The somatic cell cycle is morphologically subdivided into two periods: interphase and mitosis (or mitotic phase, M phase; Figure 2) (Lodish, 2004, Schafer, 1998).

A cell spends the majority of its time in interphase, accumulating nutrients and substances, growing, copying its DNA, and performing all functions in preparation for cell division. Interphase is composed of three sub-phases: G1 (Gap 1 phase, between M phase and S phase), S (Synthetic phase), and G2 (Gap 2 phase, between S phase and mitosis). Beside accurately duplicating the DNA and segregating the chromosomes without errors into the two genetically identical daughter cells, a cell must duplicate organelles and macromolecules, in order to maintain its size after each round of duplication; hence, G1 and G2 phases exist to coordinate cell growth with cell division. Together with granting time for cell growth, they also provide a delay to allow monitoring of internal and external environment in order to check the optimal conditions before progressing into subsequent phases (Alberts, 2008, Schafer, 1998).
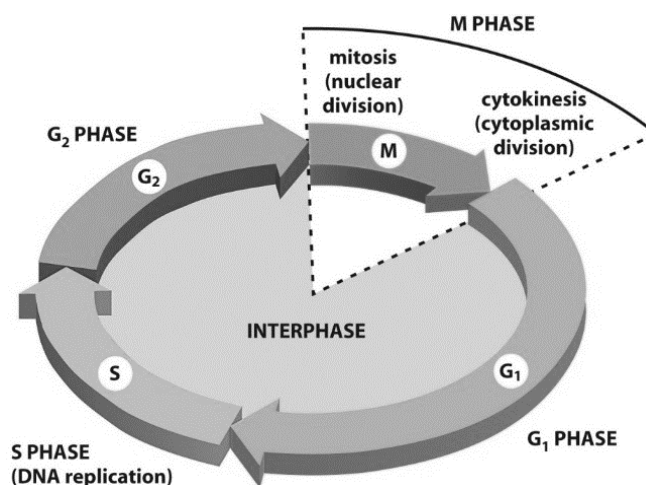
Figure 2. Phases of the cell cycle (Alberts, 2008).
Interphase is subdivided into G1, S and G2 phases and it is the longest period of the cell cycle. During G1 the cell grows and prepares for S phase. During S phase the DNA is replicated, and throughout G2 the cell prepares for cell division. Mitosis consists of the separation of the replicated DNA into two nuclei and terminates with the generation of two genetically identical daughter cells.

During G1 the cell prepares for DNA synthesis, growing, synthesizing proteins and new organelles, and increasing the volume of the cytoplasm; this phase is particularly important for the biosynthesis of enzymes and proteins required in the subsequent step. It is greatly affected by extracellular conditions, such as mitogens (growth factors present in the environment/culture medium (Sherr and Roberts, 1995)), which trigger a signal cascade that induces the transcription of specific proteins, such as the G1 cyclin-dependent kinases (CDKs, see section 1.1.2) complexes. These complexes activate transcription factors responsible for the transcription of genes coding for S phase proteins, including those required for DNA synthesis (Lodish, 2004).

If mitogenic signals are present in the environment, a cell progresses through the restriction point (R point), representing the critical event in late G1 when cells become independent from mitogen to complete division and therefore are committed to DNA replication (Pardee, 1974). If growth factors are removed before the passage of the R point, cells are not able to progress through the cell cycle (Schafer, 1998, Bertoli et al., 2013).

Following G1, a cell enters the S phase (Synthetic phase; (Lodish, 2004)), which is characterised by DNA duplication, while RNA transcription and protein synthesis are reduced. During this stage cells have aneuploid DNA content (abnormal number of chromosomes (N), e.g. <2N or 4N, where 2N is the number of chromosomes in a diploid cell; (Schafer, 1998)). At the end of DNA replication and before the entry into the mitotic phase, other checkpoints act to guarantee that the DNA is intact and fully duplicated, allowing DNA repair if necessary and preventing the cell from initiating mitosis prematurely (Nurse, 1990, Taylor and Stark, 2001, Cooper, 2006). Hence, G2 phase is the third and final phase in interphase. It is the shortest stage during which a cell prepares for

M phase, accumulating proteins and arranging structures required for mitotic progression, as well as including the G2/M checkpoint.

M phase (mitosis) is the last event in the cell cycle which culminates in the production of two daughter cells; during mitosis, the chromosomes duplicated in S phase are separated in identical sets into the two daughter nuclei. Mitosis is generally subdivided into several phases (Lodish, 2004, Alberts, 2008), summarised in Figure 3. During prophase, chromatin condenses to form the chromosomes (highly ordered structures of DNA), composed of two sister chromatids generated from the duplication of DNA during S phase, which are bound together at the level of the centromere; in addition, the already replicated centrosomes start their migration to the opposite sides of the nucleus, nucleating the microtubules necessary for the formation of the mitotic spindle. Prometaphase follows, which is characterised by the disassembling of the nuclear envelope and the formation of the kinetochore, a multiprotein complex formed at the level of the centromere. These events permit the connection of specific microtubules (kinetochore microtubules) with the chromosomes, whereas the opposite ends of these microtubules are associated with a centrosome. In the meantime, non-kinetochore microtubules interact with corresponding non-kinetochore microtubules from the opposite centrosome to form the mitotic spindle. During metaphase, chromosomes migrate and align to the metaphase plate (or equatorial plane) equidistant from the two centrosomes poles. Following these events, a cell proceeds to anaphase: sister chromatids are separated (early anaphase), cleaving the proteins that bind them together, and the so formed sister chromosomes are pulled apart by the shortening of the microtubules to which they are attached, and move toward their respective centrosome; meanwhile, non-kinetochore microtubules elongate pushing apart the centrosomes (and therefore the chromosomes attached to them) to

the opposite poles of the cell (late anaphase). The last events take place during telophase: non-kinetochore microtubules continue to elongate, corresponding sister chromosomes attach to opposite ends of the cell, and a new nuclear envelope forms around the set of separated sister chromatids, which can then unfold into chromatin.

To complete cell division, cytokinesis occurs to divide the nuclei, cytoplasm, organelles and cell membrane into two daughter cells genetically identical to each other and to their parent cell. It initiates in the late stages of mitosis (after the onset of anaphase), when deformations in the plasma membrane are created due to association with the contractile ring, a structure of actin and myosin II filaments attached to the cell cortex at the level of the mitotic spindle. The cleavage furrow is finally generated due to cell membrane ingression; its contractile action is responsible for the terminal division into the two daughter cells (Glotzer, 2005).

A fourth phase (G0) exists, which consists of a reversible quiescent state that a non-proliferative cell may enter after G1, if nutrients are not present in the environment. G0 cells are no more actively cycling, but they retain the potential to re-enter the cell cycle and to divide again under specific stimuli (Schafer, 1998).
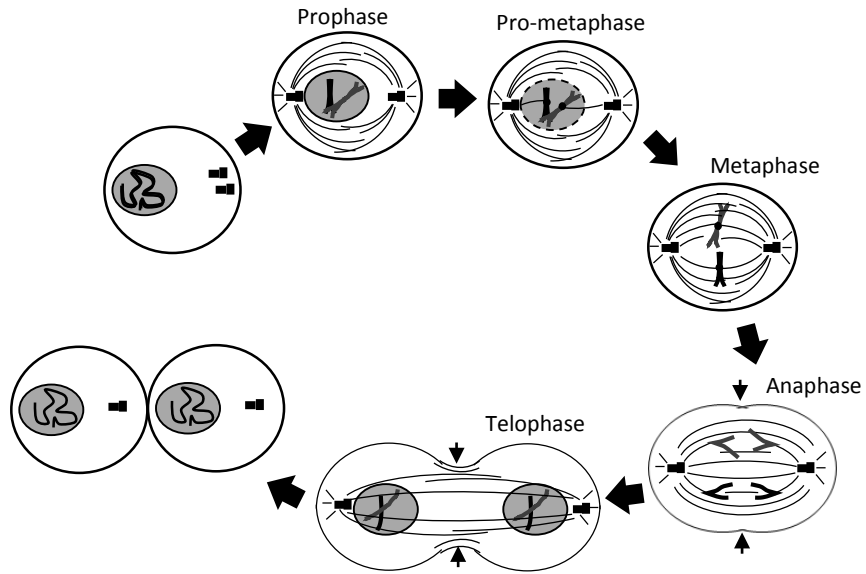
Figure 3. Diagram of the sequence of mitotic events.
DNA and centrosomes are duplicated during S phase. Mitosis starts with prophase, where the DNA condenses into chromosomes, the centrosomes migrate at the opposite sides of the nucleus and start to nucleate microtubules to form the mitotic spindle. The nuclear envelope is then disassembled and the kinetochore is formed, allowing kinetochore microtubules to interact with chromosomes. During metaphase chromosomes are aligned on the equatorial plane and in anaphase the sister chromatids are pulled apart and migrate towards opposite sides of the cell. The contractile ring is also assembled (indicated by arrows). During telophase, non-kinetochore microtubules continue to elongate, two nuclear envelopes are formed around the separated chromatids (which can now unfold) and the cleavage furrow (arrows) allows the separation into the two daughter cell.

1.1.2 Cell cycle regulation and cancer

Several regulatory proteins are present to form a control network in order to regulate the progression through the cell cycle. This system is made of an ordered series of actions which are responsible for the initiation of the main events of the cell cycle (Alberts, 2008). A central role in this network is played by CDKs, a family of serine/threonine protein kinases, which are progressively activated and inactivated to allow cell cycle progression and transition through the different phases (Ekholm and Reed, 2000, Sherr and Roberts, 2004). CDK activity is subjected to cyclical changes due to the interplay of different

Figure 4. Cyclin-CDK protein complex (Alberts, 2008). The main method of CDKs activation consists of their association with a specific cyclin.

regulatory mechanisms: association with specific activating subunits (cyclins - see further), phosphorylation by CDK-activating kinases (CAKs, (Kaldis, 1999)) and control exerted by CDK inhibitors (Cki, (Sherr and Roberts, 1995)). The main type of regulation of these enzymes consists of the association of the inactive catalytic subunit (the CDK) with its specific cyclin, a positive regulatory subunit which provides the substrate specificity, forming the cyclin-CDK complex (Figure 4).

CDKs are constitutively expressed during the cell cycle, whereas cyclins show periodical expression, undergoing cycles of synthesis and degradation; as a consequence, progression through each phase of the cell cycle is permitted by the expression of a specific class of cyclins which associate with the catalytic subunit (Table 1; (Morgan, 1997)). CDK1 and CDK2 play a central role in cell cycle regulation (Morgan, 1997, Arellano and Moreno, 1997). CDK2 associated with cyclin E triggers the transition from G1 to S phase, being for example responsible for the assembly of the pre-replication complexes at the DNA replication origins (Malumbres and Barbacid, 2005); subsequent binding with

25

cyclin A allows completion of S phase in order to progress to G2 phase. Transition from S to G2 is achieved by association of cyclin A with CDK1, which subsequently binds to cyclin B to regulate G2/M transition as well as mitotic progression (Malumbres and Barbacid, 2005, Nigg, 2001).

Table 1. Major cyclin dependent kinases (CDKs) and their associated cyclins involved in the progression of the mammalian cell cycle.

CDK	Associated cyclin	Cell-cycle phase of action
CDK4	Cyclin D	G1
CDK6	Cyclin D	G1
CDK2	Cyclin E	G1/S transition
	Cyclin A	S, early G2
CDK1 (or CDC2)	Cyclin A	G2
	Cyclin B	M

Since the cell cycle is a vital process, every step must be tightly controlled; beside the tight regulation of CDKs, many different checkpoints are active during cell cycle progression to guarantee the initiation of the subsequent phase only after the completion of the previous one, and to allow DNA repair if necessary (Cooper, 2006, Nurse, 1997). Such checkpoints comprise the restriction point in late G1, the G2/M checkpoint, and the metaphase-to-anaphase transition (spindle-assembly checkpoint, SAC (Foley and Kapoor, 2013)). The progression through each of these checkpoints is blocked if the control system detects either endogenous or exogenous problems (Alberts, 2008). However, mutations occurring in genes involved in these types of controls are responsible for the establishment of cancer (Hanahan and Weinberg, 2011). In fact, many proteins involved in cell cycle regulation have been found mutated in different types of tumours. For example, mutations in particular receptors for mitogens are responsible for signal-independent growth, which then leads to uncontrolled cell proliferation, a characteristic of malignant tumours (Hanahan and Weinberg, 2011).

1.1.3 Anti-cancer strategies to target mitosis

Several anticancer strategies to target tumour proliferation have been developed in order to disrupt the progression of the cell cycle in tumour cells. These agents can affect different stages of the cell cycle, targeting for example: mitogenic pathways such as receptor tyrosine kinases (RTKs) like EGFR (gefitinib); DNA replication (antifolates and fluoropyrimidines); cyclin-dependent kinases (CDKs inhibitors); and microtubules (taxanes and vinca alkaloids) (Espinosa et al., 2003, Manchado et al., 2012).

The work discussed in this thesis was focused on the effects of anti-mitotic drugs which act on the progression of mitosis. In this phase of the cell cycle, the bipolar spindle plays a central role in maintaining genomic stability, allowing the accurate separation of the sister chromatids at the two opposite poles of the cell, which will then generate the two daughter cells. Microtubules are the building blocks of the mitotic spindle, and components of the cytoskeleton taking part in the maintenance of the cell structure and shape (Desai and Mitchison, 1997). They consist of hollow polymers composed of α- and β-tubulin dimers (Figure 5A). These units are firstly assembled head-to-tail to produce protofilaments, which are subsequently associated in parallel to create a single microtubule (Desai and Mitchison, 1997, Wade, 2009). Microtubules are characterised by an intrinsic polarity, established by the specific interaction of the αβ tubulin dimers: they interact end-to-end, with the α-subunit of a dimer establishing contact with the β-subunit of the next dimer (Desai and Mitchison, 1997, Wade, 2009). Given that bundling of the protofilaments occurrs in a parallel fashion, there is an extremity of the microtubules exposing exclusively β-subunits (referred as plus-end), with the opposite end showing only α-subunits (minus-end) (Desai and Mitchison, 1997, Wade, 2009). Of important note is the intrinsic dynamic instability which reflects the concomitant assembly and

disassembly of microtubules at the plus-end (Desai and Mitchison, 1997). This phenomenon is dependent on the hydrolysis of GTP to GDP by the β-subunit, and is necessary for normal cell functions (Figure 5B).
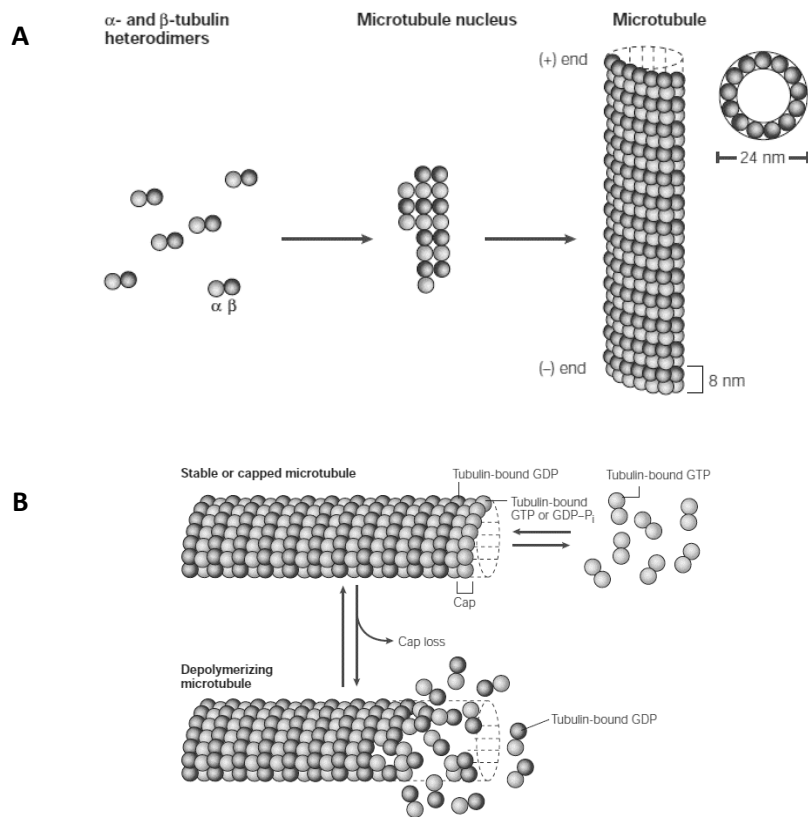
Figure 5. Microtubules structure and polymerisation/depolymerisation dynamics (Jordan and Wilson, 2004).
A) To form a microtubule, α and β tubulin subunits assemble head-to-tail to produce protofilaments (the microtubule nucleus), which are subsequently associated in parallel. This process of nucleation is followed by elongation at both ends. The final product is a cylinder composed of 13 protofilaments. Due to the specific assembly of α and β tubulin, each microtubule has a plus (+) end, exposing exclusively β tubulin, and a minus (-) end, exposing α tubulin. B) The intrinsic dynamic instability of microtubules is required for normal cell functions. It is achieved via the hydrolysis of GTP to GDP by the β subunit. When GTP or GDP+phosphate (P_i) is bound to the microtubule end, it forms a cap that stabilises the microtubule. The release of the phosphate destabilises the microtubule polymer causing catastrophes and, therefore, shortening of the microtubule.

To form the mitotic spindle, microtubules are nucleated by centrosomes, the major microtubule organising centre (MTOC; (Wade, 2009)). Specifically, the centrosome is a non-membranous organelle localised in the cytoplasm at the periphery of the nucleus in eukaryotic cells and is composed of two centrioles embedded in pericentriolar material (PCM; Figure 6A) (Fukasawa, 2002). PCM contains proteins responsible for microtubule nucleation and anchoring, such as γ tubulin. In late G1/early S phase, the centrosome is

duplicated (Figure 6B) in order to obtain two mature centrosomes by the end of late G2 phase, which could subsequently migrate to the opposite sides of the nucleus to generate the mitotic spindle (Fukasawa, 2005, Nigg and Stearns, 2011). At the onset of mitosis, cells must have exactly two centrosomes to grant the correct polarity of the mitotic spindle and avoid mitotic defects. The presence of supernumerary centrosomes will, in fact, produce genomic instability and possibly the onset of tumorigenesis (Fukasawa, 2005, Lingle et al., 2002). Indeed, centrosome hyper-amplification is implicated in chromosome instability in human tumours (Tarapore et al., 2001). Therefore, since the segregation of chromosomes into the two daughter cells during mitosis must be extremely accurate, centrosome duplication, as well as its numeral homeostasis, is strictly controlled and precisely coordinated with nuclear events taking place during the cell cycle (Fukasawa, 2005).
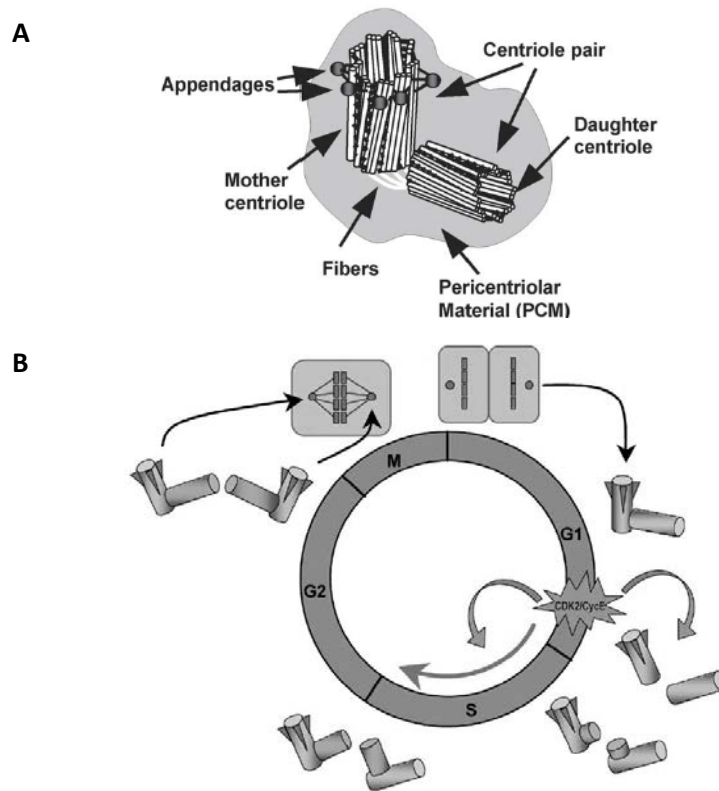
Figure 6. Centrosome structure and duplication (Fukasawa, 2005).
A) The centrosome consists of a pair of centrioles connected by fibres and surrounding proteins (the pericentriolar material, PCM). Of the two centrioles, the one defined as the daughter centriole is derived from the previous duplication of the centrosome. B) Schematic representation of the centrosome cycle. Centrosome replication is triggered by CDK2/cyclin E and is coupled with the initiation of DNA duplication during late G1. New procentrioles form at the proximal end of each pre-existing centriole and elongate during S and G2 phases. Simultaneously, components of PCM are recruited by the two maturing centrosomes. In late G2, appendages (represented by wedges) are added to the daughter centriole of the parental pair, thus generating two identical centrosomes, which form the spindle poles and direct the formation of the bipolar spindle during mitosis. When cell division is completed, each daughter cell will inherit one centrosome.

Different strategies can be employed to perturb the progression through mitosis (Figure 7; (Janssen and Medema, 2011, Manchado et al., 2012, Wood et al., 2001)). The use of microtubule poisons such as taxanes (paclitaxel and docetaxel) to disrupt microtubule dynamics, and therefore preventing the formation of a functional mitotic spindle, proved to be an effective therapy in the clinic (Jordan and Wilson, 2004, Contractor et al., 2011, Rowinsky and Donehower, 1995, Belotti et al., 1996, Calderoni and Cerny, 2001). However, microtubules-targeting drugs cannot distinguish between normal and tumour cells, thus acting on cell proliferation and microtubule dynamics in general, causing severe side-effects such as myelosuppression and neurotoxicity (Janssen and Medema, 2011,

Wood et al., 2001, Rowinsky et al., 1989). Furthermore, drug resistance is often developed by patients treated with these agents (Jordan and Wilson, 2004, Goncalves et al., 2001, Kavallaris et al., 1997, Orr et al., 2003, Dumontet and Sikic, 1999, Giannakakou et al., 1997).

These limitations have led to the development of agents which can disrupt mitosis more specifically, targeting tubulin-associated proteins or proteins involved in the formation of the mitotic spindle and completion of mitosis (Wood et al., 2001, Warner et al., 2006). Mitotic kinases such as Aurora kinases A and B and Polo-like kinase 1 (PLK1) have been identified as possible therapeutic targets (Warner et al., 2006).

Polo-like kinase 1 (PLK1) is a serine/threonine protein kinase which plays an essential role during mitosis, being involved in centrosome disengagement, i.e. separation of the paired centrioles (Nigg and Stearns, 2011, Tsou et al., 2009, Lane and Nigg, 1996, Sumara et al., 2004), as well as DNA damage response, spindle assembly, entry into mitosis and chromosome separation (Lens et al., 2010, Maire et al., 2013, Strebhardt and Ullrich, 2006, Petronczki et al., 2008).

In addition to PLK1, Aurora A and Aurora B are serine/threonine protein kinases involved in the correct progression of mitosis. Specifically, Aurora A plays a crucial role in the formation of the mitotic spindle, being associated with the duplicated centrosome and regulating its function (Andrews, 2005, Barr and Gergely, 2007, Marumoto et al., 2003, Dutertre et al., 2002, Giet et al., 2002). In contrast, Aurora B is localised at the centromere during mitosis, and then found in the midbody, a bundle of microtubules generated from the mitotic spindle at the end of anaphase (Mullins and McIntosh, 1982), during cytokinesis (Meraldi et al., 2004, Andrews, 2005, Welburn et al., 2010, Carmena and Earnshaw, 2003); it is responsible for the correct attachment of the kinetochores to

microtubules nucleating from opposite spindle poles, for the segregation of chromosomes, being defined as "chromosome passenger", and it also ensures timely cytokinesis (Andrews, 2005, Welburn et al., 2010, Lampson and Cheeseman, 2011, Ditchfield et al., 2003, Murata-Hori and Wang, 2002).

The described mitotic proteins have been found to be overexpressed in various tumour types (Janssen and Medema, 2011, Maire et al., 2013, Cammareri et al., 2010, Lok et al., 2010, Strebhardt and Ullrich, 2006, Bischoff et al., 1998, Tatsuka et al., 1998, Katayama et al., 2003). Hence, specific inhibitors to block their unique functions have been developed. Inhibition of PLK1 or Aurora A causes the formation of a monopolar spindle, resulting from the inhibition of their roles in centrosome replication and separation (Janssen and Medema, 2011, Manchado et al., 2012, Lenart et al., 2007, Gorgun et al., 2010, Hoar et al., 2007). Specific inhibition of Aurora B induces tetraploidy due to cytokinesis disruption, which results in the formation of a cell containing 4N DNA, therefore triggering efficient apoptosis (Xie et al., 2013, Hauf et al., 2003, Wilkinson et al., 2007). A clear advantage in the inhibition of Aurora B kinase is the observation that deprivation of Aurora B activity seems to have no conspicuous effects on non-proliferative cells, therefore suggesting Aurora B as a proliferation-specific target (Janssen and Medema, 2011, Manchado et al., 2012, Ditchfield et al., 2003, Stolz et al., 2009).

Inhibition of these mitotic targets causes genomic instability and therefore could lead to a delay in mitotic progression, possibly resulting in apoptotic cell death (Janssen and Medema, 2011, Manchado et al., 2012); however, there is the possibility of mitotic slippage, consisting of the ability to surmount the mitotic checkpoint and generating tetraploid cells (Figure 7). If cell-cycle checkpoints are functional, these cells can

eventually execute apoptosis, although they could also proliferate as polyploid cells (Manchado et al., 2012).
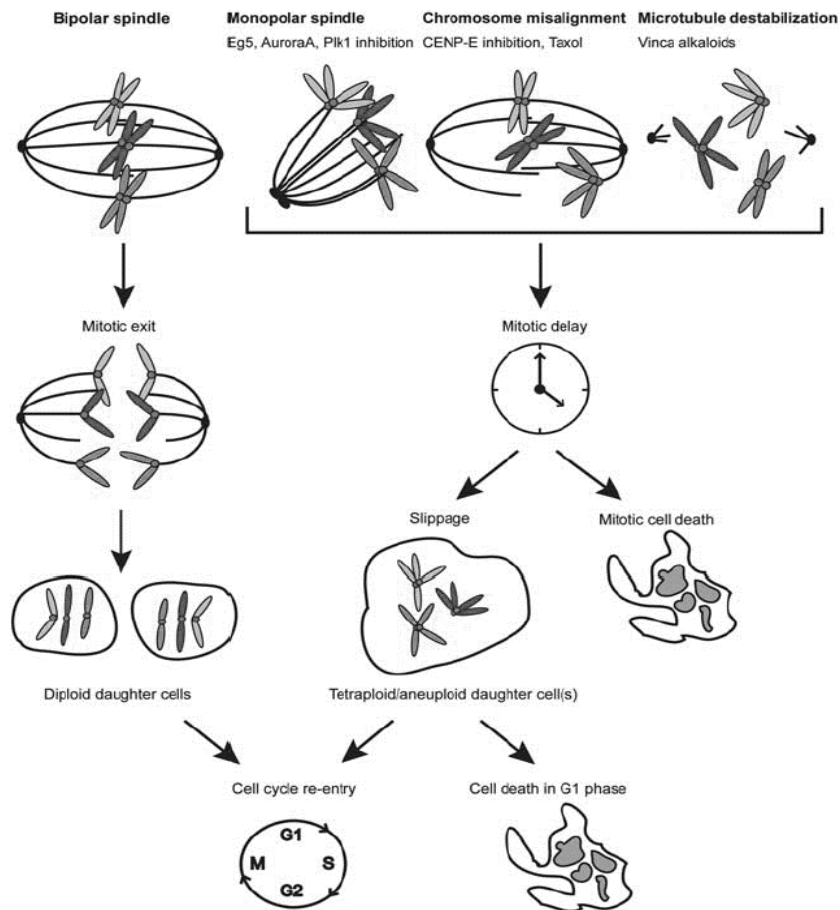
Figure 7. Schematic representation of anti-cancer strategies to induce mitotic delay (Janssen and Medema, 2011). Different phenotypes are generated by treatment with anti-mitotic drugs. As an example, Aurora A and PLK1 inhibition leads to the formation of a monopolar spindle, whereas treatment with microtubule stabilising or destabilising drugs results in aberrant spindle formation and/or incorrect attachment of the chromosomes to the spindle. In each case, the effect will be prolonged mitotic delay, which can be followed by cell death or mitotic slippage. If a cell is able to exit mitosis under these conditions (mitotic slippage), the progeny will be tetraploid. The daughter cells generated can subsequently incur into apoptosis or further progress along the cell cycle to produce aneuploid progeny.

In addition to the mitotic kinases described above, kinesin motor proteins also play a central role during mitotic events, participating in the assembly of the spindle and in chromosomes movements along the microtubules (Manchado et al., 2012). The kinesin protein KIFC1 (kinesin family member C1, also known as HSET) has started to attract attention, demonstrating to be an extremely interesting therapeutic target for cancer

therapy (Mountain et al., 1999). KIFC1 is a minus-end directed kinesin, which belongs to the non-claret disjunctional (NCD) family (Mountain et al., 1999). This family is important for the integrity of the mitotic spindle due to their action in focusing the minus-ends of microtubules (Matthies et al., 1996, Walczak and Mitchison, 1996, Mountain et al., 1999). However, KIFC1 seems to be dispensable for cell cycle progression of normal cells, but plays an important role in clustering multiple centrosomes to prevent the formation of multiple spindle poles in cells containing supernumerary centrosomes (Figure 8; (Kwon et al., 2008, Gergely and Basto, 2008)). Several cancer cells contain supernumerary centrosomes (Janssen and Medema, 2011, Tarapore and Fukasawa, 2002, Fukasawa, 2005), therefore being able to selectively kill these cells by inhibiting KIFC1 activity could be extremely valuable in terms of anti-cancer therapy. In addition, multiple centrosomes are associated with many other tumour phenotypes, e.g. p53 loss (Tarapore and Fukasawa, 2002, Carroll et al., 1999, Ouyang et al., 2001), BRCA mutations (Xu et al., 1999), Aurora overexpression (Zhou et al., 1998, Meraldi et al., 2002, Hontz et al., 2007), DNA damage (Loffler et al., 2013). Consequently, identifying patients most likely to respond to drugs targeting mitosis is equally important.
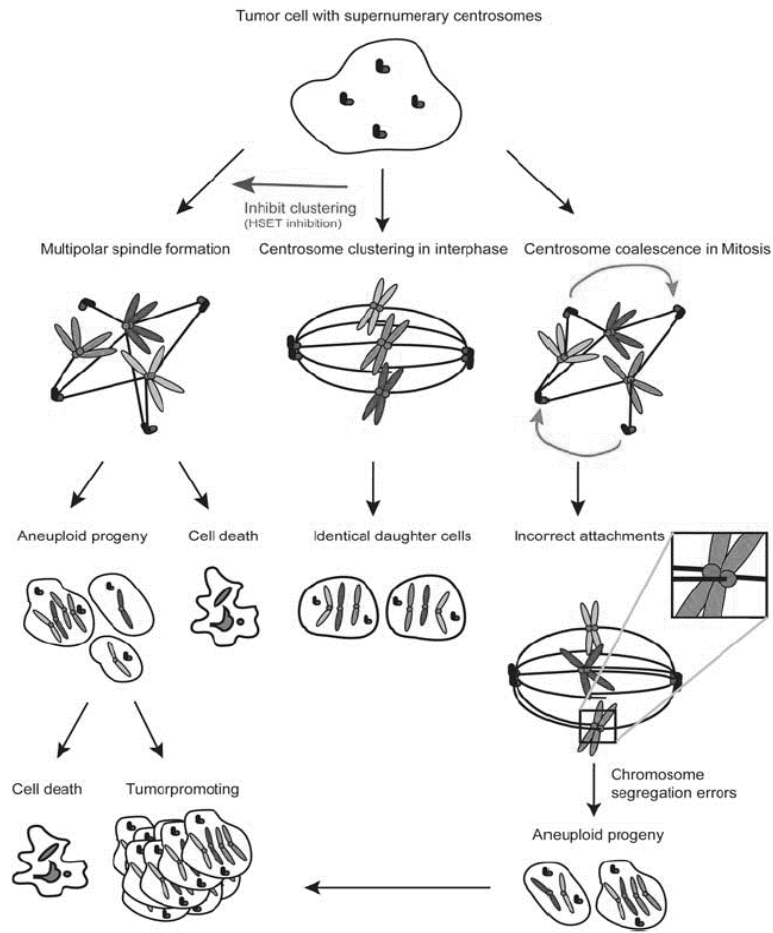
Figure 8. Schematic representation of the effects caused by supernumerary centrosomes (Janssen and Medema, 2011).

The presence of multiple centrosomes can promote the formation of multipolar spindles, which could lead to cell death or generate aneuploidy in daughter cells. The progeny can subsequently undergo cell death due to genomic instability or escape cell death and promote tumorigenesis (left panel). Tumour cells containing supernumerary centrosomes evolved mechanisms to cluster multiple centrosomes in order to produce a normal bipolar spindle. Cells can either cluster centrosomes during interphase to progress normally through mitosis (middle panel) or initially form a multipolar spindle which is subsequently converted into a bipolar spindle by clustering centrosomes following chromosome attachment to the spindle (right panel, centrosome coalescence). However, centrosome coalescence cannot resolve incorrect attachments of the chromosomes to the spindle, causing therefore mis-segregation events which lead to aneuploidy in the daughter cells. In turn, the progeny could promote tumour growth. If centrosome clustering is inhibited (e.g. KIFC1/HSET inhibition), this condition could enhance the formation of multipolar spindles, thus increasing tumour death.

1.2   The salvage pathway for DNA synthesis

The replication of nuclear DNA is the key process required for cell division. It must be tightly controlled to make sure that the genome is duplicated only once, without errors, and in a timely fashion (Takeda and Dutta, 2005). Initiation of DNA synthesis occurs at the end of G1 phase, and therefore transcription of proteins required for DNA replication is promoted at the G1/S transition (see paragraph 1.1.2). At this stage, nucleotides of the four bases (adenine, guanine, cytosine and thymine), the DNA precursors, must be available to be incorporated into the growing filament. Since thymidine is the only nucleoside exclusively incorporated into DNA, and not into RNA, it has been used to image cell proliferation with positron emission tomography (PET; see section 1.3) (Bading and Shields, 2008). For this reason, the pathways for thymidine production will be discussed in the following sections.

1.2.1   The production of dTTP through the salvage pathway

Thymidine nucleotides are supplied via two different routes (Figure 9), both of which are tightly regulated. Through the *de novo* (or endogenous) pathway for DNA synthesis, deoxyuridine monophosphate (dUMP) is methylated by thymidylate synthase (TS) to produce thymidine monophosphate (dTMP) (Bading and Shields, 2008, Krohn et al., 2001). Thymidine can also be recycled through the salvage (or exogenous) pathway, through which exogenous thymidine (TdR) is rapidly transported into the cell by facilitated nucleoside transporters (Hu and Chang, 2007, Krohn et al., 2001), and is immediately phosphorylated by thymidine kinase 1 (TK1) (Bading and Shields, 2008). Specifically, TK1 catalyses the transfer of the terminal phosphate of ATP to the 5'-hydroxyl group of thymidine, thus forming thymidylate (thymidine monophosphate, dTMP). Once

thymidine has been converted into dTMP, it is subsequently phosphorylated to thymidine diphosphate (dTDP) by thymidylate kinase (TMPK), and in turn to thymidine triphosphate (dTTP) by nucleotide diphosphate kinase (NDPK). There is continuous interconversion between the different phosphorylated forms of thymidine, which means that the phosphotranferase reactions catalysed by TMPK and NDPK are reversible. In contrast, the reaction catalysed by TK is considered almost irreversible (Hu and Chang, 2007), thus trapping TdR into the cell.

The role of the salvage pathway is to balance intracellular nucleotide pools needed for DNA replication (Grierson et al., 2004). DNA replication requires the supply of nucleosides which are imported and phosphorylated to ensure the correct amount of nucleotide triphosphates within a cell (Grierson et al., 2004). Therefore, the production of dTTP in a cell must be strictly regulated and coordinated with the replication of the DNA during the cell cycle; in particular, the amount of dTTP pool increases greatly in S phase compared to G0/G1 phase (Hu and Chang, 2007), and this oscillation results from the cell cycle-dependent regulation of enzymes involved in the salvage or *de novo* pathway (Hu and Chang, 2007).

Thymidine is also subjected to reversible degradation via cleavage of the base from the sugar moiety by thymidine phosphorylase (TP). Specifically, TP catalyses the catabolism of dTMP to produce thymine and 2-deoxyribose-1-phosphate, which can be rapidly dephosphorylated (de Bruin et al., 2003).
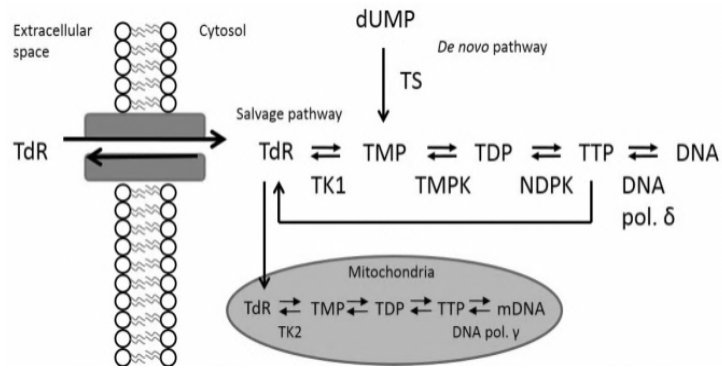
Figure 9. Salvage and *de novo* pathways for thymidylate supply.
In the salvage pathway, thymidine (TdR) is transported into the cell via facilitated diffusion. It is then phosphorylated by TK1 to produce thymidylate (TMP), which is subjected to further phosphorylation carried out by TMPK and NDPK to finally obtain thymidine triphosphate (TTP) which is incorporated into the DNA by the DNA polymerase. Thymidine can also be a substrate for TK2 in the mitochondria during the mitochondrial DNA replication. In the *de novo* pathway, thymidylate synthase (TS) converts uracil monophosphate (dUMP) to TMP via methylation.

1.2.2 Thymidine Kinase 1 (TK1) and its regulation

Thymidine kinase 1 gene is located on chromosome 17 in humans (Arner and Eriksson, 1995). It encodes for TK1 protein, responsible for the phosphorylation of thymidine to produce dTMP (Munch-Petersen et al., 1991, Bading and Shields, 2008), through the transfer of a phosphate from ATP to the 5' position of the deoxyribose of thymidine. It follows Michaelis-Menten kinetics (Arner and Eriksson, 1995).

TK1 is the most restrictive enzyme in the salvage pathway, accepting only thymine or uracil as base substrates, also with minor substitutions at the 5' or 3' positions of the sugar (Arner and Eriksson, 1995). TK1 is present in proliferating cells, being highly expressed and active in cells in S-phase (see further), and it is also widely expressed in all malignant tissues (Munch-Petersen et al., 1991, Arner and Eriksson, 1995), whereas, its activity is usually absent in quiescent cells and barely detectable in cells in the G1 phase.

In actively proliferating cells, TK1 protein concentration is low in the G1 phase, then greatly increases (10- to 20-fold) at the G1/S transition, is maintained at high levels throughout S, G2, and M, where it reaches maximum levels (Arner and Eriksson, 1995, Chang et al., 1994), before it rapidly decreases at cytokinesis; the enzyme is subsequently degraded at the onset of G1 or G0 (Sherley and Kelly, 1988, Kauffman and Kelly, 1991, Chang et al., 1994, Arner and Eriksson, 1995). Remarkably, TK1 mRNA expression changes only modestly through the cell cycle (Sherley and Kelly, 1988).

In addition to protein concentration, TK1 activity oscillates during the progression of the cell cycle, varying according to the growth state and cell cycle phase of mammalian cells. Enzyme activity is closely correlated with S phase (Arner and Eriksson, 1995, Kauffman and Kelly, 1991, Hu and Chang, 2007), and is clearly related to the level of the protein itself (Sherley and Kelly, 1988).

To achieve the oscillation in TK1 activity, several regulatory mechanisms are active at different levels: transcriptional, post-transcriptional, translational, and post-translational (Hu and Chang, 2007). Also allosteric feedback takes part in this process (Wells et al., 2004).

Tight regulation occurs at the level of the TK1 gene: in response to growth stimulation, it is transcriptionally activated during S phase (Arner and Eriksson, 1995). This induction is due to the presence of E2F (E2 transcription Factor) binding sites in a small region of the promoter (Tommasi and Pfeifer, 1997). E2Fs are a protein family of transcription factors, whose members bind to specific DNA sequences present in the promoter of several genes encoding for proteins required for S phase entry and involved in DNA synthesis (Alberts, 2008, Tommasi and Pfeifer, 1997). E2F is therefore responsible for the induction of specific genes at the G1/S transition (Tommasi and Pfeifer, 1997). If mitogens are not present in the environment, the expression of these genes is prevented by the interaction between E2F and members of the retinoblastoma protein (Rb) family; however, when mitogen stimulation occurs (i.e. mitogens interact with their specific receptors, which in turn initiate the signal cascade inside the cell), G1-CDKs are activated and phosphorylate Rb, which is therefore no more able to bind to E2F, thus releasing this transcription factor, now able to interact with its specific recognition sequences (Figure 10). Rb is usually hyper-phosphorylated in proliferating cells, whereas the hypo-phosphorylated form is more abundant in quiescent cells (Harbour and Dean, 2000a). The Rb/E2F pathway therefore regulates the transition between G1 and S phase (Harbour and Dean, 2000b).
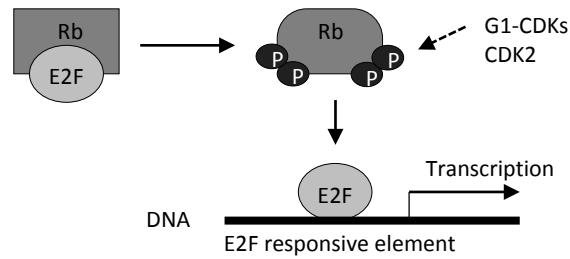
Figure 10. Schematic representation of the Rb-E2F interaction.
The transcription factor E2F is initially sequestered by the Retinoblastoma protein (Rb). When the cell is committed to enter the cell cycle, Rb is hyperphosphorylated by G1-CDKs and subsequently its phosphorylation is maintained by CDK2. This modification allows the release of E2F which is therefore able to interact with responsive elements present in the promoter of genes coding for proteins required for cell cycle progression, such as TK1.

The increase in TK1 protein expression during S phase, however, is not linked to a proportional increase of the mRNA, but the efficiency of translation of the mRNA determines the accumulation of the protein (Sherley and Kelly, 1988, Coppock and Pardee, 1987). In fact, RNA stability increases as cells approach S phase, and, in addition, translation becomes more efficient, contributing to the increase in TK1 activity at the beginning and throughout S phase (Schlosser et al., 1981, Hu and Chang, 2007, Coppock and Pardee, 1987). Although the regulation of TK1 mRNA translation is fully acknowledged, no demonstrations of the mechanism by which TK1 mRNA is regulated has been reported to date. E2F induces transcription of the gene, but the mRNA level does not drastically change when the cell enters S phase, suggesting that the mRNA might be rapidly degraded before being stabilised by a specific, not yet identified mechanism at the onset of DNA replication.

In addition, at the G1/S border TK1 activity increases also due to the formation of the tetrameric form of the protein with ATP. ATP is a cofactor which contributes to TK1 activity (Munch-Petersen et al., 1995, Barthel et al., 2005, Munch-Petersen et al., 1993) by affecting the enzyme size. In fact, the ATP pool is required to stabilize the tetramer (with a mass of 96-110 kDa, each subunit being 24 kDa; (Arner and Eriksson, 1995)).

Moreover, TK1 polypeptide concentration affects the formation of the quaternary structure of the protein. Munch-Petersen *et al.* reported a concentration-dependent mechanism in the formation of the tetrameric form of TK1 (Munch-Petersen, 2009, Munch-Petersen et al., 1993). At the onset of a new G1 phase, TK1 protein is absent following specific degradation during mitosis (see further), but the concentration starts to increase due to transcriptional regulation, resulting in a progressive accumulation of the protein in the dimeric form. As the cell progresses to G1/S, more TK1 protein is available and therefore more tetramers are formed, until TK1 concentration peak is reached and all TK1 is assembled into tetramers with higher affinity for the substrate (Munch-Petersen, 2010, Munch-Petersen, 2009, Munch-Petersen et al., 1993). Therefore, in the presence of ATP, TK1 concentration induces a more stable form of the protein, which has also higher affinity for its substrate (Arner and Eriksson, 1995, Munch-Petersen et al., 1995, Barthel et al., 2005).

Further regulation of TK1 enzymatic activity is achieved at the post-translational level via cell cycle-dependent phosphorylation (Arner and Eriksson, 1995). Chang and co-workers reported phosphorylation of serine-13 (Ser13) as the event that is responsible for strongly decreasing TK1 affinity to bind thymidine and therefore turning off enzymatic activity (Chang et al., 1998, Li et al., 2004). Evidence from a series of experiments (Hu and Chang, 2007) suggests that during S phase TK1 is present in the tetrameric form with the highest catalytic efficiency (in accordance with the formation of the tetramer following increased protein concentrations and the binding of ATP as previously discussed), whereas in G2/M phase its catalytic capability is reduced due to being in the dimeric form, acquired after phosphorylation of Ser13. This amino-acid residue was reported to be specifically phosphorylated during mitosis in HeLa and transfected mouse fibroblasts lacking

endogenous TK1 (Chang et al., 1998); moreover, phosphorylation of Ser13 appeared to be responsible for marking TK1 for degradation in a yeast system (Ke et al., 2003). However, subsequent studies in mammalian cells suggested that phosphorylation of Ser13 is not a necessary signal for mitotic degradation of TK1 (Ke and Chang, 2004). Other amino-acid residues on TK1 protein sequence, e.g. serine-30, serine-194 and serine-231, were suggested as phosphorylation sites (Chang et al., 1998), but no demonstration of their involvement in TK1 regulation has yet been provided.

In addition to these mechanisms, the intracellular concentration of thymidine also affects mitotic degradation of TK1 (Hu and Chang, 2007, Ke et al., 2007). In fact, it has been demonstrated that thymidine binding to TK1 in the tetrameric form changes the enzyme conformation so that it cannot expose the C-terminal sequence responsible for its degradation (Ke et al., 2007); however, after S phase, when thymidine is consumed during DNA replication, TK1 is found in the dimeric form which has low affinity for thymidine, and therefore this conformation allows mitotic degradation (Hu and Chang, 2007). Moreover, the thymidine triphosphate (dTTP) pool can act as a negative feedback to regulate the activity of TK1 if the dTTP concentration increases (Munch-Petersen et al., 1995, Welin et al., 2004, Carnrot et al., 2003, Lee and Cheng, 1976). This regulation has important implications when measuring the incorporation of TdR analogues by tumours treated with antineoplastic drugs, since these compounds that act by inhibiting dTTP incorporation into DNA cause an increase in the dTTP pool so decreasing TK1 activity and consequently decreasing the trapping of the labelled tracer. In contrast, inhibition of thymidylate synthase (*de novo* pathway) will deplete the dTTP pool so increasing TK1 activity and consequently analogue trapping (Bading and Shields, 2008).

Finally, at the end of mitosis (late M phase), TK1 protein is rapidly degraded when post-translational modifications occur at its carboxy-terminal (C-terminal), providing the degradation signal (Ke and Chang, 2004, Hu and Chang, 2007). This mechanism of mitotic degradation ensures that TK1 function is terminated irreversibly and allows considerable reduction of TK1 protein levels in the G1 phase of the subsequent cell cycle of the daughter cells (Hu and Chang, 2007). Furthermore, TK1 proteolysis keeps the right concentration of dTTP in the G1 phase, thus maintaining genomic stability (Hu and Chang, 2007).

To summarise, under normal conditions TK1 exists as a tetramer until late G2/M, when TK1 affinity for its substrate is reduced due to post-translational modifications (Chang et al., 1994, Chang and Huang, 1993, Chang et al., 1998, He et al., 1996, Li et al., 2004), despite high protein levels: replication of DNA is complete, and, as a result, the formation of dTTP is no longer needed. Figure 11 represents TK1 transcriptional and post-translational regulation.
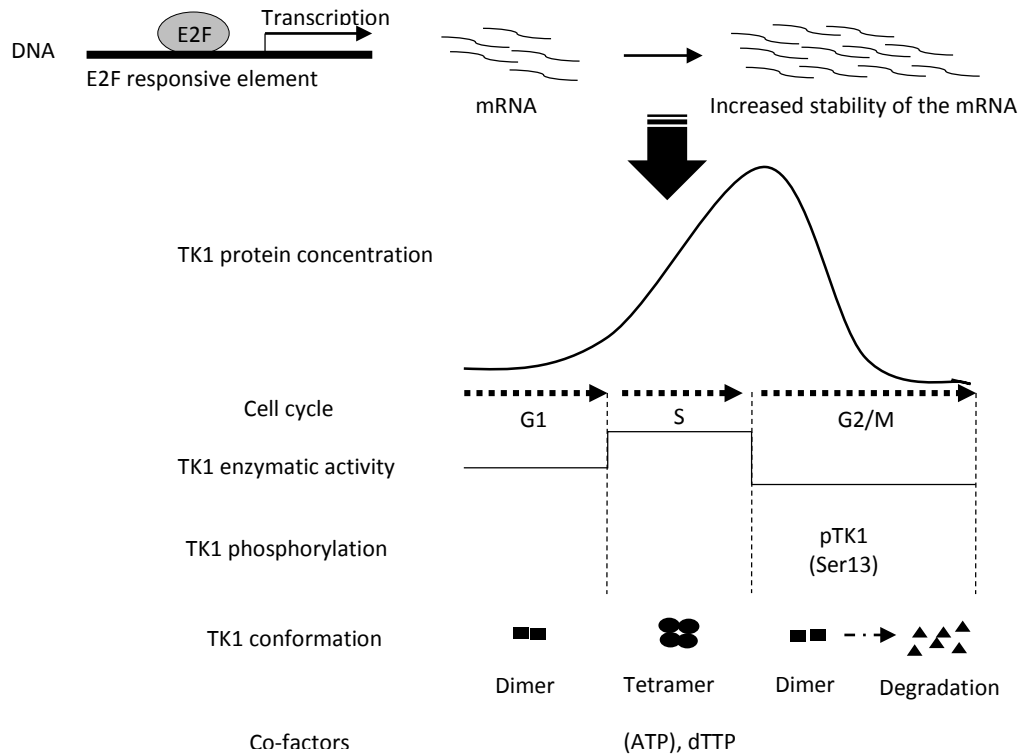
Figure 11. Regulation of thymidine kinase 1 (TK1).
The TK1 gene contains E2F recognition sequences in its promoter. When E2F binds, transcription is induced. After stabilisation of the mRNA, TK1 protein starts to accumulate. TK1 polypeptide is virtually absent in G1, it rapidly increases at the G1/S transition and reaches maximum levels during G2/M. Post-translational modifications of the protein are responsible for the oscillation of TK1 activity, which is low in G1, high in S and low during G2/M. This fluctuation is dependent on the quaternary structure. TK1 is initially assembled in homodimers; when the protein concentration increases, the formation of the tetramer contributes to TK1 increased activity during S phase, together with the binding of ATP and dTTP. At the end of S phase, TK1 enzymatic activity is no longer needed and therefore it is reduced by the formation of the dimer. Chang *et al.* proposed the phosphorylation of Ser13 as the event which triggers the formation of the dimer at the end of DNA replication.

1.2.3 TK1 and TK2

Genomic DNA is synthesized in the cytosol, but DNA synthesis occurs also in mitochondria. Two isoenzymes of thymidine kinase catalyse the reaction in the cytosol (TK1) and in the mitochondria (TK2) of mammalian cells (Hu and Chang, 2007). Expression of TK1 is S phase specific and tightly regulated together with other enzymes involved in DNA synthesis; on the contrary, TK2 is constitutively expressed and active throughout the cell cycle (Munch-Petersen et al., 1991, Arner and Eriksson, 1995, Hu and Chang, 2007, Bading and Shields, 2008). The TK2 gene is located on chromosome 16 in human cells; the protein is a monomer of 29 kDa, responsible for the lower and constant level of TK activity in resting cells, being present in both resting and proliferating cells (Munch-Petersen et al., 1991). Resting cells contain only TK2 activity, since they lack TK1; therefore, when cells are not cycling, they show limited capacity to recycle deoxyribonucleosides through the salvage pathway (Munch-Petersen et al., 1991).

1.3   PET imaging of cell proliferation

Since uncontrolled cell proliferation is one of the primary hallmarks of cancer (Hanahan and Weinberg, 2011), it is a great advantage to be able to measure tumour cell proliferation using non-invasive imaging techniques, instead of multiple biopsy methods, in order to improve the diagnosis and the understanding of the progression of cancer, as well as assessing tumour response (Bading and Shields, 2008).

Common methods to detect and monitor tumours rely on X-ray, ultrasound, computed tomography (CT) and magnetic resonance imaging (MRI), which allow the detection of alterations in growth, reflected by tumour size; however, these changes can take weeks or months before they reveal the failure or success of a treatment. This fact prevents the quick modification of a therapy in case of non-response. To overcome these limits, functional imaging techniques such as PET could be used. Nonetheless, it has to be kept in mind that each of the techniques mentioned above presents both advantages and disadvantages, so there is no elected technique to be used, but all of them can give useful information, depending on the question that needs to be investigated (Glunde et al., 2007, Alford et al., 2009).

1.3.1   Positron emission tomography (PET)

Positron emission tomography (PET) is an analytical molecular imaging technique (Phelps, 2000) based on the detection of gamma rays emitted from a positron-emitting radioisotope (Wells et al., 2004). Radioisotopes are produced by a cyclotron, and immediately incorporated into a molecule of interest (for example a thymidine analogue). The radioactive probe is then injected intravenously in a subject, e.g., rodent or patient,

which is imaged by a PET scanner (Figure 12). The tracer emits a positron, which collides with an electron nearby, thus producing two gamma rays in opposite directions. The gamma rays are detected by scintillation detectors present in the scanner and the recorded signal is then modified in order to finally generate a three-dimensional reconstructed image, where it is possible to visualise regions of interest (ROIs), drawn on the anatomical structure obtained from a CT scan and aligned with the PET scan (Wells et al., 2004, Nguyen and Aboagye, 2010). Therefore, through the use of labelled molecules, it is possible to exploit PET to image and measure biochemical processes of mammalian biology *in vivo* (Phelps, 2000, Nguyen and Aboagye, 2010).
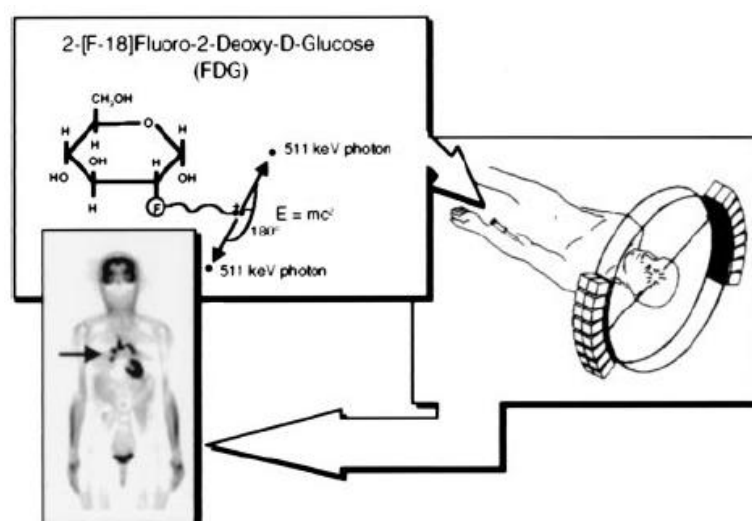
Figure 12. Principles of PET.
2-[18F]fluoro-2-deoxy-D-glucose (FDG) is a radiolabelled molecule for the detection of tumours with PET (Phelps, 2000). The radiotracer is injected intravenously into a subject who is then imaged within a dedicated scanner which records the signal emitted by the positron-emitting tracer. The image is then reconstructed to visualise the hot-spots where the radiotracer has accumulated.

Because PET can provide information about tumours *in vivo*, it has a great advantage compared to information obtained through tumour biopsies, since a single biopsy will not reflect the heterogeneity found in the tumour (Shields, 2006). In addition, PET imaging is

a powerful tool to monitor response to therapy at early stages of treatment (see section 1.3.2).

Radioisotopes used in PET imaging must be positron-emitters. Therefore radioisotopes such as ^{11}C and ^{18}F are employed to radiolabel molecules of interest (Aboagye and Price, 2003, Wells et al., 2004, Nguyen and Aboagye, 2010, Alford et al., 2009). If ^{11}C is the preferred choice to label a molecule (Carbon is found in all biological compounds), the main disadvantage resides in its short half-life (approx. 20 min), which requires extremely fast chemistry to incorporate it into the molecule of interest and inject it into the patient (Aboagye and Price, 2003, Nguyen and Aboagye, 2010). On the other hand, ^{18}F has a more practical half-life of 109 min, but it is not usually present in biological molecules. However, it is a small atom and can increase the metabolic stability of the biological compound in which it has been inserted (Alauddin, 2012).

1.3.2   Detection of cell proliferation and tumour response with PET

Tumour progression can be monitored by PET imaging; in particular, it is increasingly used in oncology for the diagnosis, staging and monitoring of tumour response to therapy (Shields et al., 1996a, Shields et al., 1998, Muzi et al., 2005b). By choosing appropriate tracers it is possible to provide images of specific metabolic pathways (Nguyen and Aboagye, 2010). Indeed, it is possible to image different aspects of tumour metabolism, according to the type of tracer used (Shields et al., 2005, Shields, 2006). For example, to image DNA synthesis and cell proliferation, thymidine analogues have been developed (Shields, 2006).

DNA synthesis, in fact, directly indicates cellular proliferation, which is increased in tumours relative to most non-tumour tissues (Shields et al., 1996a). Hence, it is possible to produce probes to assess cell proliferation by PET imaging. However, to develop a good imaging agent for this purpose, several criteria must be fulfilled (Shields et al., 1996a): 1) the probe should be readily taken up in proliferating cells and subsequently incorporated into DNA, or used in the pathway of DNA synthesis (for example it could bind to an enzyme directly involved in DNA synthesis); 2) it should produce a very low amount of metabolites, which could confound data interpretation; 3) it should be readily labelled for imaging (with a positron emitter). Another key feature for developing a probe is that it must reach the target and be retained at least for the time necessary to perform the scan, but it must not affect the biological process itself or be too toxic (Shields, 2006).

Since DNA synthesis, and therefore cell proliferation, can be measured using radiolabelled thymidine (TdR) or its analogues (Muzi et al., 2005b), in the field of oncology a lot of interest has concentrated on thymidine to develop a proliferation-specific marker of tumour treatment response (Wells et al., 2004). Thus, radiotracers for the thymidine salvage pathway have been developed. Firstly, thymidine is the only one of the four nucleotides to be incorporated exclusively into DNA, and not into RNA (Shields, 2006); since the precursor of thymidine obtained from the *de novo* pathway, e.g. uracil, is incorporated both into DNA and RNA, this pathway is not useful to monitor DNA synthesis (Bading and Shields, 2008).

TdR can enter the cell by facilitated diffusion, and is rapidly interconverted between TdR, dTMP, dTDP and dTTP ((Bading and Shields, 2008) – see section 1.2.1; Figure 9). During rapid growth and DNA synthesis, the activity of TK1 dramatically increases, which is directly related to the DNA synthesis rate ((Bading and Shields, 2008, Wells et al., 2004) –

see section 1.2.2). Although TdR is a substrate for both nuclear and mitochondrial DNA, cytosolic synthesis via TK1 dominates the use of TdR in S phase cells (Bading and Shields, 2008). Therefore, changes in thymidine uptake reflect changes in cellular growth (Krohn et al., 2001) and, by exploiting *in vivo* imaging, it is possible to observe tumour assimilation, which provides a picture of radiotracer incorporation per cell (Bading and Shields, 2008). In fact, the rate of DNA synthesis, which is the flux of nucleotides through the precursor pool, provides a quantitative measure of cell proliferation, since dividing cells must first replicate their DNA (Krohn et al., 2001). It depends on the proliferative status of the tissue, not on the concentration of precursors. The precursors pool is composed of nucleotides produced from both *de novo* and salvage pathway, and relative utilization of thymidine coming either from one or the other pathway depends on the level of extracellular TdR (Krohn et al., 2001). Cells could rely predominantly on the salvage pathway as long as enough thymidine will be present in the environment. When TdR level decreases, however, cells could enhance TdR production via the *de novo* pathway.

Additionally, cell proliferation imaging with PET can provide a measure of early therapeutic response (Muzi et al., 2005b, Nguyen and Aboagye, 2010), together with information about pharmacodynamics and pharmacokinetics of labelled drugs in tumours and normal tissues (Shields, 2006), thus allowing understanding of the mechanism of action and specific tissue localisation of a compound (Bading and Shields, 2008). The use of PET imaging, in fact, allows detection of functional and metabolic changes as well as quantification of cell proliferation in rapidly growing tumours in order to measure the effect of a treatment with specific drugs, for example against actively dividing cells (Rasey

et al., 2002, Leyton et al., 2005). Several probes have been developed for this purpose, most of them labelled with fluorine-18 (^{18}F; (Nguyen and Aboagye, 2010)).

Furthermore, with the availability of earlier information about the chemosensitivity of a patient and the failure or success of a therapy, oncologists should be able to design a specific treatment to which the patient's tumour is sensitive or modify treatment, thus eliminating possible ineffective treatment, preventing undue toxicity and reducing the costs, despite PET being an expensive imaging technique (Shields, 2006, Glunde et al., 2007, Alford et al., 2009).

Cell proliferation imaging with PET can also be useful in the development of new therapeutic agents. Drug development is a long and expensive process; clinical trials require a large number of patients before the approval of therapy, and most agents fail during the developing process. Therefore it will be more valuable to concentrate only on the most promising pharmaceuticals, instead of spending resources (time and money) on drugs which at the end reveal their therapeutic failure. In this perspective, the use of functional imaging techniques, such as PET, into early phase trials of targeted agents can provide insights on the mode of action, pharmacokinetics and pharmacodynamics of a new compound, measuring drug delivery to the specific target and therapeutic response (Shields, 2006, Gupta et al., 2002, Kelloff et al., 2005). Identification of patients who could benefit from the treatment can be carried out by means of verifying the presence of the specific biomarker via PET imaging. Subsequently, PET imaging can be used to assess target inhibition after administration of the specific agent, by following the effects on the biomarker of choice, which will provide information on the specificity for the alleged molecular target and tissue distribution. This process may therefore substitute pre- and post-treatment biopsies with non-invasive imaging techniques (Kummar et al., 2006).

1.4   Radiotracers to image cell proliferation with PET

Radiolabelled thymidine ([^{11}C-methyl]thymidine) was the first radiotracer to be developed to image cell proliferation (Christman et al., 1972, Shields et al., 1990), as it is a natural component of DNA (Figure 13), recycled via the salvage pathway, phosphorylated by TK1, and incorporated into DNA (Krohn et al., 2001, Shields, 2006). However, radioactivity was not accumulating exclusively into tumours due to the rapid catabolism of the radiotracer resulting in the production of several metabolites (Goethals et al., 1995). Synthesis of 2-[^{11}C]thymidine provided an improvement compared to [^{11}C-methyl]thymidine in terms of tumour accumulation and production of less metabolites (Vander Borght et al., 1994, Shields, 2006, Shields et al., 1996b, Eary et al., 1999), but the results still had to be corrected for thymidine metabolites in order to interpret the PET images correctly. Extensive development and validation of TdR for imaging cell proliferation with PET has been carried out in the 1990s, showing that radiolabelled thymidine was incorporated into DNA, but it was also metabolised into multiple side-products already at 2 minutes post-injection (Shields et al., 1990). Compartmental models and mathematical analysis were developed to take into account the generation of metabolites, and provide a better interpretation for PET studies (Mankoff et al., 1998, Mankoff et al., 1999).

Although thymidine would represent the gold standard to image cell proliferation with PET, it is not routinely used as an imaging agent in clinical studies due to its complex synthesis and the fact that it can only be labelled with ^{11}C (Shields, 2006). Most importantly, its rapid catabolism *in vivo* leads to two main disadvantages: first, metabolised thymidine is no longer available to be incorporated into the DNA; second,

the labelled metabolites affect the image and thus its interpretation (Krohn et al., 2001). This is due to non-specific cellular uptake into non-proliferating tissues and the contribution of the exchangeable compartment, indicating that metabolites are not irreversibly retained in the tissue, but can redistribute into the blood and other tissues (Mankoff et al., 1996).

These problems led to the development of thymidine analogues to image tumour proliferation with PET which are resistant to degradation, but, since they are not the natural components of the DNA, their uptake may not reflect directly thymidine incorporation into DNA (Shields et al., 1996a, Toyohara and Fujibayashi, 2003, Toyohara et al., 2006a, Toyohara et al., 2006b, Conti et al., 1995, Mangner et al., 2003, Krohn et al., 2001). Pyrimidine analogues mimic physiological nucleosides, since they are taken up into the cell and metabolized through the salvage pathway. They are, however, trapped intracellularly as monophosphates after phosphorylation by cytosolic TK1 and not significantly incorporated into DNA (Arner and Eriksson, 1995, Seitz et al., 2002). These compounds are usually labelled with fluorine-18 (^{18}F), since this radioisotope has a longer half-life (approx. 109 min) compared to ^{11}C and other positron emitters, and can be produced to high specific activity (Muzi et al., 2005b).

TK1 is the first enzyme in the salvage pathway and the most restrictive, accepting only thymidine and uridine as substrates (Arner and Eriksson, 1995), therefore nucleoside retention is directly dependent on phosphorylation by TK1: phosphorylation of thymidine or an analogue by TK1 is the rate limiting step to retain the nucleotide inside cells (Seitz et al., 2002).

1.4.1 FMAU

1-(2'-deoxy-2'-fluoro-β-D-arabinofuranosyl)-5-methyluracil (FMAU; Figure 13) is a 2'-fluoropyrimidine, with a fluorine atom inserted in the 2'-up position of the ribose ring. Either this position or the 5'-methyl group in the pyrimidine base could be radiolabelled (Conti et al., 1995, Mangner et al., 2003). FMAU proved to be resistant to catabolism (Bading et al., 2000) and showed uptake in tumours (Sun et al., 2005); however, it can't be efficiently phosphorylated by thymidine kinase 1 (TK1), the cytosolic, cell-cycle regulated enzyme responsible for the phosphorylation of TdR and its analogues in the salvage pathway for DNA synthesis, being instead a good substrate for thymidine kinase 2 (TK2), the mitochondrial, non cell-cycle regulated enzyme (Wang and Eriksson, 1996). This feature accounts for low sensitivity (it does not correlate with proliferation) due to its substrate specificity for the constitutively expressed TK2 enzyme (Bading and Shields, 2008).
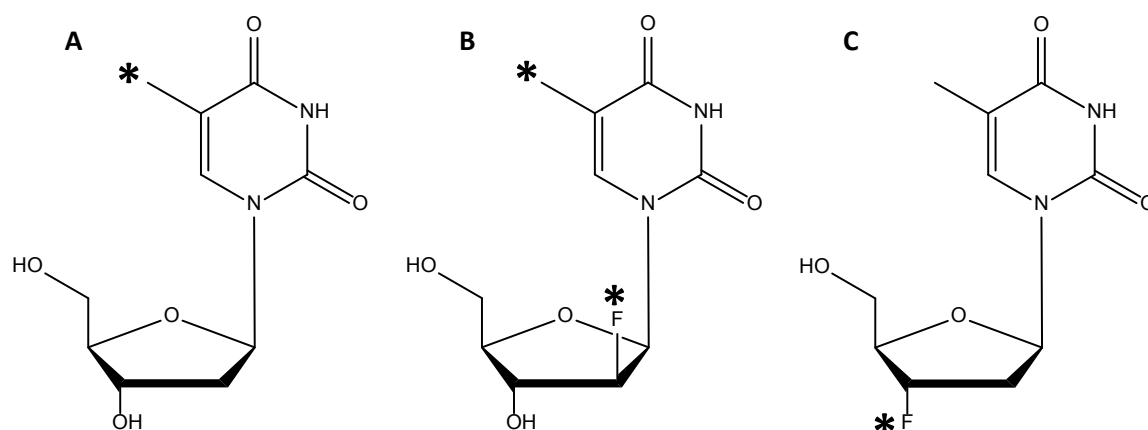
Figure 13. Chemical structures of thymidine, FMAU and FLT.
A) Thymidine is a natural component of DNA. B) FMAU is a pyrimidine analogue in which a fluorine atom is inserted into the 2'-up position of the deoxyribose ring, conferring resistance to catabolism. The 3' hydroxyl group is maintained, therefore it could potentially be incorporated into DNA. C) FLT is another pyrimidine analogue in which the substitution of the 3'-hydroxy by a fluorine atom confers resistance to catabolism. However, due to this modification it cannot be incorporated into the growing DNA chain. * = radiolabelling positions.

1.4.2 FLT

3'-deoxy-3'-fluorothymidine (FLT; Figure 13) was first developed as a chemotherapeutic agent to treat leukaemia (Blau et al., 1989). FLT anti-HIV activity was subsequently discovered (Kong et al., 1992), but, due to toxicity, its use as a drug against HIV was rejected (Shields et al., 1998, Krohn et al., 2001). However, successful labelling with ^{18}F suggested the use of FLT as a radiopharmaceutical to monitor HIV infection, but this application never reached animal experimentation. Nonetheless, this original idea formed the basis for imaging cell proliferation in tumours. FLT was, in fact, subsequently developed to image tumour proliferation with PET (Grierson and Shields, 2000, Shields et al., 1998).

[18F]FLT (Figure 13) is the most widely studied radiolabelled form of a pyrimidine nucleoside (Barthel et al., 2003, Salskov et al., 2007, Shields et al., 1998, Toyohara et al., 2002a, Vesselle et al., 2002, Barthel et al., 2005). With the exception of the replacement of the hydroxyl group in the 3' position of the deoxyribose sugar with a fluorine-18 atom (^{18}F), [18F]FLT structure remains identical to thymidine (Muzi et al., 2005b, Bading and Shields, 2008). This modification stabilizes the glycosidic bond, thus conferring resistance to catabolism by thymidine phosphorylase (TP), making [18F]FLT highly resistant to metabolic degradation (Shields et al., 1998, Schinazi et al., 1992, Grierson and Shields, 2000), even if glucuronidation (i.e. the addition of glucuronic acid to the deoxyribose) can still occur in humans (Shields et al., 2005, Muzi et al., 2005b). The resistance to degradation is the major advantage in its use (Grierson et al., 2004), since it is important to minimize the non-specific activity.

Further to its role in metabolism, the 3' position fluorination prevents the incorporation of the triphosphate form into DNA (see further), thus it acts as selective inhibitor of DNA synthesis (Barthel et al., 2003, Grierson et al., 2004): in a cell that is duplicating its DNA, it behaves as a chain terminator in the synthesis of the macromolecule (Grierson et al., 2004, Bading and Shields, 2008). Nonetheless, it tracks the salvage pathway for DNA synthesis, being efficiently phosphorylated by TK1 (Munch-Petersen et al., 1991) and less so by TK2 (Grierson et al., 2004). FLT uptake correlates with *in vitro* measures of cell proliferation, such as PCNA, Ki-67, and S phase fraction (Barthel et al., 2005, Bading and Shields, 2008). Its ability to image tumour proliferation has been reported and proved promising in several studies (Shields et al., 1998, Muzi et al., 2005b, Kenny et al., 2009, Kenny et al., 2005, Buck et al., 2003, Buck et al., 2002, Buck et al., 2006), thus it's been used as a pharmacodynamic biomarker to assess effectiveness of therapy (Dittmann et al., 2002, Barthel et al., 2003, Kenny et al., 2007, Sohn et al., 2008, Herrmann et al., 2007, Kishino et al., 2012, Contractor et al., 2012, Contractor et al., 2011).

1.4.3   Rationale of FLT uptake into proliferating cells

Since nucleosides are hydrophilic, they are not suitable for passive diffusion across membranes. Therefore, trans-membrane proteins are responsible for mediating their transport (Grierson et al., 2004). FLT permeates the cell membrane through a carrier-mediated mechanism involving equilibrative nucleoside transporter 1 (ENT1; (Paproski et al., 2008, Paproski et al., 2010)). Other nucleoside transporters are expressed on the cell surface and include additional equilibrative transporters (ENT2, 3 and 4), as well as concentrative transporters (CNT1, 2 and 3). CNTs are preferentially expressed by

specialised cells, whereas ENTs are found in most cell types and tissues. They differ in the mode of transport, with ENTs transporting nucleosides according to the concentration gradient, and CNTs concentrating nucleosides inside cells, coupling nucleoside and Na^+ transport (Cass et al., 1998, Pennycooke et al., 2001, Young et al., 2013). The distinct proteins in the same group have different cellular localisation and substrate specificity. In addition, different tumour types might rely on different transport mechanisms (see section 1.4.5). FLT mode of transport is an important aspect to take into account, since altered expression or activity of ENT1 can modulate the tracer uptake into cells and tumours. FLT flare effect has been described in pre-clinical and clinical studies, where inhibition of TS was causing redistribution of ENT1 thus increasing FLT uptake following specific treatments (Perumal et al., 2006, Kenny et al., 2009).

TK1 is the rate limiting step in FLT cellular trapping (Seitz et al., 2002). Once inside a proliferating cell (Figure 14), FLT is immediately monophosphorylated to FLTMP by TK1 (Barthel et al., 2003, Grierson et al., 2004, Shields, 2006, Rasey et al., 2002), being therefore retained in tissues at a rate proportional to TK1 activity (Muzi et al., 2005b). FLT is phosphorylated very efficiently by TK1 (Munch-Petersen et al., 1991, Rasey et al., 2002, Barthel et al., 2003), therefore reflecting metabolism via the DNA salvage pathway, and is predominantly trapped in the cell in the monophosphate form (Seitz et al., 2002, Shields, 2006, Rasey et al., 2002), representing the main labelled nucleotide pool (Grierson et al., 2004).

Subsequent phosphorylations to finally produce the triphosphate form (FLTTP) can be carried out by thymidylate kinase (TMPK), a cytosolic enzyme selectively expressed during S phase, and nucleoside diphosphate kinase (NDPK), a ubiquitous and S phase regulated

kinase responsible for the production of all nucleotide triphosphates (Grierson et al., 2004).

It has been suggested that FLTMP could also be dephosphorylated to FLT by a putative deoxynucleotidase (dNT; (Grierson et al., 2004)): although it seems that this phenomenon is perhaps a primary mechanism for tracer excretion from the cell (Grierson et al., 2004), to date there has been no evidence of the identification of this enzyme, and its role on FLT metabolism can be questioned. In fact, the predominance of FLTMP over FLTDP and FLTTP could be a consequence of reduced substrate activity of FLTMP towards TMPK, affecting the amount of FLTDP production, or NDPK, interfering with the phosphorylation to FLTTP. To support this hypothesis, 3'-azido-2',3'-dideoxythymidine (AZT), a thymidine analogue used in the treatment of HIV as antiretroviral drug, has been reported to inhibit TMPK (Furman et al., 1986). According to this report, the 3' substitution could not only affect FLT DNA incorporation, but also its ability to be phosphorylated to FLTDP by TMPK. The process by which FLTMP is converted into the different nucleotides is nonetheless reversible (Grierson et al., 2004). Hence, its metabolism is only able to show the intracellular nucleotide pool, which is subjected to reversible breakdown (Muzi et al., 2005b). If the putative dNT exists, the DNA salvage pathway will be a cycle of nucleoside phosphorylation and dephosphorylation events mediated by TK1 and dNT, respectively (Grierson et al., 2004). This will therefore cause loss of activity in cells (Grierson et al., 2004). To date, it is still assumed that FLT phosphorylation to monophosphate represents the trapping process, which is irreversible. However, nucleoside and nucleotide transporters are able to limit the intracellular pool of FLT and therefore TK1 activity measurement (Grierson et al., 2004). In fact, they could provide a mechanism for the loss of intracellular FLTMP which is not related to cellular dNT activity (Grierson et al., 2004).

FLTTP has been reported to be resistant to degradation and highly retained, but it is not (<1%) incorporated into DNA due to the lack of the 3'-hydroxy (Lu et al., 2002, Seitz et al., 2002, Toyohara et al., 2002b, Barthel et al., 2003, Grierson et al., 2004, Shields, 2006). Nonetheless, FLT has been characterised as a good biomarker for cell proliferation, due to its incorporation into cells via the salvage pathway, dependent on the cell-cycle regulated TK1 enzyme, and forming a radiolabelled pool inside cells following subsequent phosphorylation events (Muzi et al., 2005a, Muzi et al., 2005b). Its metabolic trapping, therefore, has been defined analogous to the trapping of [^{18}F]FDG (fluoro-deoxyglucose) due to its phosphorylation by the hexokinase (Rasey et al., 2002).

To summarize, TK1, TMPK and NDPK are the key known enzymes that determine intracellular radioactivity accumulation, resulting in the formation of FLT nucleotides (FLTMP, FLTDP, FLTTP). Between the three enzymes, TK1 is the most active, since FLTMP activity dominates the whole cell uptake (Grierson et al., 2004). High levels of TK1 have been found in rapidly growing cells (Sherley and Kelly, 1988, Seitz et al., 2002). As a consequence of TK1 activity, proliferating cells are able to metabolize FLT during S phase and, therefore, retain the labelled nucleotide (Grierson et al., 2004).

In addition, FLT is a very poor substrate for TK2 (Munch-Petersen et al., 1991, Bading and Shields, 2008), whereas thymidine is a substrate for this mitochondrial, constitutively expressed isoenzyme (Grierson et al., 2004).
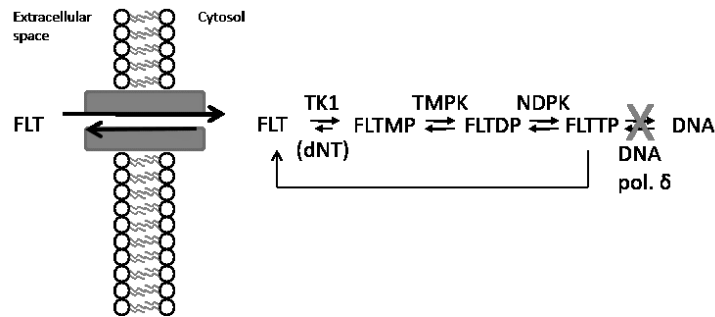
Figure 14. FLT trapping inside cells via the salvage pathway.
Transport of FLT into the cytosol occurs via facilitated diffusion by ENT1 transporters. TK1 converts FLT into the monophosphate form (FLTMP); FLTMP is subsequently phosphorylated to finally produce FLT triphosphate (FLTTP), which cannot be incorporated into the DNA. The FLT pool is subjected to reversible phosphorylations. A putative deoxynucleotidase (dNT) is proposed to dephosphorylate FLTMP, which could therefore be excreted from the cell.

Thymidine phosphorylase (TP) is an important enzyme involved in thymidine metabolism. It catalyses the cleavage of the base from the deoxyribose, forming thymine and 2-deoxyribose-1-phosphate, which is subjected to rapid dephosphorylation (de Bruin et al., 2003). Even if it does not act directly on FLT (FLT is resistant to catabolism by TP due to the 3' substitution, which prevents the cleavage of the glycosidic bond), it can modulate FLT uptake into cells by depleting the endogenous thymidine pool, thus increasing thymidine demand inside cells and consequently the accumulation of FLT. Thymidine levels, in fact, can affect the tracer uptake, since if cells contain high levels of dTTP, no more thymidine is necessary, and therefore FLT uptake will be reduced. This effect has been reported to play a role in FLT tumour accumulation (Zhang et al., 2012). Different cell lines and tumour types can, in fact, contain different levels of thymidine, affecting FLT uptake (see section 1.4.5).

1.4.4 [^{18}F]FLT-PET

[^{18}F]FLT has been one of the most promising tracers employed to image *in vivo* cell proliferation, and therefore tumours (Bading and Shields, 2008), since it reflects the early part of the DNA synthesis pathway (Grierson et al., 2004). Although, it is not incorporated

into DNA, it can provide a measure of tumour proliferation: indeed, the activity of TK1 reflects the proliferative fraction of cells (Ellims et al., 1981, Barthel et al., 2003, Rasey et al., 2002), being tightly regulated during the DNA synthetic phase (Sherley and Kelly, 1988, Toyohara et al., 2002b, Shields et al., 2005, Shields, 2006). Hence, TK1 activity provides an indirect measure of cells in S phase, and therefore changes in [^{18}F]FLT uptake are directly correlated to cell proliferation. Consequently, [^{18}F]FLT-PET imaging provides a measure of tumour proliferation *in vivo* (Shields et al., 1998, Barthel et al., 2003), even if it does not provide a direct measure (Wells et al., 2004).

FLT has been used to monitor the response of tumours to antiproliferative treatment *in vivo*, since changes in cell proliferation fraction could be visualised by changes in [^{18}F]FLT uptake (Leyton et al., 2005, Sugiyama et al., 2004, Leyton et al., 2006, Barthel et al., 2003). For example, decrease in the activities of G1 phase cyclins and in retinoblastoma hypo-phosphorylation regulates TK1 protein, leading to decrease in [^{18}F]FLT uptake (Leyton et al., 2008), reflecting the reduction in TK1 protein levels.

[^{18}F]FLT is taken up and retained in organs and tumours with high proliferative fraction (Figure 15; (Shields et al., 1998, Vesselle et al., 2002, Bading and Shields, 2008)). Its use, therefore, could provide a relatively simple, non-invasive and repetitive measure of tumour proliferation for use in clinical research and routine patient care, specifically in assessing tumour response to treatment.

FLT incorporation by tumour cells, however, is generally lower than that of FDG (Smyczek-Gargya et al., 2004, Buck et al., 2003, Cobben et al., 2004, Kameyama et al., 2009, Yamamoto et al., 2009). Consequently, the sensitivity for tumour detection can be limited because of the reduced tumour uptake. In addition, [^{18}F]FLT is not useful to image tumours within liver, bone or pelvic region (Figure 15) due to its high accumulation in non-

tumour tissues and organs (Bading and Shields, 2008). In humans FLT is, in fact, metabolised in liver (Shields et al., 2005, Shields et al., 1998), excreted through the kidneys into the bladder, and can also be accumulated in proliferating tissues such as bone marrow, other than in tumours (Shields et al., 1998).
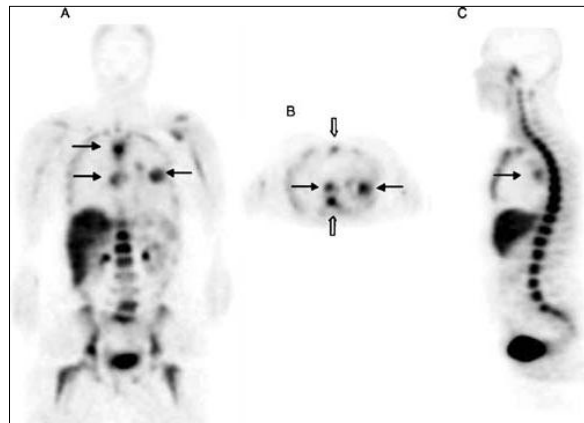
Figure 15. Physiological uptake of FLT occurs in bone marrow, bladder and liver, as well as in tumours.
The images were obtained from a whole-body scan of a patient with lung cancer following a 1h dynamic scan after the injection of 360.2 MBq of [^{18}F]FLT. A: coronal view; B: transversal view; C: sagittal view. In panel B, the dark arrows indicate the tumors, the light arrows point to the marrow. Panel A and C show high uptake in liver and bladder (Shields, 2006).

In conclusion, there are a number of features of FLT which would indicate good potential for imaging cell proliferation with PET (Rasey et al., 2002). It is resistant to catabolism by thymidine phosphorylase *in vivo* and is specifically phosphorylated inside the cell by the cytosolic thymidine kinase (TK1), the principal enzyme involved in the DNA salvage pathway which is tightly regulated during the cell cycle. In contrast, FLT is a poor substrate for the mitochondrial thymidine kinase TK2; therefore, it is a specific marker for cells that express high levels of TK1 (Rasey et al., 2002). However, a great limitation in the use of [^{18}F]FLT as a radiotracer to image cell proliferation is that it acts as a chain terminator. For this reason, its uptake could be misleading under conditions where TK1 is not rate limiting for the incorporation of exogenous TdR into DNA (see section 1.4.5 below).

1.4.5   Limitations of the use of FLT for imaging proliferation

Despite what has already been discussed in section 1.4.4, several groups recently reported discrepancies between [^{18}F]FLT tumour uptake and tumour proliferation, bringing to light the more complex relationship between FLT and cell proliferation and the potential confounding factors for PET images interpretation, as indicated by the different parameters influencing FLT uptake and described in the following list.

- **TK1 protein correlation**

Lack of direct correlation between [^{18}F]FLT uptake and TK1 protein expression has been reported (Zhang et al., 2012, Troost et al., 2010). Even though a direct association between TK1 protein levels and FLT uptake could be expected, it is important to keep in mind that FLT uptake is dependent on TK1 enzymatic activity, which is strictly regulated during the progression of the cell cycle and may not be correlated with actual protein expression. In accordance, Brockenbrough *et al.* reported lack of correlation of FLT uptake with TK1 activity, discussing other parameters (see further) that should be validated as potential confounders of FLT uptake into proliferative tissues (Brockenbrough et al., 2011).

- **Tissue thymidine content**

Tumour thymidine content competes with the incorporation and retention of FLT, causing impairment in the detection of cancer proliferation in tumour cells with an elevated thymidine pool (Zhang et al., 2012). Thymidine is in fact the natural substrate for all the enzymes involved in [^{18}F]FLT incorporation and retention. However, this effect, which has been observed in rodents, might not be translated into clinical practice, since the blood concentration of thymidine is more than 100-fold higher in rodents than in humans (Shields, 2012, Nottebrock and Then, 1977).

- **TP**

As already discussed in paragraph 1.4.3, TP is involved in the modulation of endogenous thymidine levels. Therefore, its activity has an indirect effect on the tumour uptake of FLT, modifying the endogenous thymidine pool thus increasing the radiotracer uptake, specifically in rats and mice, where thymidine concentration is elevated compared to humans. Rodents models have been developed in which pre-treatment with TP resulted in increased [^{18}F]FLT uptake (Van Waarde et al., 2004, Direcks et al., 2008).

- **FLT transport**

The extent of FLT transport should be kept in mind, as relative abundance of nucleoside and nucleotide transporters in different cell lines and tumours can affect FLT retention, as well as radioactivity loss (Paproski et al., 2010, Plotnik et al., 2011). FLT was, in fact, reported to be transported inside cells by ENT1 in RIF-1, KB and A549 cells and xenografts (Pillai et al., 2008, Perumal et al., 2006), whereas in TK6 cells both CNT and ENT transporters played a role in FLT uptake (Plotnik et al., 2011). In addition, nucleoside transporters expression can be modified following specific treatments, such as inhibition of TS (Perumal et al., 2006).

- **TS**

As [^{18}F]FLT is a direct substrate for TK1 (depending on TK1 phosphorylation in order to be retained into tissues), [^{18}F]FLT uptake could be impaired in tumours relying on the *de novo* pathway for thymidine production, as suggested by McKinley *et al.* (McKinley et al., 2013). This group reported difficulties in discriminating between tumours which are moderately proliferative and rely on the salvage pathway from those which are highly proliferating but rely on the *de novo* pathway. However, the cellular model used to measure relative contribution of salvage and *de novo* pathway (HCT116 p21$^{-/-}$) could have direct effects on TS expression. In fact, p21 plays an important role in cell cycle progression, inhibiting entry

into S phase following p53 induction of its transcription. The absence of this CDK inhibitor has been reported to induce cell cycle arrest even in S phase (Fan et al., 1997), and this event could increase TS expression during DNA synthesis (Navalgund et al., 1980). In addition, the activity of TK1 should be taken into consideration, not only its protein expression. Nonetheless, Moroz *et al.* also reported the influence of the relative usage of salvage versus endogenous (*de novo*) pathway for thymidylate supply comparing radiotracer uptake in two different xenografts models, showing that the *de novo* pathway was predominant in cells showing no difference in FLT uptake after treatment with a specific Aurora B inhibitor (Moroz et al., 2011).

[^{18}F]FLT-PET, however, proved to be useful to image TS inhibition both in pre-clinical and clinical settings, showing increase in [^{18}F]FLT uptake following treatment, a consequence of ENT1 redistribution to the cell membrane (Perumal et al., 2006, Pillai et al., 2008, Kenny et al., 2009, Viertl et al., 2011).

- **p53**

Mutations in p53 are also known to produce discrepancies in the assessment of treatment response with [^{18}F]FLT-PET (Schwartz et al., 2004). TK1 gene transcription can be regulated by p53, which induces G1 or G2 arrest, following induction of p21, in specific circumstancies, e.g. DNA damage. If p53 is depleted or its function is compromised, TK1 cell cycle regulation will be impaired (with no cell cycle specific control of TK1), thus reflecting on [^{18}F]FLT uptake (Katz et al., 2011).

- **DNA repair**

An additional factor which could have an influence on [^{18}F]FLT uptake is DNA repair. Chen *et al.* reported moderate overexpression of TK1 following DNA damage in p53-proficient cells (Chen et al., 2010). The increase in TK1 expression was more dramatic in p53-

deficient cells, as a result of the lack of p21 checkpoint arrest. They concluded that TK1 was up-regulated to provide dTTP for DNA repair; therefore an increase in the uptake of [^{18}F]FLT could be predicted following treatment with DNA-damaging agents in cells lacking p53. However, this effect could not be detected if p53 is expressed, as the increase in TK1 protein expression might not be sufficient to reflect higher uptake of [^{18}F]FLT. Additionally, they did not provide evidence of TK1 activity upon induction of DNA repair. Therefore, the effects that they reported could be simply due to G2 arrest (where TK1 protein is still expressed at high levels). If that was the case, then [^{18}F]FLT uptake will be reduced compared to cells replicating their DNA.

- **Correlation with Ki67**

Staining tumour samples with Ki67 represents the gold standard to measure tumour proliferation. Clinical studies reported conflicting correlation between [^{18}F]FLT uptake and Ki67 staining. Specifically, some reports described a positive correlation between radiotracer uptake and tumour proliferation, as measured by the Ki67 index (Buck et al., 2003, Buck et al., 2006, Brockenbrough et al., 2011), others presented lack of correlation between the two biomarkers (Yamamoto et al., 2009, Smyczek-Gargya et al., 2004, Troost et al., 2010). Chalkidou *et al.* suggested that the presence or absence of correlation with [^{18}F]FLT uptake might be due to non-standardized Ki67 analysis and depends on the tumour type (Chalkidou et al., 2012). Biopsies, however, remain problematic due to the fact that they only represent a discrete section of a tumour and, therefore, it is difficult to account for the heterogeneity of the tumour as a whole.

1.5 Layout of the thesis and hypotheses

TK1 regulation has to be kept in mind when studying TdR analogues uptake in tumours (Bading and Shields, 2008). Indeed, given that [^{18}F]FLT is a direct measure of TK1 activity (Shields et al., 1998, Rasey et al., 2002, Barthel et al., 2003), its uptake may vary according to TK1 regulation.

The work described in this thesis is focused on TK1 regulation by phosphorylation. Chang and co-workers reported TK1 hyper-phosphorylation during G2/M phase (Chang et al., 1994), suggesting that serine-13 (Ser13) was specifically phosphorylated during mitosis (Chang et al., 1998), reducing TK1 activity and marking the protein for degradation (Chang et al., 1998, Ke et al., 2003). Serine-231 (Ser231) and other residues were indicated as putative phosphorylation sites. Taking these reports as starting points, the aim of this work was to identify TK1 phosphorylation status during cell cycle progression and validate the effects of post-translational modifications on TK1 activity, hypothesising that TK1 was subjected to multiple phosphorylation events during cell cycle progression, and that these modifications affected its activity, thus [^{18}F]FLT uptake.

The $MnCl_2$-phos-tag™ system, a modified SDS-PAGE that allows separation of phosphorylated forms of a protein, was used to resolve three TK1 isoforms during cell cycle progression, with the aid of cell cycle arresting agents. Anti-cancer drugs were also used to evaluate possible effects on TK1 protein regulation. Transient transfections of TK1-deficient cells with mutant TK1 constructs were carried out to identify the phosphorylated residues responsible for the mobility shift of TK1 protein on $MnCl_2$-phos-tag™ gels. In addition, Chang *et al.* further suggested that TK1 was phosphorylated by cyclin-dependent kinases (CDKs), specifically CDK1 or CDK2 (Chang et al., 1998). However,

to the best of our knowledge, demonstration of CDK1 or CDK2 specific involvement in TK1 phosphorylation has not yet been reported. Therefore, we hypothesised that CDK1 was responsible for G2/M-specific phosphorylation, whereas CDK2 could have been involved in TK1 phosphorylation during S phase. RNA interference was exploited to selectively knock-down specific kinases to prove these hypotheses.

The different TK1 phosphorylations were thought to have specific roles in the regulation of the enzyme activity. Therefore, [18F]FLT cell uptake was performed to test 1) the effect of TK1 phosphorylation profile on radiotracer uptake during cell cycle progression, hypothesising that the G2/M-specific phosphorylation was responsible for a decrease in [18F]FLT retention during mitosis, and 2) the effects of mutant TK1 on the enzyme activity. After the *in vitro* experiments, we hypothesised that [18F]FLT-PET imaging was able to highlight early changes in tumour proliferation following treatment with paclitaxel, an anti-cancer drug which induces G2/M arrest *in vitro*. However, [18F]FLT-PET imaging did not highlight any early effect on tumour proliferation following treatment with paclitaxel. Two new radiotracers to image cell proliferation with PET were also validated. Both retained the 3'-hydroxyl group required for DNA incorporation. The original idea consisted in the development of a radiotracer with higher sensitivity when compared to [18F]FLT in order to overcome its limits. *In vitro* assays to test their ability to be phosphorylated by TK1 and to be retained into cells provided evidence that neither radiotracer was useful for imaging cell proliferation with PET.

Finally, we hypothesised that [18F]FLT could have been a useful biomarker to test G2/M arrest after inhibition of specific mitotic targets, not only following paclitaxel treatment. The effects of mitotic inhibitors on [18F]FLT retention and proteins involved in its uptake were evaluated.

Chapter 2. Materials and Methods

2.1   Cell lines and tissue culture

HCT116 cells (human colon cancer; LGC Standards, Teddington, Middlesex, UK) were cultured in RPMI-1640 (Invitrogen, Paisley, UK). A549 (lung carcinoma; ATCC, Manassas, VA), BT-20 (breast cancer; a gift from Dr Anil Chandrashekran, Department of Surgery and Cancer, Imperial College London), Hos and Ost TK1$^-$ (human osteosarcoma; a gift from Prof. Vera Bianchi, Department of Biology, University of Padua, Italy) were grown in Dulbecco's Modified Eagle's Medium (DMEM; Sigma, Poole, United Kingdom). Both types of media were supplemented with 10% fetal bovine serum (FBS; Lonza, Slough, UK), 2 mM L-glutamine and antibiotics (100U/ml penicillin and 100 µg/ml streptomycin). Cells were maintained in a 5% CO_2 humidified incubator at 37˚C.

2.2   Cell lysates preparation

For whole cell lysates, media and trypsinised cells were collected in a tube and spun at 2000 rpm at 4° C for 5 min, washed with PBS, and lysed using radioimmunoprecipitation assay buffer (RIPA; Thermo Scientific, Loughborough, UK). The buffer comprised 25mM Tris-HCl pH 7.6, 150mM NaCl, 1% NP-40, 1% sodium deoxycholate, 0.1% sodium dodecyl sulphate (SDS) containing 1:100 protease and phosphatase inhibitors (Halt protease and phosphatase inhibitor cocktail, Thermo Scientific). Lysates were sonicated on ice and stored at -20° C until ready for use. Protein concentration was determined with a bicinchoninic acid (BCA) assay (Pierce® BCA Protein Assay Kit, Thermo Scientific), according to the manufacturer's instructions.

2.3 Antibodies

Mouse anti-TK1 (34003 (3B3.E11)) was purchased from QED Biosciences, Inc. (San Diego, CA). Mouse anti-TK1 (ab57757), rabbit anti-TK1 (ab91651), mouse anti-TS (ab3145), rabbit anti-TS (ab108995), rabbit anti-ENT1 (ab48607), rabbit anti-KIFC1 (ab72452) and rabbit IgG isotype control (ab37415-5) were purchased from Abcam (Cambridge, UK). Rabbit anti-actin (A 2066) and mouse anti-γ-tubulin antibody (T6557) were purchased from Sigma-Aldrich (Gillingham, UK). Rabbit anti-Phosphoserine (61-8100) and Alexa Fluor® 488 anti-mouse (A10667) were purchased from Invitrogen. Rabbit anti-Akt (9272), rabbit anti-phospho-Akt (Ser473; 9271), rabbit anti-CDC2 (9112), rabbit anti-phospho-CDC2 (9111), rabbit anti-CDK2 (2546), rabbit anti-Wee1 (4936), rabbit anti-phospho-Wee1 (4910), and rabbit anti-TP (4307) were purchased from Cell Signaling Technology (Herts, UK). Mouse anti-tubulin (sc-8035), goat anti-mouse (sc-2005) and anti-rabbit (sc-2004) horse radish peroxidase (HRP)-conjugated were purchased from Santa Cruz Biotechnologies (Heidelberg, Germany).

2.4 Drugs

Aphidicolin, nocodazole, cisplatin, 5-fluorouracil, roscovitine and staurosporine were purchased from Sigma. Paclitaxel was obtained from Calbiochem or Hammersith Hospital pharmacy. N-[(R)-2,3-dihydroxy-propoxy]-3,4-difluoro-2-[2-fluoro-4-iodo-phenylamino]-benzamide (PD0325901) was obtained from the Division of Signal Transduction Therapy, University of Dundee, Dundee, Scotland. MLN8237, AZD1152 and BI 2536 were a kind gift from Dr Spiros Linardopoulos (Institute of Cancer Research, London, U.K.).

2.5　Small interfering RNA (siRNA)

Human CDK1, CDK2 and KIFC1 ON-TARGETplus SMARTpool siRNA and ON-TARGETplus non-targeting pool (scramble) were purchased from Dharmacon (Dharmacon Lafayette, CO, USA).

2.6　Protein dephosphorylation

2.6.1　Alkaline phosphatase (CIP)

In order to dephosphorylate TK1 protein, a reaction using alkaline phosphatase (Calf Intestinal (CIP), New England BioLabs, Herts, UK) was carried out. 100 µg of protein were incubated with 100 units (U) of CIP at 37°C for 1 hour. Samples were subsequently prepared to be electrophoresed.

2.6.2　Lambda protein phosphatase (Lambda PP)

The activity of Lambda protein phosphatase (LPP; New England Biolabs) is specific for dephosphorylating serine, threonine and tyrosine residues. In order to obtain protein dephosphorylation, 50 µg of proteins were incubated with 200 units of LPP according to the manufacturer's instructions.

2.7　Immunoblotting

1X NuPAGE® LDS sample buffer (Invitrogen) and NuPAGE® sample reducing agent (Invitrogen) were added to protein lysates, according to the manufacturer's instructions. Samples were heated at 70° C for 10 min and then resolved by SDS-polyacrylamide gel electrophoresis (SDS-PAGE).

Molecular weight marker (ColorPlus™ prestained protein ladder, broad range; New England BioLabs) was run in parallel to determine proteins molecular weights.

2.7.1 Pre-cast SDS-PAGE

NuPAGE® Novex 12% Bis-Tris gels were purchased from Invitrogen. Up to 30 µg of proteins were loaded per well. Gels were electrophoresed at 200 V for approximately 45 min using the XCell SureLock™ Mini-Cell system from Invitrogen. Separated proteins were then transferred on PVDF membrane (Amersham Hybond-P, GE healthcare) for 1 hour at 100 V using the Mini Trans-Blot Cell® from Invitrogen.

2.7.2 Mobility shift detection of phosphorylated proteins

The acrylamide-pendant Phos-tag™ ligand provides a phosphate affinity SDS-PAGE for mobility shift detection of phosphorylated proteins. It consists of a modified polyacrylamide gel in which chemical groups, known to bind to phosphorylated species, are incorporated (Kinoshita et al., 2006).

One of the major advantages of this technique resides in the avoidance of radioactivity, and in improved resolution of the different phosphorylated forms, since phospho-protein isotypes are detected as multiple bands. The binding specificity of the incorporated ligand is completely independent of the amino-acid sequence of the protein. The procedure is similar to the general SDS-PAGE, in which the gel is cast adding a specific concentration of the Phos-tag™ ligand. Its concentration, together with the percentage of acrylamide used, is dependent on the molecular weight of the protein of interest. In fact, the more acrylamide and the more Phos-tag™ are included, the slower proteins are able to migrate through the gel at room temperature.

1 mm thick 8x10 cm mini-gels were cast using Mini-PROTEAN Tetra Cell Casting Module (165-8024; Bio-Rad, Herts, UK). For $MnCl_2$-phos-tag™, gels were composed of a 12% resolving gel (12% acrylamide (Protogel, National Diagnostics, East Riding, UK), 375 mM Tris, 0.1% SDS, pH 8.8) containing 75 µM phos-tag™ (Wako Chemicals GmbH, Neuss,

Germany), 150 µM MnCl$_2$ (Sigma), and a 5% stacking gel (5% acrylamide, 125 mM Tris, 0.1% SDS, pH 6.8). To make ZnCl$_2$-phos-tag™ gels, Tris buffer was substituted by Bis-Tris pH 6.8. 1:100 10% ammonium persulfate (APS) and 1:1000 tetramethylethylendiamine (TEMED) were added to trigger polymerization. Electrophoresis was performed in a Mini-PROTEAN® Tetra cell at 200V for 1h 10 min in running buffer composed of 25 mM Tris, 190 mM glycine, 0.1% SDS, pH 8.3 for Mn-phos-tag™ gels, or of 0.1 M Tris, 0.1 M 3-(N-morpholino)propanesulfonic acid (MOPS, Sigma), 0.1% SDS and 5 mM sodium bisulfite (Sigma) for ZnCl$_2$-phos-tag™.

After electrophoretic separation, gels were washed 3 times for 10 min in 0.5 M EDTA pH 8.0. Proteins were subsequently transferred onto nitrocellulose (Hybond™ ECL nitrocellulose membrane; GE Healthcare, Little Chalfort, UK) or polyvinylidene difluoride (PVDF; Amersham Hybond-P PVDF membrane, GE Healthcare) in 20% methanol and 80% Tris buffer (25 mM, pH 8.3) containing 38 mM glycine using a Mini Trans-Blot® cell or Criterion Blotter® (Bio-Rad).

2.7.3   Protein detection

After transfer, membranes were blocked in blocking buffer (5% milk or bovine serum albumin (BSA) powder dissolved in PBS containing 0.1% Tween 20 (PBS-T)) for 1 hour, and subsequently incubated with the primary antibody appropriately diluted in antibody dilution buffer (1% milk or BSA powder dissolved in PBS-T) at 4° C overnight. Membranes were washed 3 times in PBS-T prior to 45 min room temperature incubation with the secondary antibody (goat anti-mouse or anti-rabbit HRP-conjugated), diluted 1:2000 into antibody dilution buffer containing milk. Blots were washed 3 more times in PBS-T, incubated with Amersham ECL western blot detection reagent (enhanced chemiluminescence; GE Healthcare) and developed via exposure to Amersham Hyperfilm

ECL (GE Healthcare). Membranes were probed for loading controls (α tubulin or β actin) or different primary antibodies after stripping with Restore PLUS Western Blot Stripping Buffer (Thermo Scientific) according to the manufacturer's instructions. Briefly, membranes were washed from ECL, incubated with stripping buffer at room temperature twice for 10 minutes, washed in 1X PBS-T three times for 10 minutes, and blocked in blocking buffer prior to addition of the primary antibody.

2.7.4   Densitometry

Developed films were acquired using the GS-800™ calibrated densitometer (Bio-Rad). Images were analysed using the Quantity One® 1-D analysis software (Bio-Rad). Optical densities values (OD/mm^2) were subsequently subjected to statistical analysis.

2.8   DNA cell cycle analysis

Cell cycle distribution was assessed using propidium iodide (PI, Sigma) to perform DNA-based flow cytometric analysis in fixed, permeabilized cells. Cell culture media were collected in a tube together with washes. Cells were then trypsinised and added to the same tube. After washing with PBS, the cell pellet was resuspended in 1 ml ice-cold PBS and added dropwise to 9 ml 70% ethanol (EtOH). The solution was stored at -20° C for at least 2 hours or until ready to be stained. EtOH was then discarded and cells were rehydrated in PBS for 15 min before being resuspended in staining buffer containing 100 mM Tris pH 7.4, 150 mM NaCl, 1 mM CaCl$_2$, 0.5 mM Mg Cl$_2$, 0.1% Triton-X, 0.1 mg/ml RNase A and 25 µg/ml PI. Staining was performed at 37°C for 3 hours, after which cells were analysed in a BD FACS Canto cytometer (BD, Oxford, UK), counting 10,000 cells per condition. Selective gating was applied to exclude cell debris and doublets from the

analysis. Data were subsequently processed using FlowJo software version 7.6.5 (Tree Star; Ashland, USA).

2.9 Thymidine kinase 1 (TK1) DNA plasmids

FLAG-pCMV2 DNA plasmids containing Δmet wild type TK1, Δmet S13A TK1, Δmet S13D TK1 or Δmet S231A TK1, obtained from TK1 cDNA, were kindly donated by Prof. Z.F. Chang, University of Taiwan (Chang et al., 1998).

2.10 Bacterial transformation with plasmid DNA

DH5α *Escherichia coli* (*E.coli*) competent cells (Invitrogen) were transformed with TK1 plasmids. Briefly, 50 µl of bacteria were aliquoted into pre-chilled 1.5 ml microfuge tubes. 10 ng of plasmid DNA were mixed with bacteria and placed on ice for 30 minutes. Heat shock at 42° C was applied for 30 seconds, followed by incubation on ice for 2 minutes. Recovery was allowed by adding 1 ml Super Optimal broth with Catabolite repression (SOC; Invitrogen) and incubating at 37° C with agitation for 1 hour. Bacteria were then plated on Luria Broth (LB)-agar plates supplemented with 100 µg/ml ampicillin and grown overnight at 37° C.

2.11 Plasmid DNA extraction and validation

Individual colonies were selected from bacterial plates and grown in 3 ml LB at 37° C with agitation overnight. Plasmid DNA was extracted from bacterial cultures using the GeneJET™ Plasmid Miniprep Kit (Fermentas Life Sciences, St Leon-Rot, Germany). The identity of the plasmid DNAs was verified by sequencing.

Selected colonies were expanded in 100 ml LB overnight. DNA was extracted using QIAGEN-tip 500 plasmid maxi kit (Qiagen Ltd, Manchester, UK), according to the manufacturer's instructions. After elution from the column, DNA was precipitated with 2.5X absolute ethanol and 1:10 3M sodium acetate pH 5.2 for 1 hour at -20° C. After centrifugation at 14,000g for 15 minutes, DNA was resuspended in TE buffer (10 mM Tris pH 8.0, 1 mM EDTA). DNA concentration was determined using the nano-drop ND1000 spectrophotometer (Lab Tech International, East Sussex).

2.12 Transient transfections with plasmid DNA

In order to determine the phosphorylated amino-acid residues on TK1 protein, Ost TK1⁻ cells were transiently transfected with FLAG-pCMV2 plasmids containing Δmet wild type TK1, Δmet S13A TK1, Δmet S13D TK1 or Δmet S231A TK1.

Cells were transfected using Lipofectamine™ 2000 transfection reagent (Invitrogen), according to the manufacturer's instructions. Briefly, one day prior transfection Ost TK1⁻ cells were seeded into 10 cm plates in antibiotic-free media to reach 70-80% confluency. The next day, 24 µg FLAG-pCMV2 of the desired plasmid were used to transfect Ost TK1⁻ cells. The transfection mixture was removed and replaced with fresh media, containing nocodazole as required, 6 hours post transfection. Transgene expression was tested 24 hours after transfection by western blot analysis.

The following controls were used: DNA only, in which only plasmid DNA was added to cells; Lipofectamine™ only, in which cells were treated with Lipofectamine™ 2000 without DNA; and un-transfected cells.

2.13 RNA interference (RNAi) using small interfering RNA (siRNA)

Cells were transfected with targeted or scramble siRNA for 48 hours using wet reverse transfection with RNAiMAX (Invitrogen) transfection reagent according to manufacturer's instructions. In brief, siRNA and transfection reagent dilutions were prepared, mixed and incubated for 20 minutes before adding to the cell suspension. Cells in suspension were then plated in desired plates. Validation of knockdown was done by western blotting.

2.14 Immunoprecipitation (IP)

Immunoprecipitation was performed using PureProteome™ Protein A and Protein G Magnetic Beads (Millipore, Watford, UK), according to the manufacturer's instruction. Briefly, 50 µl aliquots of Protein A were transferred into microfuge tubes, washed with PBS-0.1% Tween 20, and incubated with 5 µg p-Ser antibody or rabbit IgG control diluted in PBS-0.1% Tween 20 at room temperature with continuous mixing for 10 minutes. Bead-antibody complexes were washed 3 times with PBS-0.1% Tween 20 prior to adding 500 µg of protein lysates, and subsequently incubated at 4° C overnight with continuous mixing. Samples were washed 3 times with PBS-0.1% Tween 20, resuspended in 60 µl 1X NuPAGE® LDS sample buffer (Invitrogen) and NuPAGE® sample reducing agent (Invitrogen), and heated at 70° C for 10 minutes. Beads were removed before analysing the samples with gel electrophoresis.

2.15 Isoelectric focusing (IEF)

Cell lysates were prepared using RIPA Lysis buffer (20 mM HEPES pH 7.5, 150 mM NaCl, 1% NP40, 0.25% sodium deoxycholate, 10% glycerol; Protein Simple, Santa Clara, USA) containing phosphatase inhibitor cocktails 2 and 3 (Sigma) and protease inhibitor minitabs

(Roche). Briefly, cells were scraped in media, pelleted at 2000 rpm and 4° C for 5 minutes, washed with ice-cold PBS, lysed in RIPA buffer, and snap-frozen on dry ice. Samples were stored at -80° C.

Protein samples were diluted in 20 mM Bicine pH 7.6, 0.6% 3-[(3-cholamidopropyl)dimethylammonio]-1-propanesulfonate (CHAPS) to a final concentration of 0.8 µg/µl. 15 µl of premix composed of 14.25 µl ampholyte premix G2 pH 4-9 (Protein Simple, 040-969) and 0.75 µl pI Standard Ladder 1 (Protein Simple, 040-644) were added to 5 µl of diluted protein sample. Primary antibodies were diluted 1:50 in antibody diluents. Biotinylated secondary antibodies and horse-radish peroxidase (HRP) conjugated to streptavidin were diluted 1:100. Detection reagent was prepared as a 1:1 mix of Luminol (Protein simple, 040-652) and hydrogen peroxide (Protein Simple, 040-653). 10 µl of sample, 10 µl primary antibody and 20 µl of secondary HRP-streptavidin and detection reagent were loaded into separate wells of a 384 well plate. Samples were then analysed on a CB1000 nanopro capillary focusing automated system at 15000 microW for 40 minutes in proprietary capillaries (Protein Simple). After completion of the capillary focusing process, samples were cross-linked to the capillary surface by UV exposure for 80 seconds, and capillaries were washed prior to incubation with primary antibody for 240 minutes. Capillaries were incubated with secondary antibody for 60 minutes after a second washing step. Incubation with HRP-streptavidin occurred for 10 minutes after washing. Finally, detection was performed after incubation with Luminol-peroxide detection reagent. Images were captured with a CCD camera after 30, 60, 120, 240, 480 seconds of exposure, and processed and analysed using proprietary Compass software (Protein Simple).

2.16 Immunofluorescence microscopy (IFM)

Cells were seeded in chamber slides (BD). After appropriate treatment, cells were fixed and permeabilized in ice-cold 100% methanol for 15 minutes at -20° C. Cells were washed 3 times in PBS prior to incubation with blocking buffer (1X PBS, 5% goat serum (Dako UK Ltd, Ely, UK), 0.3% Triton X-100 (Sigma)) for 1 hour. Slides were incubated with the appropriate primary antibody diluted in antibody dilution buffer (1X PBS, 1% BSA, 0.3% Triton X-100) at 4° C overnight. Excess primary antibody was removed by washing 3 times in PBS, and cells were incubated with the fluorochrome-conjugated secondary antibody (Alexa Fluor® 488) diluted in antibody dilution buffer at room temperature for 1 hour protected from light. Slides were then rinsed in PBS, and finally the coverslips were mounted using Prolong® Gold Antifade Reagent containing DAPI (4', 6-diamidino-2-phenylindole; Invitrogen). Images were captured on imaging camera using an Olympus BX51 microscope (Olympus, Southend-on-Sea, U.K.) at 400x magnification. Nuclei, mitotic cells, centrosome number and apoptotic cells were counted in up to 6 randomly selected fields of view using 400x magnification (two repeats per experiment). The number of nuclei, mitotic/apoptotic cells and centrosomes were expressed as the percentage of the total number of counted cells.

2.17 *In vitro* cell uptake

Generally, on day 1 cells were seeded into 6-well plates in order to achieve ~60% confluence on the day of the experiment. On day 2, cells were treated with specific drugs if necessary. On the day of the experiment, cells were incubated with ~0.37 MBq/well of the desired radiotracer and incubated in a 5% CO_2 humidified incubator at 37°C. After the appropriate amount of time, cells were scraped in media, collected in a tube, and spun at

6500 rpm at 4°C for 2 minutes. Media were then aspirated and the cell pellets were washed twice with PBS or 10% perchloric acid, according to the type of experiment, before being resuspended in 200 µl RIPA buffer. Samples were transferred into counting tubes and analysed for radioactivity counts on a gamma counter (Cobra II Auto-Gamma counter, Packard Biosciences Co., Pangbourne, UK). After radioactivity decay, protein concentration was measured for each sample with a BCA assay (Thermo Scientific) and used for normalisation.

2.18 Radiotracer substrate activity for TK1

The protocol was adapted from Toyohara *et al.*, 2002 (Toyohara et al., 2002a). HCT116 cells were grown in 10 cm plates until they reached 60-70% confluency. Cells were washed and scraped in 1 ml ice-cold PBS, centrifuged at 5,000 rpm for 5 minutes at 4° C and resuspended in 0.5 ml homogenization buffer (10 mM Tris-HCl pH 7.5, 1 mM EDTA pH 8.0, 5 mM 2-mercaptoethanol). Cells were then sonicated, spun at 15,000 rpm for 5 minutes, and the supernatant was transferred into fresh microfuge tubes. Protein concentration was determined using the nano-drop ND1000 spectrophotometer (Labtech International Ltd, Uckfield, U.K.). The reaction was carried out by mixing 0.1 mg of homogenized cells (supernatant) with 90 µl of reaction buffer (50 mM Tris-HCl pH 7.5, 2.5 mM ATP, 2.5 mM MgCl$_2$), for a total volume of 100 µl. Tubes were incubated with ~1.85 MBq of the radiotracer of interest at 37° C for the desired period of time, after which the reaction was blocked by snap-freezing on dry ice. Samples were thawed on ice and diluted with 1 ml ice-cold 10% ethanol/PBS, filtered through a Millex 0.2 µm filter (Millipore), and injected on to the HPLC. Radio-HPLC conditions were as previously described (Smith et al., 2012).

2.19 *In vivo* studies

2.19.1 Tumour xenografts

All animal work was conducted in accordance with the United Kingdom Home Office

Guidance on the Operation of Animals (Scientific Procedures) Act 1986 (HMSO, London,

United Kingdom, 1990) and with guidelines established by the UK National Cancer

Research Institute Committee on Welfare of Animals in Cancer Research (Workman et al.,

2010). Tumours were induced by subcutaneous (s.c.) inoculation of 4 x 10^6 exponentially

growing HCT116 cells on the back of 6- to 8-weeks-old female BALB/c nude mice obtained

from Harlan UK Ltd. (Bicester, United Kingdom). Tumour dimensions were measured with

a calliper and tumour volumes calculated using the ellipsoid formula:

$$volume\ (mm^3) = w \cdot l \cdot h \cdot (\pi/6),$$

where *w*, *l*, and *h* represent the three orthogonal axes of the tumour. When xenografts

reached approximately 100 mm^3, mice were treated with an intraperitoneal (i.p.)

injection of paclitaxel as required and subjected to positron emission tomography-

computed tomography (PET-CT) imaging.

2.19.2 Radiotracers

[^{18}F]FLT was supplied by Siemens PETNET solutions (Nottingham, U.K.). [^{18}F]FTT and

[^{18}F]FOT were produced by Dr Graham Smith and Dr Laurence Carroll (CCIC, Imperial

College London) as described in (Smith et al., 2012).

2.19.3 PET-CT scanning and image analysis

At the selected time points, anaesthesia was induced with isoflurane/O_2/N_2O inhalation

and the tail vein of the mouse was cannulated. Animals were scanned on a dedicated

small animal PET-CT scanner (Siemens Multimodality Inveon, Siemens Molecular Imaging

Inc., Knoxville, USA). To obtain an anatomical reference and for PET data attenuation

correction, low-dose CT scans were acquired (80 kVp, 0.5 mA, 220° rotation, exposure time of 600 ms per degree, 80 μm reconstruction pixel size). Following a bolus intravenous (i.v.) injection of 2.96-3.7 MBq of the selected radiotracer ([^{18}F]FLT/FTT/FOT), dynamic emission PET scans were acquired in list-mode format over 60 min and corrected for decay and dead time. Acquired data were subsequently sorted into 0.5 mm sinogram bins and 19 time frames (4 x 15 sec, 4 x 60 sec, and 11 x 300 sec) for image reconstruction, which was performed by filtered back-projection (FBP; Fourier rebinning, 256 x 256 x 159 matrix size, 0.39 x 0.39 x 0.80 mm^3 pixel size, ramp filter with cut-off at Nyquist frequency, Full Width at Half Maximum (FWHM) 1.45 mm), ordered subset expectation maximization in 2 dimensions (OSEM2D; Fourier rebinning, 256 x 256 x 159 matrix size, 0.39 x 0.39 x 0.80 mm^3 pixel size, 4 iterations, FWHM 1.03 mm), or ordered subset expectation maximization in 3 dimensions followed by MAP reconstruction (OSEM3D/MAP; 256 x 256 x 159 matrix size, 0.43 x 0.43 x 0.80 mm^3 pixel size, 2 OSEM3D iterations, 18 MAP iterations b = 0.1 optimised for uniform resolution, FWHM 1.29 mm) (Nguyen et al., 2013). The reconstructed cumulative images of the dynamic data were used for visualization of radiotracer uptake and to define regions of interest (ROIs) with the Siemens Inveon Research Workplace software (IRW; Siemens, Frimley, UK). Three-dimensional ROIs (0.5 mm thick) were defined for each tumour. Physical decay-corrected dynamic data from the selected ROIs were averaged at each of the 19 time points to obtain time versus activity curves (TACs) for each tumour. Tumour radioactivity was then normalised to the total injected dose (ID) to obtain the normalized uptake value (NUV) as percentage of injected dose per ml of tissue (%ID/ml). NUV curves, the NUV at 60 min post-injection (NUV60) and the area under the curve (AUC), calculated as the integral of the NUV from

0 to 60 min, were used for comparison. The values obtained from each mouse were then statistically analysed with GraphPad Prism 5 for Windows, Version 5.01.

2.19.4 *In vivo* metabolism of nucleoside radiotracers

Metabolism studies were performed as previously decribed (Smith et al., 2012). Briefly, the radiotracer of interest was injected i.v. via the lateral tail vein of female BALB/c mice (Harlan). Blood samples were collected into heparinised syringes by exsanguination via cardiac puncture under general anaesthesia using 2.5% isoflurane; different mice were sacrificed at selected time points (i.e. 2, 15, 30 and 60 minutes) post-injection. Plasma was separated after centrifugation at 2000*g* for 5 minutes. Plasma, liver and urine were snap-frozen and stored on dry-ice before being thawed and kept on ice. After addition of ice-cold acetonitrile, samples were spun at 15,000*g* for 3 minutes at 4° C. The supernatant was then evaporated on a rotary evaporator and resuspended in 10% EtOH/PBS. Samples were filtered through 0.2 μm syringe filters (Millipore, Billerica, MA, USA) and approximately 1 ml injected onto HPLC for analysis. The proportion of radioactivity remaining as parental/unmetabolised compound was assessed, measuring the peak area.

2.19.5 Biodistribution analysis

Biodistribution was carried out in BALB/c mice (Harlan) as previously described (Smith et al., 2012). Briefly, 3.7 MBq of radioactivity was injected i.v. via the lateral tail vein. Mice were then sacrificed after 2, 15, 30 or 60 minutes post-injection by exsanguination via cardiac puncture under general anaesthesia using 2.5% isoflurane. Tissues were individually excised and the radioactivity was counted on a gamma counter (Cobra II Auto-Gamma counter). Values were decay-corrected and data expressed as percentage of injected dose per gram (%ID/g).

2.20 Immunohistochemistry (IHC)

Proliferative activity of tumours using Ki67 monoclonal antibody MIB-1 (Dako UK Ltd), was detected using the labelled streptavidin-biotin (LSAB) procedure. Tumours were excised and fixed in neutral buffered 10% formalin, embedded in paraffin and cut into 5.0 micron sections. Briefly, the obtained slides were deparaffinised in Histo-Clear (National Diagnostics) and rehydrated in a graded series of EtOH (100% to 50%). Heat-induced antigen retrieval was performed in citrate buffer pH 6.0 (Sigma) in heated water bath at 100° C for 20 min. Sections were allowed to cool at room temperature for approximately 15 min. Endogenous peroxidase activity was quenched with 3% hydrogen peroxide (Sigma) for 10 min. Slides were subsequently washed in PBS-T twice for 5 min. The Histostain®-*Plus* kit (Invitrogen) was used for subsequent processing, according to the manufacturer's instructions. Briefly, serum blocking solution was added for 30 min to block non-specific binding. Sections were subsequently incubated overnight at 4° C with Ki67 monoclonal antibody diluted 1:100 v/v in PBS-T containing 5% w/v BSA. Excess antibody was removed by washes in PBS-T, followed by incubation with the biotinylated secondary antibody for 30 min. Slides were rinsed with PBS-T prior to addition of enhanced horseradish peroxidase conjugated streptavidin (HRP-SA) for 15 min. Peroxidase activity was then developed by applying the chromogen 3, 3' diaminobenzidine (DAB) for 5 min. Sections were counterstained with haematoxylin (Dako) and analysed by light microscopy. Successful Ki67 staining produced brown nuclear staining. Blue nuclear stain was produced by haematoxylin.

Images were captured on imaging camera using an Olympus BX51 microscope (Olympus) at 400x magnification. For each tumour section, Ki67-positive cells (brown staining) and haematoxylin-stained cells (blue staining) were counted in up to 6 randomly selected

fields of view using a 400x magnification (two tumour sections per group). The Ki67 labelling index was expressed as the percentage of Ki67 positive cells over the total number of cells.

2.21 Tumour lysates

After excision, tumour samples were snap-frozen in liquid nitrogen (LqN$_2$) and subsequently stored at -80° C. Tumour lysates were prepared by homogenising the tumour in RIPA buffer using the Precellys® lysing kit CK14 and Precellys® 24 (Bertin Technologies, France). In brief, tumour samples were transferred in pre-chilled Precellys® tubes containing ceramic beads, submerged in an appropriate amount of RIPA buffer, and homogenised using the Precellys® 24 instrument. Protein concentration was determined after sonication using the BCA assay (Thermo Scientific) and samples were then prepared to be assessed by western blotting.

2.22 Statistical analysis

Data were analysed using GraphPad (California, U.S.A.) Prism software for Windows, version 5, and expressed as mean ± standard error of the mean (SEM). Student's un-paired two-tailed t-test was applied to compare results before and after treatment. Analysis of Variance (ANOVA) was performed on large datasets. P-values (p) ≤ 0.05 were considered statistically significant, and significant differences were expressed as * (p<0.05), ** (p<0.01) or *** (p<0.001).

Chapter 3. Results

3.1 Identification of thymidine kinase 1 (TK1) phosphorylated isoforms

3.1.1 Developing a method to isolate phosphorylated forms of TK1

Initial studies were conducted in A549 and HCT116 cells. Lung carcinoma A549 cells were chosen, analogous to the work of Rasey *et al.* (Rasey et al., 2002), in order to later validate radiotracer uptake in relation to thymidine kinase 1 (TK1) activity. Human colon cancer (HCT116) cells were used according to Leyton *et al.* (Leyton et al., 2006) to perform *in vivo* studies with a well characterised cell line, known to produce tumour xenografts in mice.

In 1993, Chang and co-workers reported for the first time phosphorylation of TK1 (Chang and Huang, 1993). Later, they demonstrated specific phosphorylation of the protein during G2/M phase in HeLa and TK1-deficient mouse fibroblasts transfected with TK1 constructs, with this modification occurring on serine-13, reducing TK1 enzymatic activity (Chang et al., 1998, Chang et al., 1994). In 1996, He *et al.* (He et al., 1996) also demonstrated the existence of phosphorylated TK1 in mouse Ehrlich ascites tumour (EAT) cells. Different residues were suggested to be phosphorylated according to bioinformatics analysis (Chang et al., 1998), but no further analysis has been carried out to date to identify these residues specifically. For this reason, there was a need to understand if there were indeed other phosphorylated forms of the protein and to determine their role in TK1 regulation during the cell cycle, in order to comprehend the effects that these modifications could have on radiotracer uptake in the context of PET imaging, where thymidine analogues are being developed to image cell proliferation via incorporation through the salvage pathway.

a) Use of 12% SDS-PAGE to separate phosphorylated forms of TK1
Firstly, detection of TK1 protein expression was assessed in different cell lines. It was essential to find an antibody that was specific for TK1, producing limited numbers of bands to permit use in assessing phosphorylation status. An antibody from QED

Biosciences Inc. was first evaluated on standard 12% SDS-PAGE (Figure 16A). TK1 signal was expected at 25 kDa; however, several bands were obtained after western blotting, with some disappearing after treatment with alkaline phosphatase (CIP). Since the signal generated by this antibody seemed to be non-specific, some optimization was performed, incubating membranes with different dilutions of the antibody (Figure 16B). These attempts did not lead to significant improvements, thus a different antibody (Abcam) was assessed (see below).

Validation of the existence of differential phosphorylations was performed by calf intestinal alkaline phosphatase (CIP) pre-treatment, since alkaline phosphatase has been previously proved to dephosphorylate proteins, including TK1 (He et al., 1996, Chang et al., 1998, Chang et al., 1994).

As a positive control to confirm the ability of CIP to dephosphorylate proteins, Akt protein phosphorylation was examined after resolution on 4-12% gels (Figure 16C). To induce Akt activating phosphorylation on Ser473, HCT116 cells were cultured in either complete media containing 10% FBS or serum-free media (0% FBS). After 24 hours, 100 nM insulin was added to culture medium and cells were incubated for 1 hour. Insulin stimulation was, in fact, known to trigger Akt hyperphosphorylation (Figure 16C, lanes 3 and 7; (Alessi et al., 1996)), with the extent of phosphorylation being enhanced if cells were deprived of serum (Figure 16C, lane 7, (Ching et al., 2010)). P-Akt corresponding bands were abolished after incubating lysates with CIP (Figure 16C; lanes 4 and 8), proving efficient dephosphorylation under these experimental conditions. Dephosphorylation was also visible in the total Akt blot (Figure 16C) with bands shifted to lower molecular weights following incubation with CIP (Figure 16C, lanes 2, 4, 6, and 8).

The same samples prepared for phosphorylated Akt detection were tested for TK1

expression, to possibly identify phosphorylated forms of TK1, highlighted by the decrease

in their signal following incubation with CIP. Figure 16D shows that the signal generated

by the TK1 antibody (QED Biosciences Inc.) was not specific enough, although there

appeared to be a decrease in the band intensity possibly corresponding to TK1 protein

(black arrow) following incubation with CIP (lanes 2 and 4).
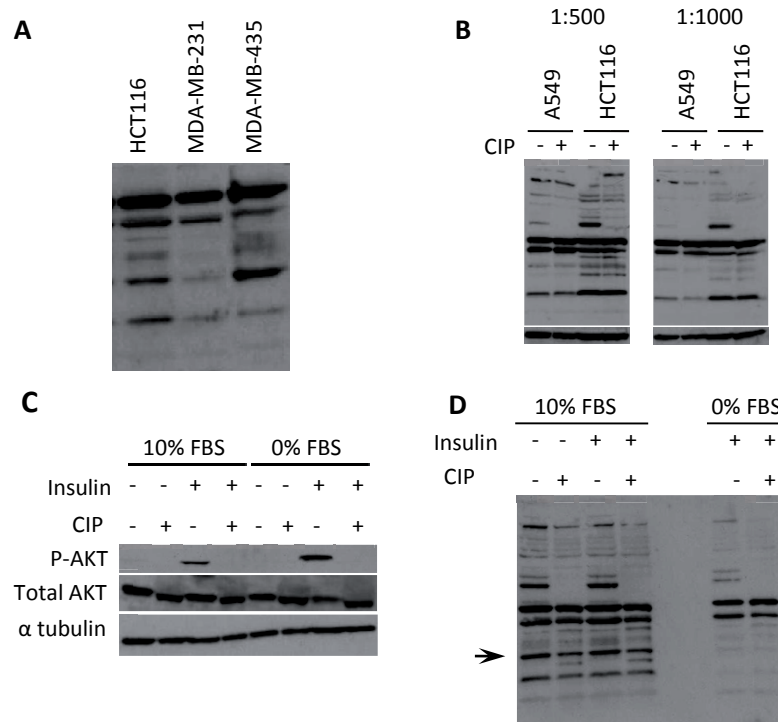
Figure 16. Detection of p-TK1 on reducing SDS-PAGE pre- and post-treatment with CIP.
A) TK1 protein expression. Cell lysates were run on SDS-PAGE and then probed with 1:500 antibody (QED Biosciences Inc.) dilution. B) QED Biosciences antibody optimization using 1:500 and 1:1000 dilutions. C) Positive control for CIP assay. Signal was detected using 1:1000 dilution of phospho-Akt rabbit antibody, 1:1000 dilution of Akt rabbit antibody, and 1:500 α tubulin mouse antibody. D) TK1 expression in HCT116 cells obtained as in C. TK1 was detected with 1:500 antibody (QED Biosciences Inc.) dilution. CIP, alkaline phosphatase.

A new antibody (Abcam) raised against recombinant full-length TK1 (as opposed to His-

tagged TK1 for the previous antibody) was tested (Figure 17) to evaluate possible

differential TK1 expression and phosphorylation. It showed higher specificity compared

to the previous one (Figure 16A). Three bands corresponding to molecular weights ~25

kDa, ~27 kDa and ~50 kDa, as judged by molecular weight markers run in parallel, were

observed, probably corresponding to the unphosphorylated TK1 monomer,

phosphorylated monomer and unphosphorylated/phosphorylated dimer, respectively. Furthermore, TK1 appeared to be more expressed in A549 and HCT116 cells, compared to MDA-MB-231 and MDA-MB-435S cells (both breast cancer cell lines). However, it was not possible to appreciate any difference in TK1 phosphorylation, even after treatment by CIP.
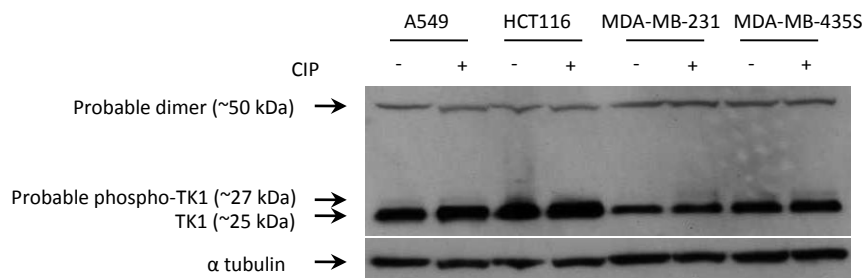
Figure 17. Western blot of TK1 protein as assessed by a specific anti-TK1 antibody.
Proteins from A549, HCT116, MDA-MB-231 and MDA-MB-435 cell lysates, untreated or pre-treated with CIP, were separated on 12% gels and probed with 1:500 dilution of anti-TK1 antibody (Abcam). A-tubulin was used as loading control. CIP, alkaline phosphatase.

The next set of studies attempted to reveal any differences in phosphorylation following anti-mitosis drug treatment.

Nocodazole was used as cell cycle arresting agent to induce mitotic arrest: its ability to induce G2/M arrest is caused by disruption of microtubules dynamics via binding to tubulin subunits, preventing their assembly to form tubulin filaments (De Brabander et al., 1976). This effect is responsible for disrupting the formation of a functional mitotic spindle. The working concentration of 0.5 µg/ml (equivalent to 1.7 µM) used for each cell line was suggested by Chang and co-workers (Chang et al., 1998), to induce Ser13 phosphorylation following G2/M arrest.

5-fluorouracil (5-FU) is a fluoropyrimidine widely used in the treatment of several cancers (Longley et al., 2003). It is a uracil analogue where the hydrogen atom in the C-5 position is substituted by a fluorine atom. It inhibits thymidylate synthase (TS), the enzyme

responsible for *de novo* production of thymidine monophosphate (Navalgund et al., 1980), thus preventing thymidylate supply, triggering deoxynucleotide imbalance, which is responsible for the disruption of DNA synthesis and repair, inducing therefore DNA damage, as well as RNA misincorporation (Longley et al., 2003). 5-FU at 100 µg/ml (0.77 mM) was used to examine differential TK1 phosphorylation (Yau et al., 2006).

cis-Dichlorodiammineplatinum(II), known as cisplatin, is another chemotherapeutic drug used in the treatment of various cancers (Niibe et al., 2004, Lesnock et al., 2013, Munoz et al., 2007). Its cytotoxicity in proliferating cells depends on the induction of cell cycle arrest by interacting with the DNA strands, thus forming inter- and intra-strand cross-links, arresting cell cycle in mitosis, and finally triggering apoptosis (Siddik, 2003). It also interacts with multiple subcellular targets, inducing cell death via apoptosis or necrosis, being the basis of its side-toxicity (Sancho-Martinez et al., 2012). Cisplatin treatment was conducted for 24 hours at a concentration of 100 µM (Nguyen et al., 2009).

Following drug treatments, cell lysates were pre-treated with CIP, increasing the incubation time, as suggested by He and co-workers (He et al., 1996). As shown in Figure 18A, TK1 signal seemed to be more intense in nocodazole treated samples (lanes 3 and 4). However, while Akt (positive control) showed dephosphorylation (Figure 18B), this was not observed with TK1 protein (Figure 18A). Furthermore, it appeared that the putative phosphorylated form of TK1 was predominant. The alternative explanation could be that the predominant band referred to total TK1, with the lower signal being non-specific signal generated by the antibody used.
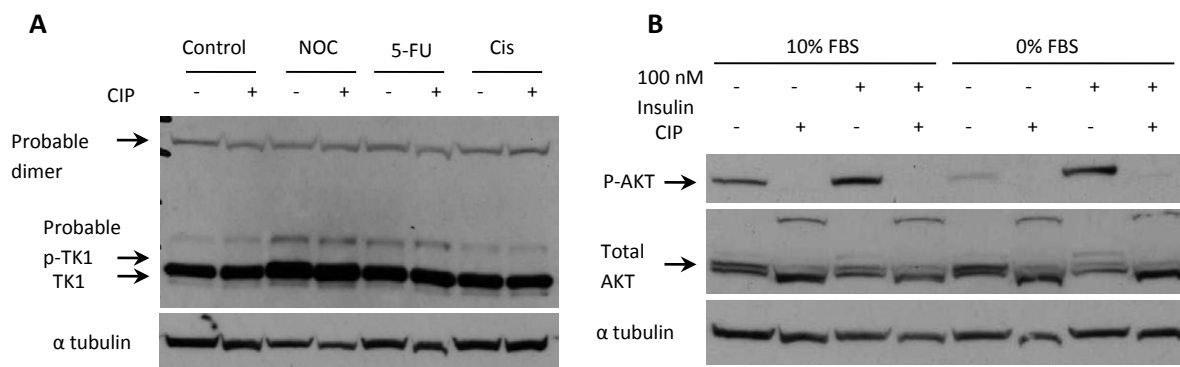
Figure 18. Western blot analysis of TK1 expression following drug treatment and dephosphorylation by alkaline phosphatase.
HCT116 were treated with the indicated drugs for 24h. Proteins from HCT116 cell lysates were incubated with alkaline phosphatase for 3h and separated on 12% SDS-PAGEs. A) TK1 protein was visualised after incubation with 1:500 anti-TK1 antibody (Abcam). B) Akt dephosporylation as a control for dephosphorylation by CIP. NOC, 0.5 μ/ml nocodazole; 5-FU, 100 μg/ml 5-fluorouracil; Cis, 100 μM cisplatin; CIP, alkaline phosphatase.

In conclusion, these studies showed that standard SDS-PAGE had poor resolving power and inability to discriminate different phosphorylated forms of TK1. A different technique was then optimised to identify TK1 phosphorylated isoforms.

b) Phos-tag™ SDS-PAGE

No specific antibodies recognising phospho-TK1 were available on the market; therefore an alternative method to determine the existence of phosphorylated forms of TK1, was needed.

Phos-tag™ acrylamide gel (Kinoshita et al., 2006) consists of a modified SDS-PAGE in which the acrylamide-pendant $MnCl_2$-Phos-tag™ ligand (a dinuclear manganese complex) provides mobility shift detection of phosphorylated proteins by interacting with the phosphates present on a protein via reversible phosphate binding, thus delaying migration through the gel (Figure 19).
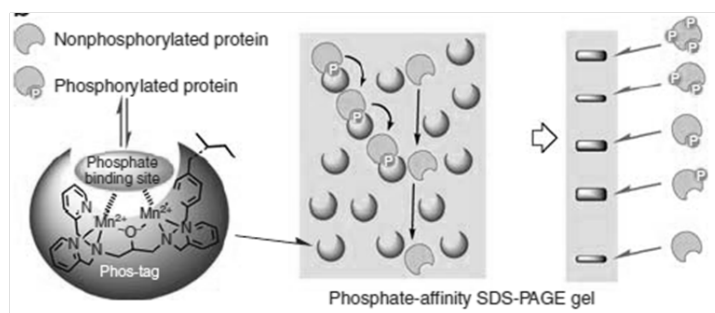
Figure 19. Schematic representation of the principle for the $MnCl_2$-phos-tag™ SDS-PAGE.
The $MnCl_2$-phos-tag™ is interspersed in the acrylamide gel and can therefore interact with phosphorylated proteins, thus separating them from the non-phosphorylated isotypes. Phosphorylated proteins are visualised on the gel as slower migrating bands in comparison to the non-phosphorylated forms (Kinoshita et al., 2009).

Phos-tag™ ligand was initially provided by Mr Chirag Patel from Dr Ramon Vilar's lab (Department of Chemistry, South Kensington Campus), and subsequently purchased from Wako Chemicals GmbH.

Optimisation was carried out to identify the gel composition which was best resolving TK1 isoforms, in terms of acrylamide and phos-tag™ type and concentration. Table 2 summarises the different conditions trialled, before achieving best resolution and good reproducibility with 12% acrylamide gels containing 75 µM $MnCl_2$-phos-tag™ (highlighted in bold). This setting was used for all subsequent studies.

Table 2. Summary of phos-tag™ optimisation using different conditions.

Type of gel	Composition	Outcome
MnCl$_2$-phos-tag™	12% acrylamide 100 µM phos-tag™	Poor resolution.
	12% acrylamide 200 µM phos-tag™	Poor resolution.
	10% acrylamide 150 µM phos-tag™	Good resolution. Not reproducible.
	15% acrylamide 150 µM phos-tag™	Reduced resolution. Long resolving time.
	12% acrylamide 75 µM phos-tag™	**Good resolution. Reproducible.**
ZnCl$_2$-phos-tag™	12% acrylamide 50 µM phos-tag™	Good resolution. Not reproducible.

Figure 20 represents HCT116 samples resolved on 12% acrylamide gels containing 75 µM MnCl$_2$-phos-tag™. Two isoforms of TK1 were resolved in control samples (lanes 1 and 2), and 3 isoforms in nocodazole-treated samples (lane 3). The two bands at the bottom were defined as band #1, running at the lowest molecular weight, and band #2 at slightly higher molecular weight. Band #3 definition was used hereon to refer to the G2/M-specific signal. This proved to be a phosphorylated form of TK1, since the signal was abolished after incubation with CIP (lane 4). Interestingly, the band #2 signal increased following nocodazole treatment, and remained unchanged in control and NOC-treated sample after incubation with CIP (lanes 2 and 4).

As proof of concept, proteins were resolved on standard 12% SDS-PAGE, demonstrating that the separation of TK1 isoforms was only achieved on gels containing phos-tag™.
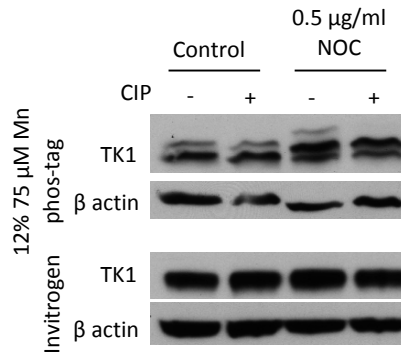
Figure 20. Multiple TK1 bands were resolved on MnCl₂-phos-tag™ gels.
HCT116 cells were treated with 0.5 μg/ml nocodazole for 24h. Prior to SDS-PAGE, HCT116 lysates were incubated with CIP for 1h. Top two panels represent resolution on 12% acrylamide + 75 μM MnCl₂-phos-tag™ gel. Bottom panels show protein detection on standard 12% SDS-PAGE. CIP, alkaline phosphatase; NOC, nocodazole.

In conclusion, 12% acrylamide gels containing 75 μM MnCl2-phos-tag™ proved to be useful to resolve 3 TK1 isoforms, one of which represented a phosphorylated species, specifically induced upon G2/M arrest with nocodazole.

c) Immunoprecipitation (IP)

As well as optimizing the phos-tag™ gel technique, immunoprecipitation was employed to attempt the isolation of phosphorylated forms of TK1 (Figure 21). 500 µg of HCT116 lysates were subjected to immunoprecipitation using phospho-serine antibody, run on a 12% pre-cast gel and then probed with 1:500 anti-TK1 antibody. Both control and lysates subjected to CIP treatment were loaded, as well as non-IP lysates (input) and lysates incubated with IgG control to account for non-specific interactions with the antibody. Results reported in Figure 21 suggested that more TK1 signal was present in control samples before dephosphorylation by CIP, although the opposite scenario emerged after treatment with nocodazole. However, no cross-linking of the antibody to the beads was performed, therefore it was difficult to interpret the results, given that the molecular weight of the light chain of the antibody run at the same level as TK1 protein (25kDa), rendering it difficult to appropriately quantify protein expression and changes in phosphorylation profile.
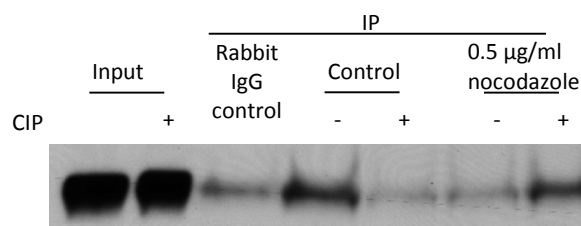
Figure 21. Detection of p-TK1 after immunoprecipitation of HCT116 cell lysates with p-Ser antibody.
HCT116 cells were treated with 0.5 µg/ml nocodazole for 24h. Cells were subsequently lysed, with aliquots being treated with CIP. Input indicates 30 µg of non-treated HCT116 cell lysates, either non-incubated or pre-treated with CIP. IP, immunoprecipitation; CIP, alkaline phosphatase.

At the same time, in the attempt to visualise TK1 changes in phosphorylation status, HCT116 cells were treated with 0.5 µg/ml nocodazole over a time course (Figure 22). Due to background generated from IgG control, it was not possible to clearly distinguish between background and actual TK1 signal, but the results shown in Figure 22 suggested

that there was already an increase in putative TK1 phosphorylation after 4 hours of

nocodazole treatment, with phosphorylation levels remaining constant until 8 hours, and

slightly increasing following overnight (O/N) and 24 hours treatments.
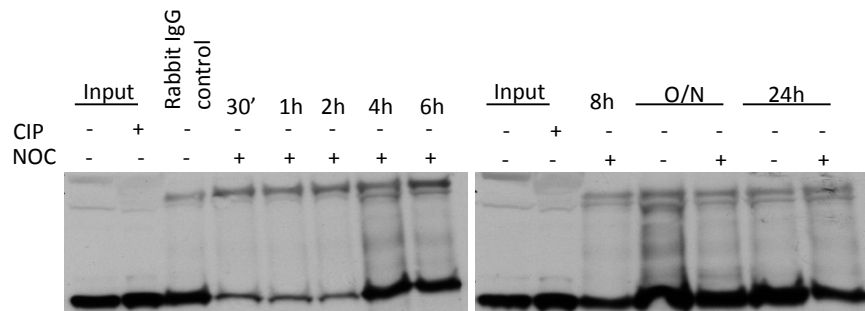
Figure 22. Immunoprecipitation of p-TK1 after time-course with 0.5 μg/ml nocodazole (NOC).
HCT116 cells were treated with nocodazole over a time course. Aliquots of each cell lysate were incubated with CIP. Input indicates 30 μg of non-treated and non-IP HCT116 cell lysates, either non-incubated or pre-treated with CIP. Rabbit IgG control refers to lysates subjected to IP using a rabbit IgG instead of p-Ser during IP. CIP, alkaline phosphatase; NOC, nocodazole; O/N, overnight.

To appropriately quantify TK1 phosphorylation on serine residues, crosslinking of the

antibody to the beads should be carried out, since the separation of the antibody chains

on SDS-PAGE produced a band at 25 kDa corresponding to the light chain, which ran at

the same level as TK1 protein. However, immunoprecipitation under the described

conditions could only suggest the existence of phosphorylated serine residues and the

time at which phosphorylation increased. Alternative methods should be used to

determine specific protein phosphorylation.

d) Iso-Electric Focusing (IEF)

It would have been valuable to validate the hypothesis of the existence of several TK1 phosphorylated isoforms using new available techniques. In collaboration with Dr Paul Clarke from the Division of Cancer Therapeutics at the Institute of Cancer Research (ICR, Sutton, UK), preliminary experiments were performed exploiting isoelectric focusing (IEF; (O'Neill et al., 2006)). This quantitative technique allows the separation of proteins according to their isoelectric point (pI), the pH at which a molecule has no net charge. The experiment was conducted in an automated system in which proteins ran in capillaries and migrated through a pH gradient until they reached their pI value (Figure 23; (Fan et al., 2009)), at which point they were cross-linked to the capillaries and probed with antibodies. The final results consisted of graphs showing the chemiluminescence signal measured at each pH for a specific sample probed with the antibody of interest (Figure 24), with peaks indicating the pH at which the protein was detected. In the case of phosphorylated proteins, the phosphate groups add negative charges to the protein, thus changing the overall charge of the molecule, and therefore causing a shift in the signal when compared to the one produced by non-phosphorylated forms of the same protein.
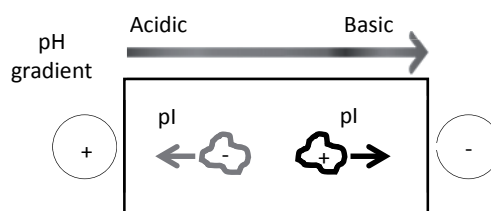
Figure 23. Schematic representation of isoelectric focusing principles.
Positively or negatively charged molecules migrate in a pH gradient, created in a capillary, towards the anode (-) or the cathode (+), respectively, until they reach their isoelectric point (pI) at which they stabilize, not having any net charge. The resolved molecules are then cross-linked to the capillary walls, becoming immobilized after separation, and probed with a specific antibody. Chemiluminescence reagents are used to detect the protein-antibody immobilized complexes, and the signal is detected by a CCD camera.

Figure 24 shows representative results obtained from a preliminary experiment, in which HCT116, A549 and Ost TK1⁻ cell lysates were prepared. An aliquot of each sample was incubated with lambda phosphatase (LPP). Lysates were then resolved via IEF.

Eukaryotic translation initiation factor 4E (eIF4E; (Rychlik et al., 1987)), an mRNA cap-binding protein, was used as a positive control for phosphorylation/dephosphorylation (Lachance et al., 2002). As shown in Figure 24A, A549 cells presented two peaks: one around pH 6.0, and the second one shifted to more acidic pH, an indication of phosphorylation (blue line, black arrow). Following incubation with lambda phosphatase (red line), the phosphorylation peak was abolished, demonstrating that the assay was inducing protein dephosphorylation. Negative control containing only phosphatase buffer with lambda phosphatase enzyme showed no background signal or artifacts (green line).

Figure 24B exemplifies the results obtained by probing IEF-separated lysates with Abcam TK1 antibody. Ost TK1⁻ cells showed high background (red line), and it was not possible to distinguish specific peaks in A549 lysates (left panel, blue line). Furthermore, there was no difference between A549 and Ost TK1⁻ even after lambda phosphatase treatment (right panel), suggesting that the antibody was not suitable for the technique. The situation did not improve with the QED Biosciences antibody (Figure 24C).
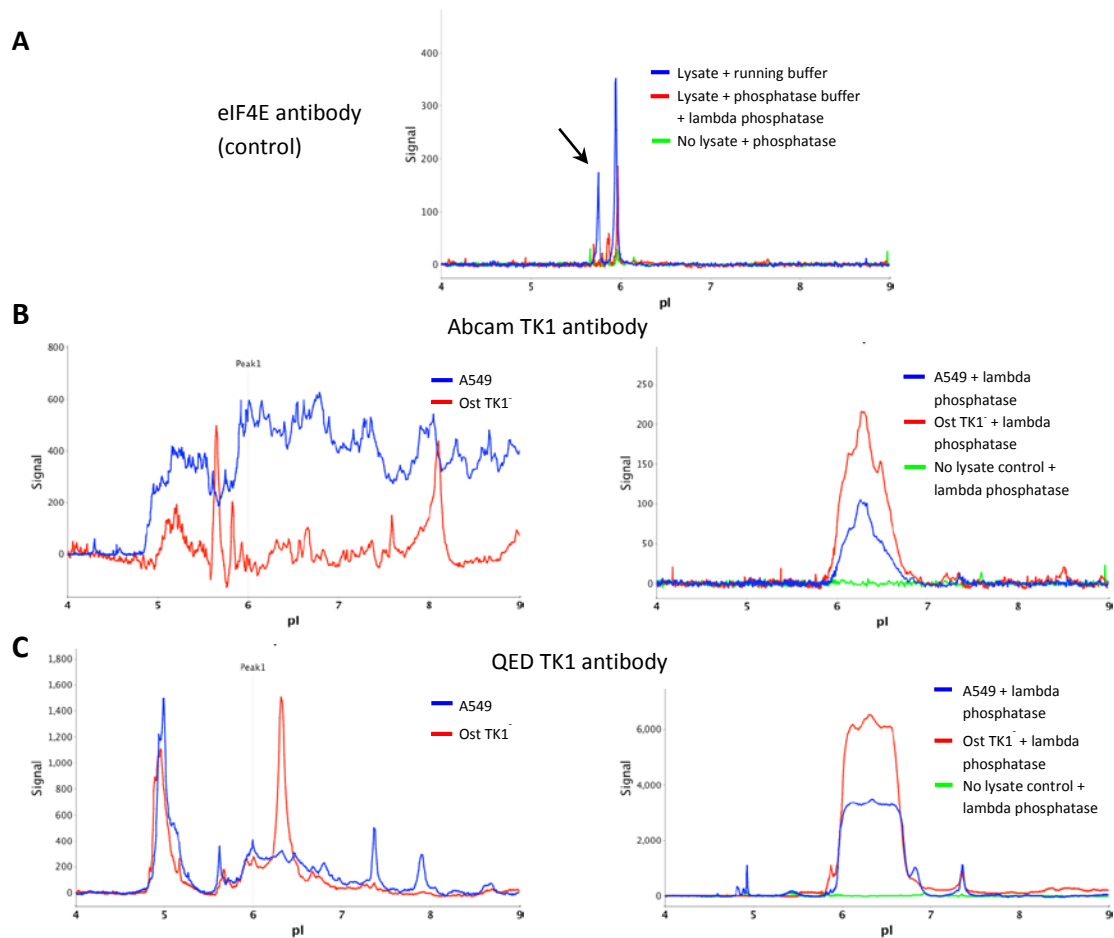
Figure 24. Iso-electric focusing (IEF) of A549 and Ost TK1⁻ cells before and after treatment with lambda phosphatase. 500,000 A549 and Ost TK1⁻ cells were seeded into 10 cm dishes. A) A549 cell lysates were subjected to IEF and subsequently probed for eIF4E protein (positive control). B) A549 and Ost TK1⁻ cell lysates were separated according to their pI and then probed for TK1 using the Abcam antibody. C) Detection of TK1 in A549 (blue) and Ost TK1⁻ (red) cells with QED Biosciences antibody.

Having a pI at pH 8.85, the TK1 signal was expected between pH 8 and 9, as predicted on

Scansite (Obenauer et al., 2003). The website also suggested that the peak would have

shifted to lower pH with addition of phosphate groups to the protein.

Unfortunately, the antibodies used to carry out these experiments did not seem to be

suitable for the technique. Testing different antibodies could help identifying TK1

phosphorylated forms.

3.1.2 Cell lines characterisation of salvage vs *de novo* pathway for thymidylate supply

TK1 expression and post-translational regulation by phosphorylation are not the only mechanisms involved in the modulation of the overall FLT signal accumulated in tumours following PET imaging. Therefore the relative usage of *de novo* vs salvage pathway could be hypothesised to contribute to the radiotracer uptake.

The relative expression of TK1 and thymidylate synthase (TS), the enzyme responsible for the conversion of uracil monophosphate (dUMP) to thymidylate (dTMP) in the *de novo* pathway for thymidylate production, was investigated in HCT116, A549, Hos (human osteosarcoma cell line) and Ost TK1$^-$ (TK1-deficient human osteosarcoma cell line), hypothesising that if cells, such as Ost TK1$^-$, lacked TK1, they could up-regulate TS in order to supply enough thymidylate during DNA replication. Amongst the four cell lines tested, HCT116 expressed significantly higher levels of TK1 compared to the other cell lines ($p<0.02$ in comparison to A549, $p<0.01$ vs Hos and $p<0.002$ vs Ost TK1$^-$), showing at least a 2-fold increase (Figure 25A, lane 1, and Figure 25B). A549 and Hos cells seemed to express comparable levels of TK1 (Figure 25A, lanes 2 and 3, respectively), although TS expression was elevated in Hos cells, which expressed double the amount of protein than HCT116 and A549 ($p<0.06$ and $p<0.04$, respectively). Higher levels of TS in the absence of TK1 were expected. Indeed, Ost TK1$^-$ cells seemed to express 3-fold higher levels of TS ($p<0.04$) compared to HCT116 and A549, with no significant difference compared to Hos cells.
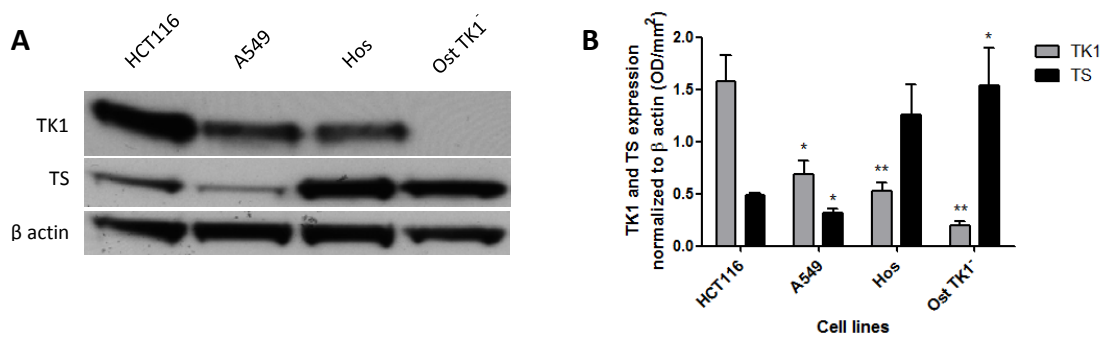
Figure 25. Thymidine kinase 1 (TK1) and thymidylate synthase (TS) expression in four cancer cell lines.
A) Representative western blot showing TK1 and TS expression in the four cell lines tested. B) Quantification of TK1 and TS expression normalized to β actin (n=3). Stars represent significant differences compared to HCT116.

The proliferation rates of the four cell lines tested were investigated to understand if the differential protein expression was correlated to the rate of cell proliferation. According to the results reported in Figure 26A, HCT116 showed faster proliferation rate (20 hours) compared to the other cell lines. A549 and Ost TK1⁻ cells exhibited similar proliferation rates, with 28 hours needed to duplicate for A549 and 27 hours for Ost Tk1⁻. However, there was imperfect correlation between cell proliferation and TK1 protein expression, as shown in Figure 26B.
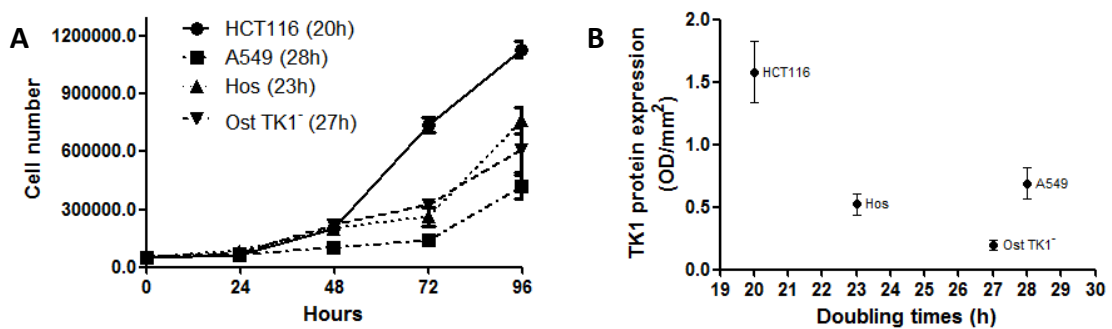
Figure 26. Comparison of HCT116, A549, Hos and Ost TK1⁻ cells doubling times and correlation with TK1 protein expression.
A) Representative growth rate and doubling times for the different cell lines. The same amount of cells for each cell line was seeded in triplicates (n=3). Cells were counted at each time point. Doubling time is indicated in brackets next to the cell line name, as calculated on http://www.doubling-time.com/compute.php?lang=en. B) Correlation plot between doubling times and TK1 expression.

In conclusion, these results confirmed HCT116 as a good model to study TK1 phosphorylation, given the expression of the protein at high levels. At the same time,

Ost TK1⁻ cells could be used to identify the phosphorylated amino-acid residues on TK1 protein, following transfections with expression plasmids encoding for TK1 variants (see paragraph 3.1.4).

Although there seemed to be an imperfect correlation between cell proliferation and TK1 expression, the enzyme regulation, achieved via post-translational regulation, e.g. phosphorylation, rather than its expression must be taken into account. This factor needs to be understood when correlating FLT uptake into tumours with TK1 expression.

3.1.3 Determination of TK1 phosphorylation profile

Having optimized a method to detect TK1 phosphorylated forms (MnCl$_2$-phos-tag™), the first challenge was to define if there was a distinctive phosphorylation profile of TK1 through the cell cycle. To determine the level of TK1 in each cell cycle phase, cells were arrested at specific stages with the aid of cell-cycle arresting agents.

To achieve accumulation in G0/G1, cells were grown in serum-free medium (0% FBS), generally for 24 hours. Aphidicolin, a DNA polymerase α and δ reversible inhibitor (Pedrali-Noy et al., 1980, Lee et al., 1985), was used to induce S phase arrest, blocking DNA polymerization. Treatment with nocodazole and paclitaxel (see below) caused G2/M phase arrest, following the impairment of microtubule dynamics, and therefore inhibition of mitotic spindle formation. Roscovitine, a cyclin-dependent kinase (CDK) inhibitor (Meijer et al., 1997), was also included to assess differences in TK1 phosphorylation.

To validate the effectiveness of nocodazole in inducing mitotic arrest, HCT116 cells were tested for their dose response to a range of concentrations after 24 hours treatment with the drug (Figure 27), as reported in literature (Long and Fairchild, 1994), and analysed for their DNA content on fluorescence-activated flow cytometry (FACS). HCT116 cells accumulated in G2/M at the lowest concentration used (0.04 μM, 82.8% of the cell population). G2/M arrest reached maximum levels at 1.2 μM, with 88% of cells accumulated in this phase of the cell cycle.
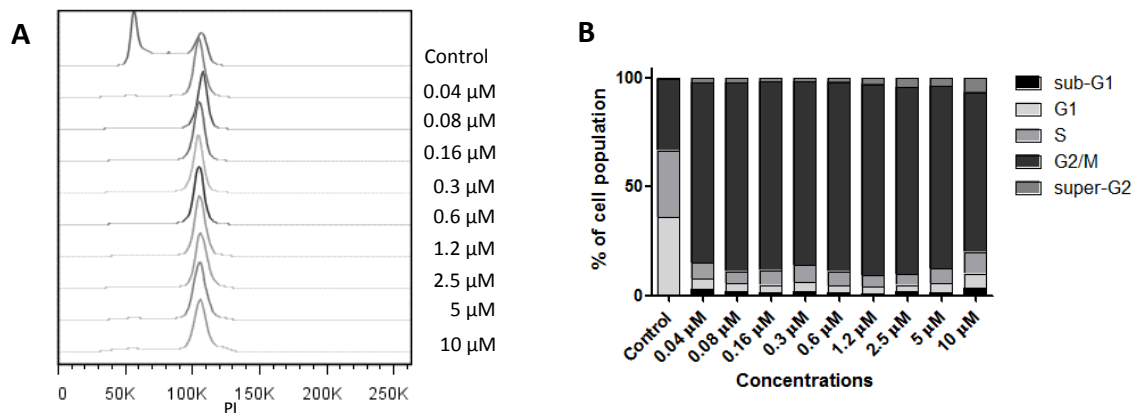
Figure 27. Cell cycle distribution of HCT116 cells after treatment with the indicated nocodazole concentrations for 24h.
A) Representative graph of cell cycle distribution after analysis of DNA content. PI, propidium iodide. B) Graph representing the percentages of cells in each phase of the cell cycle. Sub-G1, cell death; super-G2, possible endoreduplication.

G2/M arrest was also induced by treatment with paclitaxel (Taxol®), a drug that was known for its anticancer activity (Belotti et al., 1996, Rowinsky and Donehower, 1995), in order to carry out future *in vivo* experiments. Paclitaxel promotes the polymerization of tubulin by interacting with microtubule filaments, thus interfering with the microtubule dynamic instability (De Brabander et al., 1981, Manfredi et al., 1982, Schiff et al., 1979).

Preliminary experiments to assess the optimal concentration of paclitaxel to be used to treat HCT116 were performed, replicating the experiment described by Long and Fairchild in 1994 (Long and Fairchild, 1994). HCT116 cells were treated for 24h with a range of concentrations of paclitaxel and then analysed on FACS for their DNA content. As shown in Figure 28, there was increasing accumulation of cells in G2/M phase with increasing concentrations of the drug (from 30% of controls to 82% of 500 nM). Maximal accumulation (more than 80%) was reached with the highest concentrations (125, 250 and 500 nM). Intermediate concentrations (4-31 nM) seemed to produce elevated cell death compared to higher concentrations, possibly caused by paclitaxel effects on cell structure and motility, rather than microtubule dynamics (Rowinsky and Donehower, 1995, Jordan et al., 1993, Long and Fairchild, 1994).
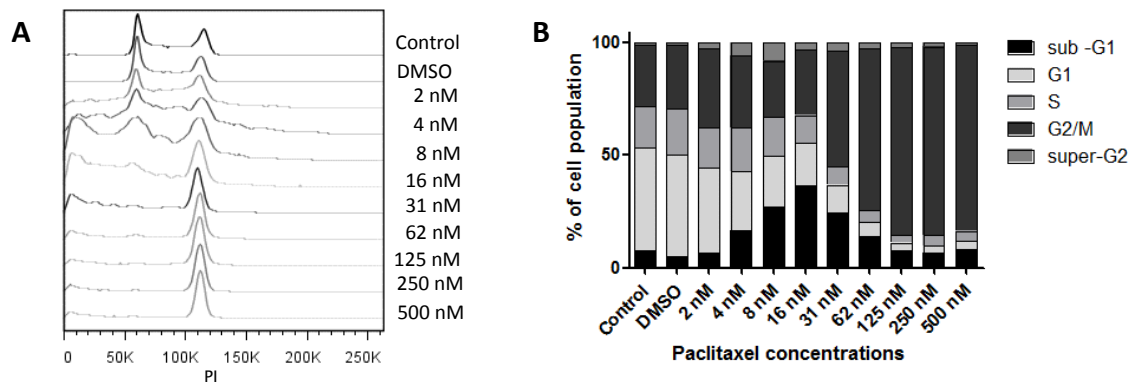
Figure 28. HCT116 dose response to paclitaxel treatment for 24h.
HCT116 cells were treated with indicated concentrations of paclitaxel (Long and Fairchild, 1994). A) Representative plots of cell cycle distribution after 24h treatment. PI, propidium iodide. B) Graph representing the relative percentages of cells accumulated in each phase of the cell cycle.

Paclitaxel concentrations of 125, 250, and 500 nM were subsequently used to treat HCT116 cells (Figure 29) to determine the working concentration for future experiments. According to these results, 250 nM paclitaxel was used for all future experiments with HCT116 cells, given that this concentration produced maximum G2/M arrest (86%) with low cell death (0.3%, as measured by percentage sub-G1 population).
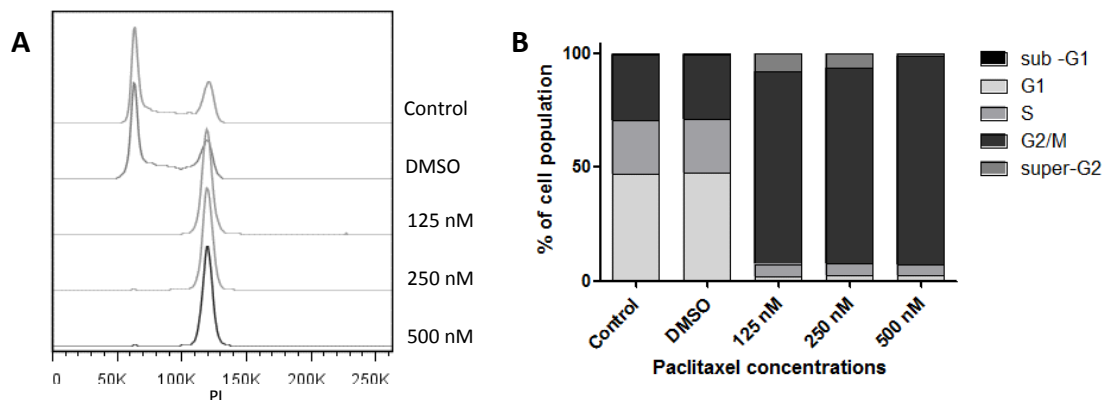
Figure 29. 24h paclitaxel treatment in HCT116 cells.
HCT116 cells were treated with indicated concentrations of paclitaxel for 24h. A) Plot representing the typical cell cycle distribution. PI, propidium iodide. B) The graph shows the relative accumulation in each phase of the cell cycle (percentages).

To test successful cell cycle arrest following treatment with the different agents, HCT116 were treated for 24 hours and analysed for DNA content via flow cytometry (Figure 30A). Normal distribution of cycling cells was detected in control and vehicle-control (DMSO) samples, with 50% of the population in G1, 20% in S and 20% in G2/M phase. Following

serum starvation, cell-cycle distribution showed prevalence of the G1 peak, with 68% of the cell population being accumulated at this stage. Aphidicolin-treatment resulted in an increase in the proportion of cells in S phase (51%). Both nocodazole and paclitaxel treatments induced accumulation in G2/M phase with 77% and 61% of cells in G2/M, respectively. Roscovitine treatment increased the sub-G1 population (57%), indicating increasing cell death compared with controls. Lysates prepared from control and treated HCT116 cells were then run on 12% acrylamide gel additioned with 75 µM $MnCl_2$-phos-tag™. Two bands were clearly detectable in each sample (band #1 and band #2, Figure 30B), with band #1 being more abundant in control samples (lane 1 and 2) compared to band #2 (2-fold reduction). Consistent with literature, total TK1 expression was low in serum starved cells (G1 enriched; lane 3; 50% reduction), and increased in aphidicolin-treated cells (S-phase enriched; lane 4), where both TK1 isoforms were overexpressed when compared to controls and different treatments (3-fold increase compared to control, 2.5-fold increase compared to nocodazole and paclitaxel); phosphorylation (band #3) was specifically induced upon nocodazole and paclitaxel treatment. Inhibition of CDKs by roscovitine was responsible for 60% reduction in the signal corresponding to band #2 compared to control, thus suggesting that band #2 could represent a phosphorylated form of TK1 which was detected in each condition. It is possible to speculate that perhaps CIP could not efficiently dephosphorylate band #2 due to TK1 structure conformation, therefore preventing CIP to access the specific phosphorylation site to remove the phosphate.
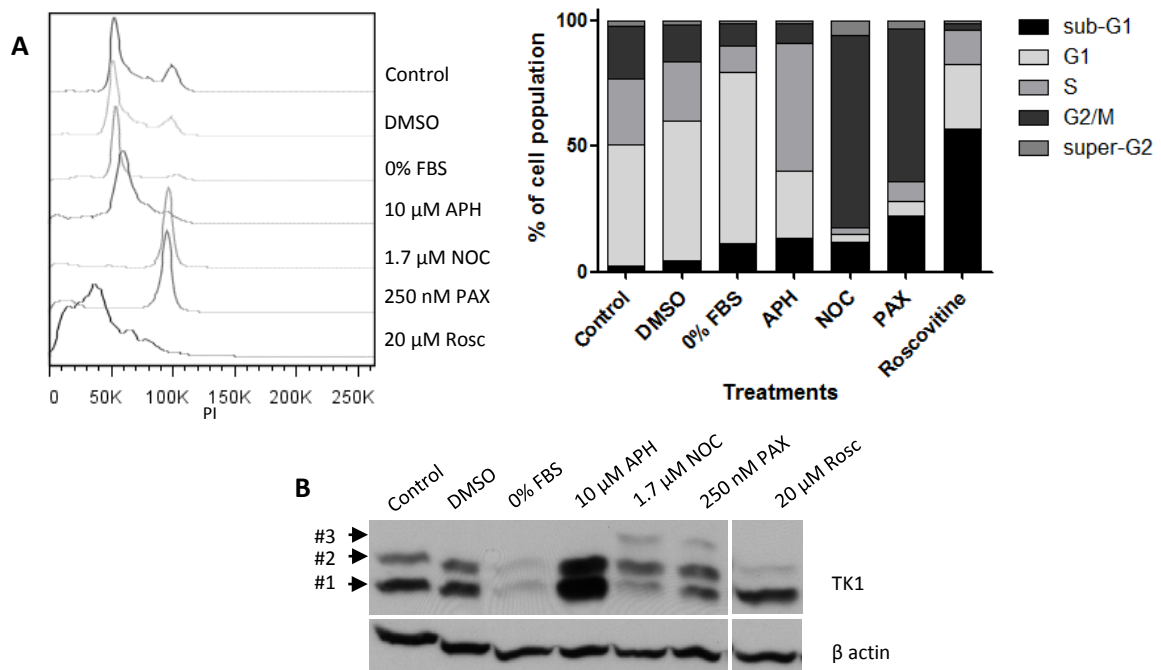
Figure 30. TK1 phosphorylation profile varies during cell cycle progression.
A) Cell cycle distribution of HCT116 cells after induction of cell cycle arrest with indicated drug concentrations for 24h. Left panel: representative plots of DNA content. Right panel: graph representing the percentages of cells accumulated in each phase of the cell cycle. B) HCT116 lysates, obtained after 24h treatment with the indicated drugs, were resolved on a 12% acrylamide gel containing 75 µM MnCl$_2$-phos-tag™. APH, aphidicolin; NOC, nocodazole; PAX, paclitaxel; Rosc, roscovitine; PI, propidium iodide.

Overnight treatment (Figure 31A) appeared to be sufficient to induce cell cycle arrest. Western blot analysis of samples in the same conditions (Figure 31B) showed very similar results to Figure 30B, with band #1, #2 and #3 presenting the same pattern. Again, total TK1 expression was reduced during G1 and increased in S phase, with the induction of specific phosphorylation in G2/M. Band #2 signal was reduced following roscovitine treatment for 4 hours, as previously discussed, without having effects on cell cycle distribution.
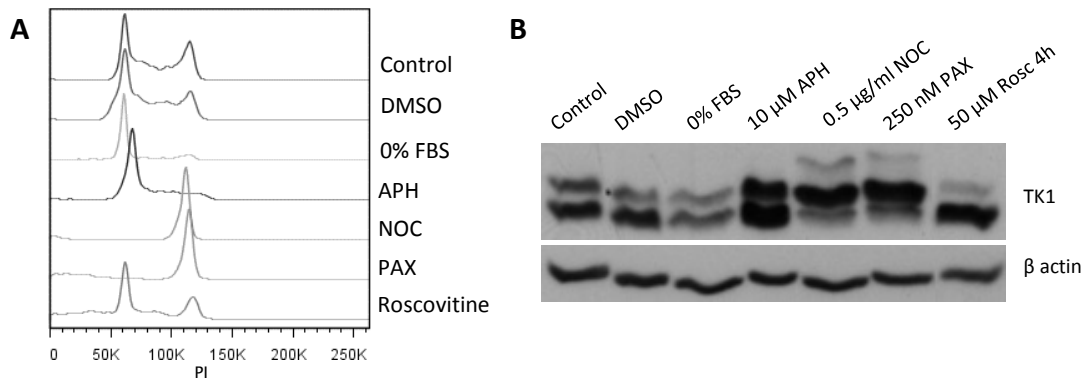
Figure 31. TK1 phosphorylation profile in HCT116 cells after overnight treatment with the indicated drugs.
Roscovitine treatment was performed for 4 hours. A) Cell cycle distribution according to DNA content. B) 12% SDS-PAGE containing 75 µM MnCl$_2$-phos-tag™. APH, aphidicolin; NOC, nocodazole; PAX, paclitaxel; Rosc, roscovitine; PI, propidium iodide.

Studies with synchronised HCT116 cells were subsequently carried out, in order to validate the presence of additional TK1 isoforms, possibly present in trace amounts. Cell synchronization was achieved by serum starvation for 24 hours, followed by release in fresh complete media, containing nocodazole or paclitaxel as required. After 18 (overnight, O/N), 24 or 48 hours, cells were subjected to western blot analysis or flow cytometry measurements. Figure 32A represents TK1 profile resolved on MnCl$_2$-phos-tag™ gel. Each sample showed the already discussed pattern of band (bands #1, #2 and #3), with the addition of an extra signal appearing following nocodazole and paclitaxel treatment (white arrows). Overall TK1 intensity was increased after treatment for 24 hours (Figure 32A, lane 5 and 6), whereas it was clearly decreased after 48 hours treatment (lane 7-9). Measurement of DNA content via flow cytometry (Figure 32B) showed progressive increase in G2/M accumulation after overnight and 24 hours treatment with nocodazole (74% and 87%, respectively). Paclitaxel increased the cell abundance in G2/M phase, already seen after overnight treatment, with 77% of the analysed cells accumulated in G2/M. Increase in cell death (suggested by the sub-G1 portion of the population) was observed following nocodazole (47%) and paclitaxel (65%) treatment for 48 hours. Even on western blots it was possible to detect a clear decrease in TK1 protein after 48 hours,

suggesting that either cells stopped cycling or were undergoing cell death. The decrease in TK1 protein expression 48 hours from release in fresh media corresponded to G0/G1 arrest due to contact inhibition due high cell density, as highlighted in Figure 32B (79% of the population accumulated in G1). Standard cell cycle distribution, with the highest peak (2N) referring to cells cycling through G1 phase (59%) and the small one (4N) representing cells in G2/M (20%), was achieved in untreated cells after 24 hours from release from serum starvation.

In conclusion, two G2/M-specific bands were induced after cell synchronization and treatment with nocodazole and paclitaxel, suggesting the existence of 3 phosphorylated forms of TK1 in HCT116: band #2, band #3 and the extra band visualised in synchronised cells (band #4).
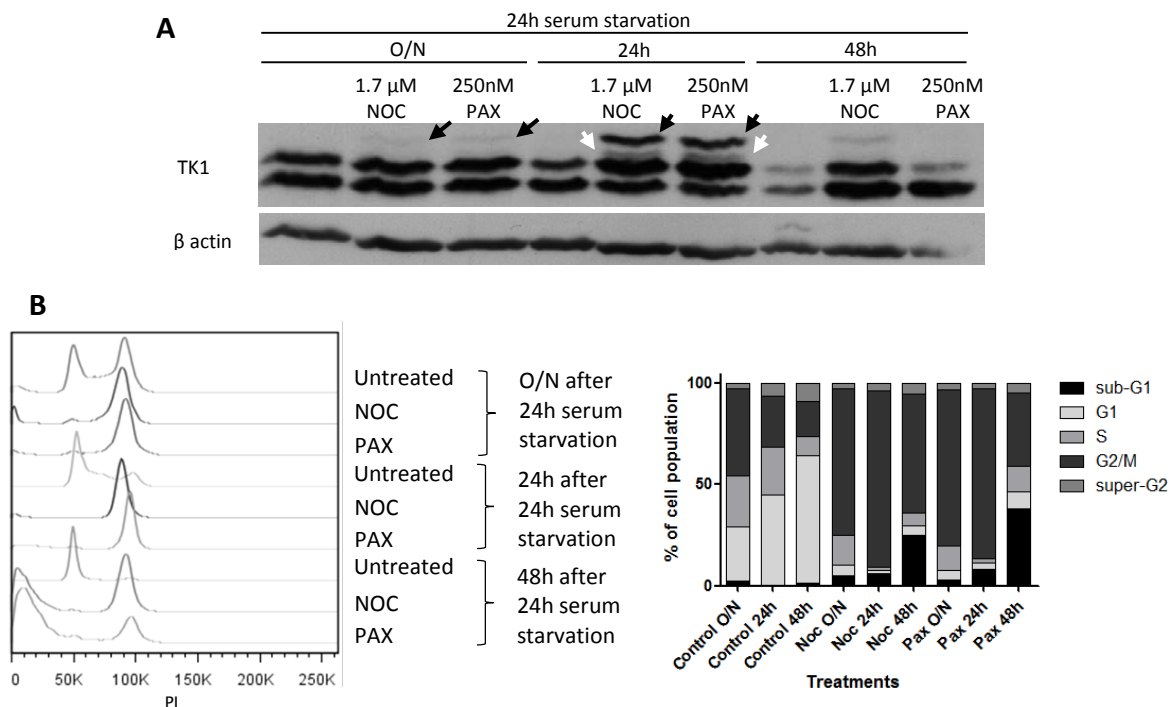
Figure 32. TK1 phosphorylation profile in synchronized HCT116 cells.
A) Representative resolution of TK1 phosphorylated isoforms on 12% acrylamide + 75 µM $MnCl_2$-phos-tag™ after cell synchronisation. Black and white arrows indicate G2/M specific bands. B) Representative cell cycle analysis of DNA content. Right panel: plots representing cellular DNA content. Left panel: analysis of the percentage of cells accumulated in each phase of the cell cycle. O/N, overnight; NOC, nocodazole; PAX, paclitaxel; PI, propidium iodide.

To determine whether or not these results could be generalised to other cell cycle phase-specific anticancer treatments, HCT116 cells were treated with 100 µM cisplatin, 100 µg/ml 5-FU or 5 µM PD0325901, a mitogenic extracellular kinase 1/2 (MEK 1/2) inhibitor (Solit et al., 2006, Sebolt-Leopold and Herrera, 2004) for 24 hours (Figure 33). Appreciating that there may be non-specific effects on signalling, 100 µM staurosporine, a CDKs inhibitor which prevents binding of ATP to the kinase (Gadbois et al., 1992), was also tested to further validate the hypothesis that band #2 represented a phosphorylated form of the protein (Figure 33B). Controls (control and DMSO; Figure 33B, lane 1 and 2), serum starved samples and treatments with aphidicolin, nocodazole, paclitaxel and roscovitine showed the same results reported in previous experiments. Specifically, G1 arrest resulted in 80% reduction of the overall TK1 signal compared to control; S phase accumulation produced a 1.5-fold increase compared to control; and nocodazole and paclitaxel treatments induced band #3 together with an overall 1.5-fold increase in TK1 expression. Treatment with PD0325901 induced G0/G1 arrest (as shown in Figure 33A), therefore TK1 protein was hardly detectable after resolution on $MnCl_2$-phos-tag™ gel (Figure 33B, lane 9; 90% decrease in overall protein expression). Cisplatin and 5-FU treatments presented the two bands identified in control samples (band #1 and #2; Figure 33B, lane 7 and 8), suggesting no specific modification of TK1, even though both treatments showed prevalence of band #1 (non-phosphorylated TK1) over #2 (phosphorylated form), specifically cisplatin.

Finally, the staurosporine concentration used in this experiment caused extensive cell death (Figure 33A), nonetheless it seemed to suggest that band #2 was reduced to 15% (Figure 33B, lane 11) compared to control samples (lane 1 and 2), where band #1 and #2

were expressed at the same level; this result is comparable to the result showed by roscovitine treatment (lane 10; 40% reduction).
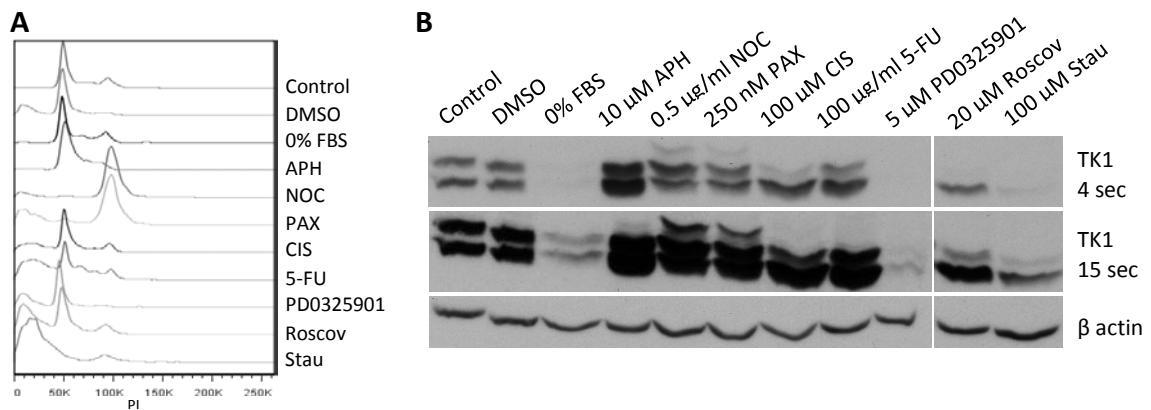
Figure 33. Cell cycle distribution and TK1 phosphorylation profile in HCT116 cells treated for 24h with cell-cycle arresting agents and anti-cancer drugs.
A) Representative cell cycle distribution following treatments for 24h. PI, propidium iodide. B) Representative resolution of p-TK1 on a 12% acrylamide + 75 μM MnCl$_2$-phos-tag gel. APH, aphidicolin; NOC, nocodazole; PAX, paclitaxel; CIS, cisplatin; 5-FU, 5-fluorouracil; Roscov, roscovitine; Stau, staurosporine.

In conclusion, the presence of different bands representing TK1 isoforms during the progression of the cell cycle was demonstrated:

- Band #1: unphosphorylated TK1, ubiquitous;

- Band #2: phosphorylated, inhibited by CDK inhibitors, but not sensitive to CIP, ubiquitous;

- Band #3: phosphorylated, induced upon nocodazole and paclitaxel treatment (synchronous or asynchronous cells) and sensitive to CIP;

- Band #4: phosphorylated, induced upon nocodazole and paclitaxel treatment (synchronised cells only due to possible low abundance), present in trace amounts.

Experiments to identify the specific amino-acid residues phosphorylated on TK1 protein and to determine the kinase responsible for TK1 phosphorylation were subsequently performed.

3.1.4 Identification of the phosphorylated amino-acid residues

Phos-tag™ gels allowed resolution of 4 bands representing TK1 and its phosphorylated species, named as band #1, #2, #3 and #4. However, the specific amino acid residues generating the different phosphorylated bands needed to be identified. Ost TK1⁻ cells, lacking endogenous TK1 expression (but still capable of undergoing proliferation via the *de novo* pathway – paragraph 3.1.2), were transiently transfected with FLAG-pCMV2 plasmid vectors encoding wild-type (WT), S13A, S13D or S231A substitutions on Δmet TK1 cDNA sequence.
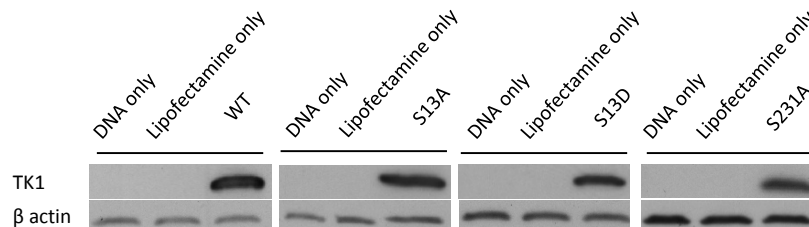
Figure 34. Transient transfections of Ost TK1⁻ cells with FLAG-pCMV2 plasmids encoding wild-type (WT), S13A, S13D or S231A Δmet TK1 cDNA sequence.
10 µg of proteins were resolved on a 12% NuPAGE gel. Transfections with DNA only (without adding Lipofectamine™ 2000) and Lipofectamine™ 2000 only (without adding plasmid DNA) were used as control to verify successful transfection.

Figure 34 shows expression of TK1 in Ost TK1⁻ cells following transfections for 24 hours with the indicated constructs. There was no detectable TK1 expression in cells incubated with plasmid DNA without Lipofectamine™ or with Lipofectamine™ without DNA vector, which were used as controls.

Subsequently, Ost TK1⁻ transfections were treated with 0.5 µg/ml nocodazole overnight, after which they were lysed and run on phos-tag™ gels, to resolve TK1 phosphorylation and identify possible changes due to serine substitutions (Figure 35).
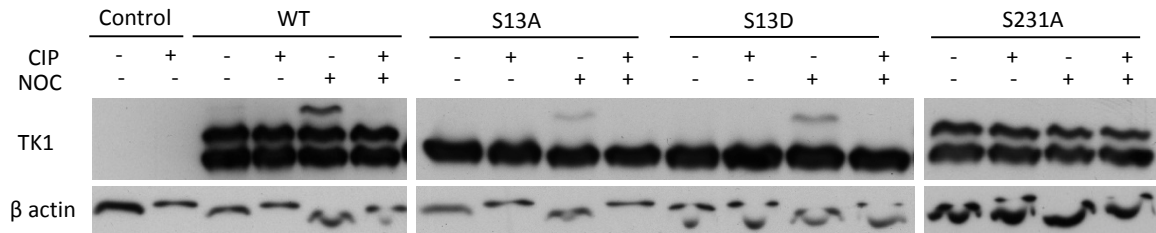
Figure 35. Identification of TK1 phospho-amino acids with transient transfections.
Ost TK1⁻ cells were transiently transfected with FLAG-pCMV2 vectors encoding wild-type (WT), S13A, S13D and S231A Δmet TK1 cDNA. 10 μg of proteins were resolved on 12% acrylamide + 75 μM $MnCl_2$-phos-tag™. CIP, alkaline phosphatase; NOC, nocodazole; Control, untransfected control; WT, wild-type.

Transfection with wild-type (WT) plasmid showed the usual TK1 phosphorylation profile (Figure 35), with non-phosphorylated band #1 and phosphorylated band #2 in each condition (lanes 3-6), and band #3 being induced following treatment with nocodazole (lane 5). This signal was then lost after incubation with CIP (lane 6). Transfection with Ser13 substituted by an alanine residue (S13A; alanine is not subjected to phosphorylation) or an aspartic acid (S13D; aspartic acid is not phosphorylated), resulted in the loss of band #2, with TK1 signal being reduced to a single band corresponding to non-phosphorylated TK1 (band #1; lanes 7-14). However, following nocodazole treatment the G2/M specific band (band #3, lanes 9 and 13) was induced, with CIP incubation confirming the band identity as a phosphorylated form (lanes 10 and 14). Expression of S231A (preventing phosphorylation at this site) showed two TK1 bands in each condition (band #1 and band #2; lanes 15-18), with no changes after G2/M arrest induced by nocodazole treatment (lanes 17 and 18). These results were in contrast to expectations. In fact, it had been demonstrated in TK1-deficient mouse fibroblasts and HeLa cells that Ser13 phosphorylation occurred specifically during mitosis (G2/M phase; (Chang et al., 1998, Ke et al., 2003)), but if that was the case, there should not have been induction of the G2/M specific signal (band #3) in S13A mutated cells. On the contrary, S231A substitution abolished the mitotic phosphorylation (band #3) and retained band #2,

suggesting that the latter corresponded to Ser13 phosphorylation and band #3 referred to Ser231 phosphorylation. The effects of these modifications on TK1 activity needed to be assessed in order to sustain our conclusions. Results are presented in Chapter 3.2.

Beta-actin resolution was compromised on pho-tag™ gels, possibly as a result of its interaction with gel components, due to the presence of charged groups on the protein.

3.1.5 CDK1 or CDK2?

Once TK1 phosphorylation profile had been determined, it became interesting to determine the kinase responsible for phosphorylating TK1, thus generating the different isoforms. Chang and co-workers suggested that either CDK2 or CDK1 (i.e. Cdc2) could phosphorylate the Ser13 residue (Chang et al., 1998). Starting from this, it was hypothesised that CDK2 could be involved in TK1 phosphorylation during S phase, whereas CDK1 could be responsible for the G2/M specific phosphorylation. Therefore, RNA interference (RNAi) experiments using CDK1 or CDK2 siRNA were performed in order to specifically knock-down the two kinases separately. CDK inhibitors such as roscovitine and staurosporine were not reliable for this purpose, as they are not specific for a unique CDK, but they inhibit several complexes.

Optimization was firstly performed to determine the siRNA concentration able to induce sufficient knock-down of the protein of interest (Figure 36). Both CDK1 and CDK2 were effectively silenced after transfection with 5 nM specific siRNA (Figure 36, lane 3 on both A and B; 80% reduction), whereas scramble siRNA did not have any significant effect on protein expression (lane 2).
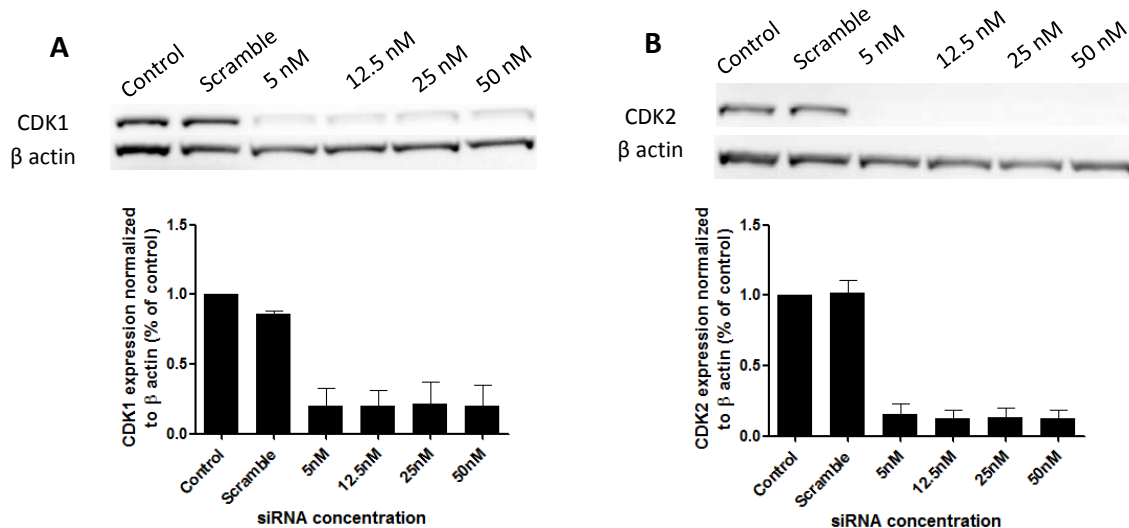
Figure 36. Optimization of CDK1 and CDK2 knock-down using RNA interference.
Indicated concentrations were used to induce protein silencing. 25 nM scramble siRNA was used as control (scramble). Upper panels show representative CDK1 (A) and CDK2 (B) protein expression after resolution on 12% NuPAGE gels and detection with specific antibodies. Lower panels represent the average values for CDK1 or CDK2 protein expression normalized to actin (n=3).

Therefore, HCT116 cells were transfected with 5 nM CDK1 or CDK2 siRNA for 48 hours and subsequently fed with fresh media containing 0.5 µg/ml nocodazole for another 18 hours (overnight). Protein lysates were then resolved on phos-tag™ gels to detect possible differences in TK1 phosphorylation profile (Figure 37). Effective knock-down was also determined by probing the same protein lysates for CDK1 and CDK2 protein expression. Indeed, 5 nM siRNA treatment effectively reduced CDK1 and CDK2 expression by 70% compared to both control and scramble control.

Interestingly, results reported in Figure 37 show the usual TK1 phosphorylation profile in control and scramble samples (lanes 1-4), with band #1 and #2 plus band #3 being induced following nocodazole treatment. Whilst band #1 and #2 were present in cells treated with CDK1 siRNA (lanes 5 and 6), there was no induction of band #3 by nocodazole (band #3; lane 6). CDK2 silencing showed a 40% reduction in band #2 in baseline condition compared to control (lane 7), although the signal generated by this band increased upon

nocodazole treatment, showing the same profile as control and scramble samples treated with nocodazole (lanes 2 and 4). In addition, band #3 was induced (lane 8).

These data suggested that CDK1 specifically phosphorylated TK1 during G2/M phase, in line with CDK1 period of action (Morgan, 1997). CDK2 knock-down seemed to have an effect on phosphorylation of band #2 only in asynchronised cells (no nocodazole treatment), with the signal coming from this form increasing after induction of G2/M arrest. This effect could be explained hypothesising that additional CDKs might have substituted CDK2 in its role of phosphorylating specific substrates (Merrick et al., 2011, Santamaria et al., 2007) or that additional residues (which could not be separated on phos- tag™ gels) were phosphorylated during G2/M. Further validation is required to confirm these results.
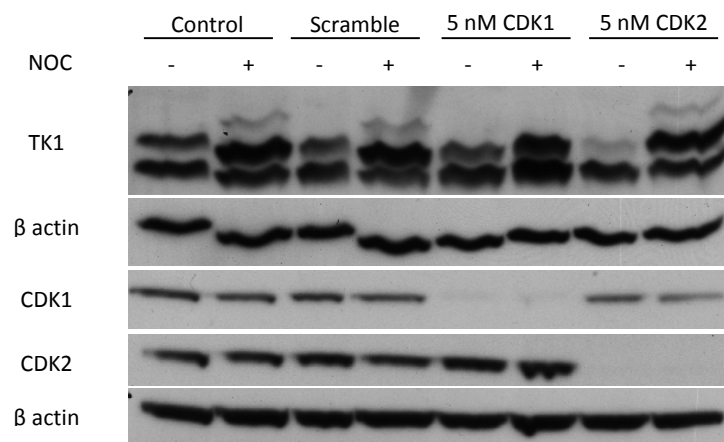
Figure 37. Effects of knock-down of CDK1 or CDK2 on TK1 protein phosphorylation.
Representative western blots showing TK1 phosphorylation profile (upper 2 panels) resolved on 12% acrylamide + 75 µM MnCl$_2$-phos-tag™ gel, and CDK1 and CDK2 expression following specific knock-down (proteins separated on 12% NuPAGE gels). HCT116 cells were transfected with 5 nM specific siRNA for 48h and then treated with nocodazole (NOC) to induce G2/M arrest overnight.

3.2 Role of thymidine kinase 1 phosphorylation in [^{18}F]FLT cell uptake *in vitro* and *in vivo*

3.2.1 Cell line comparison

Following the analysis of differential TK1 protein expression in HCT116, A549, Hos and Ost TK1$^-$ cells shown in Chapter 3.1.2 (Figure 25), [^{18}F]FLT cell uptake was assessed in the 4 cell lines to test if radiotracer uptake correlated with TK1 protein expression. [^{18}F]FLT retention, in fact, is dependent on the radiotracer phosphorylation to monophosphate via TK1.

Differences in [^{18}F]FLT cell uptake caused by differential expression of TK1 were assessed by measuring radiotracer uptake after 1 hour incubation with the radiotracer (Figure 38) to depict the activity of the thymidine salvage pathway.

Under control conditions, [^{18}F]FLT uptake was not significantly different between HCT116, A549 and Hos cells, even though HCT116 seemed to incorporate 30% more radiotracer than A549 and Hos cells. Ost TK1$^-$ cells were lacking TK1 protein expression, therefore radiotracer uptake was significantly decreased compared to HCT116 ($p < 0.01$). Furthermore, treatment with nocodazole (NOC) significantly reduced [^{18}F]FLT uptake in HCT116 cells ($p < 0.02$) as well as in A549 ($p < 0.001$) due to G2/M arrest, whereby TK1 activity is reduced following phosphorylation (Chang et al., 1998). There seemed to be a non-significant reduction also in Hos cells.

These findings confirmed HCT116 to be a good model to study TK1 protein phosphorylation and the effects on the uptake of radiotracers, which may be an indicator of proliferation; HCT116, in fact, showed higher expression of TK1 and high [^{18}F]FLT uptake. However, [^{18}F]FLT uptake was not directly proportional to the extent of TK1 protein expression, implying additional mechanisms regulating its uptake, such as TK1 regulation and additional parameters discussed in Chapter 1, section 1.4.5.
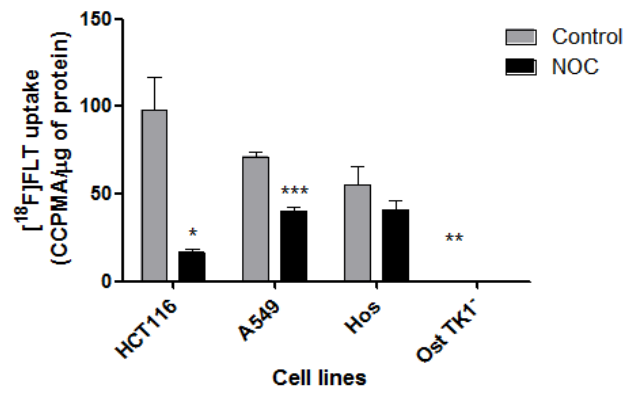
Figure 38. [^{18}F]FLT uptake in HCT116, A549, Hos and Ost TK1$^-$ cells.
Representative graph of 2 independent repeats (n=3 each). Stars indicate significant differences compared to correspondent untreated sample. For Ost TK1$^-$ stars represent significant difference compared to untreated HCT116.

3.2.2 Effects of TK1 regulation on the uptake of [18F]FLT

As shown in Chapter 3.1, TK1 is phosphorylated in several positions during cell cycle progression. It was therefore hypothesised that phosphorylation could modulate TK1 activity.

In order to validate if TK1 phosphorylation impacted [18F]FLT uptake, HCT116 cells were incubated with cell-cycle arresting agents for 24 hours (Figure 39 and Figure 40).

The first experiments were conducted at 0, 30, 60 and 120 minutes to follow [18F]FLT accumulation over time. As expected, [18F]FLT accumulation in HCT116 increased over time, due to continuous conversion of the radiotracer into the monophosphate form, which was trapped inside cells (Grierson et al., 2004, Li et al., 2011). The 0 minutes time point was included to assess non-specific binding. Serum-starved cells (0% FBS) showed a 60% decrease in radiotracer accumulation at each time point ($p<0.01$), consistent with reduced amount of TK1 protein itself. Additionally, both nocodazole and paclitaxel treatment resulted in a significant decrease (80%; $p<0.0001$) in [18F]FLT uptake at each time point, compared to the corresponding control. As shown in Chapter 3.1, mitotic arrest induced TK1 phosphorylation; this specific post-translational modification has been reported to decrease TK1 activity (Chang et al., 1998, Chang et al., 1994). Consistent with these findings, a decrease in [18F]FLT incorporation was observed. However, the signal intensity corresponding to the G2/M phosphorylation was lower than the other bands (Figure 33), but it is possible that the combination of the different phosphorylation events, as suggested by the concomitant signal increase of band #2 during G2/M (Figure 31), was responsible for the decrease in TK1 activity.
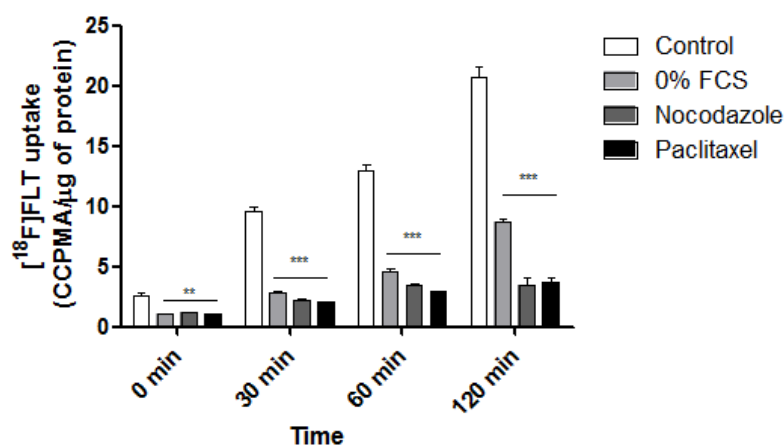
Figure 39. [¹⁸F]FLT cell uptake in HCT116 cells at the indicated time points.
HCT116 cells were seeded to 60-70% confluency and incubated with 0% FBS medium, 0.5 μg/ml nocodazole or 250 nM paclitaxel for 24h. ~0.37 MBq were added to each sample and cells were incubated at 37° C for the appropriate time. The graph represents the average values (n=3) of a representative independent repeat (3 in total) and the standard error of the mean. Stars represent significant differences compared to the corresponding control at each time point.

To have a broader understanding of TK1 activity oscillation during cell cycle progression, as well as following treatment with anti-cancer drugs, 24 hour treatments with 10 μM aphidicolin (APH), 20 μM roscovitine, 5 μM staurosporine, 100 μM cisplatin (CIS), 100 μg/ml 5-fluoruracil (5-FU) and 5 μM PD0325901 and 4 hours incubation with 50 μM roscovitine were included in a cell incorporation experiment. For clarity, the percentage of uptake calculated from Figure 40 are summarised in Table 3.

G0/G1 arrest with serum-depleted media (0% FBS) resulted in a 30% decrease in [¹⁸F]FLT uptake compared to DMSO control, corresponding with reduced TK1 expression when the protein was not needed (see Chapter 3.1, Figure 33). [¹⁸F]FLT incorporation was decreased by 70% in cells treated with aphidicolin (S-phase enriched; APH, a DNA polymerase inhibitor), even though the protein was expressed at maximum levels (see Chapter 3.1, Figure 33) and TK1 was expected to be highly active. However, it is possible that this finding was due to the negative feedback generated by increased cellular thymidine triphosphate (dTTP) which cannot be incorporated into DNA, following inhibition of DNA polymerase by aphidicolin. Under this condition, the dTTP pool increases and, as a consequence, there is no need for further thymidylate supply. For this

126

reason, TK1 activity is modulated by the binding of the final product of the salvage pathway (dTTP) to the enzyme (Munch-Petersen et al., 1993, Munch-Petersen et al., 1995).

G2/M arrest produced a 50% and 80% reduction in cell uptake with 0.5 µg/ml nocodazole (NOC) and 250 nM paclitaxel (PAX), respectively, with p values < 0.05 under each condition. In line with previous findings by Chang *et al.* (Chang et al., 1994, Chang et al., 1998), TK1 activity was reduced during mitosis, since DNA replication had been completed and cells were preparing for cell division.

Treatment with 100 µM cisplatin (CIS) also decreased [^{18}F]FLT uptake into cells by 70% (p<0.005) due to induction of DNA damage followed by cell death. As reported in Chapter 3.1, section 3.1.3, TK1 non-phosphorylated form was predominant over the phosphorylated one. It is therefore reasonable to speculate that under this condition, TK1 was no longer needed and therefore could be targeted for degradation. In addition, Leyton *et al.* reported increased G0/G1 population after 24h treatment with cisplatin *in vivo* (Leyton et al., 2005), when TK1 is not needed and therefore phosphorylation might be at minimal levels.

In contrast, incubation with 5-fluorouracil (5-FU) for 24 hours induced a 3-fold increase in radiotracer uptake (p<0.0001). The effect of 5-FU on [^{18}F]FLT cell uptake has been already reported (Perumal et al., 2006); briefly, thymidylate synthase (TS) inhibition by 5-FU caused redistribution of ENT1 transporters from the cytoplasm to the plasma membrane, without inducing transcription or translation.

Roscovitine treatment either for 4 (50 µM) or 24 hours (20 µM), as well as staurosporine treatment, decreased the incorporation of [^{18}F]FLT into HCT116 cells, suggesting that phosphorylation might be an important modification to enhance the enzyme activity.

Finally, 5 µM PD0325901 (PD) was responsible for a decrease in radiotracer uptake (45%), in line with G0/G1 arrest and reduced TK1 transcription, as discussed for the effects of serum starvation.

Figure 40. [^{18}F]FLT cell uptake in HCT116 after 24h treatment with cell-cycle arresting and anti-cancer drugs. HCT116 cells were seeded to 60-70% confluency and incubated with 0% FBS medium, 10 µM aphidicolin (APH), 0.5 µg/ml nocodazole (NOC), 250 nM paclitaxel (PAX), 100 µM cisplatin (CIS), 100 µg/ml 5-fluorouracil (5-FU), 20 µM roscovitine, 5 µM staurosporine or 5 µM PD0325901 (PD) for 24h. For the 4h treatment, roscovitine was used at 50 µM concentration. The final concentration of DMSO was 0.4%. ~0.37 MBq were added to each sample and cells were incubated at 37° C for 1h. The graph represents the average values (n=6) and the standard error of the mean. DMSO control was used as reference for statistical analysis.

Table 3. Percentages of ^{18}F-FLT cell uptake in HCT116 after the indicated treatments for 24h.

Treatment	% of uptake
Control	95%
DMSO	100%
0%FBS	-30%
10 µM Aphidicolin (APH)	-70%
0.5 µg/ml Nocodazole (NOC)	-50%
250 nM Paclitaxel (PAX)	-80%
100 µM Cisplatin (CIS)	-70%
100 µg/ml 5-fluorouracil (5-FU)	+220%
20 µM Roscovitine (24h)	-70%
50 µM Roscovitine (4h)	-80%
5 µM Staurosporine	-50%
5 µM PD0325901	-50%

- or + indicate decrease or increase, respectively, compared to DMSO control.

To conclude, [^{18}F]FLT uptake into HCT116 cells was modulated by the cell-cycle stage at which cells were arrested, in relation to specific cell cycle modulation effect on TK1 protein phosphorylation of the anti-cancer drug used.

More interestingly, radiotracer uptake did not only change in relation to S phase arrest, but also during G2/M arrest. This concept of treatments interfering with [^{18}F]FLT uptake has to be kept in mind when interpreting data generated from [^{18}F]FLT-PET.

3.2.3 Role of the different phosphorylation sites

Having determined that TK1 phosphorylation influenced [^{18}F]FLT cell uptake in HCT116,

the next step consisted of verifying the effects of the specific phosphorylations on the

enzyme activity.

As reported in Chapter 3.1 (section 3.1.4), Ser13 seemed to be phosphorylated during S

and G2/M. Additionally, a G2/M specific phosphorylation of Ser231 was inferred.

To examine the functional impact of phosphorylation of specific amino-acid residues

(Ser13 and Ser231) on [^{18}F]FLT uptake, Ost TK1$^-$ cells were tested for [^{18}F]FLT uptake.

These cells did not take up [^{18}F]FLT (Figure 41) in comparison to positive control (HCT116)

cells, indicating their suitability for studying effects of TK1 phosphorylation on [^{18}F]FLT

uptake following transfections with TK1 mutants.
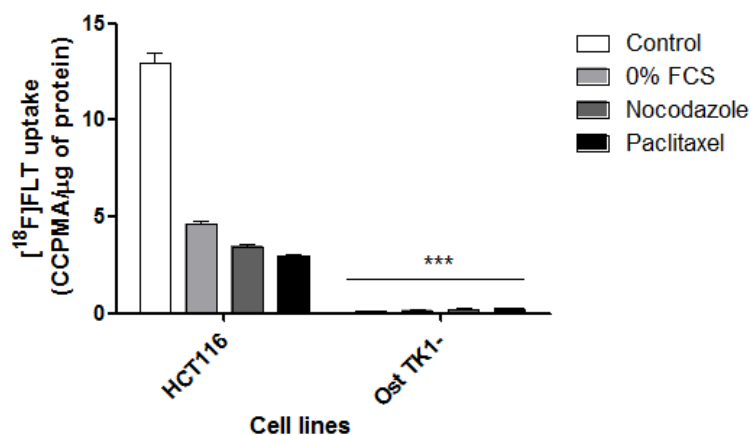
Figure 41. [^{18}F]FLT cell uptake in HCT116 and Ost TK1$^-$ cells.
Exponentially growing HCT116 and Ost TK1$^-$ cells were incubated with 0% FBS medium or treated with 0.5 µg/ml nocodazole or 250 nM paclitaxel for 24h. ~0.37 MBq were added to each condition and cells were incubated at 37° C for 1h. The graph represents the average values (n=3) and the standard error of the mean. Stars indicate highly significant difference (p<0.0001).

Ost TK1$^-$ cells were subsequently transfected with TK1 constructs encoding for different

variants of the protein (S13A, S13D and S231A); this allowed the functional consequence

of two of the known TK1 phosphorylation sites - position 13 and 231 - to be examined in

more detail (mutation of Ser13 and Ser231 to alanine was intended to eliminate

phosphorylation, while mutation of Ser13 to aspartate was intended to mimic phosphorylation).

[^{18}F]FLT uptake in transfected cells was compared with uptake in HCT116, with or without nocodazole treatment (Figure 42A). Notably, transfection with any of the plasmids induced [^{18}F]FLT uptake, even if the level of incorporation was significantly lower than that of HCT116 ($p<0.001$). A possible explanation for the lower [^{18}F]FLT incorporation in the transfected cells is the presence of the FLAG-tag on ultimate TK1 protein product; even though the FLAG epitope is only 1 kDa, it could affect TK1 activity, specifically by interfering with the formation of a fully functional tetramer. Nonetheless, it was possible to assess the effects of the different TK1 variants on [^{18}F]FLT uptake.

[^{18}F]FLT uptake in the transfected cells is shown in Figure 42B. Treatment with nocodazole for 24 hours to induce G2/M arrest significantly decreased [^{18}F]FLT uptake compared to the corresponding non-treated sample ($p<0.005$). The reduction in uptake in nocodazole treated versus untreated cells was 5-fold, 2-fold, 4-fold and 3-fold for wild-type (WT) TK1 expressing cells, S13A, S13D and S231A mutant cells, respectively. This suggested the existence of additional phosphorylation sites.
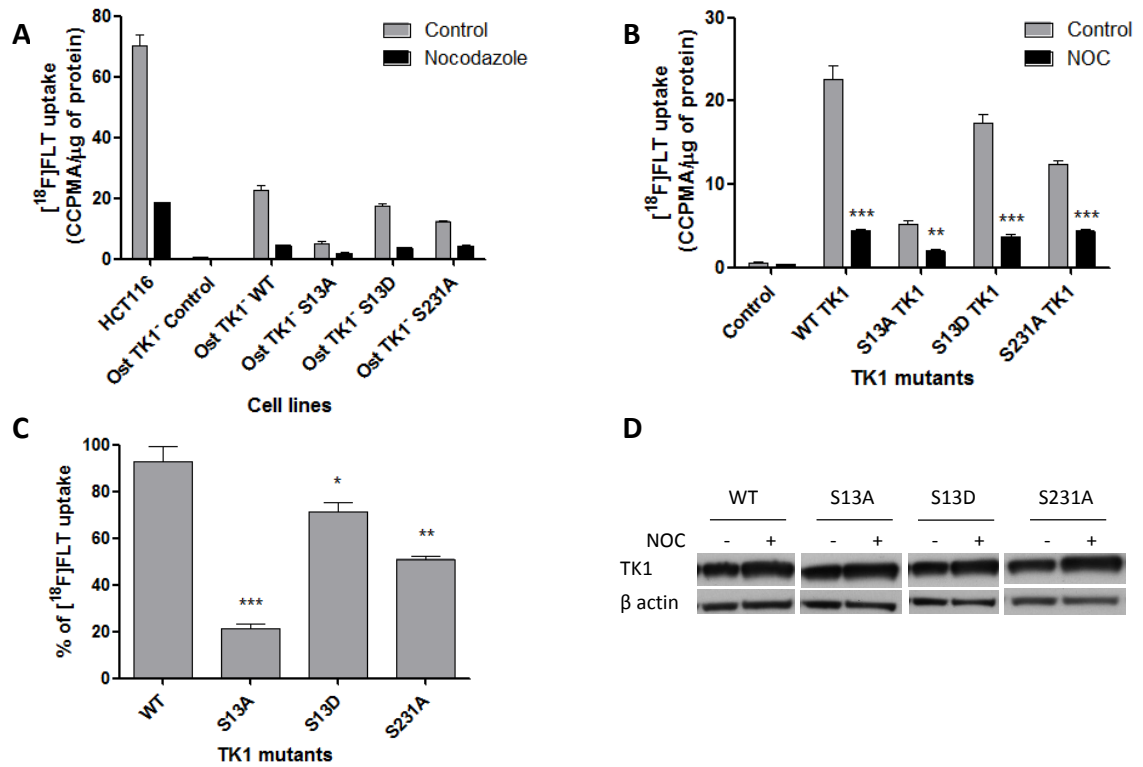
Figure 42. [¹⁸F]FLT cell uptake in Ost TK1⁻ cells after transient transfection with TK1 constructs.
Ost TK1⁻ cells were transfected with 24 µg of FLAG-pCMV2 plasmid containing the desired TK1 construct. G2/M arrest was induced using 0.5 µg/ml of nocodazole (NOC). A) Comparison of [¹⁸F]FLT uptake in HCT116 versus transfected Ost TK1⁻ (n=3). B) and C) reports the same data in A), presented in a different format. B) Radiotracer uptake in Ost TK1⁻ cells. C) Percentage of [¹⁸F]FLT uptake in cells transfected with the indicated TK1 constructs. D) Representative western blot showing TK1 expression following transfection. Protein lysates were resolved on 12% pre-cast gels.

More interestingly, Figure 42C represents the percentage of radiotracer uptake relative to cells transfected with WT TK1, assigning an arbitrary value of 100% to the uptake values measured in this sample. S13A substitution was responsible for an 80% decrease in [¹⁸F]FLT uptake compared to WT (p=0.0005), whereas S13D mutation partially rescued [¹⁸F]FLT uptake to WT levels, showing a 20% decrease (p<0.05). S231A resulted in decreased radiotracer uptake, although not as marked as with S13A, being 50% of the WT uptake (p<0.005).

Since the transfection efficiency seemed to be similar with each TK1 construct, as showed by western blot analysis on 12% gels (Figure 42D), it was reasonable to assume that the

differences in [18F]FLT uptake following transfection were a consequence of the specific mutations, rather than being originated by different levels of TK1 expression.

Taken together, these results suggested that Ser13 phosphorylation might be important for TK1 enzymatic activity, since [18F]FLT uptake was reduced after substitution with alanine, compared to WT, indicating that the ability to phosphorylate Ser13 might be required for the activation of the enzyme, not only for the decreased activity during G2/M, as previously reported (Chang et al., 1998). Radiotracer uptake was further decreased after nocodazole treatment of cells expressing TK1 with the S13A mutation, indicating that Ser13 might not be the only amino-acid residue phosphorylated during G2/M phase. Results obtained with the S13D version of TK1 seemed to further sustain this speculation, since substitution of Ser13 with Asp13 partially rescued [18F]FLT uptake, due to Asp13 mimicking the change of charge induced after phosphorylation at the same position (Ke et al., 2003, Li et al., 2004). This result is in contrast with the report from Li *et al.*, where they concluded that the phosphorylation on Ser13, mimicked by the S13D substitution, was responsible for decreased affinity for the substrate due to disassociation of the tetramer to form the dimeric form of TK1 (Li et al., 2004). However, a 20% decrease in radiotracer uptake was still notable, indicating that a change in TK1 affinity for the substrate might be involved following S13D substitution.

Finally, the results obtained with the Ser231 substitution suggested that: 1) S231A mutation had an impact on TK1 enzymatic activity, as the 50% decrease in [18F]FLT uptake indicated, and 2) there might be different residues from the ones investigated in this study which are phosphorylated on TK1 protein, since there was still a decrease in [18F]FLT uptake with nocodazole treatment, in contrast with the expected result in which there should have been no significant difference between treated and non-treated S231A

sample, as well as no marked difference between S231A and WT. In fact, if Ser231 was the only residue phosphorylated during G2/M to reduce TK1 activity, [^{18}F]FLT uptake in S231A should have been comparable to WT. Studies with different mutations should be carried out to further elucidate TK1 phosphorylation and its regulation.

3.2.4 [^{18}F]FLT-PET imaging

[^{18}F]FLT's ability to image cell proliferation in tumours is well established. Less is known about the effects on [^{18}F]FLT tumour uptake following treatment with anti-mitotic agents, therefore the impact of TK1 phosphorylation was assessed *in vivo*, using paclitaxel treatment as a means to induce TK1 mitotic phosphorylation.

HCT116 xenografts were established in BALB/c nude mice. Tumour growth was followed over 17 days from sub-cutaneous injection of 4,000,000 cells resuspended in PBS. Intra-peritoneal (i.p.) treatment with 20 mg/kg of paclitaxel (Nakayama et al., 2009) was administered when tumours reached 100 mm^3, and repeated for 3 days (schedule represented in Figure 43A), with PBS used as vehicle. Taxol® was obtained from pharmacy and diluted 1/5 with 1:1 saline solution and dextrose. 0.015 ml/g were injected intra-peritoneally in each mouse.
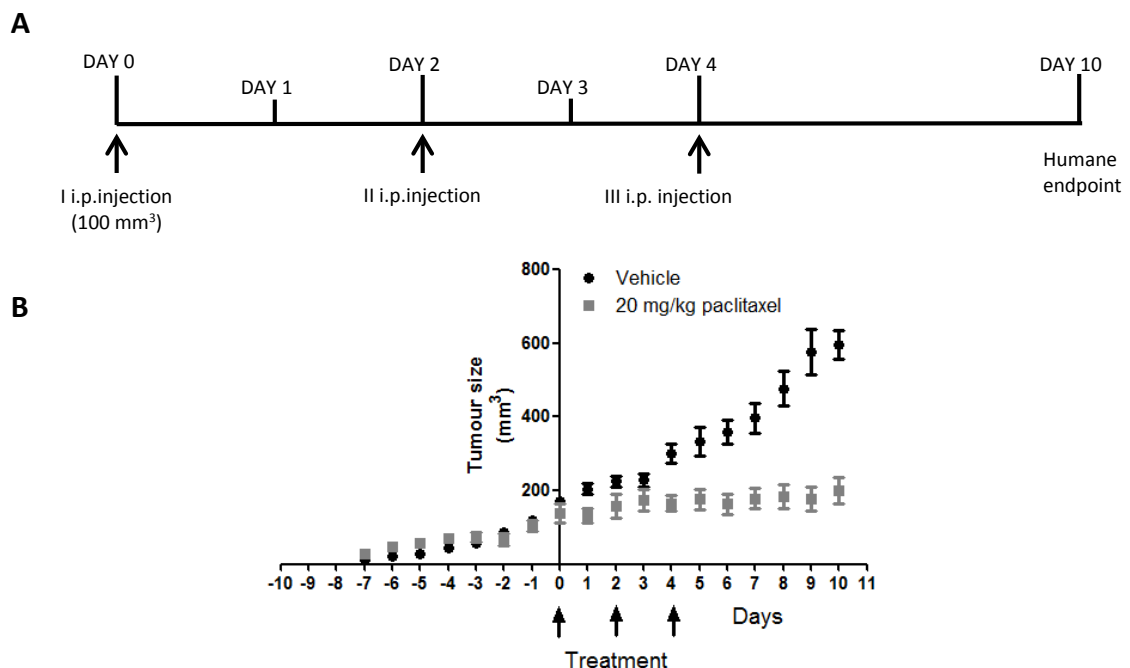
Figure 43. Tumour growth in BALB/c nude mice growing HCT116 xenografts.
HCT116 tumour xenografts were grown subcutaneously in BALB/c nude female mice. A) Schedule of treatment and humane end point. B) Tumour growth of HCT116 xenografts (n=3). PBS was used as vehicle.

Paclitaxel treatment was able to stabilize HCT116 tumour growth, maintaining tumour volume constant until the end of the experiment (Figure 43B). The growth data indicated that HCT116 tumour xenografts responded to paclitaxel treatment at 20 mg/kg with this specific regimen.

Dynamic [18F]FLT positron emission tomography (PET) imaging was performed on HCT116 tumour-bearing mice to assess early response to therapy following single treatment with 20 mg/kg paclitaxel (Figure 44).
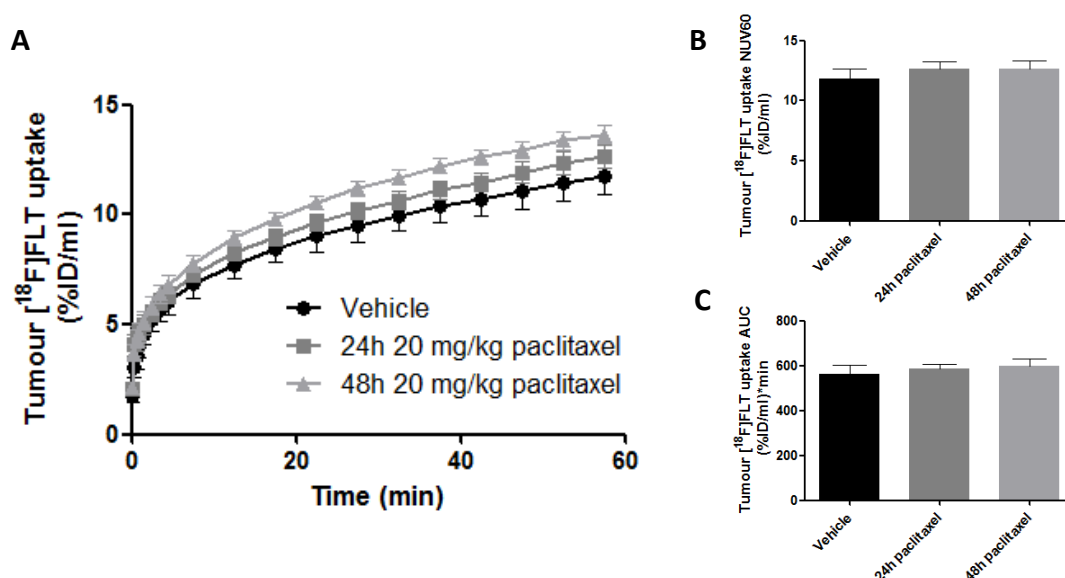
Figure 44. [18F]FLT-PET imaging after 24 and 48 hours from treatment with 20 mg/kg paclitaxel in HCT116 tumour xenografts.
HCT116 tumour bearing mice were scanned in a dedicated CT-PET scanner over 60 min. A) TACs comparison between vehicle at 24 to 48h (n=3), 24h treatment (n=8) and 48h treatment (n=6). B) Normalized Uptake Value at 60 minutes (NUV60) expressed as percentage of injected dose per ml. C) Area Under the Curve (AUC) values expressed as percentage of injected dose per ml per minute. Analysis of variance (ANOVA) was performed to compare the datasets.

[18F]FLT-PET imaging was performed on vehicle control and 24 hours or 48 hours post i.p. treatment. Figure 44 represents time-activity curves (TACs), NUV60 and AUC values for each group. [18F]FLT uptake was expected to decrease following treatment, as suggested by the *in vitro* results (Figure 39 and Figure 40). However, *in vivo* [18F]FLT-PET imaging did not highlight any significant difference following treatment at this concentration.

To validate this result, immunohistochemistry was performed on tumours to evaluate the proliferation rate with Ki67 staining. Ki67 is in fact a nuclear protein associated with cell proliferation, which is present throughout the cell cycle, and absent in non-proliferating cells such as the ones arrested in G0 (Scholzen and Gerdes, 2000).

Figure 45 shows representative results after staining with H&E to visualise cells and with Ki67 to measure proliferation. Positive Ki67 staining is indicated by brown staining of the nucleus. As the images suggested, there was no significant difference in cell proliferation (i.e. brown staining) following treatment. Ki67 expression was 66% ± 2%, 73% ± 2% and 61% ± 2% following treatment with vehicle, 24h paclitaxel and 48h paclitaxel, respectively.
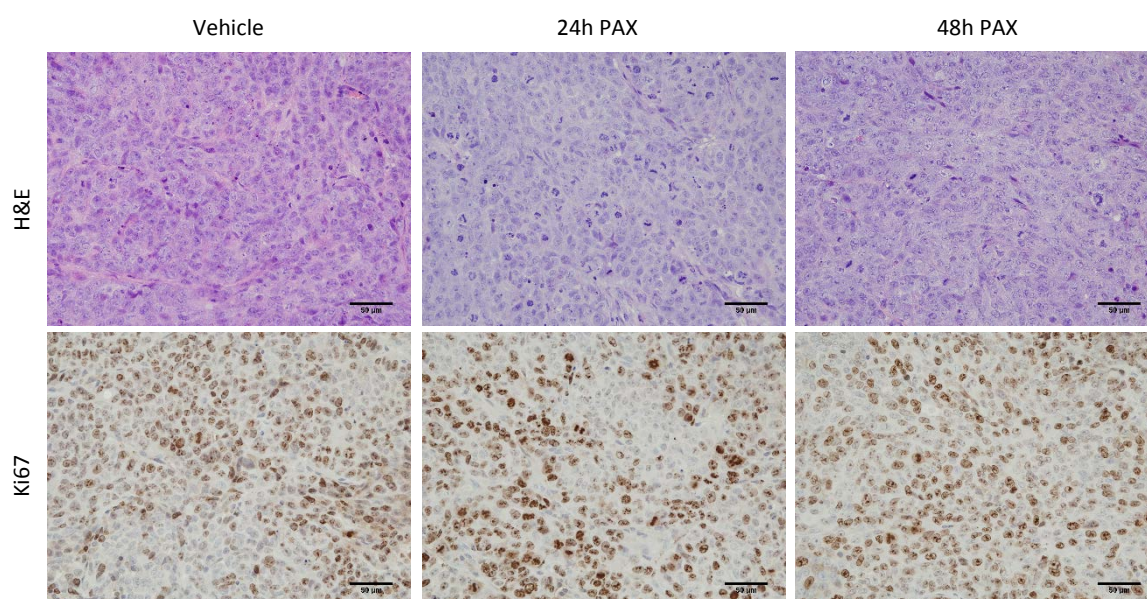
Figure 45. Representative immunohistochemistry analysis of tumour samples excised after [^{18}F]FLT-PET imaging. Mice were sacrificed at the end of the PET scan. Tumours were excised and fixed in formalin. Tissue sections were stained for haematoxylin and eosin (H&E, upper panels) or Ki67 (bottom panels).

Given these results, it was hypothesised that treatment with this dose (20 mg/kg) was not able to produce effects at early time points. Therefore, a higher concentration of 40 mg/kg paclitaxel (Nakayama et al., 2009) was administered. However, in order to reduce the injected volume/mouse, a new formulation was prepared, dissolving paclitaxel in DMSO and diluting it 1/10 in PBS. The first group was scanned as a baseline control to

assess [18F]FLT accumulation in the tumour. A different cohort was treated with 40 mg/kg paclitaxel and imaged after 24 hours from treatment. Figure 46Figure 39B shows the time-activity curves (TACs) of [18F]FLT uptake into the tumour. There was a 25% decrease in radiotracer uptake after paclitaxel treatment, with both Normalised Uptake Value at 60 minutes (NUV60) and Area Under the Curve (AUC) showing 25% decrease in uptake after drug treatment (Figure 46Figure 39C and D, respectively). Figure 46Figure 39A shows representative PET images of an un-treated mouse (left) and a treated one (right); it was possible to note a decrease in radiotracer uptake after treatment with paclitaxel. This result suggested that treatment with paclitaxel decreased [18F]FLT uptake *in vivo*, due to induction of G2/M arrest and therefore triggering TK1 phosphorylation during mitosis.
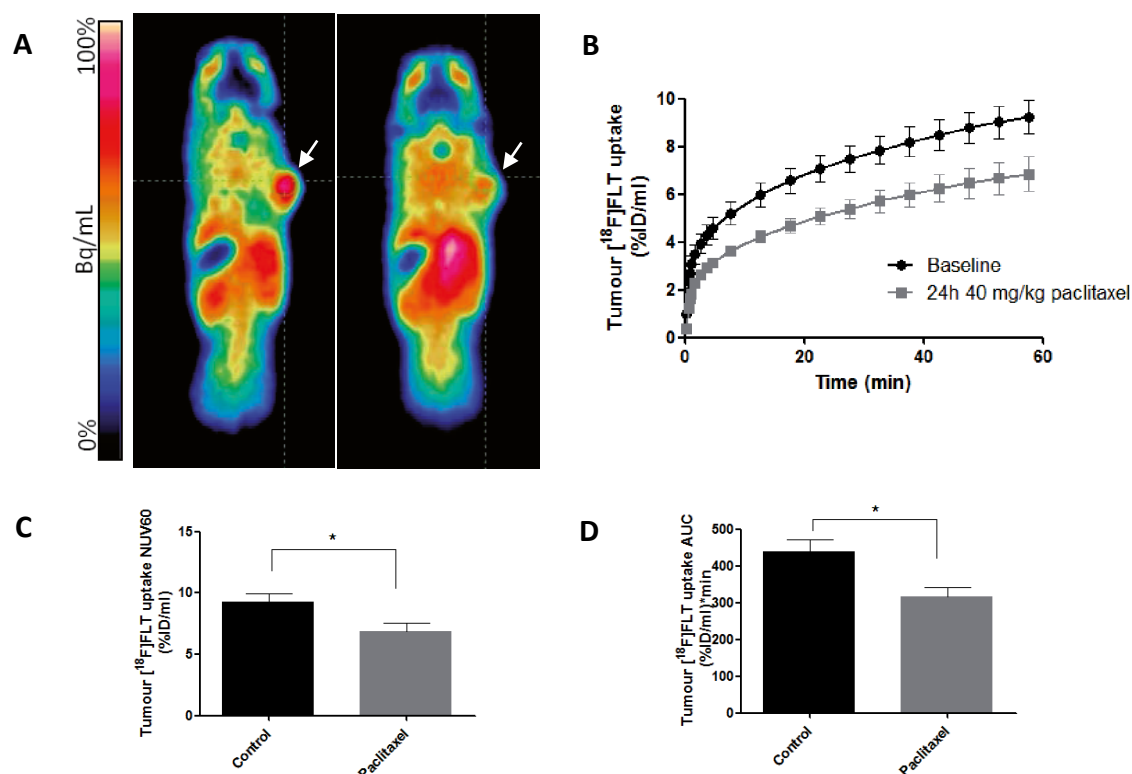
Figure 46. [18F]FLT-PET imaging after 24 hours treatment with 40 mg/kg paclitaxel in HCT116 tumour xenografts. HCT116 tumour-bearing mice were scanned in a dedicated CT-PET scanner for 60 min. Baseline = 9; 24h paclitaxel treatment = 5 mice. A) Representative axial images of [18F]FLT tumour uptake. Left: baseline, right: 24h treatment with 40 mg/kg paclitaxel. The tumour appears as a hotspot on the right side of the animal (white arrow). B) Time-activity curves (TACs) representing [18F]FLT accumulation in the tumour over 60min. C) Normalised Uptake Value at 60min (NUV60) expressed as percentage of injected dose per ml. D) Area Under the Curve (AUC) values expressed as percentage of injected dose per ml per minute. Student's t-test analysis was performed to compare differences in [18F]FLT uptake between the two cohorts (baseline and treatment).

Following this promising experiment, imaging after 48 hours treatment with a single dose of 40 mg/kg paclitaxel was performed, hypothesising that it would have produced a greater decrease in [18F]FLT tumour uptake compared to the 24 hour treatment. Figure 47 shows TACs comparison between baseline and 48 hours treatment with one dose of 40 mg/kg paclitaxel. There was no difference in tumour [18F]FLT accumulation after 48 hours from treatment compared to baseline, Figure 47 ($p > 0.05$).
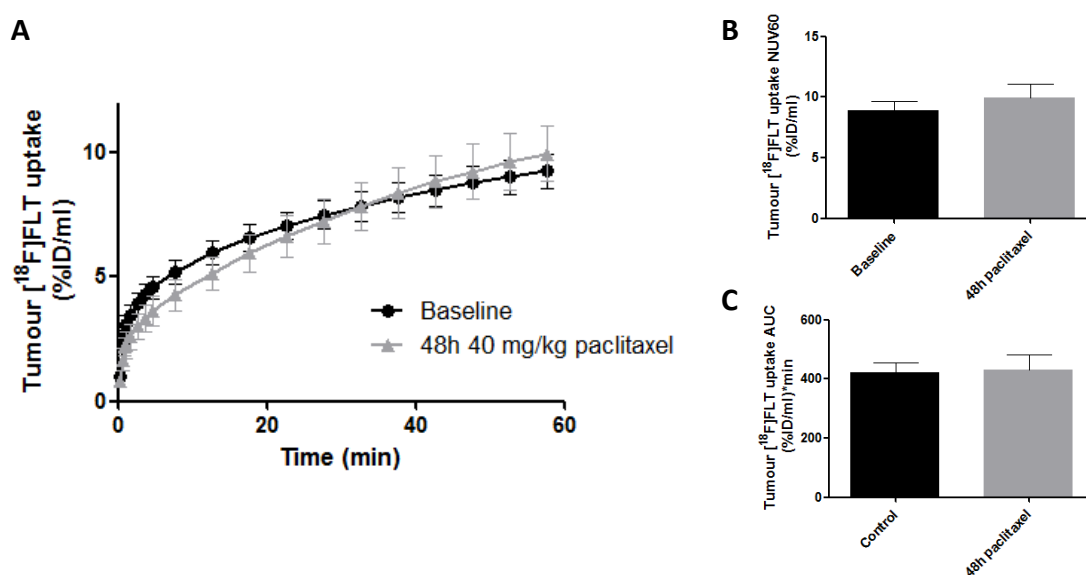
Figure 47. [18F]FLT-PET imaging after 48 hours from treatment with 40 mg/kg paclitaxel in HCT116 tumour xenografts.
A) TACs comparison between baseline (n=8) and 48h treatment (n=4). B) Normalized Uptake Value at 60 minutes (NUV60) expressed as percentage of injected dose per ml. C) Area Under the Curve (AUC) values expressed as percentage of injected dose per ml per minute. Student's t-test statistical analysis was used to compare the two datasets.

[18F]FLT-PET imaging was then carried out after a double treatment with 40 mg/kg paclitaxel within 48 hours. The second dose was administered 24 hours after the first i.p. treatment. TACs, NUV60 and AUC values are shown in Figure 48. At least the same result obtained after 24 hours treatment was expected; however, TACs showed no changes in radiotracer uptake into the tumour and no statistical difference between baseline and treatment was detected when comparing NUV60 and AUC values.
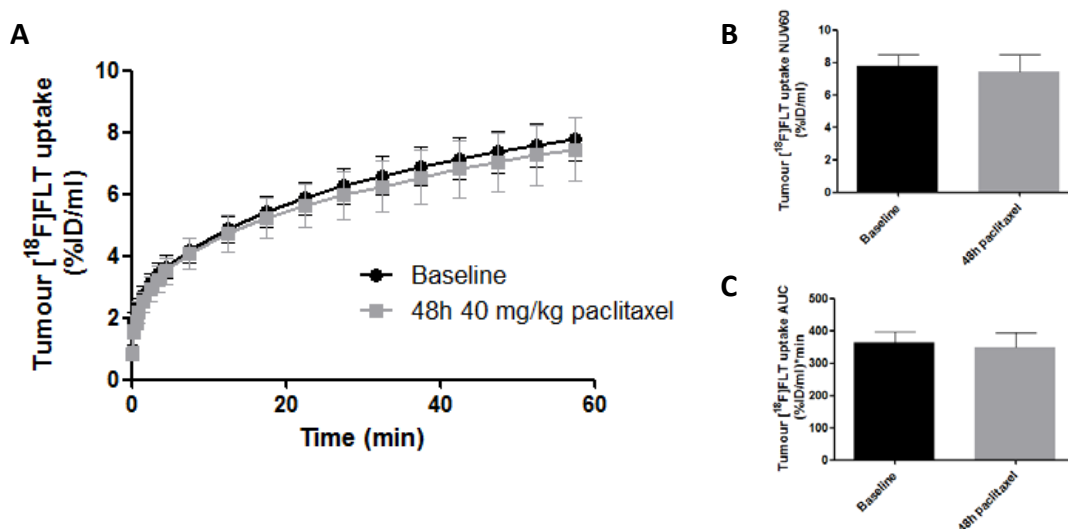
Figure 48. [¹⁸F]FLT-PET imaging after 48 hours from treatment with two doses of 40 mg/kg paclitaxel in HCT116 tumour xenografts.
A) TACs comparison between baseline (n=5) and 48h treatment (n=5). B) Normalized Uptake Value at 60 minutes (NUV60) expressed as percentage of injected dose per ml. C) Area Under the Curve (AUC) values expressed as percentage of injected dose per ml per minute. Student's t-test statistical analysis was used to compare the two datasets.

In conclusion, only the 24 hours treatment with 40 mg/kg showed a significant decrease in [¹⁸F]FLT tumour uptake. However, all the other experiments suggested that paclitaxel did not act efficiently at the dose and regimen used. It was therefore hypothesized that [¹⁸F]FLT-PET could not highlight early changes in tumour proliferation after paclitaxel treatment, regardless of the formulation and dose used.

To validate if paclitaxel was arresting tumour cells in G2/M phase, and therefore inducing TK1 phosphorylation, tumour lysates were tested for phospho-TK1 and total TK1 as well as G2/M specific markers, such as CDK1 and Wee1. For entry into mitosis, a critical step in the activation of CDK1 consists of dephosphorylation of Tyr15 and Thr14. Tyr15 is originally phosphorylated by Wee1 to prevent entry into mitosis before completion of G2 phase (McGowan and Russell, 1993). To enter mitosis Wee1 must be therefore inactivated via phosphorylation of Ser642 by Akt/PKB (Katayama et al., 2005). If samples were arrested in G2/M, an increase in P-CDK1 should have been detected, with poor

phosphorylation of Wee1. Additionally, band #3 (TK1 specific mitotic phosphorylation) should have been induced.

Western blot analysis and densitometry is reported in Figure 49. Phospho-TK1 profile consisted of the resolution of band #1 (non-phosphorylated TK1) and #2 (phosphorylated TK1), with no induction of the G2/M specific phosphorylation (band #3), similar to the results obtained from asynchronous cells *in vitro* (Figure 30, control and DMSO samples). Moreover, there appeared to be no significant difference in total TK1 protein expression, phosho-CDK1/CDK1 and phosho-Wee1/Wee1 comparing the different treatments, suggesting that the paclitaxel dose that was administered prior to [^{18}F]FLT-PET imaging was not able to induce effective G2/M arrest in any of the experiments performed, not even when a significant decrease in [^{18}F]FLT tumour uptake was highlighted after 24 hours (Figure 46). It seemed therefore sensible to assume that that single experiment provided false positive results. Additionally, the use of different cohorts of mice might have precluded small changes from being seen. This protocol was however selected due to logistical difficulties in arranging radiotracer, animal with defined tumour size and imaging scanner.
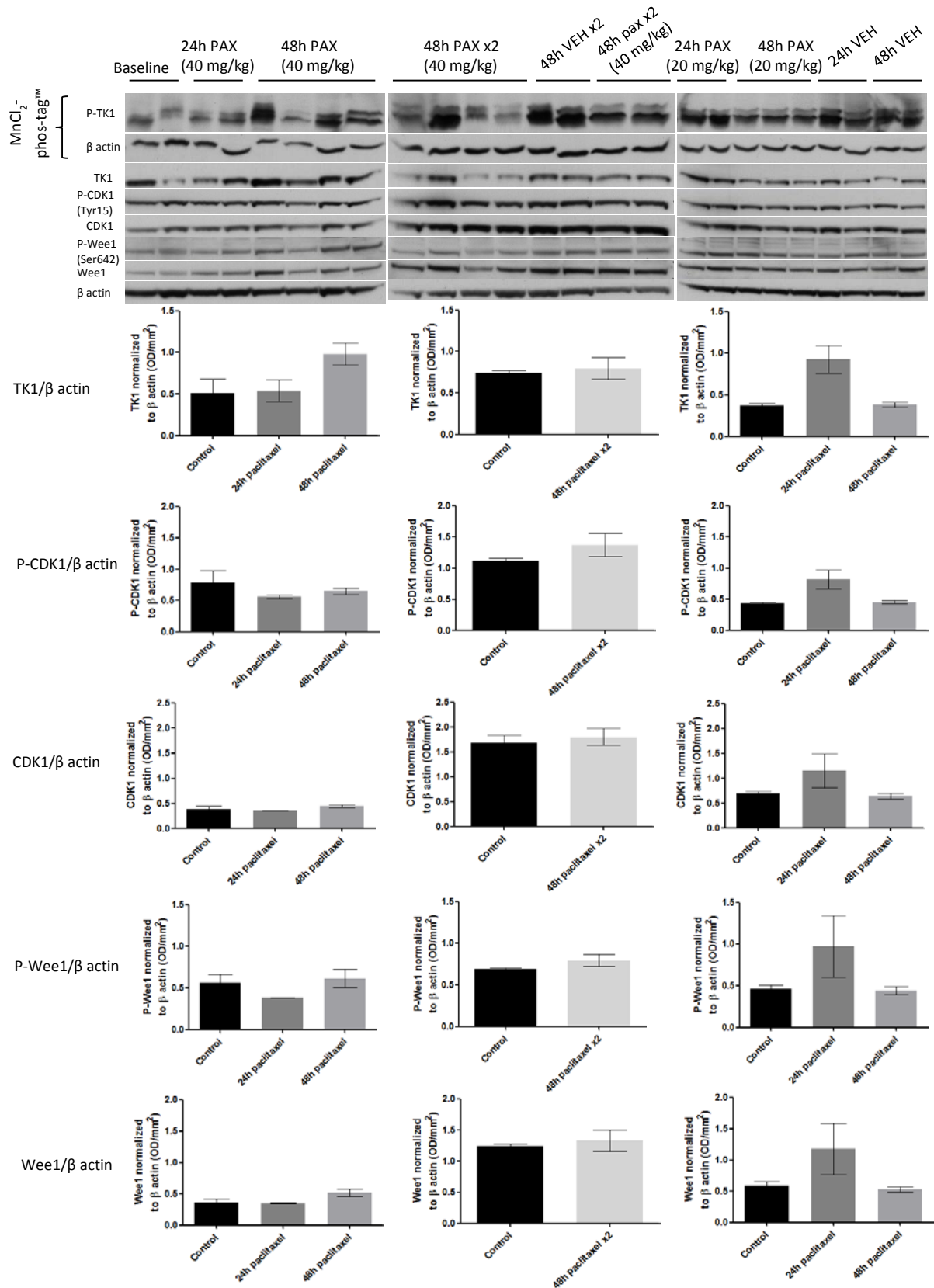
Figure 49. Expression of TK1, CDK1 and Wee1 in tumour lysates excised after [18F]FLT-PET imaging.
HCT116 lysates obtained from tumour-bearing mice were resolved on $MnCl_2$-phos-tag gels (top 2 panels) to detect phospho-TK1 (P-TK1). 12% pre-cast NuPAGE gels were used to detect total TK1, CDK1, P-CDK1, Wee1 and P-Wee1. 30 μg of proteins were resolved on each gel. Pax, paclitaxel; VEH, vehicle (PBS).

3.3 Validation of new radiotracers for cell proliferation imaging with PET

3.3.1 [^{18}F]FOT and [^{18}F]FTT

[^{18}F]FLT is used as a biomarker for tumour proliferation. However, it provides an indirect measure of proliferation, since it is phosphorylated to monophosphate by TK1 (the trapping process), but it lacks the 3'-hydroxyl group necessary for incorporation into the growing chain of the DNA. Developing new radiotracers which could be incorporated into DNA might overcome [^{18}F]FLT limits (Chapter 1, section 1.4.5).

N3-((1-(2-^{18}F-fluoroethyl)-1H-[1,2,3]-triazol-4-yl)methyl)thymidine ([^{18}F]FOT) and N3-((1-(2-^{18}F-fluoroethyl)-1H-[1,2,3]-triazol-4-yl)methyl)-4'-thio-β-thymidine ([^{18}F]FTT) (Figure 50) were developed in the group by Dr Graham Smith (Smith et al., 2012). Briefly, both radiotracers were thymidine analogues in which a fluorine atom was introduced via a linker in the N-3 position of the DNA base. This feature was inspired by the insertion of Boron Neutron Capture Therapy (BNCT) agents in the same position (Al-Madhoun et al., 2002). [^{18}F]FOT conserved the oxygen atom in the ribose ring, whereas oxygen was substituted by a sulfur atom in [^{18}F]FTT, conferring resistance to thymidine phosphorylase (TP) (Toyohara et al., 2002a); to stabilize the glycosidic bond cleaved by TP, the sugar portion of the nucleoside required a heteroatom, such as the fluorine atom in [^{18}F]FLT; since the sulfur atom in the glucose ring showed similar stability (Toyohara et al., 2002a), it was inserted into [^{18}F]FTT to be able to retain the 3'-hydroxyl group, necessary for incorporation into the growing chain of the DNA.

This feature was expected to confer an advantage, since incorporation into the DNA directly indicates the specific rate of DNA replication, providing improved accuracy in determining cell proliferation. DNA incorporation is also an irreversible step and therefore the process of reversible phosphorylations, which characterize the DNA salvage pathway and to which [^{18}F]FLT is subjected, might not be a rate limiting process. In fact, due to

limitations of [18F]FLT (see Chapter 1, section 1.4.5), it was desirable to develop new proliferation markers which could be specific, resistant to degradation and incorporated into DNA more efficiently, in order to provide higher sensitivity compared to [18F]FLT. The sulfur analogue ([18F]FTT) was meant to be more resistant to degradation compared to [18F]FOT.
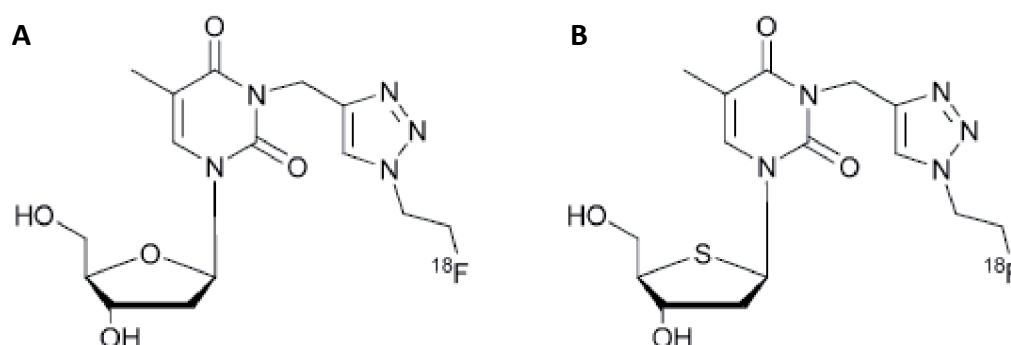
Figure 50. Structures of [18F]FOT (A) and [18F]FTT (B) (Smith et al., 2012).
The two radiotracers are thymidine analogues. A) N3-((1-(2-18F-fluoroethyl)-1H-[1,2,3]-triazol-4-yl)methyl)thymidine ([18F]FOT) retains the oxygen atom in the ribose ring. B) N3-((1-(2-18F-fluoroethyl)-1H-[1,2,3]-triazol-4-yl)methyl)-4'-thio-β-thymidine ([18F]FTT) is characterised by the presence of a sulfur atom in place of the oxygen in the ribose ring. This substitution is supposed to confer resistance to metabolism. Both radiotracers conserve the 3' hydroxyl group (OH), necessary for DNA incorporation.

Preliminary results obtained by Dr Julius Leyton in the group seemed to suggest that [18F]FTT was subjected to higher incorporation rate into DNA compared to [18F]FLT and [18F]FOT (Figure 51). Hence, validation of [18F]FTT as a radiotracer to image cell proliferation was carried out.
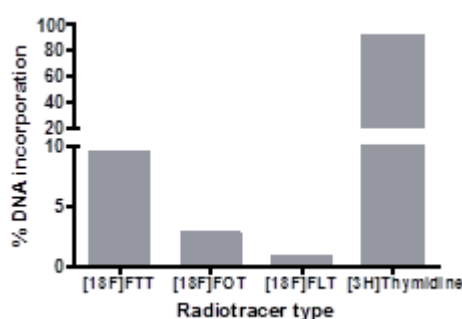
Figure 51. Rate of incorporation of the radiotracers into DNA.
Courtesy of Dr Graham Smith, CCIC, Imperial College London. [18F]FTT seemed to be incorporated into DNA more efficiently than [18F]FLT, even if to significant lower extent when compared to [3H]thymidine.

3.3.2 Phosphorylation potential of [18F]FTT and [18F]FOT

Being thymidine analogues, [18F]FTT and [18F]FOT were expected to trace cell proliferation via the salvage pathway. Therefore, TK1's ability to phosphorylate the new radiotracers was tested using HCT116 cell homogenates (prepared as described in Materials and Methods). The results are presented in Figure 52. Comparison between [18F]FTT and [18F]FLT showed that less than 8% of the total [18F]FTT analysed on HPLC was converted to a phosphorylated form after 60 minutes; on the contrary, 98% of the total [18F]FLT was phosphorylated. Under the same experimental conditions, phosphorylation of [18F]FOT was not observed (Smith et al., 2012).
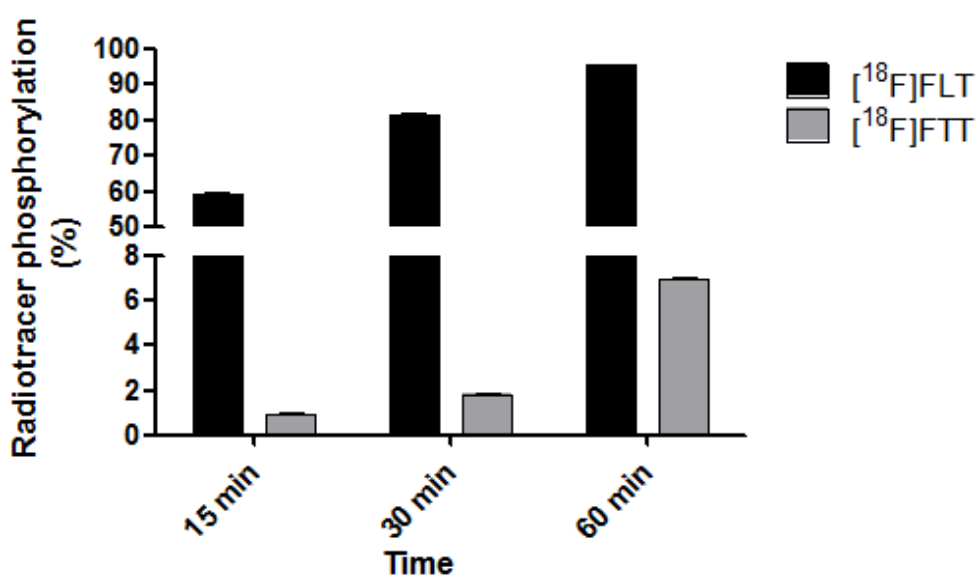
Figure 52. Phosphorylation potential of [18F]FLT and [18F]FTT by cell homogenates (TK1).
HCT116 cell homogenates were prepared as described in Chapter 2. Materials and Methods. Samples were incubated with 1.85 MBq for the indicated time points and analysed by radio-HPLC.

3.3.3 Radiotracers cell uptake and incorporation into macromolecules

In vitro cell uptake experiments were carried out to assess overall retention of the two novel radiotracers in comparison with [^{18}F]FLT. Total cell uptake together with incorporation into macromolecules by washing with 10% perchloric acid (PCA) were assessed.

There was a time-dependent increase in radiotracer accumulation into cells, with each radiotracer (Figure 53). PCA washes were performed to measure macromolecule incorporation: being a strong acid, PCA is able to wash out of cells any negative charge, i.e. a phosphorylated compound, which is not bound to macromolecules such as DNA, RNA and proteins (Schmitz et al., 1954). It was already known that [^{18}F]FLT was not incorporated into DNA, and in fact PCA washes resulted in almost complete wash-out of radioactivity from cells (5-fold reduction at 60 min, Figure 53A). The amount of [^{18}F]FTT and [^{18}F]FOT retained in HCT116 after PCA washes was also reduced (50% and 80% reduction, respectively; Figure 53B and C), suggesting that there was no or little incorporation of both radiotracers into macromolecules. Since [^{18}F]FOT was not phosphorylated, the radioactivity accumulated into cells and washed out following PCA washes possibly referred to the parent compound which was not phosphorylated; instead, radioactivity loss following PCA washes of cells incubated with [^{18}F]FTT represented phosphorylated radiotracer. [^{18}F]FTT was, in fact, subjected to phosphorylation, even if reduced compared to [^{18}F]FLT (Figure 52).
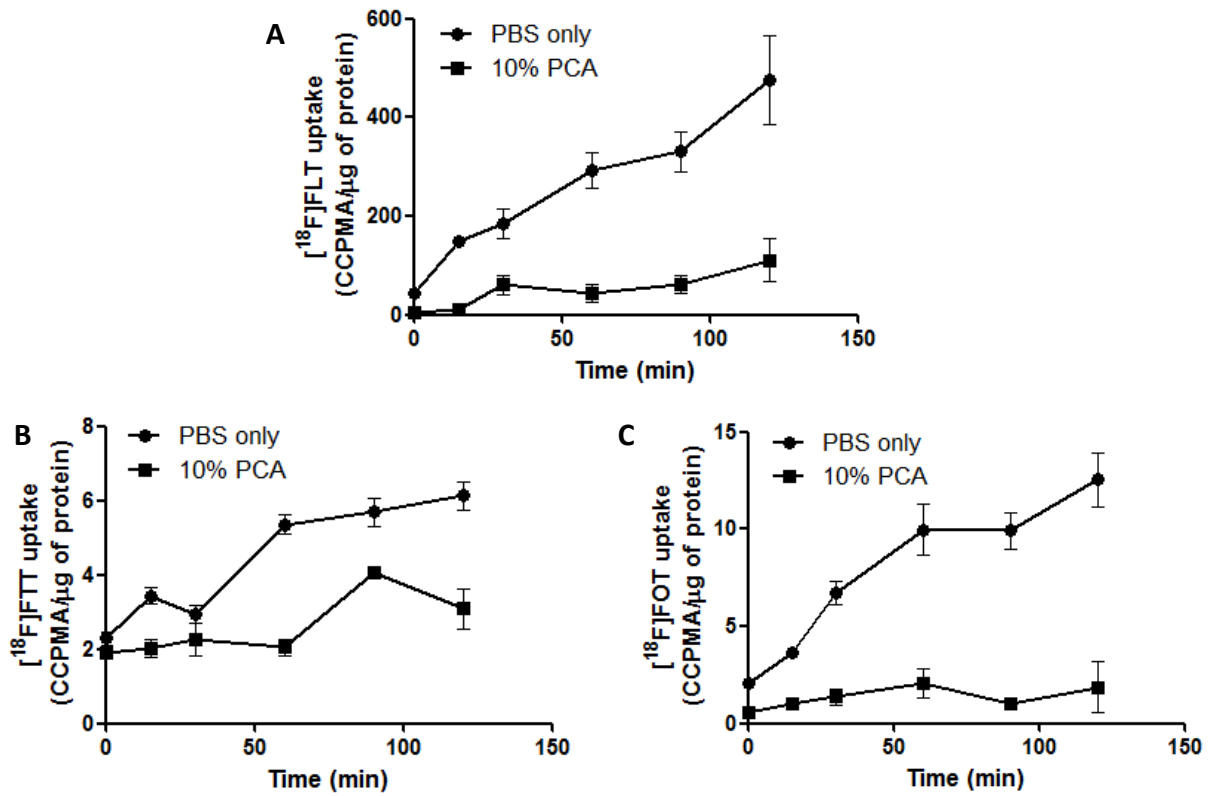
Figure 53. [¹⁸F]FLT (A), [¹⁸F]FTT (B) and [¹⁸F]FOT (C) cell uptake in HCT116 cells.
Representative graphs of 2 experiments with n=3 for each time point. After addition of the radiotracer, cells were incubated at 37°C for the indicated time points. The 0 min plates were processed immediately after addition of radioactivity. PBS only and 10% PCA (perchloric acid) refer to different types of washes.

Cell uptake experiments, together with the fact that the new radiotracers were not efficiently phosphorylated (as shown in Figure 52), clearly suggested that both [¹⁸F]FTT and [¹⁸F]FOT were not suitable radiotracer to image cell proliferation.

3.3.4 *In vivo* metabolism and biodistribution

When validating new radiotracers for PET imaging, it is important to identify possible metabolites, which could interfere with the interpretation of the results, as well as determine the biodistribution *in vivo*, identifying the route of excretion at the same time. Female BALB/c mice were injected with the specific radiotracer for metabolic analysis. Plasma, liver and urine were sampled after 2, 15, 30 or 60 minutes and analysed on radio-HPLC to visualise the evolution of the radiotracer peak as shown in Figure 54 and Figure 55. Both [^{18}F]FTT and [^{18}F]FOT seemed to be metabolically stable, with a single [^{18}F]FTT metabolite being generated after 15 minutes post-injection in plasma and liver (Figure 54), equivalent to 18% and 42% of the total signal, respectively (Smith et al., 2012). Furthermore, [^{18}F]FTT had a longer half-life compared to [^{18}F]FOT, which was in fact completely eliminated from liver after 30 minutes, and from plasma after 60 minutes (Figure 55).
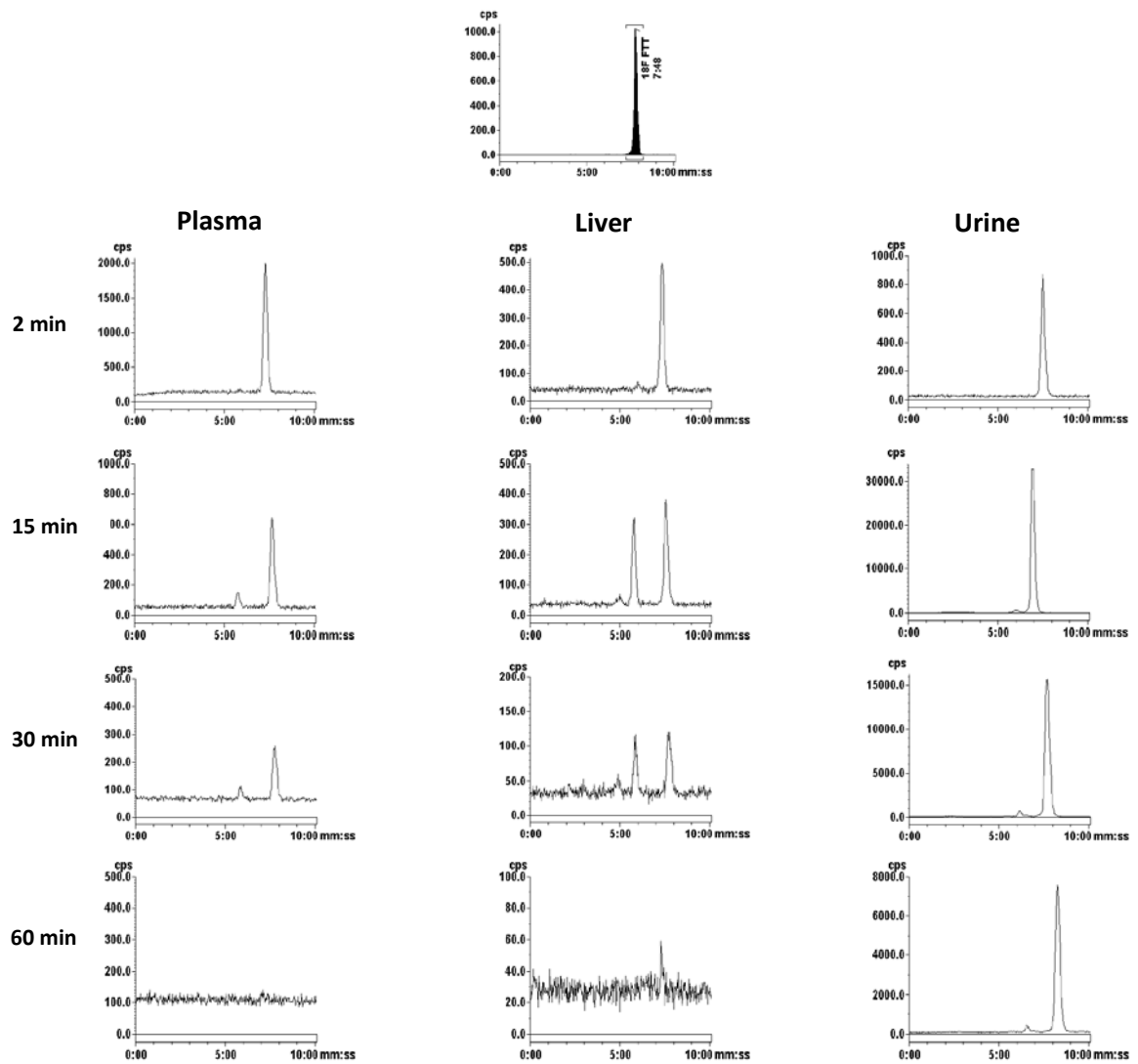
Figure 54. [¹⁸F]FTT metabolism in mouse plasma (left), liver (middle) and urine (right).
Top to bottom: reference standard, 2 minutes, 15 minutes, 30 minutes, 60 min. Representative samples were obtained from three to four mice per time point.
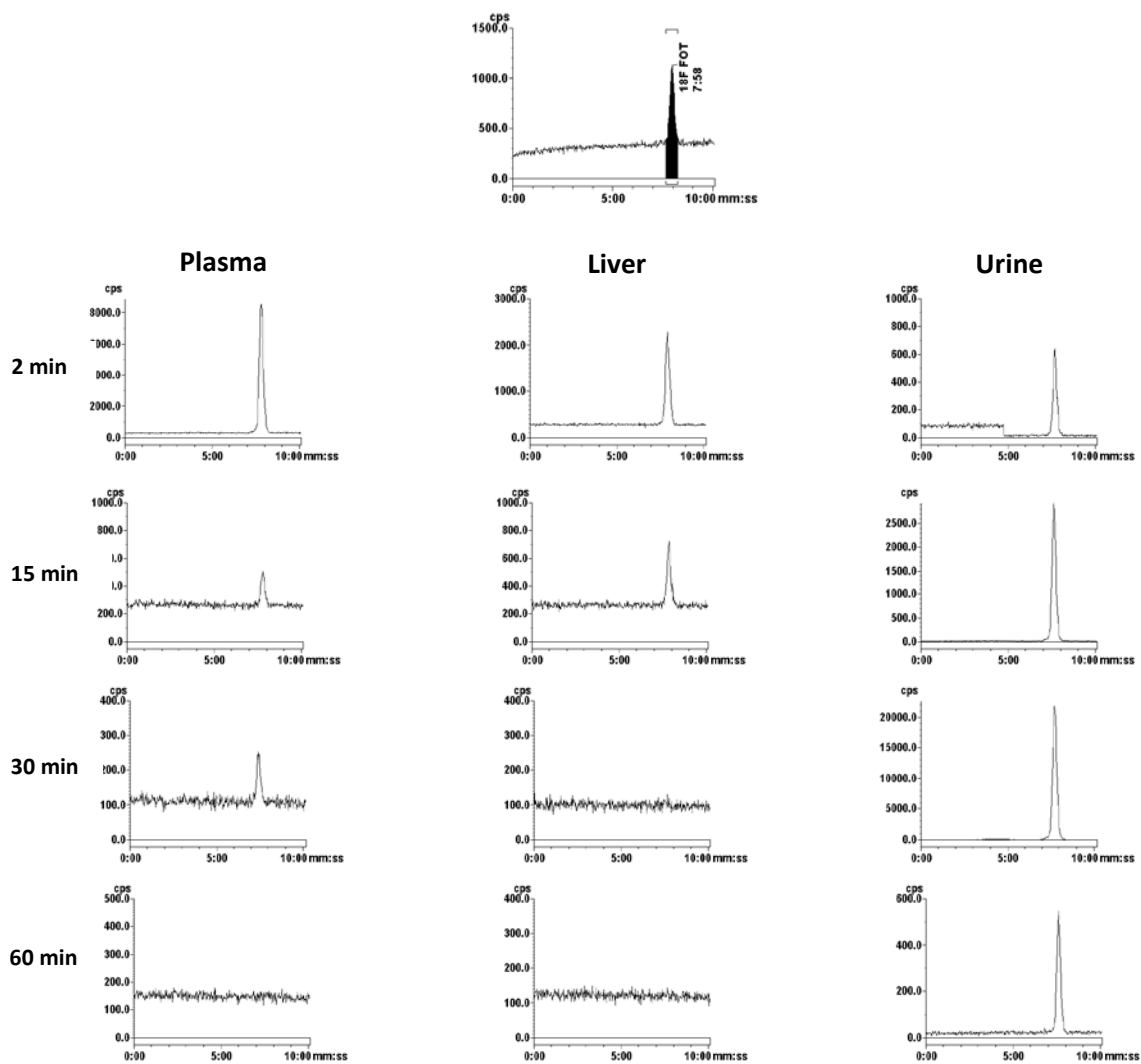
Figure 55. [¹⁸F]FOT metabolism in mouse plasma (left), liver (middle) and urine (right).
Top to bottom: reference standard, 2 minutes, 15 minutes, 30 minutes, 60 min. Representative samples were obtained from three to four mice per time point.

Biodistribution was also performed to follow the accumulation of the radiotracers in specific tissues and to trace the route of excretion (Figure 56). [¹⁸F]FOT seemed to be rapidly cleared from most of the analysed tissues via the urinary tract and the intestine, with the radioactivity being accumulated in the urine at the first time point evaluated (2 minutes, Figure 56B). [¹⁸F]FTT seemed to be accumulated in proliferative tissues such as the intestine, as well as being excreted via kidneys and intestine (Figure 56A).
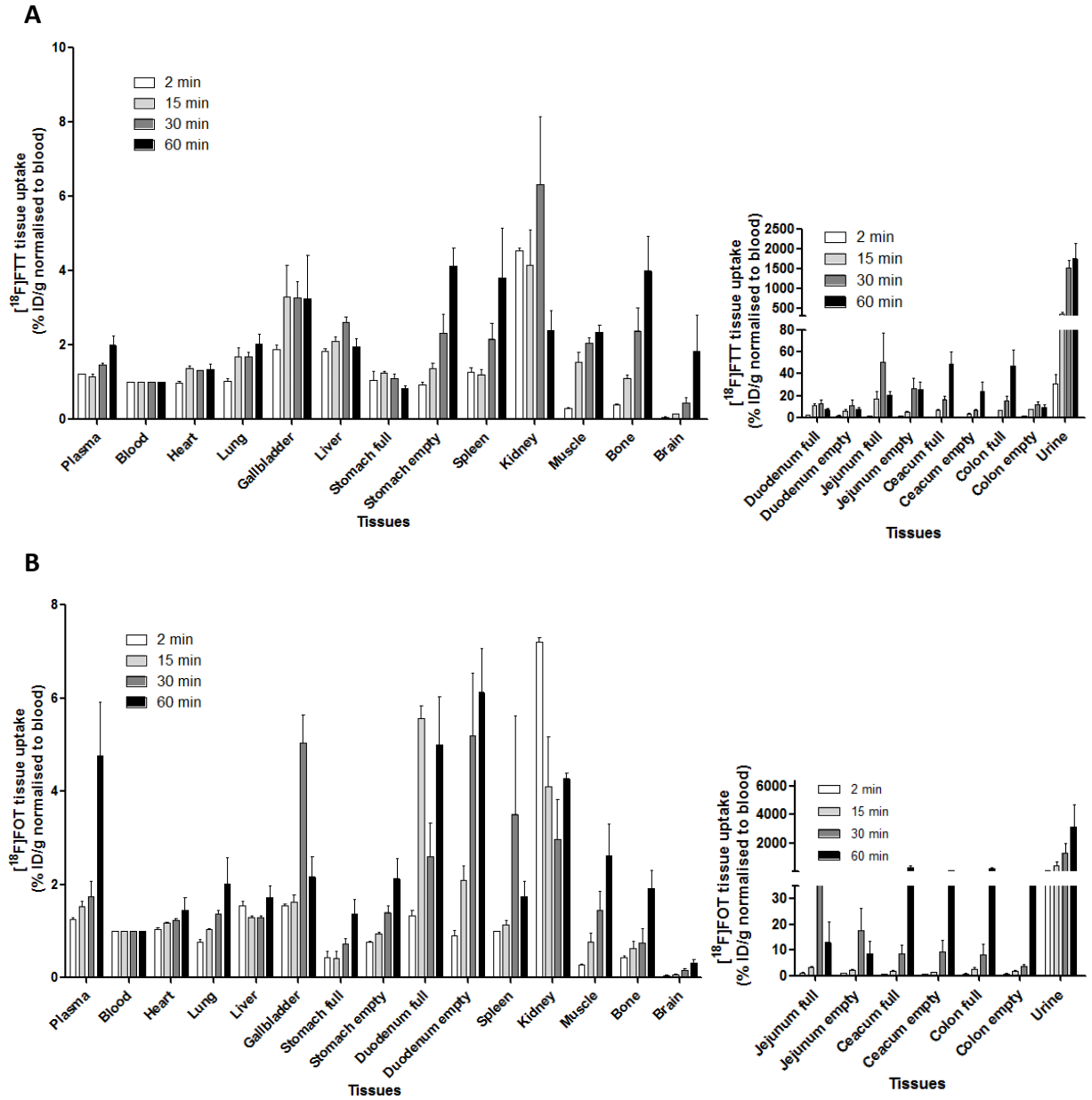
Figure 56. Time-course biodistribution of [18F]FTT and [18F]FOT.
Female BALB/c mice were injected i.v. with ~2.9-3.7 MBq. At the specified time point, mice were sacrificed by exsanguination and the various organs and tissues were excised. The radioactivity in each tissue was counted on a gamma counter and normalised to weight (g). Data are representative of n=3 per time point. A) [18F]FTT biodistribution. B) [18F]FOT biodistribution. For clarity, graphs are divided in tissues with low (left panels) and high uptake (right panels).

As a proof of concept, [18F]FTT- and [18F]FOT-PET imaging were performed to visualise tumour uptake *in vivo* after a 60 minutes dynamic scan. As represented in Figure 57A, both radiotracers failed to successfully highlight cell proliferation of the tumour, producing high background signal generated mainly by the intestine. TACs (Figure 57B and C) also showed initial uptake of both radiotracers into the tumour, followed by progressive washout with time, an indication of the fact that they could not be retained into the tissue.
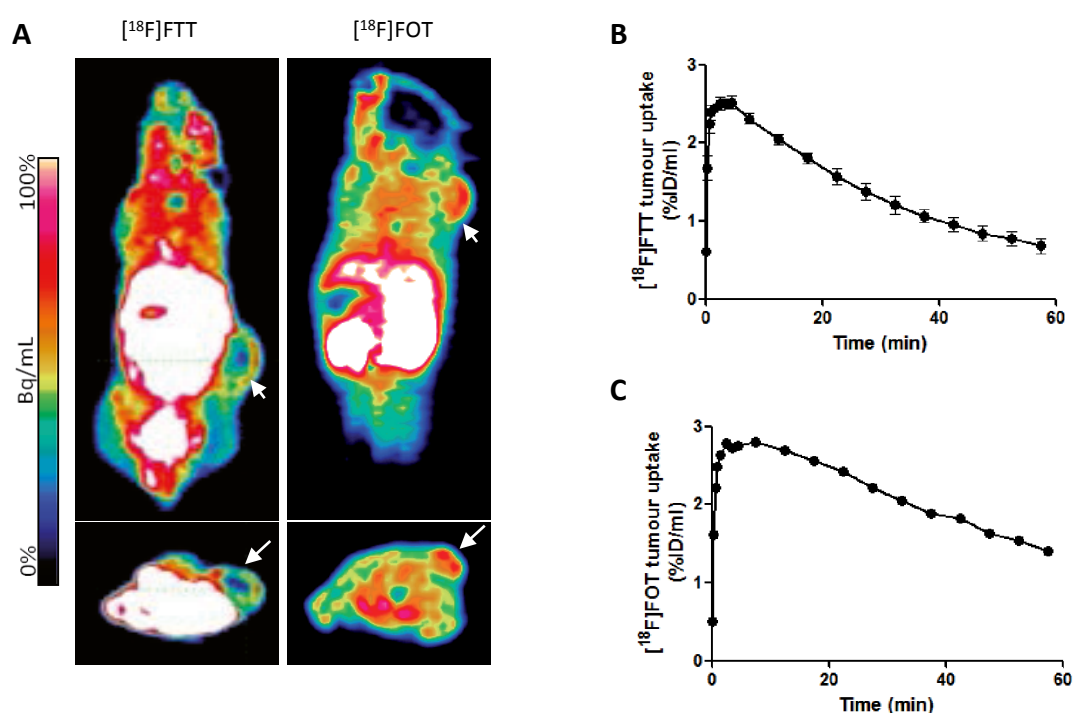
Figure 57. 60 min dynamic PET scan with [18F]FTT or [18F]FOT.
A) Coronal (top) and axial (bottom) PET images of representative tumour-bearing mice injected i.v. with 3.7 MBq [18F]FTT (left) or [18F]FOT (right, OSEM 3D reconstruction). White arrows are pointing to the tumours. B) Time-activity curve of [18F]FTT tumour uptake (n=2). B) Time-activity curve of [18F]FOT uptake into the tumour (n=1).

In conclusion, PET imaging using [18F]FTT and [18F]FOT supported the *in vitro* experiments, suggesting that the radiotracers could not provide better accuracy in the measurement of tumour proliferation compared to [18F]FLT. This result was expected in the case of [18F]FOT, having it been designed to support the oxygen substitution in [18F]FTT. However, even [18F]FTT did not show visible advantages compared to [18F]FLT.

3.4 Mitotic inhibition and [^{18}F]FLT cell uptake

3.4.1 Novel mitotic targets

Microtubule poisons are used as anti-mitotic agents to treat cancer; however, they do not selectively target cancer cells, producing a series of side effects (see Chapter 1, section 1.1.3). The use of novel agents able to target tumour cells specifically can confer a great advantage.

Paclitaxel was previously used to validate the ability of [^{18}F]FLT to highlight mitotic arrest (Chapter 3.2, section 3.2.4). Inhibitors acting on novel targets were subsequently investigated to understand if [^{18}F]FLT uptake was altered following treatment with novel mitotic inhibitors.

There is limited data available describing the effect of mitotic inhibitors on [^{18}F]FLT uptake. Nucleoside uptake is regulated by different proteins including ENT1, TK1 and thymidine phosphorylase (TP). The effect of mitotic inhibitors on the uptake of [^{18}F]FLT was examined in HCT116 and BT-20 (human breast cancer) cells in relation to these proteins together with phospho-TK1 and cell cycle dynamics. The two cell lines were selected in order to compare the effect of mitotic inhibition in cells containing normal (HCT116) or supernumerary (BT-20) centrosomes, as suggested by Dr Spiros Linardopoulos from the Division of Cancer Therapeutics at the Institute of Cancer Research (ICR). The mitotic inhibitors used included Aurora A and Aurora B specific inhibitors MLN8237 (Gorgun et al., 2010, Manfredi et al., 2011) and AZD1152 (Wilkinson et al., 2007), respectively, and the PLK1 inhibitor BI 2536 (Steegmaier et al., 2007).

Western blot analysis is represented in Figure 58. MLN8237 and AZD1152 showed no difference in TK1 protein phosphorylation compared to DMSO control in both HCT116 and BT-20 cells. In accordance, TK1 total protein expression remained constant between the different conditions. On the contrary, treatment with 500 nM of PLK1 inhibitor BI 2536

resulted in induction of the G2/M specific phosphorylation of TK1 (band #3, lanes 4 and 8, white arrows), suggesting G2/M arrest of both HCT116 and BT-20 cells. A corresponding 2-fold increase in total TK1 protein levels was visible when testing for total TK1 content. TS, TP and ENT1 expression levels were maintained at comparable levels under each condition.
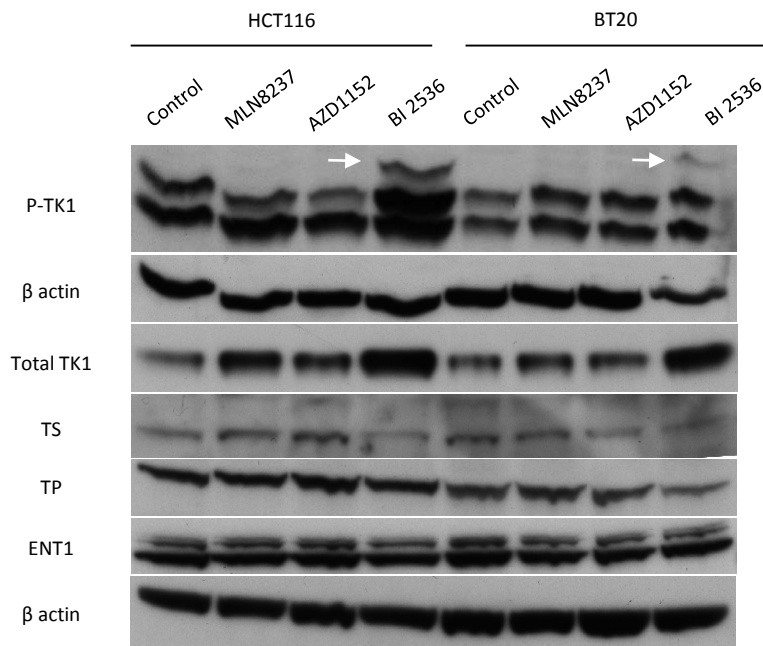
Figure 58. Protein expression in HCT116 and BT-20 cells following treatment with mitotic inhibitors.
Representative western blot analysis of HCT116 and BT-20 cells treated with 500 nM MLN8237, AZD1152 or BI 2536 for 24h. Proteins were resolved on 12% acrylamide + 75 µM MnCl₂-phos-tag™ and 12% NuPAGE gels. P-TK1, phospho-TK1; TS, thymidylate kinase; TP, thymidine phosphorylase.

Cell cycle distribution following treatment was tested (Figure 59), producing an increase of HCT116 cells arrested in G2/M phase following inhibition of Aurora kinases (2.5-fold increase following Aurora A inhibition with MLN8237; 4-fold increase after treatment with AZD1152) and PLK1 (2.5-fold; Figure 59A). AZD1152 and BI 2536 seemed to induce G2/M arrest more efficiently. Notably, AZD1152 treatment resulted in 8-fold increase in the super-G2 population of HCT116 compared to control, suggesting possible endoreduplication, in accordance with disruption of cytokinesis following Aurora B inhibition.

Treatment of BT-20 cells resulted in G2/M accumulation following PLK1 inhibition (4-fold increase compared to control), whereas treatment with MLN8237 and AZD1152 did not show major effects on cell cycle distribution (Figure 59B).
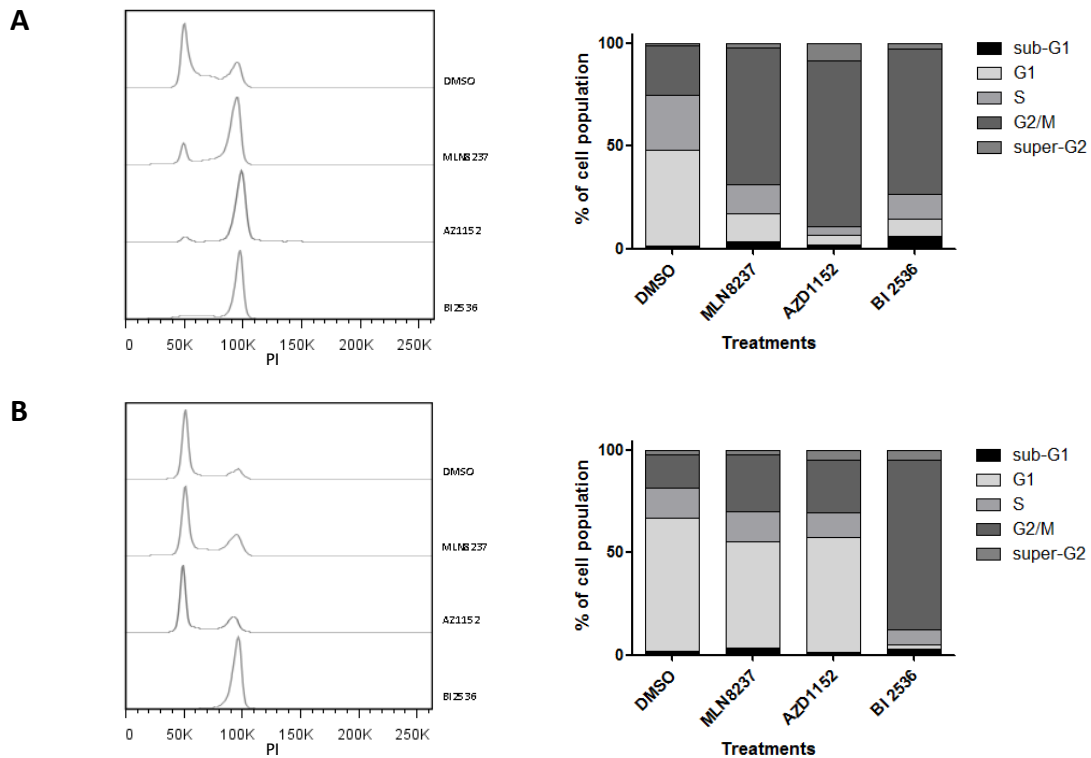
Figure 59. Representative cell cycle distribution after treatment with 500 nM of the indicated drugs.
HCT116 (A) and BT-20 (B) cells were treated with 500 nM MLN8237, AZD1152 or BI 2536 for 24h. Analysis of DNA content was performed after propidium iodide staining (PI). Left panels report representative plots of DNA content; right panels indicate the percentages of cells accumulated in the different phases of the cell cycle. Sub-G1, cell death; super-G2, possible endoreduplication.

The effects on centrosome number and mitotic spindle formation were tested by immunofluorescence staining of the γ-tubulin component of centrosomes in unsynchronised cells. Green dots in Figure 60 and Figure 61 represent centrosomes in each cell.

HCT116 contained normal centrosome number (1 in interphase, 2 during mitosis) and showed reduced proliferation, as indicated by cell number (80% less cells), following each treatment. More interestingly, MLN8237 inhibition of Aurora A resulted in the complete absence of normal mitotic spindle formation (Figure 60, second panel from left), which

was instead present in control samples as 1% of the total population (Figure 60, left panel, white arrows). This is in accordance with literature, where presence of a monopolar spindle and arrest in prometaphase and metaphase have been reported following inhibition of Aurora A. Additionally, 4% of the population contained more than 2 centrosomes, which failed to migrate at the opposite poles of the cell. Hoar *et al.* described centrosome amplification following inhibition of Aurora A with a specific inhibitor, due to defects in the previous cell cycle (Hoar et al., 2007).

Inhibition of Aurora B with AZD1152 prevented cytokinesis, as shown by the production of cells of increased size, containing multiple nuclei (Figure 60, third panel from left, red arrows; 90% of multinucleated cells). Moreover, 5% of the total population presented multiple centrosomes, consequently generating cells with multiple spindle poles (4% of the total population). These results are in accordance with the role of Aurora B in promoting cytokinesis; if the kinase is inhibited, cell division cannot be completed.

Finally, 24 hours treatment with the PLK1 inhibitor BI 2536 induced apoptosis in 40% of the analysed cells, as indicated by the presence of apoptotic bodies following DAPI staining (Figure 60, right panel, yellow arrows). BI 2536, in fact, induces mitotic arrest followed by apoptosis (Lenart et al., 2007).
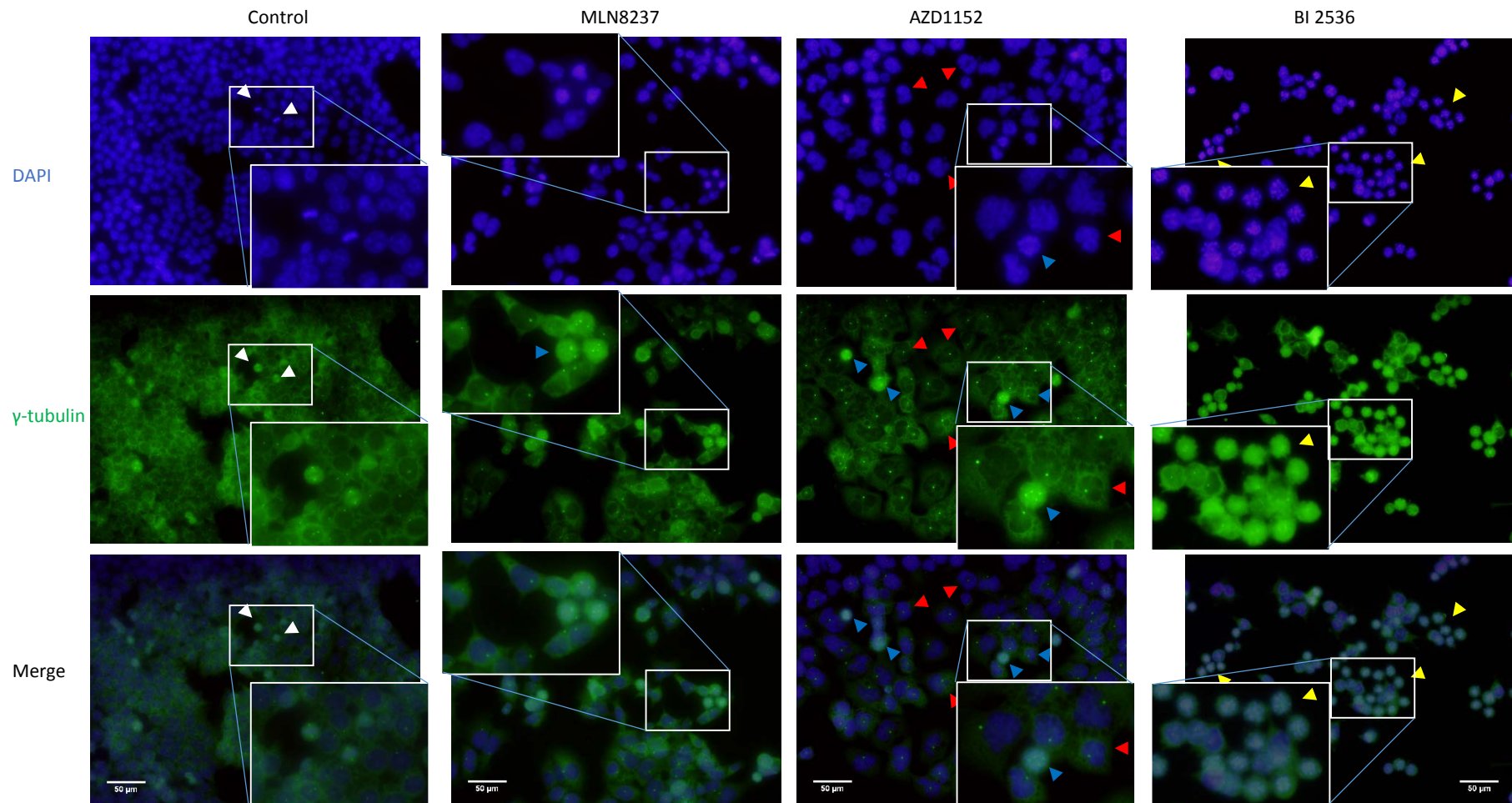
Figure 60. Effects of Aurora kinases and PLK1 inhibition in HCT116 cells.
Representative images of HCT116 cells treated with 500 nM MLN8237, AZD1152 or BI 2536 for 24h, fixed and stained for γ-tubulin (green) and DAPI (blue). Control refers to cells treated with DMSO. Green dots indicate centrosome staining. Mitotic spindle formation is highlighted by white arrows in control samples. No mitotic spindles were visible following treatments. Red arrows highlight multi-nucleated cells. Yellow arrows indicate apoptotic cells. Blue arrows point at cells containing supernumerary centrosomes. Scale bar is reported on the merged image in each panel. Selected areas are represented at higher magnitude in the smaller pictures.

BT-20 cells were characterised by the presence of supernumerary (>2) centrosomes, as indicated by red arrows in control sample (3% of the total population). Although Aurora A inhibition did not produce any major effects on TK1 phosphorylation (Figure 58) and cell cycle distribution (Figure 59B), immunofluorescence staining showed abnormalities in cell size, possibly indicating initial mitotic arrest. In addition, centrosome number was still altered as highlighted by red arrows (Figure 61, second panel from left; 13% of the total population). AZD1152 treatment did not produce major effects on cell cycle arrest, as mitotic cells represented 5% of the analysed population (Figure 61, third panel from left, white arrows). Multiple spindles were also detectable as 2% of the population (Figure 61, third panel from left, red arrows). PLK1 inhibition with BI 2536 resulted in the induction of apoptosis in 55% of the analysed cells (Figure 61, right panel, yellow arrows).

Of important note regarding treatment with BI 2536, round cells present in the culture medium and indicating mitotic arrest could not be fixed and therefore analysed by immunofluorescence. This ratio of the population was however included in western blotting and flow cytometric analysis.
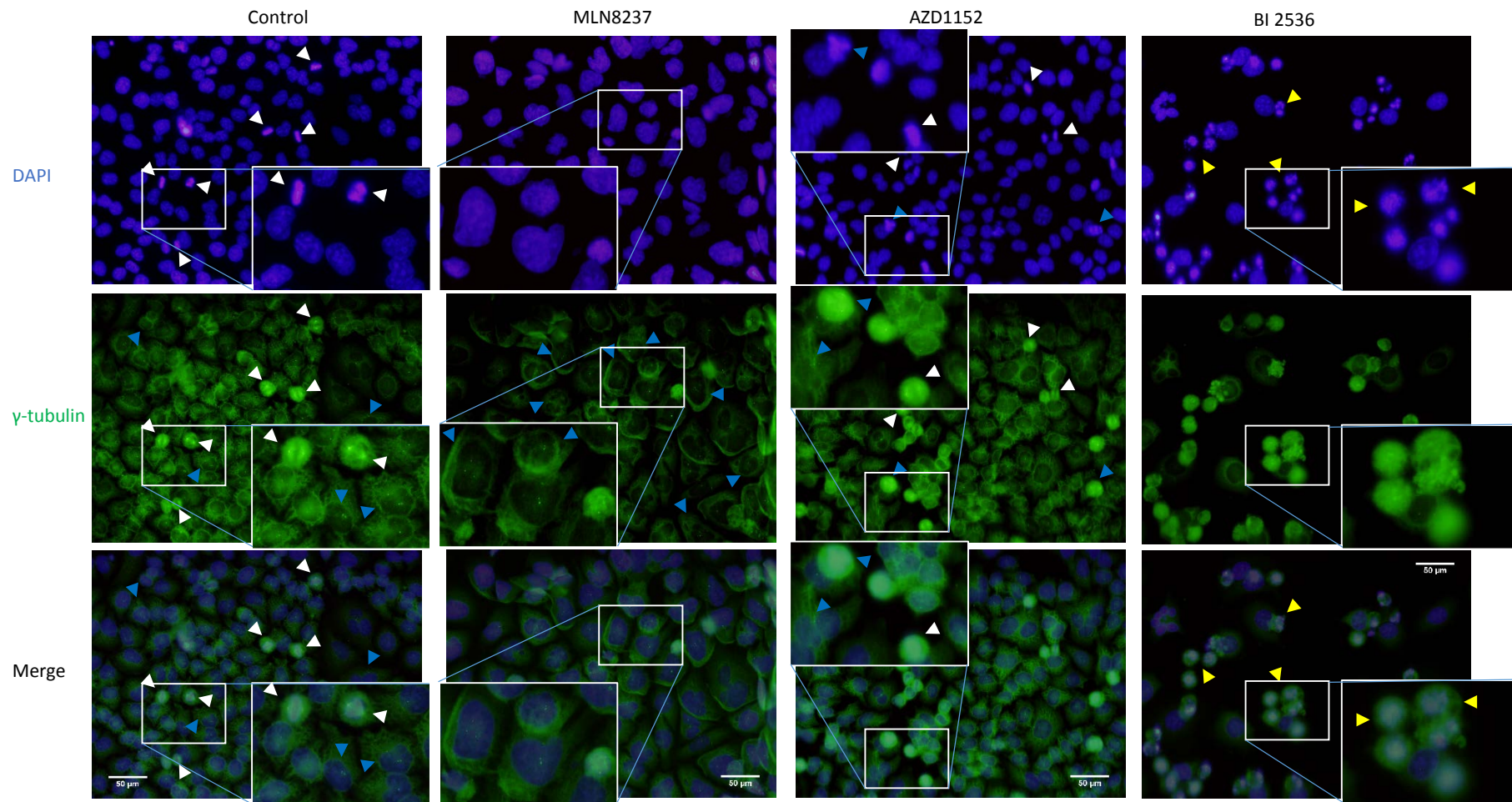
Figure 61. Effects of Aurora kinases and PLK1 inhibition in BT-20 cells.
Representative images of BT-20 cells treated with 500 nM MLN8237, AZD1152 or BI 2536 for 24h, fixed and stained for γ-tubulin (green) and DAPI (blue). Control refers to cells treated with DMSO. Green dots indicate centrosome staining. White arrows indicate normal mitotic spindle formation; blue arrows highlight the presence of supernumerary centrosomes and formation of multiple spindle poles; yellow arrows point at apoptotic cells. Scale bars are represented on the merged image of each panel. Selected areas are represented at higher magnitude in the smaller pictures.

Possible effects of inhibition of the selected mitotic targets on the uptake of [^{18}F]FLT were tested in both cell lines. As shown in Figure 62A, inhibition with MLN8237, AZD1152 and BI 2536 resulted in a significant 4-fold reduction in [^{18}F]FLT uptake in HCT116 cells (p<0.005), in accordance with mitotic arrest as shown in Figure 58 and Figure 59.

BT-20 cells showed significantly reduced [^{18}F]FLT uptake following PLK1 inhibition with BI 2536 (70% reduction compared to control; p<0.005), reflecting the induction of TK1 mitotic phosphorylation (responsible for its reduced activity) shown in Figure 58. Radiotracer uptake after Aurora kinase A inhibition with MLN8237 decreased by 30% (p<0.05); in contrast, cells treated with AZD1152 showed [^{18}F]FLT uptake similar to control (Figure 62B).
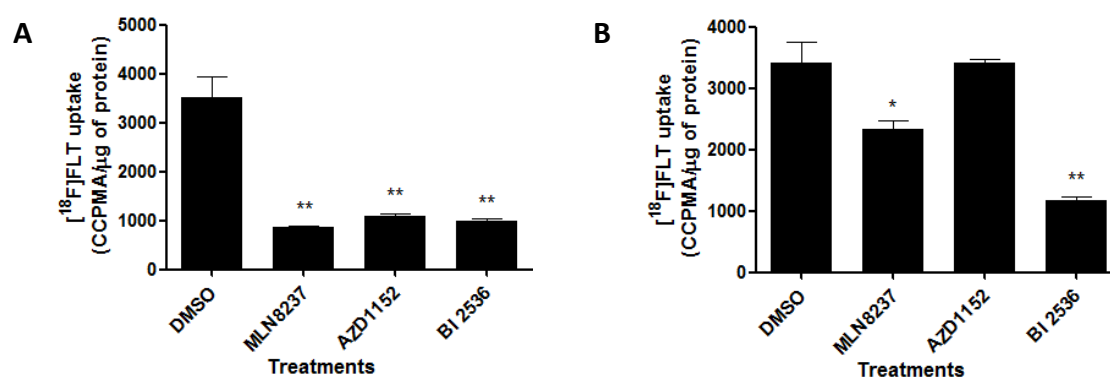
Figure 62. [^{18}F]FLT uptake in HCT116 and BT20 cells after 24h treatments with the indicated inhibitors.
HCT116 (A) and BT-20 (B) cells were treated with 500 nM of each inhibitor for 24h. DMSO was used as control. ~0.37 MBq were added to each well (n=3).

To conclude, [^{18}F]FLT is able to provide a snapshot of the success of a specific anti-mitotic treatment, but in order to interpret the results correctly, the drug effects on the radiotracer uptake must be thoroughly understood. Differences between the various tumour types must as well be taken into consideration, as differences between the two cell lines tested proved in the reported experiments.

BT-20 results could be improved by testing higher concentrations of the different drugs.

To summarise:

- In HCT116 cells, all three inhibitors led to G2/M arrest and reduction of [^{18}F]FLT uptake. Clear increase in phospho-TK1 was only seen following PLK1 inhibition (concomitant with the most pronounced G2/M arrest and apoptosis), suggesting that other mechanisms, e.g. reduction in TK1 expression, may explain the reduction in [^{18}F]FLT uptake following Aurora A and Aurora B kinase inhibition. Previous work with Aurora kinase inhibitors (Chan et al., 2007) indicated reduced TK1 expression consequent to Rb hypophosphorylation. Thus any phospho-TK1 may be masked by reduced total TK1 protein.

- In BT-20 cells, only PLK1 inhibition and to a lesser extent Aurora A inhibition led to G2/M arrest and consequent reduction in [^{18}F]FLT uptake. This reduction in [^{18}F]FLT uptake may be linked to TK1 phosphorylation during mitotic arrest.

3.4.2 Kinesins as new potential targets for cancer therapy

The kinesin protein KIFC1 (HSET) has been reported to play a role in clustering multiple centrosomes in cells containing supernumerary centrosomes in order to prevent the formation of multipolar spindles. Therefore it is an interesting target to selectively kill cancer cells, without affecting normal cell proliferation in non-cancerous cells (see Chapter 1, section 1.1.3). The effects of KIFC1 knock-down in HCT116 and BT-20 cells (containing supernumerary centrosomes) were investigated and the impact on $[^{18}F]FLT$ uptake was subsequently tested.

KIFC1 siRNA was used as a means to possibly induce selective cell death in BT-20 cells, which contain multiple centrosomes (>2). RNAi optimisation was firstly carried out (Figure 63). Knock-down of KIFC1 reduced protein expression by 60% even at the lowest concentration of siRNA (5 nM) in both cell lines.
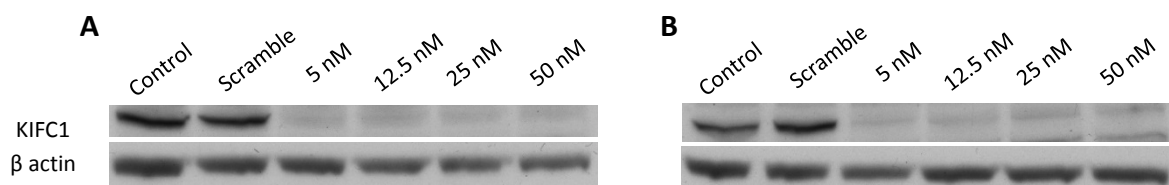
Figure 63. Optimization of KIFC1 knock-down using RNA interference.
Indicated concentrations were used to induce protein silencing. 25 nM scramble siRNA was used as control. A) Representative KIFC1 knock-down in HCT116 cells. B) Representative KIFC1 silencing in BT-20 cells. 30 µg of proteins were resolved on 12% NuPAGE gels.

TK1, TS, TP and ENT1 expression levels were subsequently tested in cells transfected with 5 nM KIFC1 siRNA.

KIFC1 knock-down proved to be successful in both cell lines (Figure 64, lanes 3 and 6). However, no significant differences in TK1, TS, TP and ENT1 protein expression were highlighted in transfected cells compared to the respective controls (Figure 64).
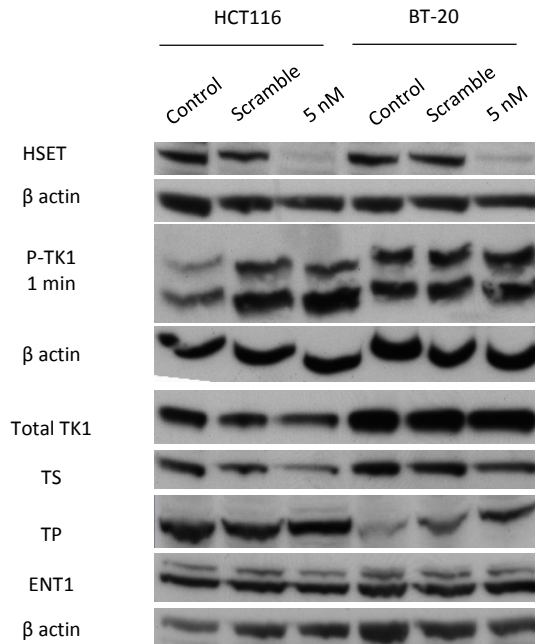
Figure 64. Protein expression in HCT116 and BT-20 cells following transfection with 5 nM KIFC1 siRNA.
Representative western blot analysis of HCT116 and BT-20 cells transfected with 5 nM non-targeting scramble or KIFC1 siRNA for 48h. Proteins were resolved on 12% acrylamide + 75 μM MnCl$_2$-phos-tag™ and 12% NuPAGE gels. P-TK1, phospho-TK1; TS, thymidylate kinase; TP, thymidine phosphorylase.

Cell cycle distribution of HCT116 and BT-20 cells following siRNA transfection is represented in Figure 65. No differences in the distribution of the population along the cell cycle were detected, suggesting no major effects on cell cycle progression following KIFC1 knock-down.
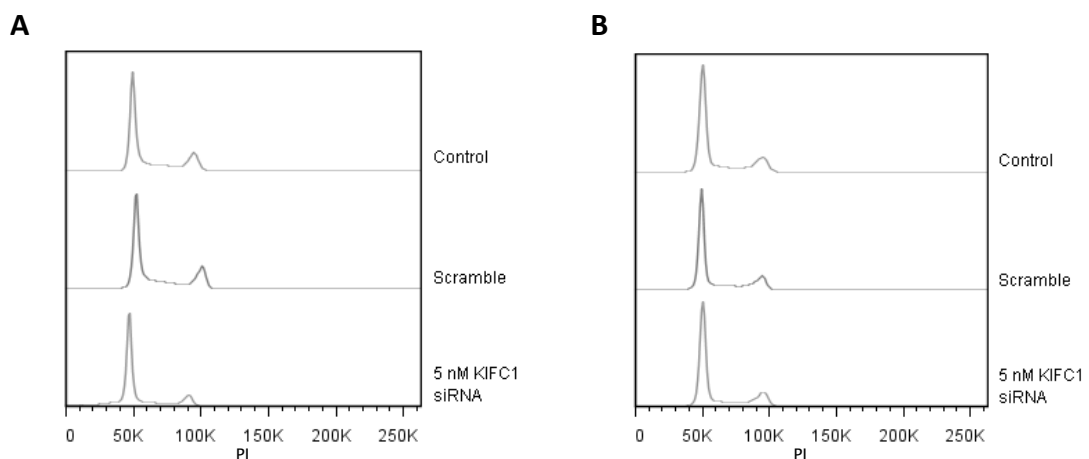
Figure 65. Cell cycle distribution following transfection with 5 nM KIFC1 siRNA.
HCT116 and BT-20 cells were transfected with 5 nM non-targeting scramble or KIFC1 siRNA for 48h and subsequently analysed for their DNA content. A) HCT116 cell cycle distribution. B) BT-20 cell cycle distribution. PI, propidium iodide.

Subsequently, preliminary [^{18}F]FLT cell uptake was also performed in HCT116 and BT-20 cells following RNAi (Figure 66). KIFC1 knock-down in HCT116 resulted in 20% reduction of radiotracer uptake compared to control (Figure 66A). However, no differences in radiotracer uptake were detected in BT-20 cells under the same experimental conditions (Figure 66B).
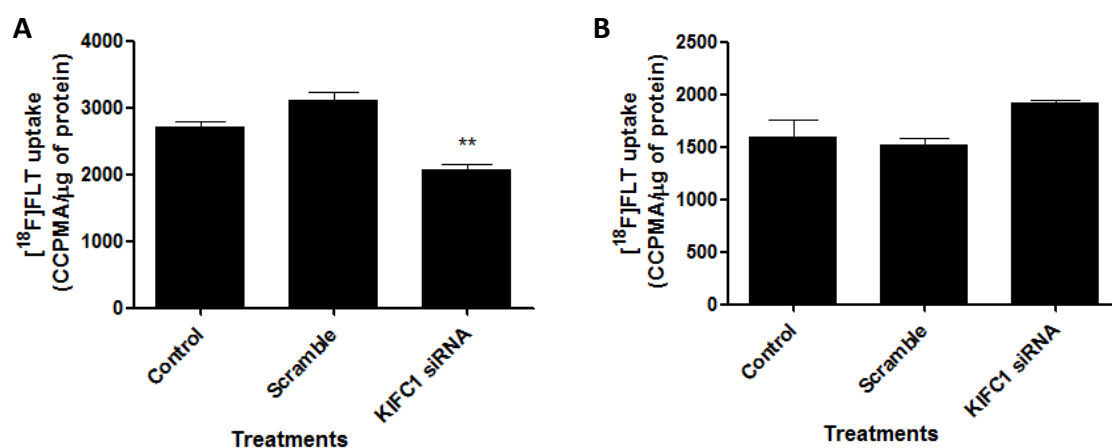
Figure 66. [^{18}F]FLT uptake in HCT116 and BT-20 cells.
[^{18}F]FLT cell uptake was tested in HCT116 (A) and BT-20 (B) following 48h transfection with5 nM non-targeting scramble or KIFC1 siRNA. 0.37 MBq were added to each well (n=4).

HCT116 and BT-20 cells were further analysed via immunofluorescence to verify the effects of KIFC1 depletion (Figure 67 and Figure 68).

Silencing of KIFC1 did not seem to produce any effect on HCT116 cells, with mitosis occurring at similar rate compared to control and scramble control (2% of the population under each condition; Figure 67). The same result was obtained with KIFC1 knock-down in BT-20 cells (Figure 68), in contrast to expectations. KIFC1 was in fact hypothesised to be important for centrosome clustering in cells with supernumerary centrosomes, like BT-20, in order to prevent the formation of multipolar spindle, therefore allowing normal mitosis. Knock-down of KIFC1 was expected to trigger cell death due to increased formation of abnormal spindles containing multiple poles. However, these results suggested that KIFC1 was dispensable in BT-20 cells, which were able to progress through

mitosis even after KIFC1 knock-down, at least under these experimental conditions (60% reduction of KIFC1 protein). Different mechanisms may act on centrosome clustering in cells containing amplified centrosomes such as BT-20 cells (Gergely and Basto, 2008); research is still ongoing to identify the specific proteins involved in this process.
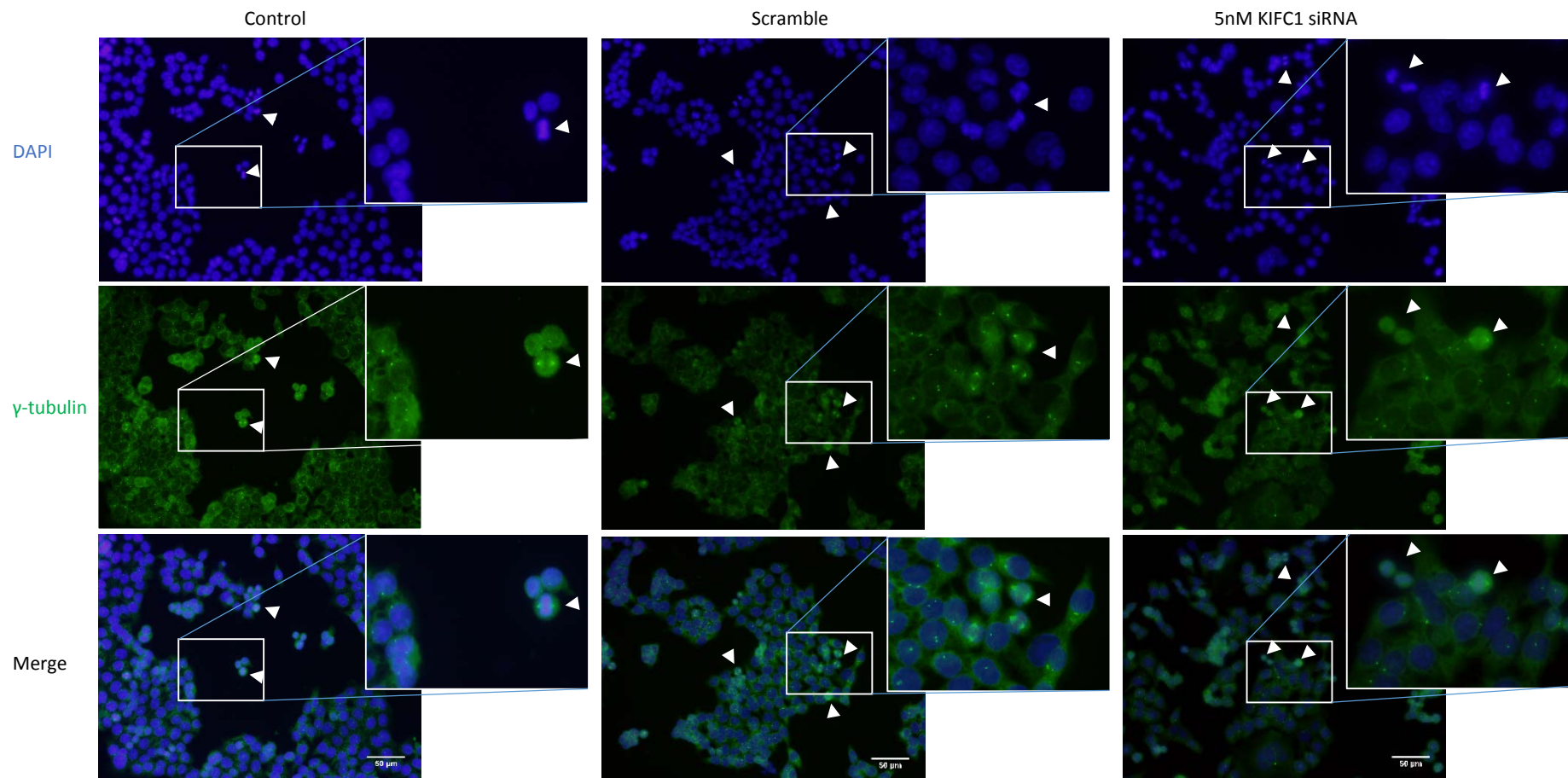
Figure 67. KIFC1 knock-down does not affect HCT116 replication.
HCT116 cells were transfected with 5 nM non-targeting scramble or KIFC1 siRNA for 48h. Green dots represent centrosomes. Mitotic spindles are highlighted by white arrows. The selected area is represented at higher magnitude in the smaller panel.
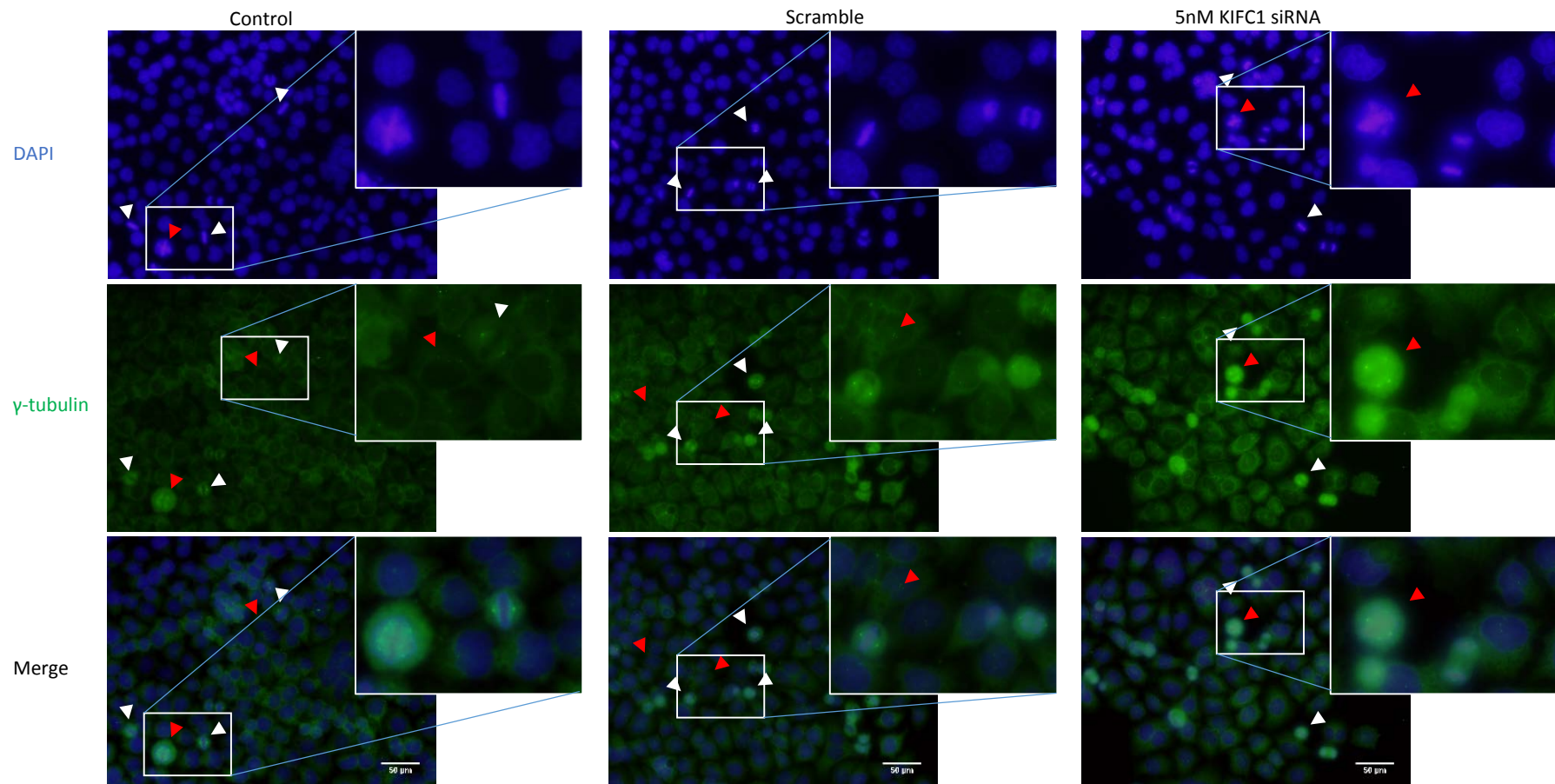
Figure 68. KIFC1 is dispensable for BT-20 progression through mitosis.
BT-20 cells were transfected with 5 nM non-targeting scramble or KIFC1 siRNA for 48h. Green dots represent centrosomes. Mitotic spindles are highlighted by white arrows. Red arrows, supernumerary centrosomes/multiple spindles. The selected area is represented at higher magnitude in the smaller panel.

In conclusion, preliminary results using RNA interference in BT-20 cells to knock-down the kinesin protein KIFC1 did not produce any significant difference compared to control cells. Additional experiments should be performed to confirm if KIFC1 is indeed dispensable for BT-20 replication, or if it is possible that the residual protein expression following knock-down could be sufficient to allow progression through mitosis. Further experiments are warranted to address these questions, and alternative cellular models could be used to further validate this hypothesis and to elucidate the effect of KIFC1 knock-down on FLT uptake.

- In HCT116 cells, knock-down of KIFC1 resulted in reduced [^{18}F]FLT uptake. This decrease, however, was not linked to a correspondent decrease in TK1 expression or differential TK1 phosphorylation, and there was no indication of G2/M arrest.

- In BT-20 cells, KIFC1 silencing did not produce any significant effect on protein expression, cell cycle distribution or [^{18}F]FLT cell uptake.

Chapter 4. Discussion

4.1 Identification of TK1 phosphorylated isoforms and the effects on [^{18}F]FLT uptake

The development and optimization of a method to investigate TK1 protein phosphorylation was necessary due to the absence of a specific antibody able to recognise phosphorylated forms of TK1. The two tested antibodies gave different specificity, possibly due to the antigen used to generate them. Use of 12% SDS NuPAGE gels failed to provide resolution of TK1 phosphorylated bands. TK1 is a small protein of 25 kDa, therefore higher percentages of gels and longer runs should be considered in order to separate different isoforms of the protein. Therefore, the phos-tag™ system was employed as a novel technique which proved to be suitable to distinguish between different types of TK1 phosphorylations. However, extensive optimization was required to obtain good resolution of the protein of interest. Several problems were encountered, possibly due to phos-tag™ and buffers instability, thus delaying the process of optimization. Alternative techniques can be employed to separate phosphorylated species of a protein, e.g. maxi gels containing higher percentage of acrylamide or native gels, but as well as phos-tag™ gels they require optimization and might not give reproducible results. Immunoprecipitation (IP) could have supported the results obtained from phos-tag™ gels, but the primary antibody should have been cross-linked to the beads to eliminate the signal generated by the light chain of the antibody used for immunoprecipitation (running at the same molecular weight as TK1 protein), therefore being able to appropriately quantify the signal. Isoelectric focusing (IEF) was trialled as well, being a quantitative technique which could help in the further validation of TK1 phosphorylated forms. It is limited by the fact that a suitable antibody which could be used with this specific system needs to be identified.

The employment of novel and high-throughput techniques to study TK1 protein phosphorylation would be extremely valuable to confirm the findings described in Chapter 3.1.

HCT116 cells proved to be a good model to study TK1 regulation during the progression of the cell cycle, expressing the protein and retaining [^{18}F]FLT at higher levels compared to A549, Hos and Ost TK1$^-$. The relative expression of TK1 and TS was investigated in order to understand the differential usage of the *de novo* or salvage pathway for DNA synthesis. TS was hypothesised to be highly expressed in cells relying on the former, with TK1 being predominant in cells mainly utilizing the salvage pathway (Pressacco et al., 1995). Results shown in Chapter 3.1.2 suggested generally higher expression of TS in cells expressing lower levels of TK1, with a consequential difference in [^{18}F]FLT cell uptake (Chapter 3.2.1). However, the difference in radiotracer uptake was not proportional to TK1 protein expression level.

Being able to identify the relative usage of the two pathways involved in thymidine supply is important in the development of new drugs targeting the two main enzymes in these pathways (TS and TK1), as well as in the field of positron emission tomography (PET) imaging, when nucleotide analogues are developed and characterised to image cell proliferation (Wells et al., 2004). Different tumours, in fact, can rely differentially on one of the two pathways, thus having an impact on the type of drug that can be effective for therapy (Pressacco et al., 1995). This has also an influence on [^{18}F]FLT tumour uptake, and therefore in the understanding of the images produced following [^{18}F]FLT-PET imaging (Brockenbrough et al., 2011).

In addition to the elucidation of TK1 protein expression in different cell lines and tumours, the determination of TK1 post-translational regulation is particularly important in the field of PET imaging, when nucleosides, specifically thymidine analogues, are developed to image cell proliferation. While a direct correlation between [^{18}F]FLT uptake and TK1 protein expression was initially reported (Barthel et al., 2005, Brockenbrough et al., 2011, Rasey et al., 2002), recent studies by several groups highlighted the need to further validate [^{18}F]FLT incorporation into tumours (McKinley et al., 2013, Zhang et al., 2012), as [^{18}F]FLT uptake did not seem to be directly proportional to TK1 protein expression. Moreover, Zhang and co-workers showed that thymidine levels in plasma and tumour tissue also influenced radiotracer uptake (Zhang et al., 2012, Shields, 2012, Van Waarde et al., 2004). However, this effect may be limited to rodents and not detected in humans due to different concentrations of plasma thymidine in the different organisms.

Chang and co-workers originally proposed the hypothesis that TK1 post-translational regulation, specifically phosphorylation, played a part in regulating its activity (Chang et al., 1998, Ke and Chang, 2004); this phenomenon could therefore influence radiotracer uptake. In their study, Chang and co-workers (Chang et al., 1998) reported the G2/M specific phosphorylation of TK1 on Ser13. Following this lead, a G2/M-specific phosphorylated isoform was successfully separated on MnCl$_2$-phos-tag™ western blots, together with another phosphorylated species present throughout the cell cycle, which was reduced after roscovitine treatment. An extra phosphorylated form appeared in synchronized cells after induction of G2/M arrest, which remains to be characterized. Following these experiments, identifying the type of phosphorylation of each isolated band became important. The determination of the phosphorylated amino-acid residues

was approached by transfecting TK1-depleted cells (Ost TK1⁻) with DNA plasmid vectors coding for mutated versions of TK1 cDNA. According to Chang *et al.* (Chang et al., 1998), Ser13 phosphorylation during G2/M was responsible for the reduced TK1 activity at this stage of the cell cycle, causing the dissociation of the tetrameric form of the protein. Our findings, however, suggested that Ser13 might be needed for TK1 enzymatic activity. In fact, if Ser13 was exclusively phosphorylated to reduce TK1 activity during G2/M, the substitution with an alanine, which cannot be phosphorylated, should maintain [^{18}F]FLT uptake, i.e. TK1 activity, close to wild type TK1, even after nocodazole treatment. On the contrary, S13A substitution caused a significant decrease in [^{18}F]FLT uptake compared to WT control, suggesting a role for Ser13 phosphorylation in maintaining the activity of the enzyme; moreover, nocodazole treatment of cells transfected with the S13A version of TK1 showed a significant decrease compared to untreated sample, suggesting at least that the phosphorylation of a different residue might have been responsible for TK1 activity reduction, since, if Ser13 specific phosphorylation was inducing a reduction in the activity of the enzyme during G2/M phase, nocodazole treatment of cells expressing S13A TK1 would have caused no changes compared to non-treated control in terms of [^{18}F]FLT uptake.

Ser231 seemed therefore to be the candidate residue to be specifically phosphorylated during mitosis; proteomic studies have shown phosphorylation of TK1 on Ser231 (Beausoleil et al., 2006, Dephoure et al., 2008), thus supporting our findings. Ser231 phosphorylation could induce the formation of the dimer (with low affinity for thymidine) and/or mark the protein for degradation. However, [^{18}F]FLT cell uptake after nocodazole treatment suggested that Ser231 might have not been the only phosphorylated residue during G2/M phase. These results, together with the observation that a fourth band was

visualised in synchronized cells and that band #2 intensity increased following nocodazole treatment, suggested the presence of additional residues involved in the process of TK1 regulation via phosphorylation. In their paper, Chang and co-workers (Chang et al., 1998) referred to two specific amino-acid residues which could be phosphorylated on TK1 protein sequence, in addition to Ser13 and Ser231: Ser30 and Ser194. Their characterization will be a priority to decipher TK1 regulation by phosphorylation, together with the determination of the enzymes responsible for these post-translational modifications.

Identification of the kinase responsible for TK1 phosphorylation was subsequently approached, following the suggestion that CDK1 and CDK2 might be the putative kinases involved in TK1 phosphorylation (Chang et al., 1998, Ke and Chang, 2004). Specifically, CDK2 might be responsible for TK1 activating phosphorylation during S phase, while CDK1 could specifically phosphorylate TK1 during G2/M. Results shown in Chapter 3.1, section 3.1.5 seemed to validate this hypothesis, with the G2/M specific phosphorylation being abolished after CDK1 knock-down and appearing in nocodazole-treated CDK2 knock-down cells. Furthermore, band #2, representing Ser13 phosphorylation, seemed to be reduced following CDK2 knock-down, suggesting that Ser13 might be phosphorylated earlier during the cell cycle (S phase) by CDK2 associated with its specific cyclin. This finding could also be in line with the result obtained following roscovitine treatment; roscovitine is supposed to be a CDK2 inhibitor, however it is known to inhibit other CDK complexes (Meijer et al., 1997). Arrest in G2/M following nocodazole treatment, however, rescued band #2 signal in CDK2 knock-down cells, suggesting that either CDK2 was substituted by other CDKs for the phosphorylation of specific substrates or additional residues, which could not be resolved on phos-tag™ gels, were

phosphorylated during mitosis. Further characterisation with additional mutant forms of TK1 is warranted to test these hypotheses.

TK1 regulation by phosphorylation should therefore be taken into account when assessing cell proliferation using [^{18}F]FLT, given that this radiotracer is a direct measure of TK1 activity. In fact, cell uptake experiments demonstrated that TK1 differential phosphorylation during the progression of the cell cycle had a direct impact on [^{18}F]FLT cell uptake, changing the efficacy of its conversion to [^{18}F]FLT-monophosphate, which is then trapped within the cell. In addition, G1 arrest produced a decrease in [^{18}F]FLT uptake due to low TK1 abundance in cells. S-phase arrest following aphidicolin treatment and G2/M arrest induced by nocodazole and paclitaxel resulted in a marked decrease in radiotracer uptake, reflecting dTTP modulation of TK1 activity during S-phase arrest (Munch-Petersen et al., 1995) and the decreased activity of the protein during G2/M, due to specific phosphorylation, respectively. Treatment with aphidicolin was expected to increase [^{18}F]FLT uptake, based on the shared view that the radiotracer measures DNA replication, even if indirectly; nevertheless, the possible dTTP negative feedback explains the results obtained with this experiment.

Treatment with PD0325901 produced a similar effect compared to serum starvation, in line with inhibition of mitotic kinases which are responsible for producing the cascade of events committing the cell to start duplicating.

Cisplatin reduced [^{18}F]FLT uptake by means of inducing DNA damage, consequently triggering apoptosis; TK1 protein expression decreased under this condition, with a marked decrease of band #2 specifically. This result suggests 1) reduced TK1 activation via phosphorylation of Ser13 and/or 2) possible TK1 degradation due to the presence of

extensive DNA damage which was inducing cell death via apoptosis. On the contrary, [^{18}F]FLT uptake increased dramatically after 5-FU treatment, confirming previous findings where redistribution of ENT1 transporters to the plasma membrane was demonstrated following treatment with the TS inhibitor in fibrosarcoma cells (Perumal et al., 2006); [^{18}F]FLT transport into cells is facilitated by ENT1, therefore redistribution of the transporters to the cell surface resulted in increased accumulation of the radiotracer inside the cell.

Finally, inhibition of phosphorylation by roscovitine and staurosporine was responsible for a reduction in [^{18}F]FLT uptake, confirming that post-translational modification of TK1 via phosphorylation plays an important role in the activation of the enzyme, beside reducing its activity as previously reported (Chang et al., 1998). To further sustain this hypothesis, we used a 4h roscovitine-treatment to reduce off-target effects associated with transcriptional induction of other proteins.

These novel findings therefore clearly suggest that [^{18}F]FLT uptake is modulated by TK1 phosphorylation. However, additional proteins which might modulate [^{18}F]FLT uptake, e.g. TS and ENT1, were not investigated; even though radiotracer retention is directly dependent on phosphorylation by TK1, ENT1 and TS might modulate the incorporation of [^{18}F]FLT into cells, specifically following treatment with anti-cancer drugs. Nonetheless, these findings change the common concept that [^{18}F]FLT uptake merely portrays alterations during DNA synthesis, showing that the radiotracer is sensitive to arrest in G2/M phase, representing therefore a broader sensitivity to proliferation. Furthermore, treatment with anti-cancer drugs and inhibitors clearly affects TK1 protein regulation via different mechanisms, which is consequently reflected on the uptake of [^{18}F]FLT. It is

therefore important to take these findings into consideration to be able to interpret [^{18}F]FLT-PET data correctly.

TK1 phosphorylation effects were further tested *in vivo*, performing [^{18}F]FLT-PET imaging after treatment with paclitaxel of HCT116 tumour-bearing mice. Even though HCT116 cells were efficiently arrested in G2/M phase *in vitro* and HCT116 xenografts responded to treatment with 3 i.p. injections of the drug over 10 days, [^{18}F]FLT-PET imaging did not show any significant reduction post-treatment. Western blotting and immunohistochemistry data seemed to support this result, suggesting that [^{18}F]FLT was acting as a true negative marker, given that there was no induction of TK1 phosphorylation and no early changes in proliferation rate of the tumours following treatment compared to control. Therefore, it was demonstrated that paclitaxel could not produce early changes in tumour proliferation at the concentrations used (20 or 40 mg/kg), possibly due to tumour microenvironment-dependent effect on pharmacokinetics and pharmacodynamics of the drug. It was speculated that sufficient levels of paclitaxel may not have reached the tumour to induce efficient G2/M arrest under the experimental conditions used: 24 hours and 48 hours 20 mg/kg or 40 mg/kg paclitaxel. The main goal of this experiment was to test early response to treatment to verify findings *in vivo*, but, given the results obtained, different doses and treatment schedules should be tested to verify these theories.

If TK1 regulation is disrupted following treatment with drugs, its activity may be impaired relative to cell cycle progression, and as a consequence [^{18}F]FLT will not always reflect cell proliferation properly. Therefore, even though there has been promising results using [^{18}F]FLT as a proliferation marker, its utility relies on the direct dependence on TK1

activity. There might be conditions under which TK1 retains its enzymatic activity when DNA synthesis has already terminated (Shields, 2003, Wells et al., 2004), thus not reflecting cell proliferation and producing false positive results. New radiotracers able to overcome the phosphorylation step carried out by TK1, but being retained in cells and efficiently incorporated into DNA might produce a more direct image of cell proliferation.

In conclusion, we demonstrated the presence of two phosphorylated residues on TK1 sequence, which are responsible for modulating the activity of the enzyme. Different residues seemed likely to be involved in this cell-cycle controlled regulation, which is achieved following the action of cyclin-dependent kinases (CDK1 and CDK2). In addition, TK1 regulation by phosphorylation modulated [^{18}F]FLT uptake *in vitro*; however, treatment of HCT116 tumour-bearing mice with paclitaxel did not show any early effect during [^{18}F]FLT-PET imaging after 24 or 48 hour treatment, due to the specific protocol used (single dose and scan after 24h, single dose and scan after 48h or double dose and scan after 48h). Later time points might have shown a decrease in [^{18}F]FLT tumour accumulation post-treatment, as suggested by HCT116-xenografts growth curve.

4.2 Validation of new radiotracers for cell proliferation imaging with PET

Two thymidine analogues were developed at the Imperial CCIC by Dr Graham Smith and tested for their suitability to be used as radiotracers for cell proliferation. Results shown in Chapter 3.3 suggested that they were not sufficiently retained in cells given their low efficiency in being phosphorylated to monophosphate, which represent the trapping process. Cell uptake and preliminary PET imaging also confirmed that both [^{18}F]FTT and [^{18}F]FOT could not be retained in cells or tumours, due to little or no phosphorylation. Nevertheless, metabolism experiments showed that [^{18}F]FOT was metabolically stable, whereas [^{18}F]FTT tissue samples generated a single metabolite 15 minutes post-injection; this species still needs to be characterized. The oxidative form, in which the sulfur atom might be oxidised *in vivo*, could be one of the possible explanations for the generation of this metabolite, where the sulfur atom present on the deoxyribose ring could incur into oxidation *in vivo*. However, [^{18}F]FTT had a longer half-life compared to [^{18}F]FOT and was taken up in proliferative tissues, such as intestines, suggesting that it may be accumulated into tumours.

In conclusion, [^{18}F]FTT was demonstrated to be unsuitable for imaging cell proliferation with PET; this result, although disappointing, confirmed the notion that TK1 is the restrictive enzyme in terms of phosphorylation of thymidine analogues, accepting only minor substitutions on the sugar portion of its substrates (Arner and Eriksson, 1995). This has led to a next generation of radiotracers within the CCIC, which could be taken up into cells hopefully avoiding phosphorylation by TK1, but being able to be incorporated into the DNA.

4.3 Mitotic inhibition and [^{18}F]FLT uptake

Mitotic inhibitors represent an important strategy to target cancer cells. Paclitaxel, together with other microtubule poisons, proved to be useful for the treatment of tumours. However, its effects are not limited to cancer cells, but affect normal cell activities, thus producing toxicity. The ability to selectively inhibit mitotic processes with specific inhibitors might confer an advantage over microtubules poisons. New mitotic drugs are being developed to inhibit the action of specific mitotic targets, thus the identification of a pharmacodynamics biomarker may be useful in their assessment.

In this thesis, novel mitotic targets have been investigated for use in cancer treatment and to assess the ability of [^{18}F]FLT to highlight mitotic inhibition. Aurora A, Aurora B and PLK1 inhibitors were studied in order to determine if [^{18}F]FLT was able to highlight G2/M arrest using these modern drugs. The results reported in Chapter 3.4 suggested that there was a difference in the response to treatment to the same drug concentrations in the two cell lines tested.

HCT116 cells treated with each inhibitor were arrested in G2/M after 24 hours treatment, which was more pronounced following Aurora A and PLK1 inhibition, as proved by cell-cycle analysis and western blot probing for phospho-TK1. Treatment of BT-20 cells with the same concentration of the three drugs produced G2/M arrest exclusively following PLK1 inhibition, whereas no major effects on cell cycle distribution were generated with inhibition of Aurora kinases, at least at the used concentration. Immunofluorescence analysis further demonstrated the effects produced by the specific inhibitors; additionally, it indicated possible initial mitotic arrest of BT-20 cells following Aurora A inhibition, suggesting that a higher concentration of the drug may induce complete mitotic arrest in this cell line.

No significant differences were found in the expression of proteins involved in thymidine metabolism, but [18F]FLT cell uptake after 24 hours treatment reflected the effects of TK1 phosphorylation during G2/M, with reduced uptake in HCT116 following inhibition of all three kinases, and BT-20 showing decreased radiotracer uptake following Aurora A and PLK1 inhibition.

Testing different drug concentrations to treat BT-20 cells should be a priority, however the small supply of drugs that was available at the time did not allow optimization. These preliminary experiments, however, further demonstrated the ability of [18F]FLT to highlight G2/M arrest, dependent on TK1 specific phosphorylation.

The enzymes involved in the thymidine salvage pathway should be taken into consideration when measuring [18F]FLT uptake into cells and tumours, as the accumulation of the radiotracer is dependent firstly on ENT1 transporters in order to enter a cell, and subsequently on the relative usage of the salvage vs the *de novo* pathway (TS), which could impair the detection of proliferation (McKinley et al., 2013). TP plays an important role in the regulation of the thymidine pool, since thymidine catabolism via TP could deplete dTTP concentration, therefore favouring [18F]FLT uptake via the salvage pathway during DNA replication. None of these parameters, however, was affected by inhibition of the three targets, supporting the fact that TK1 regulation during mitosis is responsible for the reduction in [18F]FLT uptake following mitotic inhibition.

Centrosomes also play an important role in the mitotic progression. Several tumour cells seem to over-duplicate their centrosomes. This is generally a cause of genomic instability, but cancer cells developed methods to overcome this situation. KIFC1 seems to play a

crucial role in this scenario, and being dispensable for normal cells, it could be an extremely interesting target, affecting exclusively tumour cells.

KIFC1 knock-down was induced in cells with normal number of centrosomes (HCT116) as well as in cells containing supernumerary centrosomes (BT-20). No differences in cell proliferation or viability were detected following treatment with KIFC1 siRNA in both cell lines. HCT116 were expected to show unchanged profile in terms of mitotic progression; in contrast, it was hypothesised that BT-20 cells would have been affected by the absence of KIFC1, leading to cell death due to the formation of aberrant mitotic spindles. It was therefore speculated that the residual KIFC1 expression was sufficient to allow BT-20 progression through mitosis. An alternative explanation could be that perhaps KIFC1 may be dispensable in the tested cell line (BT-20), playing instead a fundamental role in different cell lines. Additional mechanisms may be active in BT-20 cells to ensure mitotic progression (Gergely and Basto, 2008). Further experiments should be performed to validate these hypotheses.

In conclusion, the development of novel mitotic drugs may benefit from the use of [^{18}F]FLT as a pharmacodynamics biomarker, due to the ability of the specific radiotracer to detect mitotic inhibition, following regulation of TK1. Furthermore, studying the effects of novel anti-cancer treatments on [^{18}F]FLT uptake is important in order to be able to interpret PET images correctly when scanning after therapy. These new mitotic targets also need to be validated in order to understand the specific outcome for the treatment of different types of cancer.

4.4 General conclusions and future directions

[^{18}F]FLT-PET is considered to be an indirect measure of tumour proliferation due to the fact that the radiotracer is a substrate for TK1, the first enzyme of the salvage pathway for thymidylate production. TK1 is highly active in proliferating cells, with its activity reaching maximum levels during S phase. Hence, [^{18}F]FLT trapping into cells provides an indirect measure of cell proliferation. For this reason, radiotracer retention is mainly dependent on TK1 regulation, which is modulated during cell cycle progression.

Phosphorylation on different amino-acid residues appears to play a major role in regulation of TK1 activity. Our experiments using MnCl$_2$-phos-tag™ gels suggested a different role for the Ser13 phosphorylation, in contrast with previous findings by Chang *et al.* In fact, TK1 appeared to be phosphorylated on Ser13 throughout the cell cycle, not only in G2/M, being possibly required for TK1 activity, at least in transfected cells. Moreover, Ser231 seemed to be phosphorylated specifically during G2/M, possibly being the amino-acid residue responsible for the formation of the dimeric form of the protein, which has lower affinity for thymidine, and/or producing the degradation signal in the C-terminal. However, these experiments also suggested the presence of additional residues which could play a role in TK1 regulation by phosphorylation. Future works should therefore include the generation of additional TK1 mutant forms to investigate the contribution of Ser30 and Ser194 in terms of phosphorylation, together with the creation of double mutants to further validate and characterise these findings. Supplementary characterisation of the different phosphorylation sites would be also preferable, possibly optimising new available techniques such as IEF to ensure the validity of the described findings.

Figure 69 represents the proposed mechanism for the regulation of TK1 activity. It is well established that TK1 protein concentration and activity are reduced in G1 phase. Gene transcription is subsequently induced at the G1/S border. At this stage, TK1 concentration increases favouring the formation of the tetramer which has high affinity for its substrate (thymidine). ATP also plays a role in this conformational change, together with TK1 substrate. In fact, thymidine binding to TK1 has been proposed to hide the degradation signal, therefore preserving TK1 activity. Additionally, Ser13 phosphorylation may be needed to further activate the enzyme, and this modification can be carried out by CDK2. When DNA synthesis is completed, TK1 is phosphorylated by CDK1 on Ser231 and possibly additional amino acids, e.g. Ser30 and Ser194, which remain to be fully characterised. These phosphorylation events may induce the disassembly of the tetramer to the dimer with lower catalytic efficiency and provide the degradation signal. TK1 polypeptide is then degraded before the onset of the subsequent G1 phase.
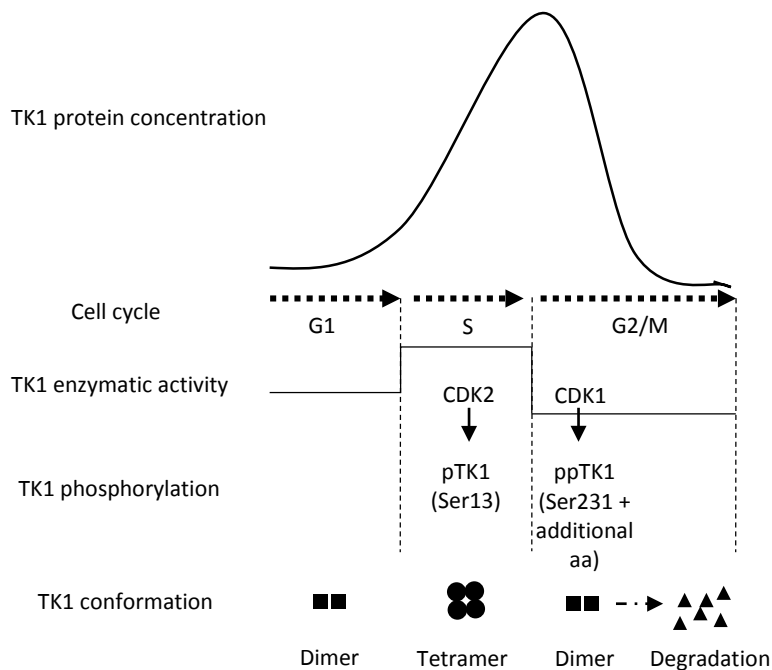
Figure 69. Proposed mechanism for the regulation of TK1 protein activity.
TK1 protein concentration is low in G1. Transcription is induced at the G1/S border and increases until it reaches maximum levels in G2/M. TK1 enzymatic activity is low in G1, maximal during S phase and decreases at the onset of mitosis (G2/M). Regulation of TK1 activity is achieved by changes in the quaternary structure of the protein (TK1 conformation). During G1, TK1 is present as a dimer; the increasing concentration of protein following the induction of its transcription favours the assembly of the tetramer, which corresponds to the most active form of the enzyme. Phosphorylation of Ser13 is also proposed to activate TK1, but the specific role of this modification (possible promotion of tetramer formation) still needs to be characterised. When DNA synthesis is complete, TK1 activity is "switched off" by phosphorylation of Ser231 and possibly additional sites. This modification might disrupt the formation of the tetramer, producing dimers with lower affinity for the substrate. Ser231 phosphorylation may also produce the degradation signal.

Moreover, our work showed that TK1 phosphorylation along the cell cycle modulates [^{18}F]FLT uptake into tumour cells, at least *in vitro*, proving that [^{18}F]FLT is not only able to reflect changes during S-phase, but additionally it is able to highlight G2/M arrest with a striking decrease in accumulation into cells under this condition, as proven following mitotic inhibition with paclitaxel and novel mitotic inhibitors.

[^{18}F]FLT is a valuable radiotracer to image cell proliferation with PET. However, it traces cell proliferation indirectly and it has some limitations which could prevent the correct interpretation of the imaging results, such as the background generated from its route of

excretion and its dependence on TK1 to be retained into cells. Nonetheless, its use is still attracting interest and being validated in clinical trials.

Importantly, any PET radiotracer developed until today for cell proliferation, which has been designed to trace the salvage pathway for thymidylate supply, needed to be a substrate for TK1, in order to be efficiently retained into cells at least for the time sufficient to perform PET imaging. However, TK1-dependency will always represent a limit in this scenario, as its expression and regulation could be impaired in certain tumour types, therefore not faithfully reflecting cell proliferation.

A thymidine analogue which could be incorporated into the growing chain of the DNA will be preferable, since it could directly trace cell proliferation. However, in order to be incorporated into the DNA each thymidine analogue will have to be phosphorylated by TK1 in order to be trapped in the cell and to form the substrate for the subsequent kinases. An alternative may be to produce a radiotracer which will not need to be phosphorylated by TK1, but could be retained into cells and finally be incorporated into the DNA. Next generation radiotracers will be designed with the idea of producing a radiotracer for cell proliferation which could overcome [^{18}F]FLT limits. PET imaging is, in fact, an extremely powerful technique able to provide biological information at the molecular level. If a better radiotracer for proliferation could be generated, it will be possible to better understand response to therapy of a vast variety of tumour types, given that the uptake will not be exclusively dependent on TK1 activity. However, general considerations about thymidine pool and transport could remain the main issues.

Finally, novel inhibitors of mitotic progression could be preferable to microtubule drugs, since they will target specific proteins involved in a precise phase of the cell cycle,

targeting exclusively proliferating cells, and therefore avoiding general toxicity due to interference with normal biological processes. Preliminary work described in this thesis confirmed the ability of [^{18}F]FLT to highlight G2/M arrest with a decrease in cell accumulation into HCT116 following inhibition of PLK1, Aurora A or Aurora B. It will therefore be interesting to perform [^{18}F]FLT-PET *in vivo* to test the radiotracer ability to detect cell-cycle arrest following inhibition of novel mitotic targets.

Knock-down of the kinesin protein KIFC1 was also performed, hypothesising that cells containing supernumerary centrosomes were dependent on KIFC1 to successfully complete mitosis. Induction of cell death was expected following transfection with siRNA; however, BT-20 cells (containing >2 centrosomes) showed no detectable effects. Transfections with shRNA might help to confirm these data. Additionally, repeating the experiments with a different cellular model could give more insight into the role of KIFC1 in the presence of supernumerary centrosomes.

References

ABOAGYE , E. O. & PRICE, P. M. (2003) Use of positron emission tomography in anticancer drug development. *Invest New Drugs,* 21, 169-81.

AL-MADHOUN, A. S., JOHNSAMUEL, J., YAN, J., JI, W., WANG, J., ZHUO, J. C., LUNATO, A. J., WOOLLARD, J. E., HAWK, A. E., COSQUER, G. Y., BLUE, T. E., ERIKSSON, S. & TJARKS, W. (2002) Synthesis of a small library of 3-(carboranylalkyl)thymidines and their biological evaluation as substrates for human thymidine kinases 1 and 2. *J Med Chem,* 45, 4018-28.

ALAUDDIN, M. M. (2012) Positron emission tomography (PET) imaging with (18)F-based radiotracers. *Am J Nucl Med Mol Imaging,* 2, 55-76.

ALBERTS (Ed.) (2008) *Molecular Biology of the Cell.*

ALESSI, D. R., ANDJELKOVIC, M., CAUDWELL, B., CRON, P., MORRICE, N., COHEN, P. & HEMMINGS, B. A. (1996) Mechanism of activation of protein kinase B by insulin and IGF-1. *EMBO J,* 15, 6541-51.

ALFORD, R., OGAWA, M., CHOYKE, P. L. & KOBAYASHI, H. (2009) Molecular probes for the in vivo imaging of cancer. *Mol Biosyst,* 5, 1279-91.

ANDREWS, P. D. (2005) Aurora kinases: shining lights on the therapeutic horizon? *Oncogene,* 24, 5005-15.

ARELLANO, M. & MORENO, S. (1997) Regulation of CDK/cyclin complexes during the cell cycle. *Int J Biochem Cell Biol,* 29, 559-73.

ARNER, E. S. & ERIKSSON, S. (1995) Mammalian deoxyribonucleoside kinases. *Pharmacol Ther,* 67, 155-86.

BADING, J. R., SHAHINIAN, A. H., BATHIJA, P. & CONTI, P. S. (2000) Pharmacokinetics of the thymidine analog 2'-fluoro-5-[(14)C]-methyl-1-beta-D-arabinofuranosyluracil ([(14)C]FMAU) in rat prostate tumor cells. *Nucl Med Biol,* 27, 361-8.

BADING, J. R. & SHIELDS, A. F. (2008) Imaging of cell proliferation: status and prospects. *J Nucl Med,* 49 Suppl 2, 64S-80S.

BARR, A. R. & GERGELY, F. (2007) Aurora-A: the maker and breaker of spindle poles. *J Cell Sci,* 120, 2987-96.

BARTHEL, H., CLEIJ, M. C., COLLINGRIDGE, D. R., HUTCHINSON, O. C., OSMAN, S., HE, Q., LUTHRA, S. K., BRADY, F., PRICE, P. M. & ABOAGYE, E. O. (2003) 3'-deoxy-3'-[18F]fluorothymidine as a new marker for monitoring tumor response to antiproliferative therapy in vivo with positron emission tomography. *Cancer Res,* 63, 3791-8.

BARTHEL, H., PERUMAL, M., LATIGO, J., HE, Q., BRADY, F., LUTHRA, S. K., PRICE, P. M. & ABOAGYE, E. O. (2005) The uptake of 3'-deoxy-3'-[18F]fluorothymidine into L5178Y tumours in vivo is dependent on thymidine kinase 1 protein levels. *Eur J Nucl Med Mol Imaging,* 32, 257-63.

BEAUSOLEIL, S. A., VILLEN, J., GERBER, S. A., RUSH, J. & GYGI, S. P. (2006) A probability-based approach for high-throughput protein phosphorylation analysis and site localization. *Nat Biotechnol,* 24, 1285-92.

BELOTTI, D., VERGANI, V., DRUDIS, T., BORSOTTI, P., PITELLI, M. R., VIALE, G., GIAVAZZI, R. & TARABOLETTI, G. (1996) The microtubule-affecting drug paclitaxel has antiangiogenic activity. *Clin Cancer Res,* 2, 1843-9.

BERTOLI, C., SKOTHEIM, J. M. & DE BRUIN, R. A. (2013) Control of cell cycle transcription during G1 and S phases. *Nat Rev Mol Cell Biol,* 14, 518-28.

BISCHOFF, J. R., ANDERSON, L., ZHU, Y., MOSSIE, K., NG, L., SOUZA, B., SCHRYVER, B., FLANAGAN, P., CLAIRVOYANT, F., GINTHER, C., CHAN, C. S., NOVOTNY, M.,

SLAMON, D. J. & PLOWMAN, G. D. (1998) A homologue of Drosophila aurora kinase is oncogenic and amplified in human colorectal cancers. *EMBO J,* 17, 3052-65.

BLAU, I. W., ELSTNER, E., WAECHTER, M., IHLE, R., VON JANTA-LIPINSKI, M. & LANGEN, P. (1989) Sensitivity of CFU-GM from normal human bone marrow and leukaemic clonogenic cells (CFU-L) from blood of patients with myelogenous leukaemia to 3'-deoxy-3'-fluorothymidine in comparison to 3'-azido-3'-deoxythymidine. *Blut,* 59, 455-7.

BROCKENBROUGH, J. S., SOUQUET, T., MORIHARA, J. K., STERN, J. E., HAWES, S. E., RASEY, J. S., LEBLOND, A., WIENS, L. W., FENG, Q., GRIERSON, J. & VESSELLE, H. (2011) Tumor 3'-deoxy-3'-(18)F-fluorothymidine ((18)F-FLT) uptake by PET correlates with thymidine kinase 1 expression: static and kinetic analysis of (18)F-FLT PET studies in lung tumors. *J Nucl Med,* 52, 1181-8.

BUCK, A. K., BOMMER, M., STILGENBAUER, S., JUWEID, M., GLATTING, G., SCHIRRMEISTER, H., MATTFELDT, T., TEPSIC, D., BUNJES, D., MOTTAGHY, F. M., KRAUSE, B. J., NEUMAIER, B., DOHNER, H., MOLLER, P. & RESKE, S. N. (2006) Molecular Imaging of proliferation in malignant lymphoma. *Cancer Research,* 66, 11055-11061.

BUCK, A. K., HALTER, G., SCHIRRMEISTER, H., KOTZERKE, J., WURZIGER, I., GLATTING, G., MATTFELDT, T., NEUMAIER, B., RESKE, S. N. & HETZEL, M. (2003) Imaging proliferation in lung tumors with PET: 18F-FLT versus 18F-FDG. *J Nucl Med,* 44, 1426-31.

BUCK, A. K., SCHIRRMEISTER, H., HETZEL, M., VON DER HEIDE, M., HALTER, G., GLATTING, G., MATTFELDT, T., LIEWALD, F., RESKE, S. N. & NEUMAIER, B. (2002) 3-deoxy-3-[F-18]fluorothymidine-positron emission tomography for noninvasive assessment of proliferation in pulmonary nodules. *Cancer Research,* 62, 3331-3334.

CALDERONI, A. & CERNY, T. (2001) Taxanes in lung cancer: a review with focus on the European experience. *Crit Rev Oncol Hematol,* 38, 105-27.

CAMMARERI, P., SCOPELLITI, A., TODARO, M., ETERNO, V., FRANCESCANGELI, F., MOYER, M. P., AGRUSA, A., DIELI, F., ZEUNER, A. & STASSI, G. (2010) Aurora-a is essential for the tumorigenic capacity and chemoresistance of colorectal cancer stem cells. *Cancer Res,* 70, 4655-65.

CARMENA, M. & EARNSHAW, W. C. (2003) The cellular geography of aurora kinases. *Nat Rev Mol Cell Biol,* 4, 842-54.

CARNROT, C., WEHELIE, R., ERIKSSON, S., BOLSKE, G. & WANG, L. (2003) Molecular characterization of thymidine kinase from Ureaplasma urealyticum: nucleoside analogues as potent inhibitors of mycoplasma growth. *Mol Microbiol,* 50, 771-80.

CARROLL, P. E., OKUDA, M., HORN, H. F., BIDDINGER, P., STAMBROOK, P. J., GLEICH, L. L., LI, Y. Q., TARAPORE, P. & FUKASAWA, K. (1999) Centrosome hyperamplification in human cancer: chromosome instability induced by p53 mutation and/or Mdm2 overexpression. *Oncogene,* 18, 1935-44.

CASS, C. E., YOUNG, J. D. & BALDWIN, S. A. (1998) Recent advances in the molecular biology of nucleoside transporters of mammalian cells. *Biochem Cell Biol,* 76, 761-70.

CHALKIDOU, A., LANDAU, D. B., ODELL, E. W., CORNELIUS, V. R., O'DOHERTY, M. J. & MARSDEN, P. K. (2012) Correlation between Ki-67 immunohistochemistry and 18F-

fluorothymidine uptake in patients with cancer: A systematic review and meta-analysis. *Eur J Cancer,* 48, 3499-513.

CHAN, F., SUN, C., PERUMAL, M., NGUYEN, Q. D., BAVETSIAS, V., MCDONALD, E., MARTINS, V., WILSHER, N. E., RAYNAUD, F. I., VALENTI, M., ECCLES, S., TE POELE, R., WORKMAN, P., ABOAGYE, E. O. & LINARDOPOULOS, S. (2007) Mechanism of action of the Aurora kinase inhibitor CCT129202 and in vivo quantification of biological activity. *Mol Cancer Ther,* 6, 3147-57.

CHANG, Z. F. & HUANG, D. Y. (1993) The regulation of thymidine kinase in HL-60 human promyeloleukemia cells. *J Biol Chem,* 268, 1266-71.

CHANG, Z. F., HUANG, D. Y. & CHI, L. M. (1998) Serine 13 is the site of mitotic phosphorylation of human thymidine kinase. *J Biol Chem,* 273, 12095-100.

CHANG, Z. F., HUANG, D. Y. & HSUE, N. C. (1994) Differential phosphorylation of human thymidine kinase in proliferating and M phase-arrested human cells. *J Biol Chem,* 269, 21249-54.

CHEN, Y. L., ERIKSSON, S. & CHANG, Z. F. (2010) Regulation and functional contribution of thymidine kinase 1 in repair of DNA damage. *J Biol Chem,* 285, 27327-35.

CHING, J. K., RAJGURU, P., MARUPUDI, N., BANERJEE, S. & FISHER, J. S. (2010) A role for AMPK in increased insulin action after serum starvation. *Am J Physiol Cell Physiol,* 299, C1171-9.

CHRISTMAN, D., CRAWFORD, E. J., FRIEDKIN, M. & WOLF, A. P. (1972) Detection of DNA synthesis in intact organisms with positron-emitting (methyl- 11 C)thymidine. *Proc Natl Acad Sci U S A,* 69, 988-92.

COBBEN, D. C., VAN DER LAAN, B. F., MAAS, B., VAALBURG, W., SUURMEIJER, A. J., HOEKSTRA, H. J., JAGER, P. L. & ELSINGA, P. H. (2004) 18F-FLT PET for visualization of laryngeal cancer: comparison with 18F-FDG PET. *J Nucl Med,* 45, 226-31.

CONTI, P. S., ALAUDDIN, M. M., FISSEKIS, J. R., SCHMALL, B. & WATANABE, K. A. (1995) Synthesis of 2'-fluoro-5-[11C]-methyl-1-beta-D-arabinofuranosyluracil ([11C]-FMAU): a potential nucleoside analog for in vivo study of cellular proliferation with PET. *Nucl Med Biol,* 22, 783-9.

CONTRACTOR, K., ABOAGYE, E. O., JACOB, J., CHALLAPALLI, A., COOMBES, R. C. & STEBBING, J. (2012) Monitoring early response to taxane therapy in advanced breast cancer with circulating tumor cells and [(18)F] 3 -deoxy-3 -fluorothymidine PET: a pilot study. *Biomark Med,* 6, 231-3.

CONTRACTOR, K. B., KENNY, L. M., STEBBING, J., ROSSO, L., AHMAD, R., JACOB, J., CHALLAPALLI, A., TURKHEIMER, F., AL-NAHHAS, A., SHARMA, R., COOMBES, R. C. & ABOAGYE, E. O. (2011) [18F]-3'Deoxy-3'-fluorothymidine positron emission tomography and breast cancer response to docetaxel. *Clin Cancer Res,* 17, 7664-72.

COOPER, S. (2006) Checkpoints and restriction points in bacteria and eukaryotic cells. *Bioessays,* 28, 1035-9.

COPPOCK, D. L. & PARDEE, A. B. (1987) Control of thymidine kinase mRNA during the cell cycle. *Mol Cell Biol,* 7, 2925-32.

DE BRABANDER, D. L., VAN DE VELRE, R. M. L., AERTS, F. E. M., BORGERS, M. & JANSSEN, P. A. J. (1976) The Effects of Methyl (5-(2-Thienylcarbonyl)-IH-benzi midazol 2-yl]carbamate, (R 17934; NSC 238159), a New Synthetic Antitumoral Drug Interfering with Microtubules, on Mammalian Cells Cultured in Vitro. *Cancer Res,* 36, 905-916.

DE BRABANDER, M., GEUENS, G., NUYDENS, R., WILLEBRORDS, R. & DE MEY, J. (1981) Taxol induces the assembly of free microtubules in living cells and blocks the organizing capacity of the centrosomes and kinetochores. *Proc Natl Acad Sci U S A,* 78, 5608-612.

DE BRUIN, M., SMID, K., LAAN, A. C., NOORDHUIS, P., FUKUSHIMA, M., HOEKMAN, K., PINEDO, H. M. & PETERS, G. J. (2003) Rapid disappearance of deoxyribose-1-phosphate in platelet derived endothelial cell growth factor/thymidine phosphorylase overexpressing cells. *Biochem Biophys Res Commun,* 301, 675-9.

DEPHOURE, N., ZHOU, C., VILLEN, J., BEAUSOLEIL, S. A., BAKALARSKI, C. E., ELLEDGE, S. J. & GYGI, S. P. (2008) A quantitative atlas of mitotic phosphorylation. *Proc Natl Acad Sci U S A,* 105, 10762-7.

DESAI, A. & MITCHISON, T. J. (1997) Microtubule polymerization dynamics. *Annu Rev Cell Dev Biol,* 13, 83-117.

DIRECKS, W. G., VAN GELDER, M., LAMMERTSMA, A. A. & MOLTHOFF, C. F. (2008) A new rat model of human breast cancer for evaluating efficacy of new anti-cancer agents in vivo. *Cancer Biol Ther,* 7, 532-7.

DITCHFIELD, C., JOHNSON, V. L., TIGHE, A., ELLSTON, R., HAWORTH, C., JOHNSON, T., MORTLOCK, A., KEEN, N. & TAYLOR, S. S. (2003) Aurora B couples chromosome alignment with anaphase by targeting BubR1, Mad2, and Cenp-E to kinetochores. *J Cell Biol,* 161, 267-80.

DITTMANN, H., DOHMEN, B. M., KEHLBACH, R., BARTUSEK, G., PRITZKOW, M., SARBIA, M. & BARES, R. (2002) Early changes in [18F]FLT uptake after chemotherapy: an experimental study. *Eur J Nucl Med Mol Imaging,* 29, 1462-9.

DUMONTET, C. & SIKIC, B. I. (1999) Mechanisms of action of and resistance to antitubulin agents: microtubule dynamics, drug transport, and cell death. *J Clin Oncol,* 17, 1061-70.

DUTERTRE, S., DESCAMPS, S. & PRIGENT, C. (2002) On the role of aurora-A in centrosome function. *Oncogene,* 21, 6175-83.

EARY, J. F., MANKOFF, D. A., SPENCE, A. M., BERGER, M. S., OLSHEN, A., LINK, J. M., O'SULLIVAN, F. & KROHN, K. A. (1999) 2-[C-11]thymidine imaging of malignant brain tumors. *Cancer Res,* 59, 615-21.

EKHOLM, S. V. & REED, S. I. (2000) Regulation of G(1) cyclin-dependent kinases in the mammalian cell cycle. *Curr Opin Cell Biol,* 12, 676-84.

ELLIMS, P. H., VAN DER WEYDEN, M. B. & MEDLEY, G. (1981) Thymidine kinase isoenzymes in human malignant lymphoma. *Cancer Res,* 41, 691-5.

ESPINOSA, E., ZAMORA, P., FELIU, J. & GONZALEZ BARON, M. (2003) Classification of anticancer drugs--a new system based on therapeutic targets. *Cancer Treat Rev,* 29, 515-23.

FAN, A. C., DEB-BASU, D., ORBAN, M. W., GOTLIB, J. R., NATKUNAM, Y., O'NEILL, R., PADUA, R. A., XU, L., TAKETA, D., SHIRER, A. E., BEER, S., YEE, A. X., VOEHRINGER, D. W. & FELSHER, D. W. (2009) Nanofluidic proteomic assay for serial analysis of oncoprotein activation in clinical specimens. *Nat Med,* 15, 566-71.

FAN, S., CHANG, J. K., SMITH, M. L., DUBA, D., FORNACE, A. J., JR. & O'CONNOR, P. M. (1997) Cells lacking CIP1/WAF1 genes exhibit preferential sensitivity to cisplatin and nitrogen mustard. *Oncogene,* 14, 2127-36.

FOLEY, E. A. & KAPOOR, T. M. (2013) Microtubule attachment and spindle assembly checkpoint signalling at the kinetochore. *Nat Rev Mol Cell Biol,* 14, 25-37.

FUKASAWA, K. (2002) Introduction. Centrosome. *Oncogene,* 21, 6140-5.

FUKASAWA, K. (2005) Centrosome amplification, chromosome instability and cancer development. *Cancer Lett,* 230, 6-19.

FURMAN, P. A., FYFE, J. A., ST CLAIR, M. H., WEINHOLD, K., RIDEOUT, J. L., FREEMAN, G. A., LEHRMAN, S. N., BOLOGNESI, D. P., BRODER, S., MITSUYA, H. & ET AL. (1986) Phosphorylation of 3'-azido-3'-deoxythymidine and selective interaction of the 5'-triphosphate with human immunodeficiency virus reverse transcriptase. *Proc Natl Acad Sci U S A,* 83, 8333-7.

GADBOIS, D. M., CRISSMAN, H. A., TOBEY, R. A. & BRADBURY, E. M. (1992) Multiple kinase arrest points in the G1 phase of nontransformed mammalian cells are absent in transformed cells. *Proc Natl Acad Sci U S A,* 89, 8626-30.

GERGELY, F. & BASTO, R. (2008) Multiple centrosomes: together they stand, divided they fall. *Genes & Development,* 22, 2291-2296.

GIANNAKAKOU, P., SACKETT, D. L., KANG, Y. K., ZHAN, Z., BUTERS, J. T., FOJO, T. & PORUCHYNSKY, M. S. (1997) Paclitaxel-resistant human ovarian cancer cells have mutant beta-tubulins that exhibit impaired paclitaxel-driven polymerization. *J Biol Chem,* 272, 17118-25.

GIET, R., MCLEAN, D., DESCAMPS, S., LEE, M. J., RAFF, J. W., PRIGENT, C. & GLOVER, D. M. (2002) Drosophila Aurora A kinase is required to localize D-TACC to centrosomes and to regulate astral microtubules. *J Cell Biol,* 156, 437-51.

GLOTZER, M. (2005) The molecular requirements for cytokinesis. *Science,* 307, 1735-1739.

GLUNDE, K., PATHAK, A. P. & BHUJWALLA, Z. M. (2007) Molecular-functional imaging of cancer: to image and imagine. *Trends Mol Med,* 13, 287-97.

GOETHALS, P., VANEIJKEREN, M., LODEWYCK, W. & DAMS, R. (1995) Measurement of [Methyl-Carbon-11]Thymidine and Its Metabolites in Head and Neck Tumors. *Journal of Nuclear Medicine,* 36, 880-882.

GONCALVES, A., BRAGUER, D., KAMATH, K., MARTELLO, L., BRIAND, C., HORWITZ, S., WILSON, L. & JORDAN, M. A. (2001) Resistance to Taxol in lung cancer cells associated with increased microtubule dynamics. *Proc Natl Acad Sci U S A,* 98, 11737-42.

GORGUN, G., CALABRESE, E., HIDESHIMA, T., ECSEDY, J., PERRONE, G., MANI, M., IKEDA, H., BIANCHI, G., HU, Y., CIRSTEA, D., SANTO, L., TAI, Y. T., NAHAR, S., ZHENG, M., BANDI, M., CARRASCO, R. D., RAJE, N., MUNSHI, N., RICHARDSON, P. & ANDERSON, K. C. (2010) A novel Aurora-A kinase inhibitor MLN8237 induces cytotoxicity and cell-cycle arrest in multiple myeloma. *Blood,* 115, 5202-13.

GRIERSON, J. R., SCHWARTZ, J. L., MUZI, M., JORDAN, R. & KROHN, K. A. (2004) Metabolism of 3'-deoxy-3'-[F-18]fluorothymidine in proliferating A549 cells: validations for positron emission tomography. *Nucl Med Biol,* 31, 829-37.

GRIERSON, J. R. & SHIELDS, A. F. (2000) Radiosynthesis of 3'-deoxy-3'-[(18)F]fluorothymidine: [(18)F]FLT for imaging of cellular proliferation in vivo. *Nucl Med Biol,* 27, 143-56.

GUPTA, N., PRICE, P. M. & ABOAGYE, E. O. (2002) PET for in vivo pharmacokinetic and pharmacodynamic measurements. *Eur J Cancer,* 38, 2094-107.

HANAHAN, D. & WEINBERG, R. A. (2011) Hallmarks of cancer: the next generation. *Cell,* 144, 646-74.

HARBOUR, J. W. & DEAN, D. C. (2000a) Rb function in cell-cycle regulation and apoptosis. *Nat Cell Biol,* 2, E65-7.

HARBOUR, J. W. & DEAN, D. C. (2000b) The Rb/E2F pathway: expanding roles and emerging paradigms. *Genes Dev,* 14, 2393-409.

HAUF, S., COLE, R. W., LATERRA, S., ZIMMER, C., SCHNAPP, G., WALTER, R., HECKEL, A., VAN MEEL, J., RIEDER, C. L. & PETERS, J. M. (2003) The small molecule Hesperadin reveals a role for Aurora B in correcting kinetochore-microtubule attachment and in maintaining the spindle assembly checkpoint. *J Cell Biol,* 161, 281-94.

HE, Q., SKOG, S., WU, C., JOHANSSON, A. & TRIBUKAIT, B. (1996) Existence of phosphorylated and dephosphorylated forms of cytosolic thymidine kinase (TK1). *Biochim Biophys Acta,* 1289, 25-30.

HERRMANN, K., WIEDER, H. A., BUCK, A. K., SCHOFFEL, M., KRAUSE, B. J., FEND, F., SCHUSTER, T., MEYER ZUM BUSCHENFELDE, C., WESTER, H. J., DUYSTER, J., PESCHEL, C., SCHWAIGER, M. & DECHOW, T. (2007) Early response assessment using 3'-deoxy-3'-[18F]fluorothymidine-positron emission tomography in high-grade non-Hodgkin's lymphoma. *Clin Cancer Res,* 13, 3552-8.

HOAR, K., CHAKRAVARTY, A., RABINO, C., WYSONG, D., BOWMAN, D., ROY, N. & ECSEDY, J. A. (2007) MLN8054, a small-molecule inhibitor of Aurora A, causes spindle pole and chromosome congression defects leading to aneuploidy. *Mol Cell Biol,* 27, 4513-25.

HONTZ, A. E., LI, S. A., LINGLE, W. L., NEGRON, V., BRUZEK, A., SALISBURY, J. L. & LI, J. J. (2007) Aurora a and B overexpression and centrosome amplification in early estrogen-induced tumor foci in the Syrian hamster kidney: implications for chromosomal instability, aneuploidy, and neoplasia. *Cancer Res,* 67, 2957-63.

HU, C. M. & CHANG, Z. F. (2007) Mitotic control of dTTP pool: a necessity or coincidence? *J Biomed Sci,* 14, 491-7.

JANSSEN, A. & MEDEMA, R. H. (2011) Mitosis as an anti-cancer target. *Oncogene,* 30, 2799-809.

JORDAN, M. A., TOSO, R. J., THROWER, D. & WILSON, L. (1993) Mechanism of mitotic block and inhibition of cell proliferation by taxol at low concentrations. *Proc Natl Acad Sci U S A,* 90, 9552-6.

JORDAN, M. A. & WILSON, L. (2004) Microtubules as a target for anticancer drugs. *Nat Rev Cancer,* 4, 253-65.

KALDIS, P. (1999) The cdk-activating kinase (CAK): from yeast to mammals. *Cell Mol Life Sci,* 55, 284-96.

KAMEYAMA, R., YAMAMOTO, Y., IZUISHI, K., TAKEBAYASHI, R., HAGIIKE, M., MUROTA, M., KAJI, M., HABA, R. & NISHIYAMA, Y. (2009) Detection of gastric cancer using 18F-FLT PET: comparison with 18F-FDG PET. *Eur J Nucl Med Mol Imaging,* 36, 382-8.

KATAYAMA, H., BRINKLEY, W. R. & SEN, S. (2003) The Aurora kinases: role in cell transformation and tumorigenesis. *Cancer Metastasis Rev,* 22, 451-64.

KATAYAMA, K., FUJITA, N. & TSURUO, T. (2005) Akt/protein kinase B-dependent phosphorylation and inactivation of WEE1Hu promote cell cycle progression at G2/M transition. *Mol Cell Biol,* 25, 5725-37.

KATZ, S. I., ZHOU, L., FERRARA, T. A., WANG, W., MAYES, P. A., SMITH, C. D. & EL-DEIRY, W. S. (2011) FLT-PET may not be a reliable indicator of therapeutic response in p53-null malignancy. *Int J Oncol,* 39, 91-100.

KAUFFMAN, M. G. & KELLY, T. J. (1991) Cell cycle regulation of thymidine kinase: residues near the carboxyl terminus are essential for the specific degradation of the enzyme at mitosis. *Mol Cell Biol,* 11, 2538-46.

KAVALLARIS, M., KUO, D. Y., BURKHART, C. A., REGL, D. L., NORRIS, M. D., HABER, M. & HORWITZ, S. B. (1997) Taxol-resistant epithelial ovarian tumors are associated with altered expression of specific beta-tubulin isotypes. *J Clin Invest,* 100, 1282-93.

KE, P. Y. & CHANG, Z. F. (2004) Mitotic degradation of human thymidine kinase 1 is dependent on the anaphase-promoting complex/cyclosome-CDH1-mediated pathway. *Mol Cell Biol,* 24, 514-26.

KE, P. Y., HU, C. M., CHANG, Y. C. & CHANG, Z. F. (2007) Hiding human thymidine kinase 1 from APC/C-mediated destruction by thymidine binding. *FASEB J,* 21, 1276-84.

KE, P. Y., YANG, C. C., TSAI, I. C. & CHANG, Z. F. (2003) Degradation of human thymidine kinase is dependent on serine-13 phosphorylation: involvement of the SCF-mediated pathway. *Biochem J,* 370, 265-73.

KELLOFF, G. J., KROHN, K. A., LARSON, S. M., WEISSLEDER, R., MANKOFF, D. A., HOFFMAN, J. M., LINK, J. M., GUYTON, K. Z., ECKELMAN, W. C., SCHER, H. I., O'SHAUGHNESSY, J., CHESON, B. D., SIGMAN, C. C., TATUM, J. L., MILLS, G. Q., SULLIVAN, D. C. & WOODCOCK, J. (2005) The progress and promise of molecular imaging probes in oncologic drug development. *Clin Cancer Res,* 11, 7967-85.

KENNY, L., COOMBES, R. C., VIGUSHIN, D. M., AL-NAHHAS, A., SHOUSHA, S. & ABOAGYE, E. O. (2007) Imaging early changes in proliferation at 1 week post chemotherapy: a pilot study in breast cancer patients with 3'-deoxy-3'-[18F]fluorothymidine positron emission tomography. *Eur J Nucl Med Mol Imaging,* 34, 1339-47.

KENNY, L. M., CONTRACTOR, K. B., STEBBING, J., AL-NAHHAS, A., PALMIERI, C., SHOUSHA, S., COOMBES, R. C. & ABOAGYE, E. O. (2009) Altered tissue 3'-deoxy-3'-[18F]fluorothymidine pharmacokinetics in human breast cancer following capecitabine treatment detected by positron emission tomography. *Clin Cancer Res,* 15, 6649-57.

KENNY, L. M., VIGUSHIN, D. M., AL-NAHHAS, A., OSMAN, S., LUTHRA, S. K., SHOUSHA, S., COOMBES, R. C. & ABOAGYE, E. O. (2005) Quantification of cellular proliferation in tumor and normal tissues of patients with breast cancer by [18F]fluorothymidine-positron emission tomography imaging: evaluation of analytical methods. *Cancer Res,* 65, 10104-12.

KISHINO, T., HOSHIKAWA, H., NISHIYAMA, Y., YAMAMOTO, Y. & MORI, N. (2012) Usefulness of 3'-deoxy-3'-18F-fluorothymidine PET for predicting early response to chemoradiotherapy in head and neck cancer. *J Nucl Med,* 53, 1521-7.

KONG, X. B., ZHU, Q. Y., VIDAL, P. M., WATANABE, K. A., POLSKY, B., ARMSTRONG, D., OSTRANDER, M., LANG, S. A., JR., MUCHMORE, E. & CHOU, T. C. (1992) Comparisons of anti-human immunodeficiency virus activities, cellular transport, and plasma and intracellular pharmacokinetics of 3'-fluoro-3'-deoxythymidine and 3'-azido-3'-deoxythymidine. *Antimicrob Agents Chemother,* 36, 808-18.

KROHN, K. A., MANKOFF, D. A. & EARY, J. F. (2001) Imaging cellular proliferation as a measure of response to therapy. *J Clin Pharmacol,* Suppl, 96S-103S.

KUMMAR, S., GUTIERREZ, M., DOROSHOW, J. H. & MURGO, A. J. (2006) Drug development in oncology: classical cytotoxics and molecularly targeted agents. *Br J Clin Pharmacol,* 62, 15-26.

KWON, M., GODINHO, S. A., CHANDHOK, N. S., GANEM, N. J., AZIOUNE, A., THERY, M. & PELLMAN, D. (2008) Mechanisms to suppress multipolar divisions in cancer cells with extra centrosomes. *Genes Dev,* 22, 2189-203.

LACHANCE, P. E., MIRON, M., RAUGHT, B., SONENBERG, N. & LASKO, P. (2002) Phosphorylation of eukaryotic translation initiation factor 4E is critical for growth. *Mol Cell Biol,* 22, 1656-63.

LAMPSON, M. A. & CHEESEMAN, I. M. (2011) Sensing centromere tension: Aurora B and the regulation of kinetochore function. *Trends Cell Biol,* 21, 133-40.

LANE, H. A. & NIGG, E. A. (1996) Antibody microinjection reveals an essential role for human polo-like kinase 1 (Plk1) in the functional maturation of mitotic centrosomes. *J Cell Biol,* 135, 1701-13.

LEE, L. S. & CHENG, Y. (1976) Human deoxythymidine kinase II: substrate specificity and kinetic behavior of the cytoplasmic and mitochondrial isozymes derived from blast cells of acute myelocytic leukemia. *Biochemistry,* 15, 3686-90.

LEE, M. Y., TOOMEY, N. L. & WRIGHT, G. E. (1985) Differential inhibition of human placental DNA polymerases delta and alpha by BuPdGTP and BuAdATP. *Nucleic Acids Res,* 13, 8623-30.

LENART, P., PETRONCZKI, M., STEEGMAIER, M., DI FIORE, B., LIPP, J. J., HOFFMANN, M., RETTIG, W. J., KRAUT, N. & PETERS, J. M. (2007) The small-molecule inhibitor BI 2536 reveals novel insights into mitotic roles of polo-like kinase 1. *Curr Biol,* 17, 304-15.

LENS, S. M., VOEST, E. E. & MEDEMA, R. H. (2010) Shared and separate functions of polo-like kinases and aurora kinases in cancer. *Nat Rev Cancer,* 10, 825-41.

LESNOCK, J. L., DARCY, K. M., TIAN, C., DELOIA, J. A., THRALL, M. M., ZAHN, C., ARMSTRONG, D. K., BIRRER, M. J. & KRIVAK, T. C. (2013) BRCA1 expression and improved survival in ovarian cancer patients treated with intraperitoneal cisplatin and paclitaxel: a Gynecologic Oncology Group Study. *Br J Cancer,* 108, 1231-7.

LEYTON, J., ALAO, J. P., DA COSTA, M., STAVROPOULOU, A. V., LATIGO, J. R., PERUMAL, M., PILLAI, R., HE, Q., ATADJA, P., LAM, E. W., WORKMAN, P., VIGUSHIN, D. M. & ABOAGYE, E. O. (2006) In vivo biological activity of the histone deacetylase inhibitor LAQ824 is detectable with 3'-deoxy-3'-[18F]fluorothymidine positron emission tomography. *Cancer Res,* 66, 7621-9.

LEYTON, J., LATIGO, J. R., PERUMAL, M., DHALIWAL, H., HE, Q. & ABOAGYE, E. O. (2005) Early detection of tumor response to chemotherapy by 3'-deoxy-3'-[18F]fluorothymidine positron emission tomography: the effect of cisplatin on a fibrosarcoma tumor model in vivo. *Cancer Res,* 65, 4202-10.

LEYTON, J., SMITH, G., LEES, M., PERUMAL, M., NGUYEN, Q. D., AIGBIRHIO, F. I., GOLOVKO, O., HE, Q., WORKMAN, P. & ABOAGYE, E. O. (2008) Noninvasive imaging of cell proliferation following mitogenic extracellular kinase inhibition by PD0325901. *Mol Cancer Ther,* 7, 3112-21.

LI, C. L., LU, C. Y., KE, P. Y. & CHANG, Z. F. (2004) Perturbation of ATP-induced tetramerization of human cytosolic thymidine kinase by substitution of serine-13 with aspartic acid at the mitotic phosphorylation site. *Biochem Biophys Res Commun,* 313, 587-93.

LI, W., ARAYA, M., ELLIOTT, M., KANG, X., GERK, P. M., HALQUIST, M. S., KARNES, H. T., ZHANG, C. & O'BRIEN, P. J. (2011) Monitoring cellular accumulation of 3'-deoxy-3'-fluorothymidine (FLT) and its monophosphate metabolite (FLT-MP) by LC-MS/MS as a measure of cell proliferation in vitro. *J Chromatogr B Analyt Technol Biomed Life Sci,* 879, 2963-70.

LINGLE, W. L., BARRETT, S. L., NEGRON, V. C., D'ASSORO, A. B., BOENEMAN, K., LIU, W., WHITEHEAD, C. M., REYNOLDS, C. & SALISBURY, J. L. (2002) Centrosome amplification drives chromosomal instability in breast tumor development. *Proc Natl Acad Sci U S A,* 99, 1978-83.

LODISH (Ed.) (2004).

LOFFLER, H., FECHTER, A., LIU, F. Y., POPPELREUTHER, S. & KRAMER, A. (2013) DNA damage-induced centrosome amplification occurs via excessive formation of centriolar satellites. *Oncogene,* 32, 2963-72.

LOK, W., KLEIN, R. Q. & SAIF, M. W. (2010) Aurora kinase inhibitors as anti-cancer therapy. *Anticancer Drugs,* 21, 339-50.

LONG, B. H. & FAIRCHILD, C. R. (1994) Paclitaxel inhibits progression of mitotic cells to G1 phase by interference with spindle formation without affecting other microtubule functions during anaphase and telephase. *Cancer Res,* 54, 4355-61.

LU, L., SAMUELSSON, L., BERGSTROM, M., SATO, K., FASTH, K. J. & LANGSTROM, B. (2002) Rat studies comparing 11C-FMAU, 18F-FLT, and 76Br-BFU as proliferation markers. *J Nucl Med,* 43, 1688-98.

MAIRE, V., NEMATI, F., RICHARDSON, M., VINCENT-SALOMON, A., TESSON, B., RIGAILL, G., GRAVIER, E., MARTY-PROUVOST, B., DE KONING, L., LANG, G., GENTIEN, D., DUMONT, A., BARILLOT, E., MARANGONI, E., DECAUDIN, D., ROMAN-ROMAN, S., PIERRE, A., CRUZALEGUI, F., DEPIL, S., TUCKER, G. C. & DUBOIS, T. (2013) Polo-like kinase 1: a potential therapeutic option in combination with conventional chemotherapy for the management of patients with triple-negative breast cancer. *Cancer Res,* 73, 813-23.

MALUMBRES, M. & BARBACID, M. (2005) Mammalian cyclin-dependent kinases. *Trends Biochem Sci,* 30, 630-41.

MANCHADO, E., GUILLAMOT, M. & MALUMBRES, M. (2012) Killing cells by targeting mitosis. *Cell Death Differ,* 19, 369-77.

MANFREDI, J. J., PARNESS, J. & HORWITZ, S. B. (1982) Taxol binds to cellular microtubules. *J Cell Biol,* 94, 688-96.

MANFREDI, M. G., ECSEDY, J. A., CHAKRAVARTY, A., SILVERMAN, L., ZHANG, M., HOAR, K. M., STROUD, S. G., CHEN, W., SHINDE, V., HUCK, J. J., WYSONG, D. R., JANOWICK, D. A., HYER, M. L., LEROY, P. J., GERSHMAN, R. E., SILVA, M. D., GERMANOS, M. S., BOLEN, J. B., CLAIBORNE, C. F. & SELLS, T. B. (2011) Characterization of Alisertib (MLN8237), an investigational small-molecule inhibitor of aurora A kinase using novel in vivo pharmacodynamic assays. *Clin Cancer Res,* 17, 7614-24.

MANGNER, T. J., KLECKER, R. W., ANDERSON, L. & SHIELDS, A. F. (2003) Synthesis of 2'-deoxy-2'-[18F]fluoro-beta-D-arabinofuranosyl nucleosides, [18F]FAU, [18F]FMAU, [18F]FBAU and [18F]FIAU, as potential PET agents for imaging cellular proliferation. Synthesis of [18F]labelled FAU, FMAU, FBAU, FIAU. *Nucl Med Biol,* 30, 215-24.

MANKOFF, D. A., SHIELDS, A. F., GRAHAM, M. M., LINK, J. M., EARY, J. F. & KROHN, K. A. (1998) Kinetic analysis of 2-[carbon-11]thymidine PET imaging studies: compartmental model and mathematical analysis. *J Nucl Med,* 39, 1043-55.

MANKOFF, D. A., SHIELDS, A. F., GRAHAM, M. M., LINK, J. M. & KROHN, K. A. (1996) A graphical analysis method to estimate blood-to-tissue transfer constants for tracers with labeled metabolites. *J Nucl Med,* 37, 2049-57.

MANKOFF, D. A., SHIELDS, A. F., LINK, J. M., GRAHAM, M. M., MUZI, M., PETERSON, L. M., EARY, J. F. & KROHN, K. A. (1999) Kinetic analysis of 2-[11C]thymidine PET imaging studies: validation studies. *J Nucl Med,* 40, 614-24.

MARUMOTO, T., HONDA, S., HARA, T., NITTA, M., HIROTA, T., KOHMURA, E. & SAYA, H. (2003) Aurora-A kinase maintains the fidelity of early and late mitotic events in HeLa cells. *J Biol Chem,* 278, 51786-95.

MATTHIES, H. J., MCDONALD, H. B., GOLDSTEIN, L. S. & THEURKAUF, W. E. (1996) Anastral meiotic spindle morphogenesis: role of the non-claret disjunctional kinesin-like protein. *J Cell Biol,* 134, 455-64.

MCGOWAN, C. H. & RUSSELL, P. (1993) Human Wee1 kinase inhibits cell division by phosphorylating p34cdc2 exclusively on Tyr15. *EMBO J,* 12, 75-85.

MCKINLEY, E. T., AYERS, G. D., SMITH, R. A., SALEH, S. A., ZHAO, P., WASHINGTON, M. K., COFFEY, R. J. & MANNING, H. C. (2013) Limits of [18F]-FLT PET as a biomarker of proliferation in oncology. *PLoS One,* 8, e58938.

MEIJER, L., BORGNE, A., MULNER, O., CHONG, J. P., BLOW, J. J., INAGAKI, N., INAGAKI, M., DELCROS, J. G. & MOULINOUX, J. P. (1997) Biochemical and cellular effects of roscovitine, a potent and selective inhibitor of the cyclin-dependent kinases cdc2, cdk2 and cdk5. *Eur J Biochem,* 243, 527-36.

MERALDI, P., HONDA, R. & NIGG, E. A. (2002) Aurora-A overexpression reveals tetraploidization as a major route to centrosome amplification in p53-/- cells. *EMBO J,* 21, 483-92.

MERALDI, P., HONDA, R. & NIGG, E. A. (2004) Aurora kinases link chromosome segregation and cell division to cancer susceptibility. *Curr Opin Genet Dev,* 14, 29-36.

MERRICK, K. A., WOHLBOLD, L., ZHANG, C., ALLEN, J. J., HORIUCHI, D., HUSKEY, N. E., GOGA, A., SHOKAT, K. M. & FISHER, R. P. (2011) Switching Cdk2 on or off with small molecules to reveal requirements in human cell proliferation. *Mol Cell,* 42, 624-36.

MORGAN, D. O. (1997) Cyclin-dependent kinases: engines, clocks, and microprocessors. *Annu Rev Cell Dev Biol,* 13, 261-91.

MOROZ, M. A., KOCHETKOV, T., CAI, S., WU, J., SHAMIS, M., NAIR, J., DE STANCHINA, E., SERGANOVA, I., SCHWARTZ, G. K., BANERJEE, D., BERTINO, J. R. & BLASBERG, R. G. (2011) Imaging colon cancer response following treatment with AZD1152: a preclinical analysis of [18F]fluoro-2-deoxyglucose and 3'-deoxy-3'-[18F]fluorothymidine imaging. *Clin Cancer Res,* 17, 1099-110.

MOUNTAIN, V., SIMERLY, C., HOWARD, L., ANDO, A., SCHATTEN, G. & COMPTON, D. A. (1999) The kinesin-related protein, HSET, opposes the activity of Eg5 and cross-links microtubules in the mammalian mitotic spindle. *J Cell Biol,* 147, 351-66.

MULLINS, J. M. & MCINTOSH, J. R. (1982) Isolation and initial characterization of the mammalian midbody. *J Cell Biol,* 94, 654-61.

MUNCH-PETERSEN, B. (2009) Reversible tetramerization of human TK1 to the high catalytic efficient form is induced by pyrophosphate, in addition to tripolyphosphates, or high enzyme concentration. *FEBS J,* 276, 571-80.

MUNCH-PETERSEN, B. (2010) Enzymatic regulation of cytosolic thymidine kinase 1 and mitochondrial thymidine kinase 2: a mini review. *Nucleosides Nucleotides Nucleic Acids,* 29, 363-9.

MUNCH-PETERSEN, B., CLOOS, L., JENSEN, H. K. & TYRSTED, G. (1995) Human thymidine kinase 1. Regulation in normal and malignant cells. *Adv Enzyme Regul,* 35, 69-89.

MUNCH-PETERSEN, B., CLOOS, L., TYRSTED, G. & ERIKSSON, S. (1991) Diverging substrate specificity of pure human thymidine kinases 1 and 2 against antiviral dideoxynucleosides. *J Biol Chem,* 266, 9032-8.

MUNCH-PETERSEN, B., TYRSTED, G. & CLOOS, L. (1993) Reversible ATP-dependent transition between two forms of human cytosolic thymidine kinase with different enzymatic properties. *J Biol Chem,* 268, 15621-5.

MUNOZ, F., FRANCO, P., CIAMMELLA, P., CLERICO, M., GIUDICI, M., FILIPPI, A. R. & RICARDI, U. (2007) Squamous cell carcinoma of the prostate: long-term survival after combined chemo-radiation. *Radiat Oncol,* 2, 15.

MURATA-HORI, M. & WANG, Y. L. (2002) Both midzone and astral microtubules are involved in the delivery of cytokinesis signals: insights from the mobility of aurora B. *J Cell Biol,* 159, 45-53.

MUZI, M., MANKOFF, D. A., GRIERSON, J. R., WELLS, J. M., VESSELLE, H. & KROHN, K. A. (2005a) Kinetic modeling of 3'-deoxy-3'-fluorothymidine in somatic tumors: mathematical studies. *J Nucl Med,* 46, 371-80.

MUZI, M., VESSELLE, H., GRIERSON, J. R., MANKOFF, D. A., SCHMIDT, R. A., PETERSON, L., WELLS, J. M. & KROHN, K. A. (2005b) Kinetic analysis of 3'-deoxy-3'-fluorothymidine PET studies: validation studies in patients with lung cancer. *J Nucl Med,* 46, 274-82.

NAKAYAMA, S., TORIKOSHI, Y., TAKAHASHI, T., YOSHIDA, T., SUDO, T., MATSUSHIMA, T., KAWASAKI, Y., KATAYAMA, A., GOHDA, K., HORTOBAGYI, G. N., NOGUCHI, S., SAKAI, T., ISHIHARA, H. & UENO, N. T. (2009) Prediction of paclitaxel sensitivity by CDK1 and CDK2 activity in human breast cancer cells. *Breast Cancer Res,* 11, R12.

NAVALGUND, L. G., ROSSANA, C., MUENCH, A. J. & JOHNSON, L. F. (1980) Cell cycle regulation of thymidylate synthetase gene expression in cultured mouse fibroblasts. *J Biol Chem,* 255, 7386-90.

NGUYEN, Q. D. & ABOAGYE, E. O. (2010) Imaging the life and death of tumors in living subjects: Preclinical PET imaging of proliferation and apoptosis. *Integr Biol (Camb),* 2, 483-95.

NGUYEN, Q. D., LAVDAS, I., GUBBINS, J., SMITH, G., FORTT, R., CARROLL, L. S., GRAHAM, M. A. & ABOAGYE, E. O. (2013) Temporal and spatial evolution of therapy-induced tumor apoptosis detected by caspase-3-selective molecular imaging. *Clin Cancer Res,* 19, 3914-24.

NGUYEN, Q. D., SMITH, G., GLASER, M., PERUMAL, M., ARSTAD, E. & ABOAGYE, E. O. (2009) Positron emission tomography imaging of drug-induced tumor apoptosis with a caspase-3/7 specific [18F]-labeled isatin sulfonamide. *Proc Natl Acad Sci U S A,* 106, 16375-80.

NIGG, E. A. (2001) Mitotic kinases as regulators of cell division and its checkpoints. *Nature Reviews Molecular Cell Biology,* 2, 21-32.

NIGG, E. A. & STEARNS, T. (2011) The centrosome cycle: Centriole biogenesis, duplication and inherent asymmetries. *Nat Cell Biol,* 13, 1154-60.

NIIBE, Y., KARASAWA, K. & HAYAKAWA, K. (2004) Ten-year disease-free survival of a small cell lung cancer patient with brain metastasis treated with chemoradiotherapy. *Anticancer Res,* 24, 2097-100.

NOTTEBROCK, H. & THEN, R. (1977) Thymidine concentrations in serum and urine of different animal species and man. *Biochem Pharmacol,* 26, 2175-9.

NURSE, P. (1990) Universal control mechanism regulating onset of M-phase. *Nature,* 344, 503-8.

NURSE, P. (1997) Checkpoint pathways come of age. *Cell,* 91, 865-7.

O'NEILL, R. A., BHAMIDIPATI, A., BI, X., DEB-BASU, D., CAHILL, L., FERRANTE, J., GENTALEN, E., GLAZER, M., GOSSETT, J., HACKER, K., KIRBY, C., KNITTLE, J., LODER, R., MASTROIENI, C., MACLAREN, M., MILLS, T., NGUYEN, U., PARKER, N., RICE, A., ROACH, D., SUICH, D., VOEHRINGER, D., VOSS, K., YANG, J., YANG, T. & VANDER HORN, P. B. (2006) Isoelectric focusing technology quantifies protein signaling in 25 cells. *Proc Natl Acad Sci U S A,* 103, 16153-8.

OBENAUER, J. C., CANTLEY, L. C. & YAFFE, M. B. (2003) Scansite 2.0: Proteome-wide prediction of cell signaling interactions using short sequence motifs. *Nucleic Acids Res,* 31, 3635-41.

ORR, G. A., VERDIER-PINARD, P., MCDAID, H. & HORWITZ, S. B. (2003) Mechanisms of Taxol resistance related to microtubules. *Oncogene,* 22, 7280-95.

OUYANG, X., WANG, X., XU, K., JIN, D. Y., CHEUNG, A. L., TSAO, S. W. & WONG, Y. C. (2001) Effect of p53 on centrosome amplification in prostate cancer cells. *Biochim Biophys Acta,* 1541, 212-20.

PAPROSKI, R. J., NG, A. M., YAO, S. Y., GRAHAM, K., YOUNG, J. D. & CASS, C. E. (2008) The role of human nucleoside transporters in uptake of 3'-deoxy-3'-fluorothymidine. *Mol Pharmacol,* 74, 1372-80.

PAPROSKI, R. J., WUEST, M., JANS, H. S., GRAHAM, K., GATI, W. P., MCQUARRIE, S., MCEWAN, A., MERCER, J., YOUNG, J. D. & CASS, C. E. (2010) Biodistribution and uptake of 3'-deoxy-3'-fluorothymidine in ENT1-knockout mice and in an ENT1-knockdown tumor model. *J Nucl Med,* 51, 1447-55.

PARDEE, A. B. (1974) A restriction point for control of normal animal cell proliferation. *Proc Natl Acad Sci U S A,* 71, 1286-90.

PEDRALI-NOY, G., SPADARI, S., MILLER-FAURES, A., MILLER, A. O., KRUPPA, J. & KOCH, G. (1980) Synchronization of HeLa cell cultures by inhibition of DNA polymerase alpha with aphidicolin. *Nucleic Acids Res,* 8, 377-87.

PENNYCOOKE, M., CHAUDARY, N., SHURALYOVA, I., ZHANG, Y. & COE, I. R. (2001) Differential expression of human nucleoside transporters in normal and tumor tissue. *Biochem Biophys Res Commun,* 280, 951-9.

PERUMAL, M., PILLAI, R. G., BARTHEL, H., LEYTON, J., LATIGO, J. R., FORSTER, M., MITCHELL, F., JACKMAN, A. L. & ABOAGYE, E. O. (2006) Redistribution of nucleoside transporters to the cell membrane provides a novel approach for imaging thymidylate synthase inhibition by positron emission tomography. *Cancer Res,* 66, 8558-64.

PETRONCZKI, M., LENART, P. & PETERS, J. M. (2008) Polo on the Rise-from Mitotic Entry to Cytokinesis with Plk1. *Dev Cell,* 14, 646-59.

PHELPS, M. E. (2000) Inaugural article: positron emission tomography provides molecular imaging of biological processes. *Proc Natl Acad Sci U S A,* 97, 9226-33.

PILLAI, R. G., FORSTER, M., PERUMAL, M., MITCHELL, F., LEYTON, J., AIBGIRHIO, F. I., GOLOVKO, O., JACKMAN, A. L. & ABOAGYE, E. O. (2008) Imaging pharmacodynamics of the alpha-folate receptor-targeted thymidylate synthase inhibitor BGC 945. *Cancer Res,* 68, 3827-34.

PLOTNIK, D. A., MCLAUGHLIN, L. J., CHAN, J., REDMAYNE-TITLEY, J. N. & SCHWARTZ, J. L. (2011) The role of nucleoside/nucleotide transport and metabolism in the uptake

and retention of 3'-fluoro-3'-deoxythymidine in human B-lymphoblast cells. *Nucl Med Biol,* 38, 979-86.

PRESSACCO, J., MITROVSKI, B., ERLICHMAN, C. & HEDLEY, D. W. (1995) Effects of thymidylate synthase inhibition on thymidine kinase activity and nucleoside transporter expression. *Cancer Res,* 55, 1505-8.

RASEY, J. S., GRIERSON, J. R., WIENS, L. W., KOLB, P. D. & SCHWARTZ, J. L. (2002) Validation of FLT uptake as a measure of thymidine kinase-1 activity in A549 carcinoma cells. *J Nucl Med,* 43, 1210-7.

ROWINSKY, E. K., BURKE, P. J., KARP, J. E., TUCKER, R. W., ETTINGER, D. S. & DONEHOWER, R. C. (1989) Phase I and pharmacodynamic study of taxol in refractory acute leukemias. *Cancer Res,* 49, 4640-7.

ROWINSKY, E. K. & DONEHOWER, R. C. (1995) Paclitaxel (taxol). *N Engl J Med,* 332, 1004-14.

RYCHLIK, W., DOMIER, L. L., GARDNER, P. R., HELLMANN, G. M. & RHOADS, R. E. (1987) Amino acid sequence of the mRNA cap-binding protein from human tissues. *Proc Natl Acad Sci U S A,* 84, 945-9.

SALSKOV, A., TAMMISETTI, V. S., GRIERSON, J. & VESSELLE, H. (2007) FLT: measuring tumor cell proliferation in vivo with positron emission tomography and 3'-deoxy-3'-[18F]fluorothymidine. *Semin Nucl Med,* 37, 429-39.

SANCHO-MARTINEZ, S. M., PRIETO-GARCIA, L., PRIETO, M., LOPEZ-NOVOA, J. M. & LOPEZ-HERNANDEZ, F. J. (2012) Subcellular targets of cisplatin cytotoxicity: an integrated view. *Pharmacol Ther,* 136, 35-55.

SANTAMARIA, D., BARRIERE, C., CERQUEIRA, A., HUNT, S., TARDY, C., NEWTON, K., CACERES, J. F., DUBUS, P., MALUMBRES, M. & BARBACID, M. (2007) Cdk1 is sufficient to drive the mammalian cell cycle. *Nature,* 448, 811-5.

SCHAFER, K. A. (1998) The cell cycle: a review. *Vet Pathol,* 35, 461-78.

SCHIFF, P. B., FANT, J. & HORWITZ, S. B. (1979) Promotion of microtubule assembly in vitro by taxol. *Nature,* 277, 665-7.

SCHINAZI, R. F., PECK, A. & SOMMADOSSI, J. P. (1992) Substrate specificity of Escherichia coli thymidine phosphorylase for pyrimidine nucleosides with anti-human immunodeficiency virus activity. *Biochem Pharmacol,* 44, 199-204.

SCHLOSSER, C. A., STEGLICH, C., DEWET, J. R. & SCHEFFLER, I. E. (1981) Cell cycle-dependent regulation of thymidine kinase activity introduced into mouse LMTK-cells by DNA and chromatin-mediated gene transfer. *Proc Natl Acad Sci U S A,* 78, 1119-23.

SCHMITZ, H., POTTER, V. R., BURLBERT, R. B. & WHITE, D. M. (1954) Alternative pathways of glucose metabolism. II. Nucleotides from the acid-soluble fraction of normal and tumor tissues and studies on nucleic acid synthesis in tumors. *Cancer Res,* 14, 66-74.

SCHOLZEN, T. & GERDES, J. (2000) The Ki-67 protein: from the known and the unknown. *J Cell Physiol,* 182, 311-22.

SCHWARTZ, J. L., TAMURA, Y., JORDAN, R., GRIERSON, J. R. & KROHN, K. A. (2004) Effect of p53 activation on cell growth, thymidine kinase-1 activity, and 3'-deoxy-3'fluorothymidine uptake. *Nucl Med Biol,* 31, 419-23.

SEBOLT-LEOPOLD, J. S. & HERRERA, R. (2004) Targeting the mitogen-activated protein kinase cascade to treat cancer. *Nat Rev Cancer,* 4, 937-47.

SEITZ, U., WAGNER, M., NEUMAIER, B., WAWRA, E., GLATTING, G., LEDER, G., SCHMID, R. M. & RESKE, S. N. (2002) Evaluation of pyrimidine metabolising enzymes and in vitro uptake of 3'-[(18)F]fluoro-3'-deoxythymidine ([(18)F]FLT) in pancreatic cancer cell lines. *Eur J Nucl Med Mol Imaging,* 29, 1174-81.

SHERLEY, J. L. & KELLY, T. J. (1988) Regulation of human thymidine kinase during the cell cycle. *J Biol Chem,* 263, 8350-8.

SHERR, C. J. & ROBERTS, J. M. (1995) Inhibitors of mammalian G1 cyclin-dependent kinases. *Genes Dev,* 9, 1149-63.

SHERR, C. J. & ROBERTS, J. M. (2004) Living with or without cyclins and cyclin-dependent kinases. *Genes & Development,* 18, 2699-2711.

SHIELDS, A. F. (2003) PET imaging with 18F-FLT and thymidine analogs: promise and pitfalls. *J Nucl Med,* 44, 1432-4.

SHIELDS, A. F. (2006) Positron emission tomography measurement of tumor metabolism and growth: its expanding role in oncology. *Mol Imaging Biol,* 8, 141-50.

SHIELDS, A. F. (2012) PET Imaging of Tumor Growth: Not as Easy as It Looks. *Clin Cancer Res,* 18, 1189-1191.

SHIELDS, A. F., BRISTON, D. A., CHANDUPATLA, S., DOUGLAS, K. A., LAWHORN-CREWS, J., COLLINS, J. M., MANGNER, T. J., HEILBRUN, L. K. & MUZIK, O. (2005) A simplified analysis of [18F]3'-deoxy-3'-fluorothymidine metabolism and retention. *Eur J Nucl Med Mol Imaging,* 32, 1269-75.

SHIELDS, A. F., GRIERSON, J. R., DOHMEN, B. M., MACHULLA, H. J., STAYANOFF, J. C., LAWHORN-CREWS, J. M., OBRADOVICH, J. E., MUZIK, O. & MANGNER, T. J. (1998) Imaging proliferation in vivo with [F-18]FLT and positron emission tomography. *Nat Med,* 4, 1334-6.

SHIELDS, A. F., GRIERSON, J. R., KOZAWA, S. M. & ZHENG, M. (1996a) Development of labeled thymidine analogs for imaging tumor proliferation. *Nucl Med Biol,* 23, 17-22.

SHIELDS, A. F., LIM, K., GRIERSON, J., LINK, J. & KROHN, K. A. (1990) Utilization of labeled thymidine in DNA synthesis: studies for PET. *J Nucl Med,* 31, 337-42.

SHIELDS, A. F., MANKOFF, D., GRAHAM, M. M., ZHENG, M., KOZAWA, S. M., LINK, J. M. & KROHN, K. A. (1996b) Analysis of 2-carbon-11-thymidine blood metabolites in PET imaging. *J Nucl Med,* 37, 290-6.

SIDDIK, Z. H. (2003) Cisplatin: mode of cytotoxic action and molecular basis of resistance. *Oncogene,* 22, 7265-79.

SMITH, G., SALA, R., CARROLL, L., BEHAN, K., GLASER, M., ROBINS, E., NGUYEN, Q. D. & ABOAGYE, E. O. (2012) Synthesis and evaluation of nucleoside radiotracers for imaging proliferation. *Nucl Med Biol,* 39, 652-65.

SMYCZEK-GARGYA, B., FERSIS, N., DITTMANN, H., VOGEL, U., REISCHL, G., MACHULLA, H. J., WALLWIENER, D., BARES, R. & DOHMEN, B. M. (2004) PET with [18F]fluorothymidine for imaging of primary breast cancer: a pilot study. *Eur J Nucl Med Mol Imaging,* 31, 720-4.

SOHN, H. J., YANG, Y. J., RYU, J. S., OH, S. J., IM, K. C., MOON, D. H., LEE, D. H., SUH, C., LEE, J. S. & KIM, S. W. (2008) [18F]Fluorothymidine positron emission tomography before and 7 days after gefitinib treatment predicts response in patients with advanced adenocarcinoma of the lung. *Clin Cancer Res,* 14, 7423-9.

SOLIT, D. B., GARRAWAY, L. A., PRATILAS, C. A., SAWAI, A., GETZ, G., BASSO, A., YE, Q., LOBO, J. M., SHE, Y., OSMAN, I., GOLUB, T. R., SEBOLT-LEOPOLD, J., SELLERS, W. R.

& ROSEN, N. (2006) BRAF mutation predicts sensitivity to MEK inhibition. *Nature,* 439, 358-62.

STEEGMAIER, M., HOFFMANN, M., BAUM, A., LENART, P., PETRONCZKI, M., KRSSAK, M., GURTLER, U., GARIN-CHESA, P., LIEB, S., QUANT, J., GRAUERT, M., ADOLF, G. R., KRAUT, N., PETERS, J. M. & RETTIG, W. J. (2007) BI 2536, a potent and selective inhibitor of polo-like kinase 1, inhibits tumor growth in vivo. *Curr Biol,* 17, 316-22.

STOLZ, A., VOGEL, C., SCHNEIDER, V., ERTYCH, N., KIENITZ, A., YU, H. & BASTIANS, H. (2009) Pharmacologic abrogation of the mitotic spindle checkpoint by an indolocarbazole discovered by cellular screening efficiently kills cancer cells. *Cancer Res,* 69, 3874-83.

STREBHARDT, K. & ULLRICH, A. (2006) Targeting polo-like kinase 1 for cancer therapy. *Nat Rev Cancer,* 6, 321-30.

SUGIYAMA, M., SAKAHARA, H., SATO, K., HARADA, N., FUKUMOTO, D., KAKIUCHI, T., HIRANO, T., KOHNO, E. & TSUKADA, H. (2004) Evaluation of 3'-deoxy-3'-18F-fluorothymidine for monitoring tumor response to radiotherapy and photodynamic therapy in mice. *J Nucl Med,* 45, 1754-8.

SUMARA, I., GIMENEZ-ABIAN, J. F., GERLICH, D., HIROTA, T., KRAFT, C., DE LA TORRE, C., ELLENBERG, J. & PETERS, J. M. (2004) Roles of polo-like kinase 1 in the assembly of functional mitotic spindles. *Curr Biol,* 14, 1712-22.

SUN, H., SLOAN, A., MANGNER, T. J., VAISHAMPAYAN, U., MUZIK, O., COLLINS, J. M., DOUGLAS, K. & SHIELDS, A. F. (2005) Imaging DNA synthesis with [18F]FMAU and positron emission tomography in patients with cancer. *Eur J Nucl Med Mol Imaging,* 32, 15-22.

TAKEDA, D. Y. & DUTTA, A. (2005) DNA replication and progression through S phase. *Oncogene,* 24, 2827-43.

TARAPORE, P. & FUKASAWA, K. (2002) Loss of p53 and centrosome hyperamplification. *Oncogene,* 21, 6234-40.

TARAPORE, P., HORN, H. F., TOKUYAMA, Y. & FUKASAWA, K. (2001) Direct regulation of the centrosome duplication cycle by the p53-p21Waf1/Cip1 pathway. *Oncogene,* 20, 3173-84.

TATSUKA, M., KATAYAMA, H., OTA, T., TANAKA, T., ODASHIMA, S., SUZUKI, F. & TERADA, Y. (1998) Multinuclearity and increased ploidy caused by overexpression of the aurora- and Ipl1-like midbody-associated protein mitotic kinase in human cancer cells. *Cancer Res,* 58, 4811-6.

TAYLOR, W. R. & STARK, G. R. (2001) Regulation of the G2/M transition by p53. *Oncogene,* 20, 1803-15.

TOMMASI, S. & PFEIFER, G. P. (1997) Constitutive protection of E2F recognition sequences in the human thymidine kinase promoter during cell cycle progression. *J Biol Chem,* 272, 30483-90.

TOYOHARA, J. & FUJIBAYASHI, Y. (2003) Trends in nucleoside tracers for PET imaging of cell proliferation. *Nucl Med Biol,* 30, 681-5.

TOYOHARA, J., HAYASHI, A., GOGAMI, A. & FUJIBAYASHI, Y. (2006a) Alkyl-fluorinated thymidine derivatives for imaging cell proliferation II. Synthesis and evaluation of N3-(2-[18F]fluoroethyl)-thymidine. *Nucl Med Biol,* 33, 765-72.

TOYOHARA, J., HAYASHI, A., GOGAMI, A., HAMADA, M., HAMASHIMA, Y., KATOH, T., NODE, M. & FUJIBAYASHI, Y. (2006b) Alkyl-fluorinated thymidine derivatives for

imaging cell proliferation I. The in vitro evaluation of some alkyl-fluorinated thymidine derivatives. *Nucl Med Biol,* 33, 751-64.

TOYOHARA, J., HAYASHI, A., SATO, M., TANAKA, H., HARAGUCHI, K., YOSHIMURA, Y., YONEKURA, Y. & FUJIBAYASHI, Y. (2002a) Rationale of 5-(125)I-iodo-4'-thio-2'-deoxyuridine as a potential iodinated proliferation marker. *J Nucl Med,* 43, 1218-26.

TOYOHARA, J., WAKI, A., TAKAMATSU, S., YONEKURA, Y., MAGATA, Y. & FUJIBAYASHI, Y. (2002b) Basis of FLT as a cell proliferation marker: comparative uptake studies with [3H]thymidine and [3H]arabinothymidine, and cell-analysis in 22 asynchronously growing tumor cell lines. *Nucl Med Biol,* 29, 281-7.

TROOST, E. G., BUSSINK, J., SLOOTWEG, P. J., PEETERS, W. J., MERKX, M. A., VAN DER KOGEL, A. J., OYEN, W. J. & KAANDERS, J. H. (2010) Histopathologic validation of 3'-deoxy-3'-18F-fluorothymidine PET in squamous cell carcinoma of the oral cavity. *J Nucl Med,* 51, 713-9.

TSOU, M. F., WANG, W. J., GEORGE, K. A., URYU, K., STEARNS, T. & JALLEPALLI, P. V. (2009) Polo kinase and separase regulate the mitotic licensing of centriole duplication in human cells. *Dev Cell,* 17, 344-54.

VAN WAARDE, A., COBBEN, D. C. P., ALBERT J.H. SUURMEIJER, A. J. H., MAAS, B., VAALBURG, W., DE VRIES, E. F. J., JAGER, P. L., HOEKSTRA, H. J. & ELSINGA, P. H. (2004) Selectivity of 18F-FLT and 18F-FDG for Differentiating Tumor from Inflammation in a Rodent Model. *J Nucl Med,* 45, 695-700.

VANDER BORGHT, T., PAUWELS, S., LAMBOTTE, L., LABAR, D., DE MAEGHT, S., STROOBANDT, G. & LATERRE, C. (1994) Brain tumor imaging with PET and 2-[carbon-11]thymidine. *J Nucl Med,* 35, 974-82.

VESSELLE, H., GRIERSON, J., MUZI, M., PUGSLEY, J. M., SCHMIDT, R. A., RABINOWITZ, P., PETERSON, L. M., VALLIERES, E. & WOOD, D. E. (2002) In vivo validation of 3'deoxy-3'-[(18)F]fluorothymidine ([(18)F]FLT) as a proliferation imaging tracer in humans: correlation of [(18)F]FLT uptake by positron emission tomography with Ki-67 immunohistochemistry and flow cytometry in human lung tumors. *Clin Cancer Res,* 8, 3315-23.

VIERTL, D., BISCHOF DELALOYE, A., LANZ, B., POITRY-YAMATE, C., GRUETTER, R., MLYNARIK, V., AMETAMEY, S. M., ROSS, T. L., LEHR, H. A., ANDRE, P. A., PERILLO-ADAMER, F., KOSINSKI, M., DUPERTUIS, Y. M. & BUCHEGGER, F. (2011) Increase of [(18)F]FLT tumor uptake in vivo mediated by FdUrd: toward improving cell proliferation positron emission tomography. *Mol Imaging Biol,* 13, 321-31.

WADE, R. H. (2009) On and around microtubules: an overview. *Mol Biotechnol,* 43, 177-91.

WALCZAK, C. E. & MITCHISON, T. J. (1996) Kinesin-related proteins at mitotic spindle poles: function and regulation. *Cell,* 85, 943-6.

WANG, J. & ERIKSSON, S. (1996) Phosphorylation of the anti-hepatitis B nucleoside analog 1-(2'-deoxy-2'-fluoro-1-beta-D-arabinofuranosyl)-5-iodouracil (FIAU) by human cytosolic and mitochondrial thymidine kinase and implications for cytotoxicity. *Antimicrob Agents Chemother,* 40, 1555-7.

WARNER, S. L., GRAY, P. J. & VON HOFF, D. D. (2006) Tubulin-associated drug targets: Aurora kinases, Polo-like kinases, and others. *Semin Oncol,* 33, 436-48.

WELBURN, J. P., VLEUGEL, M., LIU, D., YATES, J. R., 3RD, LAMPSON, M. A., FUKAGAWA, T. & CHEESEMAN, I. M. (2010) Aurora B phosphorylates spatially distinct targets to differentially regulate the kinetochore-microtubule interface. *Mol Cell,* 38, 383-92.

WELIN, M., KOSINSKA, U., MIKKELSEN, N. E., CARNROT, C., ZHU, C., WANG, L., ERIKSSON, S., MUNCH-PETERSEN, B. & EKLUND, H. (2004) Structures of thymidine kinase 1 of human and mycoplasmic origin. *Proc Natl Acad Sci U S A,* 101, 17970-5.

WELLS, P., WEST, C., JONES, T., HARRIS, A. & PRICE, P. (2004) Measuring tumor pharmacodynamic response using PET proliferation probes: the case for 2-[(11)C]-thymidine. *Biochim Biophys Acta,* 1705, 91-102.

WILKINSON, R. W., ODEDRA, R., HEATON, S. P., WEDGE, S. R., KEEN, N. J., CRAFTER, C., FOSTER, J. R., BRADY, M. C., BIGLEY, A., BROWN, E., BYTH, K. F., BARRASS, N. C., MUNDT, K. E., FOOTE, K. M., HERON, N. M., JUNG, F. H., MORTLOCK, A. A., BOYLE, F. T. & GREEN, S. (2007) AZD1152, a selective inhibitor of Aurora B kinase, inhibits human tumor xenograft growth by inducing apoptosis. *Clin Cancer Res,* 13, 3682-8.

WOOD, K. W., CORNWELL, W. D. & JACKSON, J. R. (2001) Past and future of the mitotic spindle as an oncology target. *Curr Opin Pharmacol,* 1, 370-7.

WORKMAN, P., ABOAGYE, E. O., BALKWILL, F., BALMAIN, A., BRUDER, G., CHAPLIN, D. J., DOUBLE, J. A., EVERITT, J., FARNINGHAM, D. A., GLENNIE, M. J., KELLAND, L. R., ROBINSON, V., STRATFORD, I. J., TOZER, G. M., WATSON, S., WEDGE, S. R. & ECCLES, S. A. (2010) Guidelines for the welfare and use of animals in cancer research. *Br J Cancer,* 102, 1555-77.

XIE, H., LEE, M. H., ZHU, F., REDDY, K., PENG, C., LI, Y., LIM DO, Y., KIM, D. J., LI, X., KANG, S., LI, H., MA, W., LUBET, R. A., DING, J., BODE, A. M. & DONG, Z. (2013) Identification of an Aurora kinase inhibitor specific for the Aurora B isoform. *Cancer Res,* 73, 716-24.

XU, X., WEAVER, Z., LINKE, S. P., LI, C., GOTAY, J., WANG, X. W., HARRIS, C. C., RIED, T. & DENG, C. X. (1999) Centrosome amplification and a defective G2-M cell cycle checkpoint induce genetic instability in BRCA1 exon 11 isoform-deficient cells. *Mol Cell,* 3, 389-95.

YAMAMOTO, Y., KAMEYAMA, R., IZUISHI, K., TAKEBAYASHI, R., HAGIIKE, M., ASAKURA, M., HABA, R. & NISHIYAMA, Y. (2009) Detection of colorectal cancer using (1)(8)F-FLT PET: comparison with (1)(8)F-FDG PET. *Nucl Med Commun,* 30, 841-5.

YAU, K., PRICE, P., PILLAI, R. G. & ABOAGYE, E. (2006) Elevation of radiolabelled thymidine uptake in RIF-1 fibrosarcoma and HT29 colon adenocarcinoma cells after treatment with thymidylate synthase inhibitors. *Eur J Nucl Med Mol Imaging,* 33, 981-7.

YOUNG, J. D., YAO, S. Y., BALDWIN, J. M., CASS, C. E. & BALDWIN, S. A. (2013) The human concentrative and equilibrative nucleoside transporter families, SLC28 and SLC29. *Mol Aspects Med,* 34, 529-47.

ZHANG, C. C., YAN, Z., LI, W., KUSZPIT, K., PAINTER, C. L., ZHANG, Q., LAPPIN, P. B., NICHOLS, T., LIRA, M. E., AFFOLTER, T., FAHEY, N. R., CULLINANE, C., SPILKER, M., ZASADNY, K., O'BRIEN, P., BUCKMAN, D., WONG, A. & CHRISTENSEN, J. G. (2012) [(18)F]FLT-PET imaging does not always "light up" proliferating tumor cells. *Clin Cancer Res,* 18, 1303-12.

ZHOU, H., KUANG, J., ZHONG, L., KUO, W. L., GRAY, J. W., SAHIN, A., BRINKLEY, B. R. & SEN, S. (1998) Tumour amplified kinase STK15/BTAK induces centrosome amplification, aneuploidy and transformation. Nat Genet, 20, 189-93.